Waterborne Polysulfide Dispersions for Coatings Application

Justine Elgoyhen

Supervised by: Radmila Tomovska

Chemical Engineering Group
University of the Basque Country UPV/EHU
Donostia-San Sabastián
(2023)

eman ta zabal zazu
Universidad del País Vasco
Euskal Herriko Unibertsitatea

Acknowledgements

I would like to express my sincere gratitude to my supervisor Prof. Radmila Tomovska for giving me the opportunity to perform my PhD in the Polymerization Process Group. I would like to sincerely acknowledge her guidance, advice and support in the execution of this PhD.

I would like to thank all the group members from the Polymerization Process Group and POLYMAT, students, professors and Ines. I would like to thank Prof. Alejandro J. Müller, his group, and Valentina Pirela for their collaboration in the crystallization part.

I acknowledge the financial support from the European Union's Horizon 2020 Research and Innovation Program under the Marie Skłodowska-Curie grant agreement no. 765341 (Project PHOTO-EMULSION, MSCA-ITN-2017) and would like to thank all the members from the project.

Je souhaite remercier tous mes amis de Bayonne, qui m'encouragent depuis toujours. Merci pour vos mots, votre enthousiasme à l'égard de mon travail! Merci pour ces moments partagés, et ceux à venir.

Enfin, et surtout, je remercie ma famille. Je mesure la chance que j'ai de vous avoir à mes côtés, et je n'aurais pas pu concrétiser ce projet sans vous. Je ne peux achever ces remerciements sans une pensée particulière pour ma maman, qui me soutient dans tout ce que

j’entreprends et qui m’a particulièrement accompagnée en période d’écriture. Cette thèse est aussi un peu la tienne finalement.

Diciembre 2018

Diciembre 2022

Content

Chapter 1. Introduction

Chapter 2. Challenges of thiol-ene chemistry in the field of polymer synthesis

Chapter 3. Development of waterborne poly(thioether) coatings by polymerization in dispersed media

Chapter 4. Study on the crystallization of film-forming poly(thioethers)

Chapter 5. Crystallization of aliphatic poly(thioethers)

Chapter 6. Biobased polysulfide coatings

Chapter 7. Conclusions

Chapter 1. Introduction

1.1. Main motivation and objectives

Today, the polymer industry is going through significant changes in priorities driven by the growing awareness of ecological issues. In this context, the development of eco-efficient and sustainable processes and products has become an absolute necessity.

Nowadays, many industrial coating processes involve the use of waterborne products obtained by polymerization in dispersed media[1–4]. These VOC-free polymer products are indeed a greener alternative to the traditional solvent borne coatings, as water is used as the disperse phase. Although the market of waterborne coatings is constantly increasing, the variety of polymer dispersions commercially available is restricted and relies mainly on (meth)acrylic, styrene or acrylonitrile monomers and chain growth radical polymerization using thermal[1,2,5,6] or redox radical initiator[1,7]. Hence, the development of polymerization technologies to expand the range of products and to make the process even more efficient and environmental friendly is needed. To answer to this need, we propose an approach that unites a photopolymerization in dispersed media technique, as energy efficient and more versatile process[8–11], with thiol-ene step-growth radical polymerization, as a process to produce novel polysulfide aqueous dispersed products and widen the application possibilities.

Thiol-ene chemistry has been widely studied, and its application in coating has recently emerged[12] because of its numerous advantages such as rapid kinetics, control of the polymer architecture, and insensitivity to oxygen.[13] Thiol-ene photopolymerization has been used in UV-cured coating formulations[12,14,15], although its application is restricted to surface and thin-layer. The feasibility of thiol-ene photopolymerization in aqueous dispersed media is well documented in the literature, and has been performed in emulsion[16,17], miniemulsion[18–25] and suspension[26], giving rise to linear or crosslinked poly(thioether) dispersions in water, also called latexes. Among these processes, thiol-ene polymerization in miniemulsion turns out to be a privileged mean to obtain high sulfur content products with controlled colloidal properties and architecture, while minimising cost and environmental impact because of the lower consumption of energy and the use of a VOC-free process.

In the scope of aimed applications of novel thiol-ene dispersions, the oxygen barrier waterborne coatings for food packaging is a highly open market for innovations. Even though the current industrial barrier coatings based on waterborne polyvinylidene chloride (PVDC) present outstanding barrier properties, driven by the growing awareness of an ecological issue they need to be replaced by halogen-free and more sustainable options. Pertaining to waterborne barrier coatings, the polymer microstructure is of the utmost importance in combining excellent barrier properties and good film-forming ability. Therefore, an additional objective of the thesis is to synthesize linear and crystallisable polymer chains that will be embedded within soft amorphous polymer matrix, and to study their crystalline behaviour by the mean of advance differential scanning calorimetry (DSC) analysis.

1.2. Basics of thiol-ene chemistry in polymer synthesis

The so-called thiol-ene reaction was first observed by Theodor Posner in 1905. [27] In his work, he describes the additions of mercaptans to mono or bi unsaturated olefin, following an anti-markovnikov arrangement. Thiol-ene chemistry has been extensively studied in the field of polymer synthesis and material science, based on polymers produced principally by bulk and solution polymerization.[12,28–32]

Herein, we focus on the synthesis of poly(thioethers) by radical-mediated thiol-ene polymerization, which follows a step growth mechanism. This synthetic pathway can be either initiated thermally[33,34], or photochemically[35–38]. The latter is more frequently used in polymer synthesis, as it is considered energetically more efficient and provides a spatial and temporal control of the polymerization.

The mechanism of thiol-ene step-growth photopolymerization is schematically presented in Figure 1.1, in the case of bifunctionnal thiol and ene monomers that do not homopolymerize. In a first step, radicals are produced by decomposition of a radical photoinitiator. These radicals readily abstract the hydrogen of the thiol moiety, as the sulfur hydrogen bond is very labile,[39] yielding thiyl radicals. The latter then propagate across the ene goup, by addition to the less substituted side of the ene moiety (anti-markovnikov addition) forming a carbon centered radical. Subsequently, a chain reaction transfer occurs, in which the carbonyl abstract the hydrogen of another thiol moiety. The step growth polymerization takes place by alternation of

thiyl radical propagation and chain transfer reaction. Termination reactions occur by radical recombination.

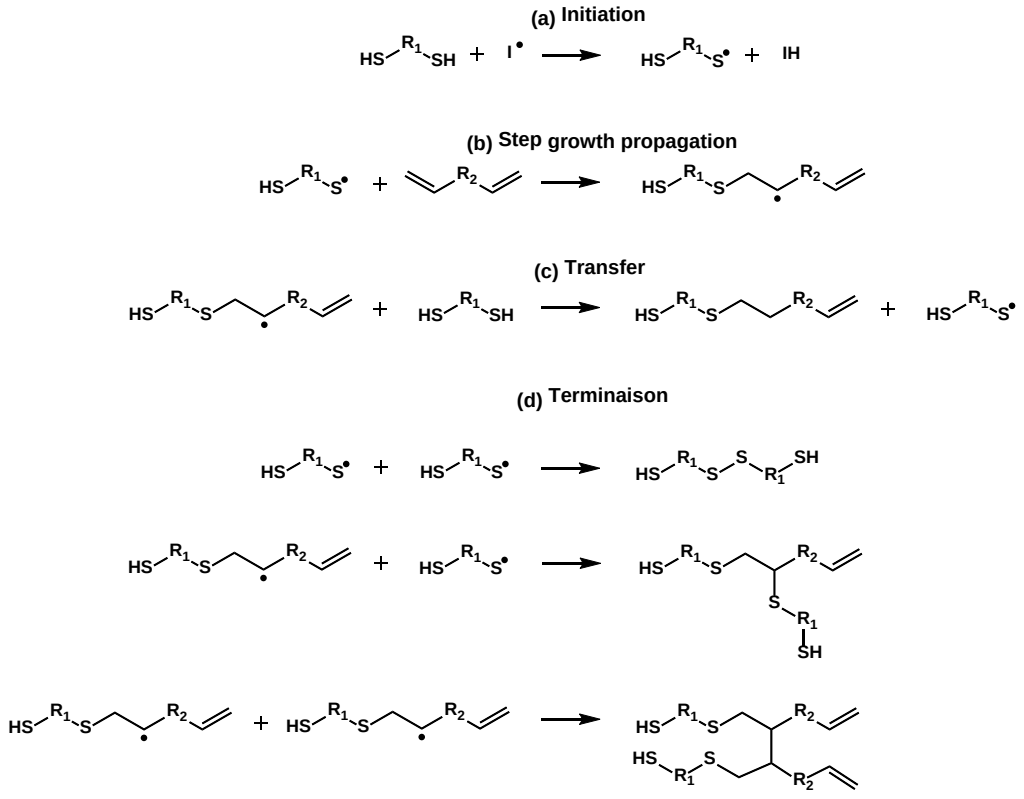

Figure 1.1. Thiol-ene radical step-growth polymerization mechanism[13]

Interest in thiol-ene chemistry has dramatically increased over the past few decades in the field of material science. Indeed, it appears to be a preferred technology because of the simplicity to obtain various polymer architectures and lack of production of undesired products, so there is no need of product purification. Namely, thiol-ene bifunctional monomers lead to the

synthesis of linear step-grown polymers, while branching/cross-linking can be finely tuned by increasing monomer functionality[15]. Thiol-ene polymerization is considered as a "click" chemistry, an approach initially described by Sharpless *et al.*[40]. Among the list of criteria described by the authors, a reaction can be classified as "click" chemistry if it can be effectively performed under mild conditions, and leads to the formation of a single product, stereospecificately, with very few and inoffensive by products and with high yields. In addition, the reaction conditions should be simple, with solvent that are benign or easily removable. Noteworthy, thiol-ene polymerization is readily implemented under atmospheric conditions, as it is insensitive to oxygen (unlike acrylate radical mediated chain growth polymerization for example). Indeed, in conventional radical polymerization, radicals react very fast with oxygen to form peroxy radicals, which stop chain propagation. In thiol-ene polymerization, the peroxy radicals, although not participating in propagation, can readily abstract the hydrogen from the thiol moiety yielding to thiyl radicals that can continue the polymerization process.[41]

Besides the advantages drawn by the click nature of thiol-ene polymerization, it suffers from some drawbacks when it comes to practical applications. Because of the step-growth mechanism, the synthesis of high molar mass polymers with practical significance can be challenging compared to chain-grown polymers. Indeed, in the case of A-A and B-B monomers combination into linear addition polymers through step-growth mechanism, the Carothers equation (Eq. 1.1) relates the degree of polymerization to the extent of reaction and the stoichiometric ratio between functionality, where $\bar{X}_n$ is the number-average degree of polymerization, p is the conversion and r is the monomers stoichiometric ratio (Eq. 1.2).[42]

$$\bar{X}_n = \frac{1+r}{1+r-2pr} \text{ ……. (1.1)}$$

$$r = \frac{[\mathrm{A}-\mathrm{A}]}{[\mathrm{B}-\mathrm{B}]} \text{ …….. (1.2)}$$

$$\text{with } [\mathrm{A}-\mathrm{A}] \leq [\mathrm{B}-\mathrm{B}]$$

The Carothers equation highlights the stringent requirements of the stoichiometric balance between thiol and ene monomers and conversion to enable molar mass control in step growth polymerization. Another consequence arising from step-growth mechanism is that reproducibility in terms of molar masses is unlikely to occur from one reaction to another, as small stoichiometric imbalance that induces large difference in molar masses are inevitable.[42]

Another drawbacks reported in the literature is the chemical instability of thiol ene system.[43–47] Thiol-ene systems readily undergo premature polymerization even without initiator, and this lack of control may worsen reproducibility already difficult to achieve due to the nature of step growth mechanism. In the literature, thiol-ene spontaneous reaction, also known as thiol-ene dark reaction, is mainly attributed to the presence of impurities capable to initiate the step-growth mechanism through different pathways. Namely, the presence of residues coming from the monomers synthesis, such as peroxide or hydroperoxide species with concentrations as low as traces can initiate the radical mediated polymerization.[43] Indeed, thiol-ene step growth reaction can be initiated by very low amount of radical species, capable to abstract the hydrogen from the thiol moiety yielding a thiyl radical. This thiyl radical then initiates the propagation cycle, and thiol and ene monomers' consumption mainly occurs through the rapid chain transfer step during propagation.[37] The presence of basic or nucleophilic impurities in the formulation

can initiate another polymerization pathway, the catalyst-mediated thiol Michael addition.[32,39,48] Unfortunately, the presence of impurities, which could be diminished by purification of starting material, is not the only cause of premature polymerization. There are several works reported on self-initiated mechanisms responsible for the radical mediated thiol-ene polymerization. After showing evidence of a premature polymerization by UV spectroscopy and DSC[46], Klemm *et al*. reported that in dark and inert conditions, radicals were formed spontaneously in dithiol and diene mixtures.[44] The spontaneous formation of radicals, evidenced by electron spin resonance (ESR) spectroscopy, only occurred when dithiol were mixed with diene. Hence, the authors attribute the appearance of radicals to the formation of a charge transfer complex between thiol and ene monomers, followed by an electron transfer with the formation of a thiyl radical. Another possible self-initiated mechanism responsible for premature polymerization is the production of thiyl radicals from the thiol-oxidation by molecular oxygen.[47,49,50] Kharasch *et al.*[49] postulated in 1950 that mercaptan could yield to thiyl free radicals by the attack of an oxidant upon the thiol moiety in presence of oxygen. In a more recent contribution, Bagiyan *et al.*[50] reported that the self-oxidation of thiol compounds by molecular oxygen in aqueous solutions is induced by the presence of catalytically active impurities of variable-valence metals that generate thiyl radicals in neutral and alkaline solutions. In the recent work of Le *et al.*[47], it is shown that the thiol oxidation by molecular oxygen plays a leading role in the premature polymerization of the studied systems by creating thiyl radicals that set up the radical mediated step growth polymerization. The nature of the initiating radicals was confirmed by ESR spin-trapping analysis. It appears that the main driving force of thiol air oxidation is the polarization of the S-H bond. Finally, another mechanism that could explain the premature polymerization

in thiol-ene system would be the homolytic cleavage of the S-H bond. Thiols are indeed very good hydrogen donor because of the low dissociation energy of the sulphur-hydrogen bond[51,52]. Depending on the reaction conditions, thiols can undergo heterolytic or homolytic dissociation[39], leading to the formation of sulfur centred ion or radical[53]. This mechanism as a possible route to premature initiator-free thiol-ene polymerization has not been demonstrated, yet.

1.3. Thiol-ene photopolymerization in miniemulsion

Thiol-ene polymerization in miniemulsion is a privileged mean to obtain high sulfur content products with controlled colloidal properties and architecture. In this process, after mixing the hydrophobic thiol-ene monomers with water and formation of coarse emulsion, small monomer droplets are formed in aqueous continuous phase by high-efficient homogenization device.[1] The small monomer droplets are stabilized against diffusional degradation (Ostwald ripening) and droplet coagulation by using respectively a costabilizer and a surfactant.[1,3,54] The key feature of miniemulsion polymerization compared to conventional emulsion polymerization is that no transfer of the monomer through the aqueous phase is required to perform the polymerization, as the monomer droplets are nucleated to form particles and turn to be the loci of the reaction, acting as nanoreactors. This feature is particularly suited for thiol-ene step-growth polymerization, in which a 1:1 ratio between the ene and thiol functionalities is essential to obtain sufficiently high molar mass polymer. Otherwise, according to the individual water solubility of both thiols and enes, each of them will diffuse towards the water phase, creating stoichiometric imbalance. In addition, miniemulsions are submicron

dispersions, with an average droplet diameter ranging between 50-500nm. In the case of photoinitiated polymerization, working with small size droplets the light scattering is lower, thus, it provides improved light penetration.[55]

In 2014, Lobry *et al*[56] reported for the first time the synthesis of thiol-ene nanoparticles by photopolymerization in a continuous microreactor. A 15% solids content poly(thioether) dispersion based on the bifunctional monomers diallyl adipate (DAA) and ethylene glycol dithiol (EGDT) was prepared with a molar mass above 105 kDa and a polydispersity of 3.5. In addition, the polymer presented a relatively high degree of crystallinity (55%), attributed to the linearity of its chemical structure, more likely to organize into ordered patterns, and interactions between ester and thioether groups. DSC analysis revealed that the materials presented a low T_g of -63ºC, and that the crystals melt at 18ºC. The use of microreactor, however, displays some limitation as only small-scale production is permitted.

In another work, crosslinked poly(thioether) particles were produced by photopolymerization in miniemulsion of the trifunctional monomers 1,3,5-triallyl-1,3,5-triazine-2,4,6 (1H, 3H, 5H) trione (TTT) and pentaerythritol tetra(3-mercaptopropionate) (PETMP)[18]. The particles, produced with excess of thiol moieties, could further capture fluorescent agent via post-polymerization modification. Although the synthesis of crosslinked thiol-ene particles deviates from our objective, this work is important because of the introduction of a radical inhibitor into the formulation to preclude thiol-ene premature polymerization, especially during the miniemulsification step. Namely during this step by sonication, as high energy is provided to the system to break the large monomer droplets,

premature polymerization led to high monomer conversion. Amato et al. in this work reported that without radical inhibitor 4-p-methoxy phenol (MEHQ), or when the latter is used at too low concentration, the thiol-ene system undergoes a sonopolymerization process during miniemulsification, which could be followed by proton nuclear magnetic resonance (^{1}H NMR). This result is supported by the work of Skinner *et al.*[57], in which thiol-ene coupling reaction between 1-butanethiol or cysteamine hydrochloride with a number of monofunctional alkenes could be initiated by generating radicals through sonication. In addition, the authors report that sonochemical initiation was particularly efficient when performed in water compared to the organic solvent butanol, as hydroxyl radicals can be generated. As explained previously in the case of thiol-ene polymerization, hydroxyl radical can initiate thiol-ene coupling reaction by abstraction of the hydrogen of the thiol moiety.

Following these works, Le *et al.*[21] prepared linear poly(thioethers) based on diallyl phthalate (DAP), 2,2-(ethylenedioxy)diethanedithiol (EDDT), 1,6-hexanedithiol (HMDT) and 2,2′-thiodiethanethiol (DMDS) by photopolymerization in miniemulsion. To prevent premature polymerization, the radical inhibitors 2,5-di-tert-butylhydroquinone (DBHQ) and pyrogallol (PYR) were employed. This work, for the first time, gives an insight on the miniemulsion polymerization process in the case of step-grown poly(thioethers), with a special emphasis on nucleation mechanism. Indeed, attention was turned toward determining the reaction conditions to promote droplet nucleation, and the effect of initiator and monomers solubility and droplet size were studied. They reported that the use of the water-soluble photoinitiator lithium phenyl(2,4,6-tri- methylbenzoyl)phosphinate (TPO-Li) promoted –unfavourable- homogeneous nucleation.[58] In this nucleation mechanism, common for emulsion polymerization, but also

observed in miniemulsion, radicals are formed in the aqueous phase and initiate polymerization of monomers also dissolved in the aqueous phase, yielding to oligoradicals. Once the oligoradicals reach a critical length and become too hydrophobic, they precipitate and are stabilized by the surfactant present in the aqueous phase. Polymerization continues by diffusion of monomers from large monomer droplet present in the emulsion.[1] When using the water-soluble photoinitiator, homogeneous nucleation occurred independently on monomer solubility, but was affected by droplet size. Indeed, when droplet size was low enough (100nm and below), droplet nucleation was prevalent, probably due to large surface area offered by so small droplets for oligoradicals to enter into the particles instead of precipitation in aqueous phase. Nevertheless, the use of the oil soluble photoinitiator turned out to be the more efficient way to promote droplet nucleation.

In the recent contribution of Teixeira *et al.*[22], the authors studied thiol-ene photopolymerization reaction of the monomers DAA as the diene, and EDDT, and compared kinetics and polymer molecular weight in bulk and miniemulsion. Polymerization rate was higher when thiol-ene reaction was performed in miniemulsion than in bulk, which was attributed to the radicals' confinement effect. For the same reason, higher conversions were reached in miniemulsion, generating polymers with higher molecular weight (approximately 19kDa) than in bulk (approximately 12.5 kDa). It is explained that radical compartmentalisation in the miniemulsion process promotes the obtainment of such high molecular weight polymers: the propagating radicals, isolated in the droplet loci, are less likely to terminate by recombination. Similar observations were reported by Jasinski *et al.*[19], who also obtained substantially higher molar masses (with a molar mass of 54.3 kDa and PDI of 2.7) in thiol-ene

miniemulsion photopolymerization of EDDT and DAP, than in bulk and solution (with a molar mass of 36 kDa and PDI of 3.1 and a molar mass of 23.6kDa and PDI 2.1 in bulk and solution respectively). In addition, Teixeira *et al.*[22] also studied the effect of photoinitiator concentration, stoichiometric ratio between thiol and ene functionalities on the final polymer properties and kinetics. In all cases, photopolymerization in miniemulsion turned out to be more beneficial to obtain fast kinetics and high molar mass poly(thioethers).

In the literature, few works deal with the synthesis of thiol-ene polymer dispersions, also called latexes, with an intended application in waterborne coatings and crystallization. Noteworthy, Jasinski *et al.*[20] reported the synthesis of linear poly(thioether ester) particles with film forming ability by photopolymerization in miniemulsion. The linear chains, based on the bifunctional monomers DAA and EGDT present a low T_g of -63ºC and yield an elastomeric film after water evaporation at room temperature. The semicystalline behaviour of the latter was evidenced by DSC analysis, with a melting point at 18ºC and recrystallization peak at 6ºC, and the degree of crystallinity of the materials was 55%, as reported previously by Lobri *et al*[56] for the same polymer obtained via continuous photopolymerization. However, despite the low solids content of the final dispersions that lack practical significance, the authors acknowledged the restraint utility of such film, due to the low melting point leading to poor mechanical properties. To stiffen significantly the final films for targeted coating applications, rigid polymer chains are required, which on the other hand, may affect the complex process of film formation.

Introducing aromatic units in the polymer backbone is one of the strategies to stiffen significantly the final films obtained from thiol-ene aqueous dispersions. In another

contribution, Jasinski *et al.* synthesized a film-forming poly(thioether) latex based on the monomers DAP and EGDT.[19] Introducing a rigid aromatic ring into the polymer building block resulted in increased T_g of -42ºC due to the less flexible and mobile chains. As a consequence of the enhanced rigidity, the organization into crystalline domains was prevented and no melting point was observed by DSC analysis.

1.4. Film formation from waterborne polymer dispersions

The latex film formation is the process to obtain a coherent continuous film after water evaporation from the polymer dispersion (i.e. latex).[59]

The latex film formation can be divided in three steps,[59] as schematically presented in Figure 1.2.

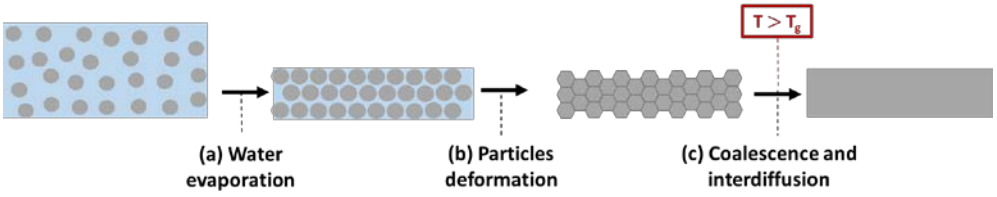

Figure1.2. Film formation process[59]

After casting the dispersion, the first step is the water evaporation, leading to the ordering of polymer particles and close packaging. In the second step, the interstitial water remaining in-between polymer particles disappears, allowing their deformation into a tetrahedral or honeycomb like shape. At this stage, the polymer particles integrity remains intact and the

"pre-film" becomes optically clear as only one phase is present. The last step involves particle coalescence and subsequent interdiffusion of polymer chains across particle interfaces to fuse the particles boundaries. This last step is of primary importance when it comes to mechanical properties, usually required for coating applications and subsequent testing. Interdiffusion of polymer chains occurs at temperature above their T_g and is driven by Brownian motion. Indeed, obtaining of continuous coating films through film formation process from waterborne dispersions is very challenging, as each step affects drastically the final film morphology and therefore its properties. Good cohesion of a latex film is achieved when polymer particles deformed sufficiently and polymer chains from different particles have interdiffused between them and created entanglements. For this, it is important that the T_g of the polymer is lower than the film forming temperature (lower than ambient temperature if the films should be formed at ambient conditions). On the other hand, too low T_g may result in very soft polymer film that does not respond to the minimum requirements of mechanical resistance. These two contradictory requirements are the main challenges of the film forming ability of polymer latex, especially when good mechanical properties are expected for targeted applications, such as barrier coating.

1.5. Study on polymer crystallization

In the case of newly synthesized material or polymers that need to respond to specific application, a deep understanding of their behaviour is required to grasp and reach their full potential. It is well known that the crystallization behaviour of semi-crystalline polymers is directly related to the final properties of the material. Therefore, thermal properties with a

special emphasis on crystallization behaviour are being explored in this work, by the mean of advanced DSC techniques, X-ray diffraction and microscopy technique. It is important to note that this section does not provide an exhaustive list of crystallization concepts that can be used to study crystallization kinetics, and is restricted to the one that were used in this work.

1.5.1. Crystallization theories

The crystallization of polymers is attributed to their ability to organise into ordered arrangement, typically chains parallel to each other. Polymers always display a semi-crystalline behaviour, with crystalline and amorphous (unordered) regions, as they never crystallize 100%.[42,60] As an attempt to describe the nature of polymer crystallinity, two main theories were developed: the fringed micelle theory and the chain folded theory.

In the fringed micelle theory,[42,60,61] also called the micellar theory, one polymer chain can be constituted of a series of amorphous and crystalline portions randomly distributed. In this theory, crystalline regions are composed of different polymer chains aligned in parallel as depicted in Figure1.3 and are linked by amorphous areas. Therefore, one polymer chain pass through several different crystalline and amorphous regions.

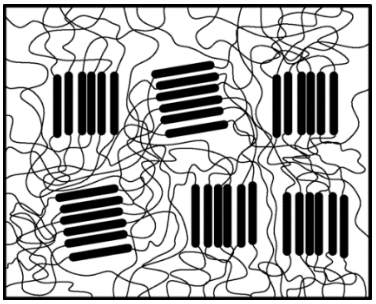

Figure 1.3. Fringed micelle theory [62]. Reproduced with permission from American Physical Society.

In the chain folded theory,[42,60,61] crystalline structures are composted of folded chains forming lamella, with the chain direction perpendicular to the lamellar surface. Two main models emerged from this theory. In the first one, known as the adjacent re-entry model and schematically presented in Figure 1.4.a, chains come back and forth into the lamella forming loops with equal length at the lamellar surface. The other concept, the "switchboard model" can be described as an irregular version of the re-entry model. As seen in Figure 1.4.b chains come back and forth into the lamella and loops with different length are formed. The pendant chains can enter into a neighbouring lamella[62].

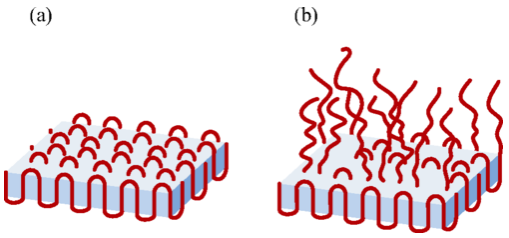

Figure 1.4. Chain folded theory with the (a) adjacent re-entry and (b) switchboard models [62] Reproduced with permission from American Physical Society.

Typically, two spontaneous mode of crystallization are observed: crystallization from the melt and crystallization from solution. In this work, crystallization was performed from the melt. With this mode, crystals grow as spherical units, termed spherulites, and the chain folded theory is used to describe this morphology.[42] With this theory, the presence of amorphous phases consists of defects in the chain folding structure, which excludes some polymer chains from the ingrowing crystal.

1.5.2. Crystallization process

The process of crystallization of polymer chains, or their ordering into crystalline structures, can be divided in two mains steps: the primary and secondary crystallization[63].

Namely, the first step of the crystallization, denoted as primary crystallization, is the process in which crystalline structures are formed from isotropic melt and grow until they impinge on each other. It can be subdivided in two different steps: nucleation and crystal growth. The nucleation consists in the formation of nuclei, typically from existing heterogeneities (heterogeneous nucleation) or spontaneous aggregation of polymer chain segments

(homogeneous nucleation), that will act as the starting point of the subsequent crystal growth. Nucleation occurs at various nuclei, and crystals grow until they impinge on one another, which marks the end of primary crystallization. The subsequent step, also called secondary crystallization implies several complex phenomena, such as the thickening of existing crystals.

1.6. Crystallization concepts implemented

1.6.1. Isothermal crystallization

This section is devoted to explain the methodology that was followed to study the overall crystallization kinetics of the poly(thioethers) that were investigated in this work, and to give a practical approach on how to measure it experimentally.

The typical procedure to study crystallization kinetics is to rapidly quench the sample from its molten state to a certain temperature, which we shall name crystallization temperature (T_c) and monitor the formation of crystals at this temperature. This procedure is called isothermal crystallization. In this work, the nucleation and growth of crystals were followed under optical microscope or by the mean of DSC. For the latter, the isothermal crystallization methodology is described below.

In a first step, the minimum isothermal crystallization temperature ($T_{c,min}$), at which the material can be rapidly cooled down without crystallizing, has to be determined. Indeed, precluding crystallization during the cooling step, preceding isothermal crystallization is of primary importance to be able to determine the overall crystallization rate isothermally. To do so, Lorenzo *et al.*[64] propose the following DSC protocol: first, the polymer sample is heated 30ºC

above its melting temperatures to erase thermal history, and rapidly cooled at a selected rate (which will be used in the conventional isothermal experiment) to the temperature T_c to be tested. Generally, the chosen T_c is estimated from a previous non-isothermal DSC experiment, and is the temperature at which the polymer starts to crystallize under cooling[63]. Once the sample reaches the selected T_c, it is directly heated up. $T_{c,min}$ is the minimum temperature for which no melting peak is observed in the latter heating scan, attesting that no crystals were formed during the cooling scan to T_c.

Once $T_{c,min}$ is determined, one can perform the conventional isothermal protocol. First, the polymer sample is heated to its molten state at and kept long enough at this temperature to erase thermal history. Then, the sample is rapidly cooled down to a range of crystallization temperatures T_c with $T_c \geq T_{c,min}$, and kept at this temperature for some time allowing the monitoring of crystal growth. In the last step, the sample is heated up to record the melting of the crystals formed isothermally. The schematic presentation of isothermal thermal procedure is depicted in Figure 1.5.

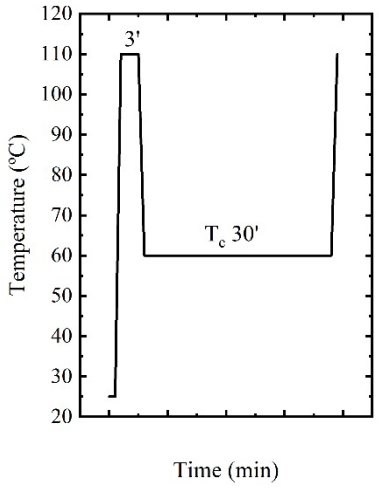

Figure 1.5. Schematic representation of an isothermal experiment, with heating rate of 20ºC/min and cooling rate of 60ºC/min

Once the isothermal crystallization experimental data are obtained, they can be fitted to the Avrami equation from the Avrami theory, which is used to analyse the bulk growth.[42,61,64,65] Lorenzo *et al.*[64] developed an Origins application software, designed to analyze the DSC isotherms, which is a straightforward tool to obtain the values of interest, such as the experimental half-crystallization time ($\tau_{50\%,exp}$), the Avrami index (n), the induction time (t_0) and the correlation coefficient R^2 (that should be 0.9990 or larger[64]).

The first parameter to consider is the induction time (t_0), which is the time required to form stable nuclei. The inverse of the induction time give us information about the nucleation rate[66]. Another data that can be deduced from Avrami fitting is the measured half-crystallization

time $\tau_{50\%,exp}$. The inverse of the half–crystallization time provides an experimental measure of the overall crystallization rate (which includes both nucleation and growth)[66].

Finally, the Avrami index obtained from the fitting gives an additional indication of the morphology of the crystals that are formed isothermally[66].

Crystallization rate can also be monitored under PLOM, as stated previously. The sample thermal treatment is the same that the one used for DSC (Figure 1.5). Typically, the radii of spherulites is measured over time, which gives an accurate growth rate value. However, compared to the DSC procedure, determining crystallization kinetics by PLOM can be more time-consuming, and not applicable for polymers with high nucleation densities, as spherulites rapidly impinged on each other.[65]

1.6.2. Self-nucleation process

The self-nucleation (SN) procedure arises from the melt memory effect, which accelerates the polymer's crystallization kinetics by the presence of nuclei or a "memory" from a previous crystalline state that was not erased thermally.[67] As already stated, this thermal history can be erased by heating the sample up to a temperature high enough to yield an isotropic melt. When the polymer is recrystallized from this temperature and above, the overall crystallization kinetics remain unchanged. Nucleation can occur by aggregation of polymer chains, but mostly occurs from thermally resistant heterogeneities that are present in the sample,[61] followed by crystal growth.

If the polymer sample is heated to lower temperature, some "memory" from the previous crystalline state subsists, and influences the polymer crystalline kinetics. This melt-memory effect can be studied by performing SN experiments. Indeed, SN procedure is a thermal protocol in which self-nuclei are generated within the material at a selected self-nucleation temperature (T_s).[67–72] It was first reported by Keller *et al.*[73], and was further implemented through DSC analysis by Fillon *et al.*[71] SN allows control of the nucleation step, preceding the crystal growth. This step is substantially sped up when polymer chains nucleate on pre-existing surfaces, in our case self-seed or self-nuclei which are the best nucleating agent for the polymers. Nucleation density is greatly increased and the overall crystallization kinetics are sped up.[72] Therefore, SN strategy can be used for studying the kinetics of slow-crystallization material, in which isothermal crystallization experiments are made difficult because of extended time frame.[68] By performing a SN procedure previous to isothermal crystallization analysis, nucleation step is substantially step up and crystal growth can be monitored isothermally.

In this work, the SN procedure was mainly implement through DSC technique, and the typical thermal treatment is shown in Figure 1.6.[67]

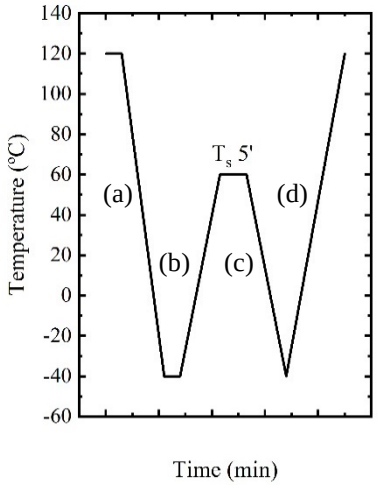

Figure 1.6. Typical SN thermal treatment[67,68]

In a first step (a) Figure 1.6, the sample is heated up to a temperature high enough (at least 30ºC above its melting temperature) and kept sufficient time (at least 3 minutes) to erase any thermal history and yield to an isotropic melt. In the subsequent step (b), the sample is cooled, typically at a rate of 10ºC/min or 20ºC/min, to a temperature low enough to allow the crystallization of the material until saturation. In this step, a standard thermal history is set up, and the crystallization peak observed in the DSC heating scan is denoted as the standard crystallization temperature (T_c). The sample is then heated to a selected T_s (Figure 1.6 step (b)), and kept 5 minutes at this temperature. During this thermal conditioning, the samples can melt, self-nucleate, or self-nucleate and anneal. In the following cooling step (Figure 1.6 step (c)), the DSC cooling scan is recorded to observe the sample recrystallization. Finally, the melting of the crystals is monitored in the last heating scan (Figure 1.6 step (d)).

To study the melt-memory effect, Fillon *et al.*[71] described three SN *Domains* that can be deduced from the DSC traces of steps (c) and (d). Figure 1.7 schematically illustrates the polymer chain at a molecular level in each SN *Domain.* These *Domains* are defined as below:

- *Domain I* which occurs for T_s well above the melting temperature (T_m) of the polymer. In this domain, the polymer is completely melted in step (b) (Figure 1.6). The thermal history and memory effect induced by previous crystallization are erased, and the crystallization temperatures (T_c) obtained upon cooling in step (c) (Figure 1.6) are constant: the overall crystallization kinetics do not depend on T_s, and nucleation step occurs spontaneously. At a molecular level, the polymer chain adopts an isotropic random coil conformation (Figure 1.7)
- *Domain II*, or self-nucleation *Domain*, in which the range of T_s is high enough to melt most of the crystals and low enough to intentionally produce self-nuclei from the melt memory effect. Indeed, these self-nuclei results from some residual segmental orientation (Figure 1.7) that was not be erased thermally during step (b) (Figure 1.6), and provide a perfect lattice for the subsequent crystal growth. They increase greatly the nucleation density and crystallization kinetics, which is reflected by a recrystallization peak shifted to higher temperatures.[67,68,71]
- *Domain III*, or self-nucleation and annealing domain, in which the range of T_s is lower than in *Domain II*, so that crystal fragments remain unmolten and are annealed for 5 minutes (Figure 1.7). Therefore, *Domain III* can be differentiated from *Domain II* by the presence of annealing traces in the final heating scan of the experiment. In

this domain too, nucleation density is increased leading to faster crystallization kinetics.

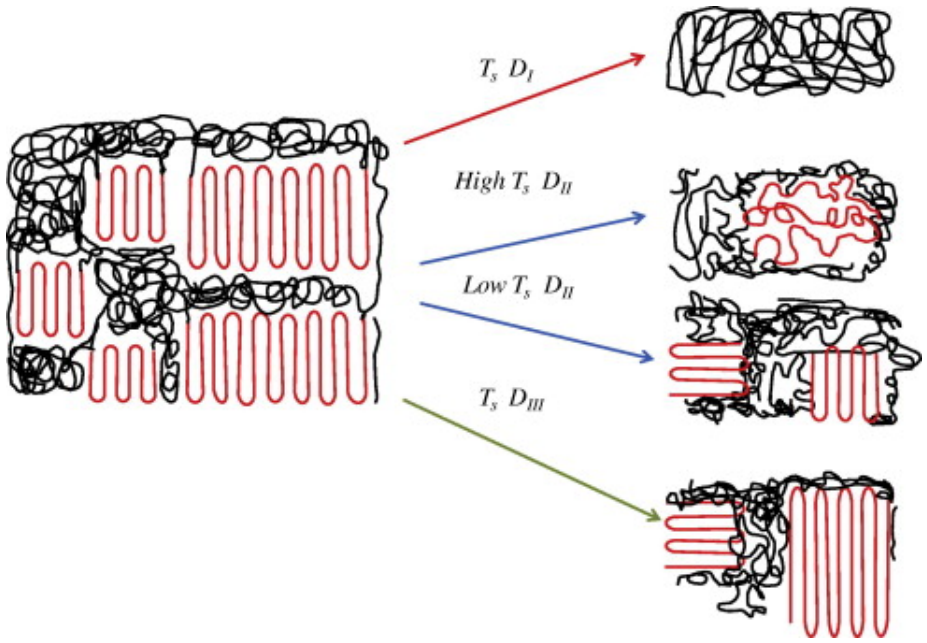

Figure 1.7. Schematic molecular representation of the different self-nucleation Domains[69]. Reproduced with permission from Elsevier.

In this work, SN strategy was used as a tool to speed up crystallization kinetics of slow crystallizing material, but also to evaluate the melt-memory effect of poly(thioethers) varying in chemical structure, as studied by Sangroniz *et al.*[72] for polycarbonate, polyesters, polyethers, and polyamides.

1.7. Thesis outline

The main aims of this thesis are the synthesis of novel film forming semi-crystalline poly(thioethers) by employing photopolymerization in dispersed media technique, and the study of their crystalline behaviour to develop application possibilities as waterborne barrier coatings for food packaging. In addition, the possibility to carry out polymerization in dispersed system to yield biobased polymer dispersions and coatings has been implemented, with an aimed application in decorative coating.

This thesis is subdivided into seven Chapters. **Chapter 1** provides a general introduction with the main objectives of the work. In this chapter, a literature review on thiol-ene chemistry and on thiol-ene (photo)polymerization in miniemulsion with a special emphasis on waterborne coatings is proposed. The general crystallization concepts employed in this work (namely crystallization kinetics by isothermal crystallization experiments and SN concept) are described.

In **Chapter 2**, the challenges of thiol-ene chemistry in polymer synthesis are addressed. The effect of photoinitiator concentration, reaction time, stoichiometric balance between thiol and ene functionality on the final poly(thioethers) were investigated. The chemical instability is also addressed, and strategies to overcome it are proposed.

Chapter 3 is devoted to the synthesis of waterborne thiol-ene polymer dispersions. In this work, a novel synthesis approach of high solids content film forming waterborne poly(thioether) polymers, based on initiator-free step-growth sonopolymerization and photopolymerization is reported.

In **Chapter 4**, the crystalline behaviour of the film-forming poly(thioethers) synthesized in Chapter 3 is investigated, by the mean of advanced DSC analysis and X-ray diffraction. Self-nucleation experiments

In **Chapter 5**, a study of other linear poly(thioethers) crystallization behaviour is proposed. These poly(thioethers), although not film forming, present interesting crystalline features that are being studied by DSC, Wide-angle X-ray diffraction, and optical microscope. An insight on crystalline kinetics is presented, with the concepts of SN and isothermal crystallization.

In **Chapter 6** newly synthesized biobased monomers were implemented in bulk or miniemulsion thiol-ene photopolymerization. The resulting polymer dispersions yielded to consistent films after water evaporation, with an aimed application in decorative coatings. Coating properties were studied for that aim.

Finally, **Chapter 7** summarizes the main conclusions of the thesis.

1.8. References

(1) Asua, J. M. Miniemulsion Polymerization. *Prog. Polym. Sci.* **2002**, *27* (7), 1283–1346. https://doi.org/10.1016/S0079-6700(02)00010-2.

(2) Asua, J. M. Emulsion Polymerization: From Fundamental Mechanisms to Process Developments. *J. Polym. Sci. Part A Polym. Chem.* **2004**, *42* (5), 1025–1041. https://doi.org/10.1002/pola.11096.

(3) Asua, J. M. Challenges for Industrialization of Miniemulsion Polymerization. *Prog. Polym. Sci.* **2014**, *39* (10), 1797–1826. https://doi.org/10.1016/j.progpolymsci.2014.02.009.

(4) Taylor, M. A. Synthesis of Polymer Dispersions. *Polym. Dispersions Their Ind. Appl.* **2002**, *7*, 15–40. https://doi.org/10.1002/3527600582.ch2.

(5) Alduncin, J. A.; Forcada, J.; José, A. Miniemulsion Polymerization Using Oil-Soluble Initiators. *Macromolecules* **1994**, *27* (8), 2256–2261. https://doi.org/10.1021/ma00086a041.

(6) Wang, S.; Schork, F. J. Miniemulsion Polymerization of Vinyl Acetate with Nonionic Surfactant. *J. Appl. Polym. Sci.* **1994**, *54* (13), 2157–2164. https://doi.org/10.1002/app.1994.070541318.

(7) Huang, H.; Zhang, H.; Hu, F.; Ai, Z.; Tan, B.; Cheng, S.; Li, J. Miniemulsion Copolymerization of Styrene and Butyl Acrylate Initiated by Redox System at Lower Temperature: Reaction Kinetics and Evolution of Particle-Size Distribution. *J. Appl. Polym. Sci.* **1999**, *73* (3), 315–322. https://doi.org/10.1002/(SICI)1097-4628(19990718)73:3<315::AID-APP2>3.0.CO;2-4.

(8) Jasinski, F.; Zetterlund, P. B.; Braun, A. M.; Chemtob, A. Photopolymerization in Dispersed Systems. *Prog. Polym. Sci.* **2018**, *84*, 47–88. https://doi.org/10.1016/j.progpolymsci.2018.06.006.

(9) Daniloska, V.; Tomovska, R.; Asua, J. M. Hybrid Miniemulsion Photopolymerization in a Continuous Tubular Reactor-A Way to Expand the Characteristics of Polyurethane/Acrylics. *Chem. Eng. J.* **2012**, *184*, 308–314. https://doi.org/10.1016/j.cej.2012.01.040.

(10) Daniloska, V.; Tomovska, R.; Asua, J. M. Designing Tubular Reactors to Avoid Clogging in High Solids Miniemulsion Photopolymerization. *Chem. Eng. J.* **2013**, *222*, 136–141. https://doi.org/10.1016/j.cej.2013.02.015.

(11) Daniloska, V.; Carretero, P.; Tomovska, R.; Asua, J. M. High Performance Pressure Sensitive Adhesives by Miniemulsion Photopolymerization in a Continuous Tubular Reactor. *Polymer (Guildf).* **2014**, *55* (20), 5050–5056. https://doi.org/10.1016/j.polymer.2014.08.038.

(12) Resetco, C.; Hendriks, B.; Badi, N.; Du Prez, F. Thiol-Ene Chemistry for Polymer Coatings and Surface Modification-Building in Sustainability and Performance. *Mater. Horizons* **2017**, *4* (6), 1041–1053. https://doi.org/10.1039/c7mh00488e.

(13) Hoyle, C. E.; Lee, T. Y.; Roper, T. Thiol-Enes: Chemistry of the Past with Promise for the Future. *J. Polym. Sci. Part A Polym. Chem.* **2004**, *42* (21), 5301–5338. https://doi.org/10.1002/pola.20366.

(14) Wutticharoenwong, K.; Soucek, M. D. Influence of the Thiol Structure on the Kinetics of Thiol-Ene Photopolymerization with Time-Resolved Infrared Spectroscopy. *Macromol. Mater. Eng.* **2008**, *293* (1), 45–56. https://doi.org/10.1002/mame.200700175.

(15) Li, Q.; Zhou, H.; Hoyle, C. E. The Effect of Thiol and Ene Structures on Thiol-Ene Networks: Photopolymerization, Physical, Mechanical and Optical Properties. *Polymer (Guildf).* **2009**, *50* (10), 2237–2245. https://doi.org/10.1016/j.polymer.2009.03.026.

(16) Durham, O. Z.; Chapman, D. V.; Krishnan, S.; Shipp, D. A. Radical Mediated Thiol-Ene Emulsion Polymerizations. *Macromolecules* **2017**, *50* (3), 775–783. https://doi.org/10.1021/acs.macromol.6b02228.

(17) Quoc Le, C. M.; Schmutz, M.; Chemtob, A. Ab Initio Batch Emulsion Thiol–Ene Photopolymerization. *Macromolecules* **2020**. https://doi.org/10.1021/acs.macromol.0c00265.

(18) Amato, D. V.; Amato, D. N.; Flynt, A. S.; Patton, D. L. Functional, Sub-100 Nm Polymer Nanoparticles via Thiol-Ene Miniemulsion Photopolymerization. *Polym. Chem.* **2015**, *6* (31), 5625–5632. https://doi.org/10.1039/c4py01449a.

(19) Jasinski, F.; Rannée, A.; Schweitzer, J.; Fischer, D.; Lobry, E.; Croutxé-Barghorn, C.; Schmutz, M.; Le Nouen, D.; Criqui, A.; Chemtob, A. Thiol-Ene Linear Step-Growth Photopolymerization in Miniemulsion: Fast Rates, Redox-Responsive Particles, and Semicrystalline Films. *Macromolecules* **2016**, *49* (4), 1143–1153. https://doi.org/10.1021/acs.macromol.5b02512.

(20) Jasinski, F.; Lobry, E.; Tarablsi, B.; Chemtob, A.; Croutxé-Barghorn, C.; Nouen, D. Le; Criqui, A. Light-Mediated Thiol-Ene Polymerization in Miniemulsion: A Fast Route to Semicrystalline Polysul Fide Nanoparticles. *ACS Macro Lett.* **2014**, *3* (9), 958–962. https://doi.org/10.1021/mz500458s.

(21) Le, C. M. Q.; Vidal, L.; Schmutz, M.; Chemtob, A. Droplet Nucleation in Miniemulsion Thiol-Ene Step Photopolymerization. *Polym. Chem.* **2021**, *12* (14), 2084–2094. https://doi.org/10.1039/d1py00139f.

(22) Infante Teixeira, L.; Landfester, K.; Thérien-Aubin, H. Nanoconfinement in Miniemulsion Increases Reaction Rates of Thiol-Ene Photopolymerization and Yields High Molecular Weight Polymers. *Polym. Chem.* **2022**, 2831–2841. https://doi.org/10.1039/d2py00350c.

(23) Walley, S. E. Synthesis of Polythioether Nanoparticles via Thiol- Alkene / Alkyne Photopolymerization in Miniemulsion. **2017**, 34.

(24) Machado, T. O.; Cardoso, P. B.; Feuser, P. E.; Sayer, C.; Araújo, P. H. H. Thiol-Ene Miniemulsion Polymerization of a Biobased Monomer for Biomedical Applications. *Colloids Surfaces B Biointerfaces* **2017**, *159*, 509–517. https://doi.org/10.1016/j.colsurfb.2017.07.043.

(25) Infante Teixeira, L.; Landfester, K.; Thérien-Aubin, H. Selective Oxidation of Polysulfide Latexes to Produce Polysulfoxide and Polysulfone in a Waterborne Environment. *Macromolecules* **2021**, *54* (8), 3659–3667. https://doi.org/10.1021/acs.macromol.1c00382.

(26) Durham, O. Z.; Shipp, D. A. Suspension Thiol-Ene Photopolymerization: Effect of Stabilizing Agents on Particle Size and Stability. *Polymer (Guildf).* **2014**, *55* (7), 1674–1680. https://doi.org/10.1016/j.polymer.2014.02.044.

(27) Posner, T. Beiträge Zur Kenntniss Der Ungesättigten Verbindungen. II. Ueber Die Addition von Mercaptanen an Ungesättigte Kohlenwasserstoffe. *Berichte der Dtsch. Chem. Gesellschaft* **1905**, *38* (1), 646–657. https://doi.org/10.1002/cber.190503801106.

(28) Lowe, A. B. Thiol-Ene "Click" Reactions and Recent Applications in Polymer and Materials Synthesis: A First Update. *Polym. Chem.* **2014**, *5* (17), 4820–4870. https://doi.org/10.1039/c4py00339j.

(29) Lowe, A. B. Thiol-Ene "Click" Reactions and Recent Applications in Polymer and Materials Synthesis. *Polym. Chem.* **2010**, *1* (1), 17–36. https://doi.org/10.1039/b9py00216b.

(30) Machado, T. O.; Sayer, C.; Araujo, P. H. H. Thiol-Ene Polymerisation: A Promising Technique to Obtain Novel Biomaterials. *Eur. Polym. J.* **2017**, *86*, 200–215. https://doi.org/10.1016/j.eurpolymj.2016.02.025.

(31) Hoyle, C. E.; Lowe, A. B.; Bowman, C. N. Thiol-Click Chemistry: A Multifaceted Toolbox for Small Molecule and Polymer Synthesis. *Chem. Soc. Rev.* **2010**, *39* (4), 1355–1387. https://doi.org/10.1039/b901979k.

(32) Hoyle, C. E.; Bowman, C. N. Thiol-Ene Click Chemistry. *Angew. Chemie - Int. Ed.* **2010**, *49* (9), 1540–1573. https://doi.org/10.1002/anie.200903924.

(33) Cook, W. D.; Chen, F.; Pattison, D. W.; Hopson, P.; Beaujon, M. Thermal Polymerization of Thiol–ene Network-Forming Systems. *Polym Int* **2007**, *56*, 1572–1579. https://doi.org/10.1002/pi.

(34) dos Santos, P. C. M.; Machado, T. O.; Santin, J. V. C.; Feuser, P. E.; Córneo, E. S.; Machado-de-Ávila, R. A.; Sayer, C.; de Araújo, P. H. H. Superparamagnetic Biobased Poly(Thioether-Ester) via Thiol-Ene Polymerization in Miniemulsion for Hyperthermia. *J. Appl. Polym. Sci.* **2021**, *138* (4), 1–10. https://doi.org/10.1002/app.49741.

(35) Lillie, L. M.; Tolman, W. B.; Reineke, T. M. Degradable and Renewably-Sourced Poly(Ester-Thioethers) by Photo-Initiated Thiol-Ene Polymerization. *Polym. Chem.* **2018**, *9* (23), 3272–3278. https://doi.org/10.1039/c8py00502h.

(36) Cramer, N. B.; Bowman, C. N. Kinetics of Thiol-Ene and Thiol-Acrylate Photopolymerizations with Real-Time Fourier Transform Infrared. *J. Polym. Sci. Part A Polym. Chem.* **2001**, *39* (19), 3311–3319. https://doi.org/10.1002/pola.1314.

(37) Cramer, N. B.; Reddy, S. K.; O'Brien, A. K.; Bowman, C. N. Thiol - Ene Photopolymerization Mechanism and Rate Limiting Step Changes for Various Vinyl Functional Group Chemistries. *Macromolecules* **2003**, *36* (21), 7964–7969. https://doi.org/10.1021/ma034667s.

(38) Cramer, N. B.; Davies, T.; O'Brien, A. K.; Bowman, C. N. Mechanism and Modeling of a Thiol-Ene Photopolymerization. *Macromolecules* **2003**, *36* (12), 4631–4636. https://doi.org/10.1021/ma034072x.

(39) Mutlu, H.; Ceper, E. B.; Li, X.; Yang, J.; Dong, W.; Ozmen, M. M.; Theato, P. Sulfur Chemistry in Polymer and Materials Science. *Macromol. Rapid Commun.* **2019**, *40* (1), 1–51. https://doi.org/10.1002/marc.201800650.

(40) Kolb, H. C.; Finn, M. G.; Sharpless, K. B. Click Chemistry: Diverse Chemical Function from a Few Good Reactions. *Angew. Chemie - Int. Ed.* **2001**, *40* (11), 2004–2021. https://doi.org/10.1002/1521-3773(20010601)40:11<2004::AID-ANIE2004>3.0.CO;2-5.

(41) Cramer, N. B.; Bowman, C. N. CHAPTER 1. Thiol-ene and Thiol-yne Chemistry in Ideal Network Synthesis. **2013**, No. 6, 1–27. https://doi.org/10.1039/9781849736961-00001.

(42) Odian, G. *Principles of Polymerization*, 4th ed.; Sons., J. W. &, Ed.; 2004.

(43) Esfandiari, P.; Ligon, S. C.; Lagref, J. J.; Frantz, R.; Cherkaoui, Z.; Liska, R. Efficient Stabilization of Thiol-Ene Formulations in Radical Photopolymerization. *J. Polym. Sci. Part A Polym. Chem.* **2013**, *51* (20), 4261–4266. https://doi.org/10.1002/pola.26848.

(44) Sensfua, S.; Friedrich, M.; Kiemm, E. Untersuchungen Zur ThioVEn-Polymerisation: **1991**, *2900*, 2895–2900.

(45) Klemm, E.; Sensfuß, S.; Holfter, U.; Flammersheim, H. J. Free-Radical Stabilizers for the Thiol/Ene-systems. *Die Angew. Makromol. Chemie* **1993**, *212* (1), 121–127. https://doi.org/10.1002/apmc.1993.052120111.

(46) Klemm, E.; St. Sensfuß. Untersuchungen Zum Selbstinitiierungs-Mechanismus Der Thiol/En-Polymerisation. *Die Makromol. Chemie* **1991**, *192* (1), 159–164. https://doi.org/10.1002/macp.1991.021920114.

(47) Le, C. M. Q.; Morlet-Savary, F.; Chemtob, A. Role of Thiol Oxidation by Air in the Mechanism of the Self-Initiated Thermal Thiol-Ene Polymerization. *Polym. Chem.* **2021**, *12* (45), 6594–6605. https://doi.org/10.1039/d1py01301g.

(48) Nair, D. P.; Podgórski, M.; Chatani, S.; Gong, T.; Xi, W.; Fenoli, C. R.; Bowman, C. N. The Thiol-Michael Addition Click Reaction: A Powerful and Widely Used Tool in Materials Chemistry. *Chem. Mater.* **2014**, *26* (1), 724–744. https://doi.org/10.1021/cm402180t.

(49) Kharasch, M. S.; Nudenberg, W.; Mantell, G. J. Reactions of Atoms and Free Radicals in Solution. XXV. the Reactions of Olefins with Mercaptans in the Presence of Oxygen. *J. Org. Chem.* **1951**, *16* (4), 524–532. https://doi.org/10.1021/jo01144a005.

(50) Bagiyan, G. A.; Koroleva, I. K.; Soroka, N. V.; Ufimtsev, A. V. Oxidation of Thiol Compounds by Molecular Oxygen in Aqueous Solutions. *Russ. Chem. Bull.* **2003**, *52* (5), 1135–1141. https://doi.org/10.1023/A:1024761324710.

(51) KOOYMAN, E. C.; Leiden. Thiyl Radicals. *Pure Appl. Chem.* **1967**, No. 15, 81. https://doi.org/10.1002/9780470034408.ch8.

(52) Bertrand, M. P.; Ferreri, C. Sulfur-Centered Radicals. *Radicals Org. Synth.* **2008**, 485–504. https://doi.org/10.1002/9783527618293.ch49.

(53) Dénès, F.; Pichowicz, M.; Povie, G.; Renaud, P. Thiyl Radicals in Organic Synthesis. *Chem. Rev.* **2014**, *114* (5), 2587–2693. https://doi.org/10.1021/cr400441m.

(54) Crespy, D.; Landfester, K. Miniemulsion Polymerization as a Versatile Tool for the Synthesis of Functionalized Polymers. *Beilstein J. Org. Chem.* **2010**, *6*, 1132–1148. https://doi.org/10.3762/bjoc.6.130.

(55) Jasinski, F.; Lobry, E.; Chemtob, A.; Croutxé-Barghorn, C.; Criqui, A. Photopolymerizable Monomer Miniemulsions: Why Does Droplet Size Matter? *Macromol. Chem. Phys.* **2013**, *214* (15), 1669–1676. https://doi.org/10.1002/macp.201300278.

(56) Lobry, E.; Jasinski, F.; Penconi, M.; Chemtob, A.; Croutxé-Barghorn, C.; Oliveros, E.; Braun, A. M.; Criqui, A. Continuous-Flow Synthesis of Polymer Nanoparticles in a Microreactor via Miniemulsion Photopolymerization. *RSC Adv.* **2014**, *4* (82), 43756–43759. https://doi.org/10.1039/c4ra06814a.

(57) Skinner, E. K.; Whiffin, F. M.; Price, G. J. Room Temperature Sonochemical Initiation of Thiol-Ene Reactions. *Chem. Commun.* **2012**, *48* (54), 6800–6802. https://doi.org/10.1039/c2cc32457a.

(58) Priest, W. J. Particle Growth in the Aqueous Polymerization of Vinyl Acetate. *J. Phys. Chem* **1952**, *56* (3), 1077–1082.

(59) Keddie, J. L.; Routh, A. F. *Fundamentals of Latex Film Formation: Processes and Properties*; Springer US: Berlin, 2010.

(60) Gedde, U. W. *Polymer Physics*; Dordrecht, Ed.; Kluwer, 1995.

(61) Van Krevelen, D. W.; Te Nijenhuis, K. *Properties of Polymers*; 2009. https://doi.org/10.1016/B978-0-08-054819-7.X0001-5.

(62) Dargazany, R.; Khiêm, V. N.; Poshtan, E. A.; Itskov, M. Constitutive Modeling of Strain-Induced Crystallization in Filled Rubbers. *Phys. Rev. E - Stat. Nonlinear, Soft Matter Phys.* **2014**, *89* (2), 1–12. https://doi.org/10.1103/PhysRevE.89.022604.

(63) Pérez, R. Phd. Crystallization and Morpholgy of Multiphasic Polymeric Systems: Random Copolymers, Nanocomposites and Polymers with Complex Chain Topologies. **2019**.

(64) Lorenzo, A. T.; Arnal, M. L.; Albuerne, J.; Müller, A. J. DSC Isothermal Polymer Crystallization Kinetics Measurements and the Use of the Avrami Equation to Fit the Data: Guidelines to Avoid Common Problems. *Polym. Test.* **2007**, *26* (2), 222–231. https://doi.org/10.1016/j.polymertesting.2006.10.005.

(65) Müller, A. J.; Michell, R. M.; Lorenzo, A. T. Isothermal Crystallization Kinetics of Polymers. *Polym. Morphol. Princ. Charact. Process.* **2016**, 181–203. https://doi.org/10.1002/9781118892756.ch11.

(66) Coba-Daza, S.; Carmeli, E.; Otaegi, I.; Aranburu, N.; Guerrica-Echevarria, G.; Kahlen, S.; Cavallo, D.; Tranchida, D.; Müller, A. J. Effect of Compatibilizer Addition on the Surface Nucleation of Dispersed Polyethylene Droplets in a Self-Nucleated Polypropylene Matrix. *Polymer (Guildf).* **2022**, *263* (June), 125511. https://doi.org/10.1016/j.polymer.2022.125511.

(67) Sangroniz, L.; Cavallo, D.; Müller, A. J. Self-Nucleation Effects on Polymer Crystallization. *Macromolecules* **2020**, *53* (12), 4581–4604. https://doi.org/10.1021/acs.macromol.0c00223.

(68) Michell, R. M.; Mugica, A.; Zubitur, M.; Muller, A. J. Self-Nucleation of Crystalline Phases within Homopolymers, Polymer Blends, Copolymers, and Nanocomposites. *Adv. Polym. Sci.* **2017**, *276* (August 2015), 215–256. https://doi.org/10.1007/12_2015_327.

(69) Müller, A. J.; Michell, R. M.; Pérez, R. A.; Lorenzo, A. T. Successive Self-Nucleation and Annealing (SSA): Correct Design of Thermal Protocol and Applications. *Eur. Polym. J.* **2015**, *65*, 132–154. https://doi.org/10.1016/j.eurpolymj.2015.01.015.

(70) Müller, A. J.; Arnal, M. L. Thermal Fractionation of Polymers. *Prog. Polym. Sci.* **2005**, *30* (5), 559–603. https://doi.org/10.1016/j.progpolymsci.2005.03.001.

(71) Fillon, B.; Wittmann, J. C.; Lotz, B.; Thierry, A. Self-nucleation and Recrystallization of Isotactic Polypropylene (α Phase) Investigated by Differential Scanning Calorimetry. *J. Polym. Sci. Part B Polym. Phys.* **1993**, *31* (10), 1383–1393. https://doi.org/10.1002/polb.1993.090311013.

(72) Sangroniz, L.; Meabe, L.; Basterretxea, A.; Sardon, H.; Müller, A. J.; Cavallo, D. Chemical Structure Drives Memory Effects in the Crystallization of Homopolymers †. *Macromolecules* **2020**, *53* (12), 4874–4881. https://doi.org/10.1021/acs.macromol.0c00751.

(73) Blundell, D. J.; Keller, A.; Kovacs, A. J. A New Self-Nucleation Phenomenon and Its Application to the Growing of Polymer Crystals from Solution. *J. Polym. Sci. Part B Polym. Lett.* **1966**, *4* (7), 481–486. https://doi.org/10.1002/pol.1966.110040709.

Chapter 2. Challenges of thiol-ene chemistry in the field of polymer synthesis

2.1. Introduction

Thiol-ene chemistry in the field of polymer synthesis and material science has been extensively studied, based on polymers produced principally by bulk and solution polymerization.[1–4] As emphasized in the introduction, one of the main drawbacks reported in the literature is the chemical instability of thiol-ene systems.[5–9] In the literature dealing with polymers synthesized by radical mediated thiol-ene reaction, there are few reports[9,10] mentioning a lack of control and irreproducibility of molar masses of thiol-ene step growth polymers (due to excessive reactivity of some thiols). Nevertheless, except in the recent work of Teixeira *et al*,[11] there is no information of this principal challenge of thiol-ene polymers. This lack of knowledge how to control and reproduce the polymer synthesis is the main drawback to the implementation of this type of chemistry into more complex systems, such as polymerization in aqueous dispersed media.[10] Hence, this chapter presents the efforts to fully understand the thiol-ene systems and monomers' reactivity, by comparing and verifying existing literature data and thiol-ene main rules with experimental data. For that aim, the model monomer couple diallyl terephthalate (DATP) and glycol dimercaptoacetate (GDMA) (Figure 2.1) was selected, and their photopolymerization study was performed in bulk for sake of practical simplicity.

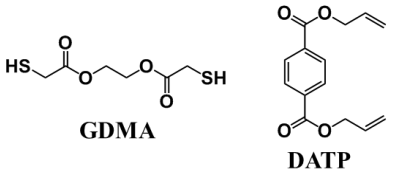

Figure 2.1 Chemical structures of dithiol monomer glycol dimercaptoacetate (GDMA) and diene monomer diallyl terephthalate (DATP)

In the first part, the effect of reaction conditions, namely photoinitiator concentration, reaction time, stoichiometric balance between thiol and ene functionality were investigated. In the following parts, challenging concerns about thiol-ene reproducibility and chemical stability are addressed. Some strategies to overcome the latter are proposed. This preliminary study also includes in a last part the observation of the spontaneous degradation of thiol-ene polymers obtained from GDMA-DATP photopolymerization.

2.2. Experimental

2.2.1.Materials

Diallyl Terephthalate (DATP, >98%) and 2,5-Di-tert-butylhydroquinone (DBHQ, >98%) were purchased from TCI chemicals. Glycol dimercaptoacetate (GDMA, >95%) was kindly supplied by Bruno Bock. Diphenyl(2,4,6-trimethylbenzoyl)phosphine oxide (TPO, >97%) and Pyrogallol (PYR, >98%) were purchased from Sigma Aldrich. Tetrahydrofuran THF (99.9% GPC) was purchased from Scharlab and used as solvent for the GPC analysis.

All chemicals were used as received without further purification.

2.2.2. Bulk photopolymerization

In a typical bulk experiment, a targeted 1:1 stoichiometric amount of the dithiol GDMA and diene DATP was mixed in presence of the photoinitiator TPO. Once completely miscible, the reactional mixture was subjected to UV light, in a (model BS-03, Dr. Grobel UV-Elektronik GmbH) equipped with 20 mercury lamps with a maximum wavelength intensity at 368 nm and an irradiance of 7 mW/cm^2.

2.2.3. Characterizations

Gel permeation chromatography (GPC) with tetrahydrofuran THF as a carrier, was utilized to determine the average molar mass (M_w) and polydispersity (PDI), at 35ºC with a THF flow rate of 1 mL/ min. The GPC instrument consisted of an injector, a pump (Waters 510), three columns in series (Styragel HR2, HR4, and HR6), and a differential refractometer detector (Waters 2410). The equipment was calibrated using polystyrene standards. The molar masses reported were obtained by comparison with the polystyrene standards.

Proton nuclear magnetic resonance (^{1}H NMR) was used for the measurement of the final ene conversion, and the method is detailed in Appendix V. NMR spectra were recorded on a Bruker 400 MHz at 25 °C. Samples were prepared by dissolving 20mg aliquots in 0.5 mL of deuterated chloroform ($CDCl_3$-d^6) or deuterated Dimethylsulfoxide (DMSO-d^6).

Matrix assisted laser desorption/ionization–time of flight mass spectrometry (MALDI-ToF MS) measurements were performed on a Bruker Autoflex Speed system equipped with a

355 nm NdYAG laser. Both positive reflectron and linear modes were used to obtain the spectra. Trans-2-[3-(4-tert-butylphenyl)-2-methyl-2-propenylidene] malonitrile (DCTB, Fluka) was used as a matrix, dissolved in tetrahydrofuran (THF) at a concentration of 20 mg mL^{-1} silver trifluoroacetate (AgTFA) was added as the ionization agent (10 mg mL−1dissolved in THF). Polymer samples were dissolved in THF at a concentration of 10mgmL^{-1}.The matrix, the salt, and the polymer were premixed at a ratio 10:1:1.Around 0.5μL of the mixture was hand spotted on a ground steel target plate. For each spectrum, 10 000 laser shots were accumulated. The spectra were externally calibrated with a mixture of different polyethylene glycol standards (PEG, Varian).

Electron Paramagnetic Resonance (EPR) spectra were carried out at room temperature using a Bruker ELEXSYS E500 spectrometer operating at the X-band. The spectrometer was equipped with a super-high-Q resonator ER-4123-SHQ, the magnetic field was calibrated by a NMR probe and the frequency inside the cavity (~9.39 GHz) was determined with an integrated MW-frequency counter. All measurements were performed on liquid samples at room temperature. 0.5 mL of GDMA, or the monomer mixture GDMA and DATP, were dissolved with 0.5ml of a solution of N-tert-butyl-α-phenylnitrone (PBN) in DMSO (5mg/ml). Data were collected and processed using the Bruker Xepr suite.

Raman measurements were done by using a Renishaw InVia Raman spectrometer, joined to a Leica DMLM microscope. The spectra were acquired with the Leica 50x N Plan (0.75 aperture) objective. The spatial resolution for the 50x objectives is 2 μm.

For the focusing and searching of the points of interest, the microscope implements a Prior scientific motorised stage (XYZ) with a joystick.

The spectrometer has two lasers, 514 nm (ion-argon laser, Modu-Laser) and 785 nm (diode laser, Torsana). The laser of 514 nm has a nominal power at the source of 50 mW, being the maximum power at the sample of 20 mW. In the case of the 785 nm laser, the power at the source is 350 mW, being the maximum power at the sample 150 mW. For the 514 nm laser, a holographic net of 1800 lines/mm is used, whereas for the 785 nm laser a holographic net of 1200 lines/mm is used. In all the measurements, the power of the laser was reduced in order to avoid the photo-decomposition of the samples (burning) by using neutral density filters. For each spectrum 20 seconds were employed and 5 scans were accumulated with the 50% of the maximum power of the 785 nm laser in the spectral window from 150 cm^{-1} to 3200 cm^{-1}.

2.3. Results and discussion

As emphasized in the introduction, to understand better the system based on bulk polymerization of GDMA-DATP monomers, the effect of reaction conditions on the final molar masses are studied in this chapter. The effect of photoinitiator concentration was assessed by performing three bulk reactions with TPO weight percent (wt%) of 0.25, 0.5, and 1. The three reaction mixtures were subjected to UV light with an irradiance of 7 mW/cm^2 for three hours, and ene conversion was monitored by ^1H NMR, polymers' molar mass and polydispersity index (PDI) were obtained by GPC and are reported in Figure 2.3.a. It is important to note that experiments with 0.5 and 1wt% of TPO were performed in triplicates, and the mean values of

molar mass, PDI and conversion are reported in Figure 2.3.a., with error bars showing the disparity of the results.

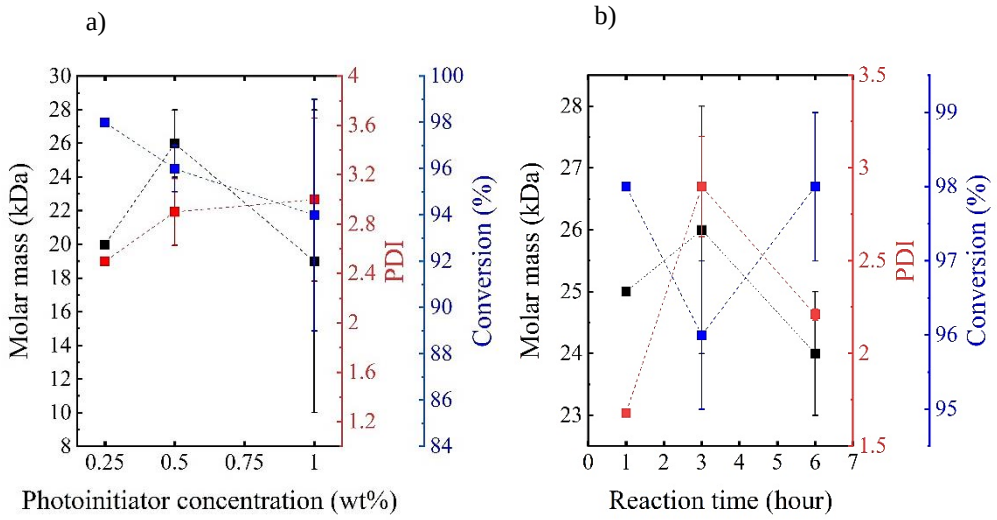

Figure 2.3. a) Molar masses, polydispersity index (PDI) and conversion of GDMA-DATP polymers synthesized by step growth polymerization as a function of the photoinitiator concentration used in the reaction. The reactions were performed for 3hours. In b) the molar masses, polydispersity index (PDI) and conversion of GDMA-DATP polymers synthesized by step growth polymerization in presence of 0.5wt% of photoinitiator as a function of reaction time. For a) and b), reactions were performed with an irradiance of 7 mW/cm^2. The error bars show the disparity of the results obatined for the experiments that were reproduced (triplicates).

As seen in Figure 2.3.a, the conversion decreases with initiator concentration, indicating that higher radical flux created from the larger initiator concentration induced significant radical recombination, as already reported in bulk polymerization of diallyl adipate (DAA) and 2,2′-(ethylenedioxy) diethanethiol (EDDT).[11] On the other hand, the molar mass of the polymers

first increases by increasing initiator concentration to 0.5 %, and decreases with further augmentation of the initiator quantity to 1%. Slight increase in the initiating species induced simultaneous growing of large number of chains, which after termination by combination increased the final molar masses. Further increase of initiating species results obviously in important radical recombination and drop in molar masses. This feature is explained by the step-growth mechanism, schematically presented in Figure 2.4

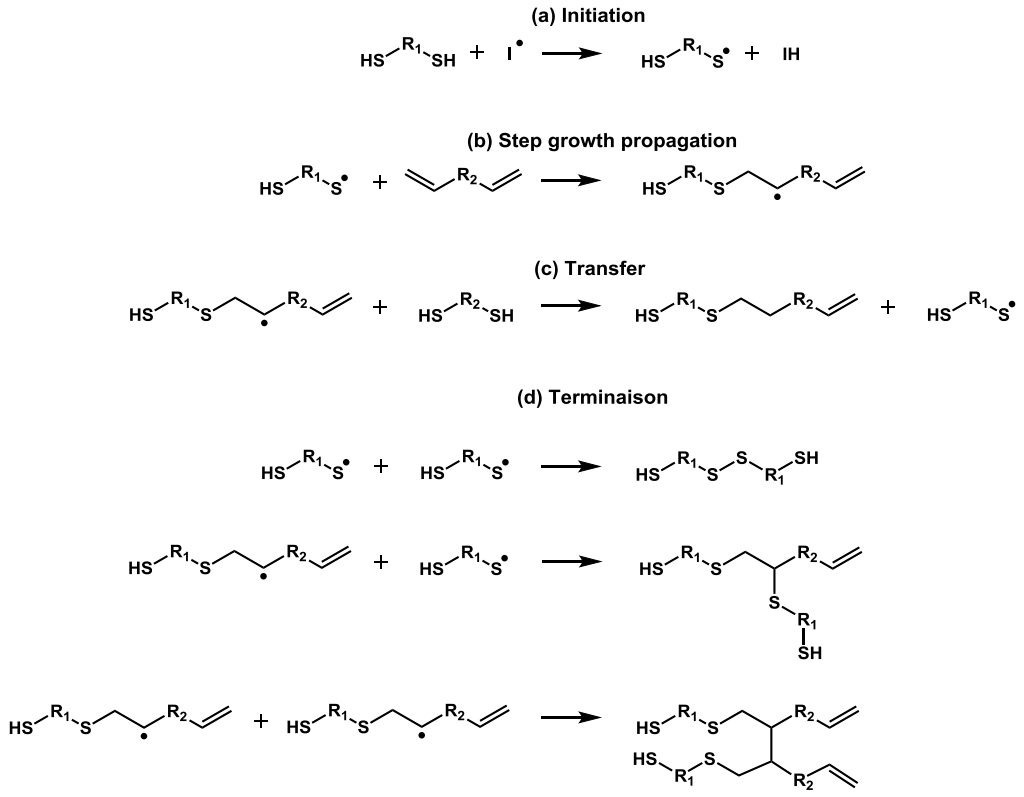

Figure 2.4. Thiol-ene radical step-growth polymerization mechanism[12]

With this mechanism, initiation occurs by activation of a radical initiator, which abstracts the hydrogen of the thiol moiety yielding to a thiyl radicals. The latter initiate thiol-ene step-growth by alternating thiyl radical propagation and chain transfer reaction (Steps b and c in Figure 2.4). Hence, in theory, very low concentration of radical initiator is required as the consumption of thiol and ene monomers by initiator radicals is assumed to be negligible relative to their consumption by propagation.[13] In our experiments, a minimal amount of photoinitiator

should be present in the reactional mixture to be efficiently decomposed by UV-light and generates radicals because of light penetration constrains when working in bulk.

When the concentration of photoinitiator was increased up to 1wt%, a drop in the polymer final molar mass is observed (Figure 2.3.a). Indeed, a high concentration of radical species (thiyl radicals and TPO radicals) promotes the occurrence of termination reaction by radical recombination (Step d Figure 2.4). This results, also reported in the case of DAA and EDDT[11], is supported by the increase of the molar mass distribution with a PDI up to 3 (Figure 2.3.a) when 1wt% of TPO is used, showing that recombination must occur.

In Figure 2.3.a., it is shown that conversion did not follow the same trend as molar masses when increasing the photoinitiator concentration and slightly decreased when working with higher amount of TPO. Noteworthy, the overall reaction conversion was approximated to the double bond consumption of the ene monomer, because homopolymerization of any of the monomers is not expected, which supposes proportional consumption of thiol and ene in a first-order step-growth polymerizations, as reported in other works.[5,10,11,14,15] Noticeably, the higher conversion, reached for 0.25wt% of photoinitiator yields to a polymer with a molar mass of 20 kDa, whereas the lower conversion reached with 0.5wt% of photoinitiator leads to a 26 kDa polymer (Figure 2.3.a). This results can be explained by the Carothers equation (Eq. 2.1), which describes the evolution of the degree of polymerization ($\bar{X}_n$) in the case of linear addition polymers with the conversion of the reaction (p) and the stoichiometric ratio of thiol and ene monomers (r)[16].

$$\bar{X}_n = \frac{1+r}{1+r-2pr} \quad \text{..... (2.1)}$$

This equation shows that besides the monomers' conversion, molar masses also strongly depends on the stoichiometric balance between thiol and ene functionality. The bulk experiments depicted in Figure 2.3.a. were prepared independently, and the differences in the stoichiometric ratio are likely to happen from one reaction to another even though big efforts are implemented to reach the same reaction conditions. Hence, in thiol-ene step growth polymerization, polymer with lower molar masses can be obtained for higher conversions because of off-stoichiometric ratio of thiols and enes effect. This effect could also explains the high irreproduicibility of the results obtained for experiments performed with 0.5 and 1wt% of photoinitiator as stressed by the error bars in Figure 2.3.a.

For the model monomer pair composed of DATP and GDMA, the effect of reaction time on polymer's molar mass was investigated. Three reactions were prepared and subjected to UV-light for 1 hour, 3 hours and 6 hours with an irradiance of 7 mW/cm^2 and in presence of 0.5wt% of TPO and results are reported in Figure 2.3.b. Reactions performed for 3 and 6 hours were reproduced in triplicate, and the mean values of molar mass, PDI and conversion are reported in Figure 2.3.b., with error bars.

Unexpectedly, the lowest chain length is obtained for the reaction exposed 6 hours under UV, which is in contradiction with the existing literature[11,16]. In addition, the error bars for the reaction performed for 3 and 6 hours shows again a high irreproducibility.

In order to see if the peculiar results depicted in Figure 2.3 can be explained by a preponderant effect of stoichiometric imbalance between reactants, the latter was studied by preparing four formulations with slightly different stoichiometric ratio r, which was calculated as according Equation 2.2

$$r = \frac{[\mathrm{GDMA}]}{[\mathrm{DATP}]} \quad \ldots\ldots\ldots \quad (2.2)$$

$$\text{with } [\mathrm{GDMA}] \leq [\mathrm{DATP}]$$

The four reactional mixtures were subjected to UV light for 3 hours in presence of 0.5wt% of photoinitiator, and polymers' molar mass and ene conversion are reported in Figure 2.5.a

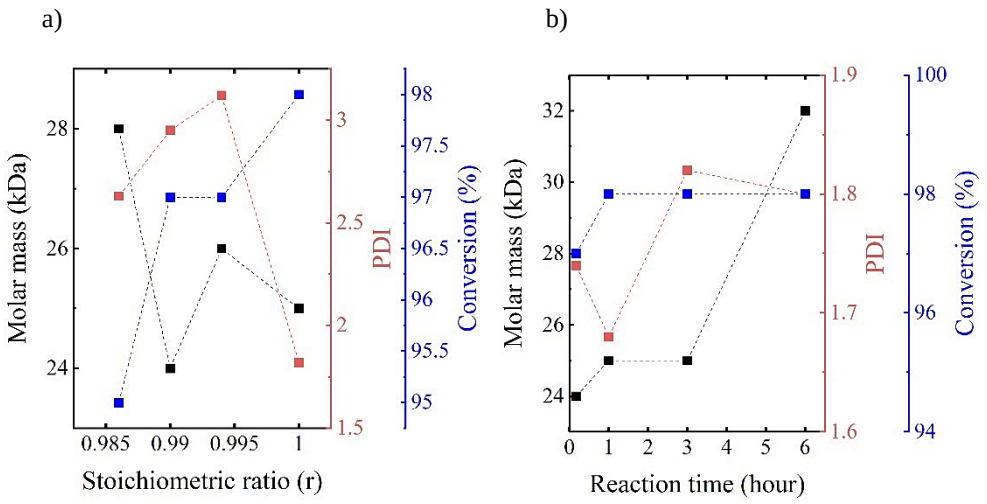

Figure 2.5. a) Molar masses, polydispersity index (PDI) and conversion of GDMA-DATP polymers synthesized by step growth polymerization as a function of stoichiometric ratio (r). The reactions were performed for 3hours and b) Molar masses, polydispersity index (PDI) and conversion of a GDMA-DATP polymer synthesized by step growth polymerization as a function of reaction time (10 min, 1 hour, 3 hours and 6 hours). The reaction was performed from the same bulk preparation, hence the molar ratio was constant and equal to 1.000. Reactions from a) and b) were performed in presence of 0.5wt% of photoinitiator with an irradiance of 7 mW/cm^2.

As depicted in Figure 2.5.a, the expected dependence between stoichiometric imbalance and final molar mass is not achieved, with the highest molar mass obtained when the ene monomer is in the largest excess. The apparent perfect stoichiometric ratio of 1,000:1,000 between thiol and ene functionality did not yield to a substantially higher molar mass polymers (Figure 2.5.a), as one would expect from Carothers' equation (Eq. 2.1). From these results, the occurrence of side reactions such as homopolymerization or the presence of dimers in the starting material is suspected. The latter would indeed biased the calculated stoichiometric ratio

between dithiol GDMA and diene DATP before the onset of polymerization, or cause stoichiometric imbalance during the reaction advancement. Nevertheless, the UV exposure of GDMA and DATP separately in presence of photoinitiator did not yield a synthesis of polymers or oligomers, which completely discarded homopolymerization of DATP and GDMA. Because it is well known that thiols can create dimmers and oligomers through S-S bonding,[17–19] the starting GDMA was analysed by diffusion ordered (DOSY) NMR spectroscopy (Figure 2.6). showing an absence of dimers or oligomers.

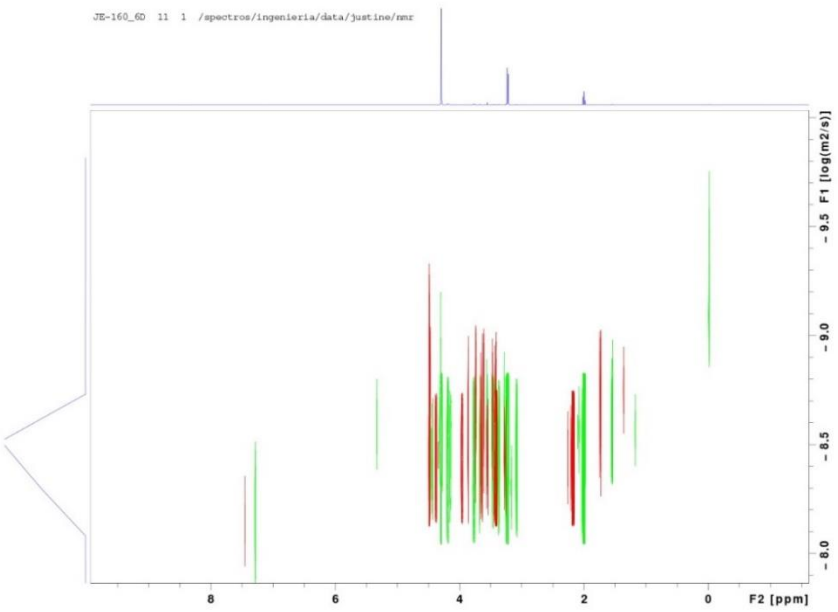

Figure 2.6. Diffusion ordered (DOSY) NMR spectroscopy analysis of the neat glycol dimercaptoacetate (GDMA) monomer.

Taking all these considerations into account, the rather strange results observed previously indicates important irreproducibility.

In order to eliminate the effect of stoichiometric ratio when the reaction time parameter was investigated, the same study was performed again, in which one DATP/GDMA mixture was used in all reactions performed in parallel for different reaction times. In that way, stoichiometric ratio between GDMA and DATP was kept strictly constant (r = 1,000) for the four samples. The results are presented in Figure 2.5.b, in which indeed only the effect of

reaction time parameter can be appreciated. The four reaction mixtures were subjected to UV-light for 10 min, 1 hour, 3 hours and 6 hours with an irradiance of 7 mW/cm^2 and in presence of 0.5wt% of TPO.

As seen in Figure 2.5.b, the effect of reaction time on molar mass and conversion can be noticed at constant stoichiometric ratio. As expected, molar masses of the polymers increase with reaction time, even when conversion was not varied importantly (between 1h and 6h), indicating very few disappearance of the functional groups, but important augmentation of molar masses due to termination between large chains.

In view of the previous results, it is clear that reproducibility in terms of thiol-ene polymer's molar masses is very challenging in practice. Reproducibility issue could be one limitation of thiol-ene chemistry applied to material synthesis, as molar mass variation could affect the thermomechanical properties of thiol-ene polymers and their crystalline behaviour for example. Very stringent reaction conditions, unattainable at the laboratory scale, need to be achieved to obtained reproducibility.

Searching for possible source behind this thiol-ene behaviour, it was found that thiol-ene systems, just after creating a contact between the both thiol and ene monomers, undergo premature reaction.[5–9] This lack of chemical stability and control of the polymerization onset could indeed worsen reproducibility.

The premature polymerization between GDMA and DATP was readily noticed qualitatively by a heat release when preparing formulations with the neat monomers.

Furthermore, it was evidenced by a series of reactions in which GDMA and DATP monomers were mixed with and without the photoinitiator TPO and in various reaction conditions detailed in Table 2.1.

Table 2.1. GDMA and DATP monomers mixture subjected to different reaction conditions and the final molar mass obtained by GPC.

Entry	Reaction conditions	Thiol:Ene	Reaction time (hours)	Mw (Da)
A.1	Dark and sealed vial	1.000:1.020	150	1911
A.2.TPO	Dark, 1wt% of TPO and sealed vial	1.000:0.980	150	1952
B.1	Natural light and sealed vial	1.000:0.969	150	1692
B.2.TPO	Natural light, 1wt% of TPO and sealed vial	1.000:0.978	150	10768
B.3	Natural light and sealed vial	1.000:1.000	96	2649
B.3.O	Natural light and open vial	1.000:1.000	96	2410
B.3.N_2	Natural light, purged with N_2 and sealed vial	1.000:1.000	96	2586

In Table 2.1, the nomenclature was chosen as follow: the GDMA-DATP mixtures kept in dark conditions are denoted A.X, (Entries A.1 and A.2.TPO) and the mixtures kept under natural light are labelled B.X. (Entries B.1, B.2.TPO, B.3, B.3.O and B.3.N_2). The second feature highlights the different bulk preparation. As an example, reactions A.1 and A.2.TPO were prepared from two different monomer mixtures, an therefore displays different thiol:ene stoichiometric ratios, whereas reactions B.3, B.3.O and B.3.N_2 were prepared from the same GDMA-DATP mixture and hence exhibit the same ratio between thiol and ene moieties. Finally, the last feature points out additional reaction conditions. Namely, reactions A.2.TPO and

B.2.TPO were performed in presence of 1wt% of TPO, reaction B.3.O was performed in an open vial and reaction B.3.N_2 was purged with nitrogen to work under inert atmosphere.

Spontaneous polymerization takes place in the neat monomer mixture (without the addition of a radical initiator) both in complete dark conditions or under sunlight (Entries A.1 and B.1, Table 2.1) creating oligomers of almost 2 kDa. From this results, sun light does not contribute to the self-initiating, as no significant difference in molar mass is observed for oligomers A.1 and B.1 after a couple of days light exposure. The presence of 1wt% of the photoinitiator TPO in dark conditions does not affect the molar masses and hence the premature polymerization (Entry A.2.TPO, Table 2.1), meaning that the photoinitiator is stable at this condition. However, under sun light the photoinitiator TPO is activated and forms radicals yielding to the synthesis of 11 kDa polymers through radical step growth polymerization (Entry B.2.TPO, Table 2.1). Upon low light intensity type I photoinitiators based on phosphine oxides like TPO have been reported to efficiently initiate polymerizations[20,21].

In order to investigate the effect of oxygen on the system based on GDMA and DATP, the reactions B.3, B.3.O and B.3.N_2 were prepared from the neat monomer mixture and subjected to different conditions. In entry B.3, as the sample was sealed under atmospheric conditions, oxygen is present in the sample at a certain concentration. In entry B.3.O, the sample was left open. In entry B.3.N_2, the monomer mixture was purged with N_2 and performed in a sealed vial, so that no oxygen is present in the surrounding or dissolved in the reactional mixture. Surprisingly, no effect of oxygen on the spontaneous polymerization could be detected by comparing the polymers' molar mass after 96 hours, as no significant difference is obtained.

This result differs from the data reported by Le *et al*[9]., for another system based on the monomer pair GDMA and diallyl phthalate (DAP), in which premature polymerization was completely prevented in inert atmosphere. Because of the longer time frame in our experiment B.3.N_2, some oxygen might have penetrated within the sealed samples and dissolve in the reactional mixture, causing the onset of spontaneous polymerization. Also, their study showed that for other monomer combinations, premature polymerization occurred in inert atmosphere at lower rate, showing that this process is oxygen assisted but also relies on other pathways, such as the homolytic cleavage of the S-H bond, assisted by a hydrogen transfer to alkene to form a C-H bond[9,26]. In addition, they emphasized that radicals may be present in the neat thiol monomer (i.e. before mixing with the ene) because of the slow oxidation of thiols by air during storage.

As emphasized in the introduction Chapter 1, in the literature, thiol-ene spontaneous reaction is mainly attributed to the presence of impurities capable to initiate the step-growth mechanism through different pathways. Namely, the presence of residues coming from the monomers synthesis, such as peroxide or hydroperoxide species with concentrations as low as traces can initiate the radical mediated polymerization. The presence of basic or nucleophilic impurities in the formulation can initiate another polymerization pathway, the catalysed-mediated thiol Michael addition.[17,22,23] Unfortunately, the presence of impurities, which could be diminished by purification of starting material, is not the only cause of premature polymerization. There are several works reported on self-initiated mechanisms responsible for the radical mediated thiol-ene polymerization. Klemm *et al*. reported that in dark and inert conditions, radicals were formed spontaneously in dithiol and diene mixtures.[6] The authors attribute the appearance of radicals to the formation of a charge transfer complex between thiol

and ene monomers, followed by an electron transfer with the formation of a thiyl radical. Another possible self-initiated mechanism responsible for premature polymerization is the production of thiyl radicals from the thiol-oxidation by molecular oxygen.[9,24,25] In the recent work of Le *et al.*[9], it is shown that the thiol oxidation by molecular oxygen plays a leading role in the premature polymerization of the studied systems by creating thiyl radicals setting up the radical mediated step growth polymerization. The nature of the initiating radicals was confirmed by ESR spin-trapping analysis. It appears that the main driving force of thiol air oxidation is the polarization of the S-H bond. However, in our systems, this mechanism does explain the premature polymerization observed in absence of oxygen (Table 2.1, Entry B.3.N_2). Therefore, another self-initiating mechanism may be occurring, in which oxygen is not involved. In that line, self-initiation could imply the homolytic cleavage of the S-H bond, assisted by a hydrogen transfer to alkene to form a C-H bond[9,26]. Noteworthy, Le *et al.* acknowledged that the mechanism they propose (i.e. the thiol oxidation by molecular oxygen, yielding to thiyl radicals by electron transfer) resembles to the initiation of a thiol-olefin cooxidation (TOCO) reaction[27], thiol oxidation into disulfide[18] or thiol-disulfide exchange[19].

To gain deeper understanding of our thiol-ene system and determinate the mechanism responsible for premature polymerization, Electron Paramagnetic Resonance (EPR) analysis of monomers GDMA, and DATP were performed at room temperature in presence of spin trapper PBN. The spectra shown in Figure 2.7 reveals the presence of a signal characteristic of radical species in the neat thiol monomer GDMA, whereas no signal was detected for the neat monomer DATP.

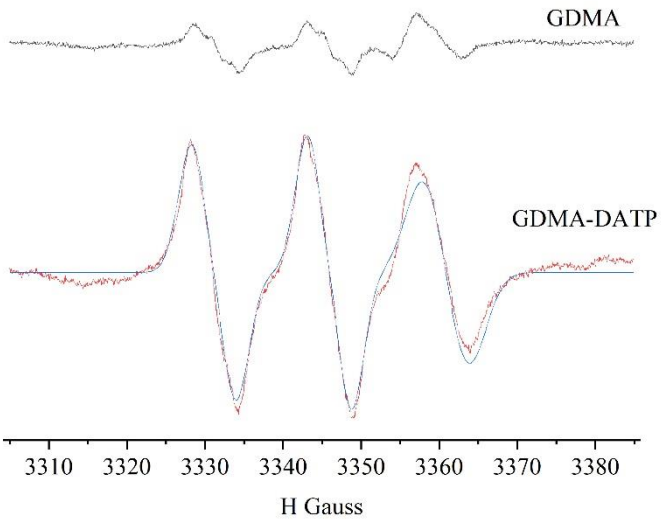

Figure 2.7. Electron Paramagnetic Resonance (EPR) spectra of neat monomer GDMA, and the mixture GDMA-DATP. The analysis was performed at room temperature in presence of spin trapper N-tert-butyl-α-phenylnitrone (PBN).

When GDMA is mixed with DATP, the radical signal is stronger in intensity, meaning that radical concentration is increased due to spontaneous polymerization taking place. From this result, it is obvious that the radical-mediated pathway is involved in the premature polymerization process. This results is supported by the recent study from Le *et al.*[9] The authors performed similar analysis and concluded that the radical specie present in GDMA is a thiyl radical. To determine the nature of radicals, they intentionally formed thiyl radicals by mixing GDMA with isopropyl thioxanthone (ITX) known to induce an intermolecular abstraction of a hydrogen atom from RSH upon irradiation. The EPR spectra of neat GDMA and GDMA mixed

with ITX showed the same traces, leading to the conclusion that the radical adducts in the neat GDMA are thiyls.

In our case, MALDI-ToF mass spectroscopy analysis were performed on the neat monomer GDMA, as an attempt to determine the origin of the radicals but also to analyse the purity of the sample, as impurities can contribute to the spontaneous reaction. No traces of peroxide, hydroperoxide or other impurity could be found on the spectra, but significant amounts of dimers, trimers and quadrimers were revealed.

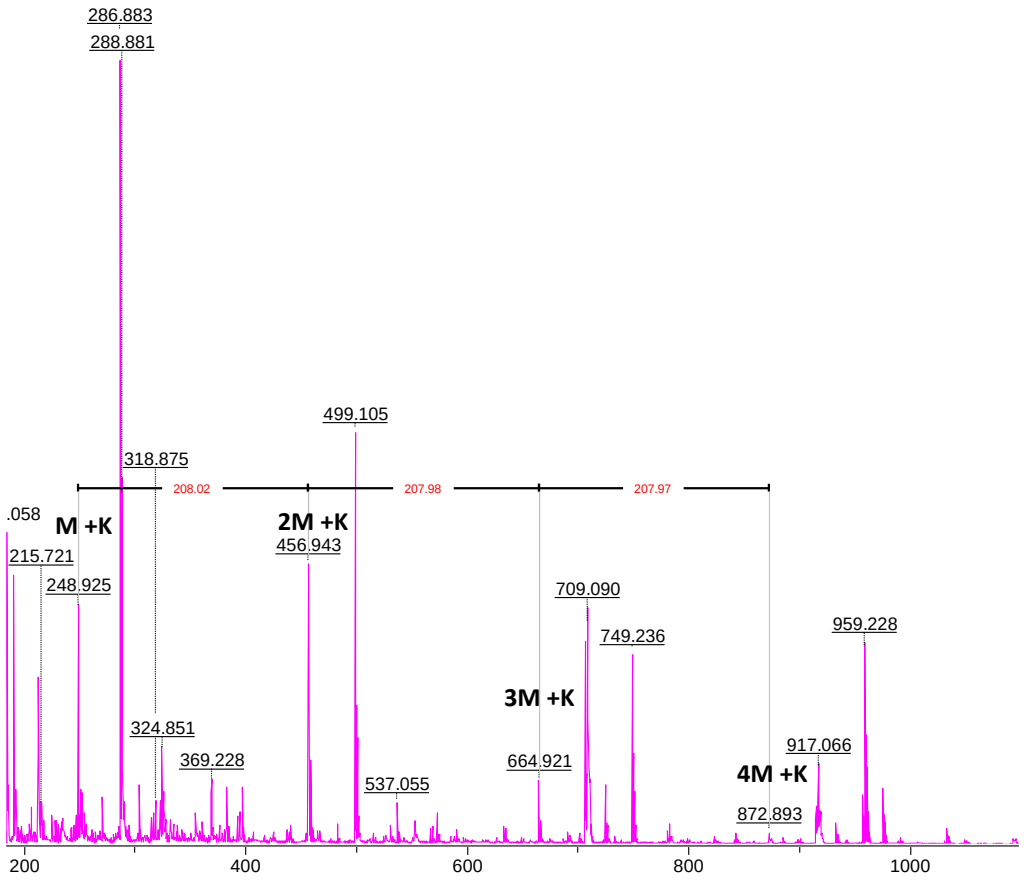

Figure 2.8. MALDI-TOF mass spectroscopy analysis of the neat monomer GDMA after 2 hours under atmospheric conditions.

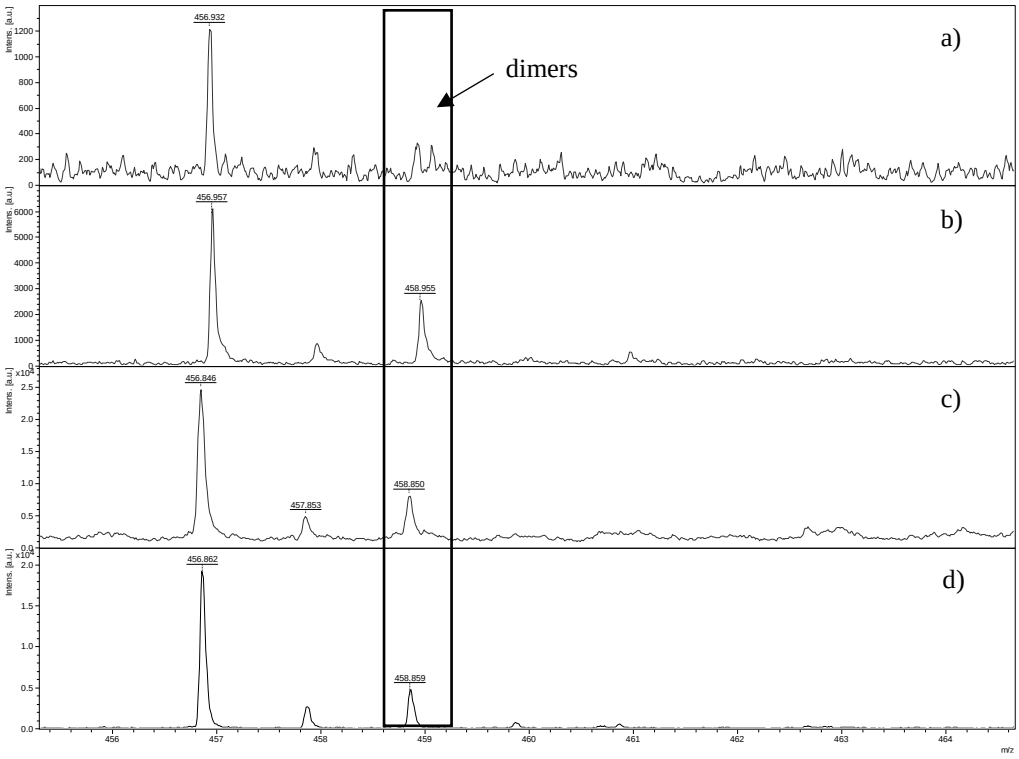

Figure 2.9. MALDI-TOF mass spectroscopy analysis of the neat monomer GDMA after different time of atmosphere exposure. a) Spectras of GDMA after opening of fresh bottle, b) after 2 hours under atmospheric conditions, c) after 72 hours under atmospheric conditions and d) after 6 days under atmospheric conditions.

Figure 2.8 presents the MALDI-TOF mass spectra of the GDMA that was kept under atmospheric conditions (in an open vial) for 2 hours. At 249 m/z, the peak is attributed to the monomer GDMA cationized with potassium ion $[M + K]^+$ (M being monomer GDMA). Spaced at m/z 208 Da, which represents the molar mass of the monomer GDMA, another peak at 457 m/z is attributed to the presence of dimers cationized with potassium ion $[2M + K]^+$. From the latter, two other peaks at 665 m/z and 873 m/z, equally spaced at m/z = 208 Da, highlight the

presence of trimers $[3M + K]^+$ and quadrimers $[4M + K]^+$ in the sample. In Figure 2.9, it is shown that the presence of dimers depends on the exposure time of the sample to atmospheric conditions. Indeed, in a freshly open bottle of monomer, the MALDI-TOF mass spectra (Figure 2.9.a) does not show any traces of the peak at 457 m/z from $[2M + K]^+$. However, when the same GDMA sample was kept in an open vial, the MALDI-TOF mass spectrum after 2hours, 72 hours and 6 days of exposure to atmospheric conditions clearly show the appearance of the peak at 457 m/z from $[2M + K]^+$.

The concentration of dimers, trimers and quadrimers increases with time exposure of the sample to atmosphere (Figure 2.9). Probably, these species were not visible by DOSY NMR (Figure 2.6) because their appearance depends on the aging of the sample and its exposure to atmosphere. These results also highlights that the stability of neat monomer is very limited, and that the targeted stoichiometric ratio between thiol and ene functionality is biased. As a consequence, stoichiometric imbalance cannot be properly calculated, and explains why we did obtain a polymer with higher molar mass for the highest stoichiometric imbalance in the experiments presented Figure 2.5.a. Attempts to calculate the molar mass were made by using the Carothers equation (Eq. 2.1), but the experimental values usually differ from the ones expected. This result can also be explained by the formation of dimers, trimers and quadrimers within the sample.

Moreover, dimers, trimers and quadrimers are known to be oxidation products from thiols[18], and could be involved in the premature polymerization mechanism. Actually, the oxidation of thiols by atmospheric oxygen could be responsible for the formation of disulfide

bonds, capable to undergo rapid exchange with thiyl radicals[25,28,29] which could initiate the radical mediated step growth mechanism. For the latter, a possible mechanism is proposed in Figure 2.10. For sake of clarity, the mechanism is depicted in the case that only dimers are present in the thiol monomer (herein GDMA).

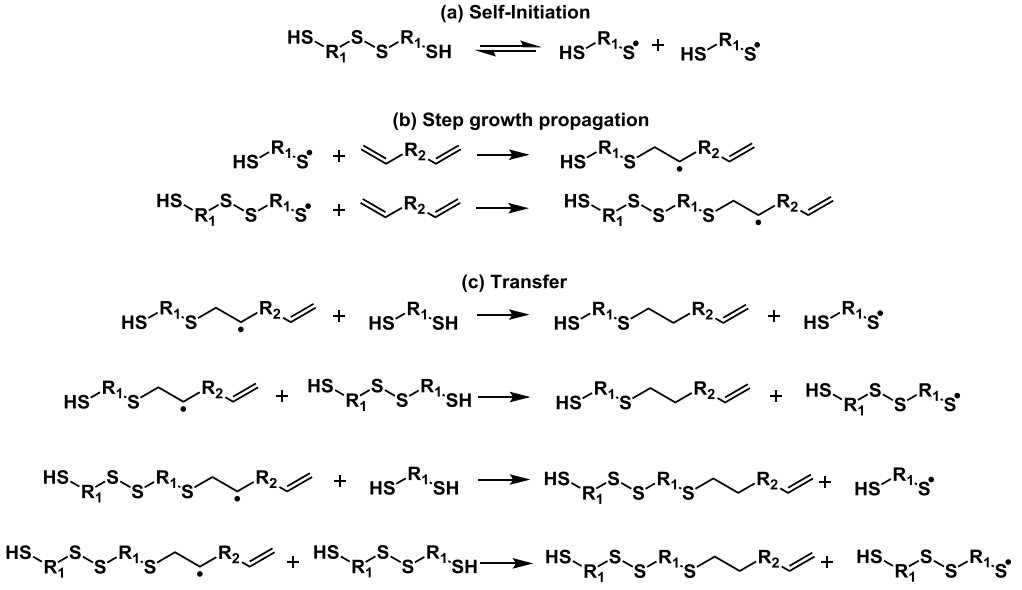

Figure 2.10. Thiol-ene radical mediated step-growth mechanism, self-initiated by the rapid exchange of disulfide bonds from dimers with thiyl radicals.

In a first step, radicals are produced by the rapid exchange of disulfide bonds from dimers with thiyl radicals. The latter then propagate across the ene goup by addition, forming a carbon centered radical. Subsequently, a chain reaction transfer occurs, in which the carbonyl abstract the hydrogen of another thiol moiety from a monomer, or a dimer. The step growth polymerization takes place by alternation of thiyl radical propagation and chain transfer reaction

and yields to the synthesis of thiol-ene polymers. As emphasized in the Figure 2.9., the presence of dimers (and trimers, quadrimers) implies that disulfide bonds are incorporated into the polymer backbone. Indeed, disulfide bonds are not only present in the neat monomer GDMA, but also in the polymer's backbone based on GDMA DATP, as seen on the Raman spectra Figure 2.11.

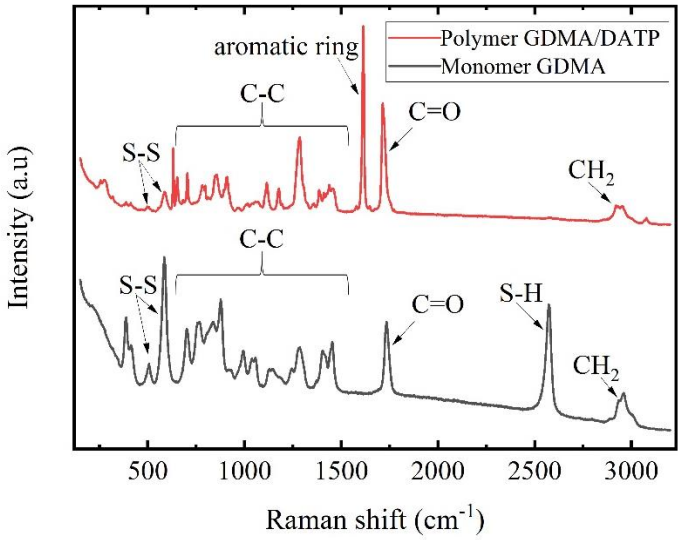

Figure 2.11. Raman spectra of the neat monomer GDMA and of the polymer based on GDMA-DATP

The presence of disulfide bond within the final backbone of the polymer affect its final properties. Indeed, it is known that disulfide bonds are dynamic bonds, which may induce polymer decomposition. For this matter, the evolution of molar mass with time was observed by GPC analysis for a range of GDMA-DATP polymers (P.1 to P.5), and results are depicted in Figure 2.11.

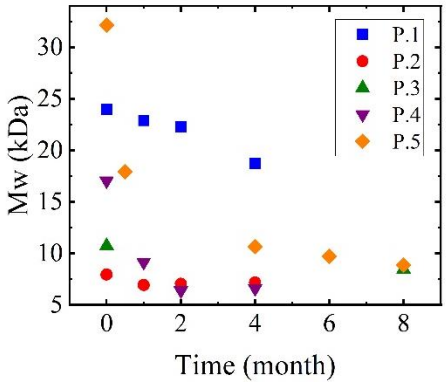

Figure 2.12. Evolution of the molar mass of GDMA-DATP polymers with time.

As shown in Figure 2.12, all polymers displayed molar mass loss, and the molar mass drop vary from one polymer to another. The more pronounced depolymerization is observed for the polymer P.5, with a drop of molar mass from 32kDa to 18kDa after two weeks, and to 9kDa after 8 months. The presence of disulfide bond, known to be dynamic covalent bond, within the polymer backbone could explain this drop in molar masses, and deeper investigation would be necessary to determine if the rate of decomposition is a function of the concentration of disulphide bonds. Polymers with disulfide backbone are reported in the literature, as they present good properties such as robust polymers presenting dynamic properties.[30] Indeed, disulfide bonds have a high dissociation energy (60kCal.mol^{-1}),[31] yet reversible under mild condition due to the fast thiol-disulfide exchange.[19,32] Degradation of poly(disulfide) is a critical consideration, as it can also be considered as a limitation if it happens within the time scale of the utilization of the material. When material evolving in terms of molar masses are usually precluded, depolymerization could be an interesting feature for recycling purpose.

Thiol-ene spontaneous polymerization may be one of the main limitation when it comes to its application. Indeed, the limited shelf life does not allow its storage, but also its utilization in 3D printing for example. Extensive work have been done to control the spontaneous polymerization by using radical scanvengers such as pyrogallol[33] or hydroquinone monomethyl ether[34] or stabilizer systems[5] combining radical scavenger (to prevent the radical mediated pathway of spontaneous reaction) and acidic compound to prevent the nucleophilic pathway of spontaneous reaction.

Herein, results showed that the radical mediated self-initiating process contribute to the spontaneous reaction occurring in the system based on GDMA-DATP. Attempts to overcome the chemical instability was performed by using radical scavenger at different concentration, DBHQ[35] and PYR[5,33], both used in other work to stabilize thiol-ene system. As depicted in Table 2.2, the use of radical scavenger alone, with 0.002 equivalent calculated with regards to GDMA, is enough to prevent completely the spontaneous reaction for at least 3 days for PYR and 5 days for DBHQ and hence control the onset of polymerization (Entries C.2 and D.2, Table 2.2).

Table 2.2. Ene conversion for GDMA DATP formulations with different concentration of radical scavenger Pyrogallol (PYR) and 2,5-Di-tert-butylhydroquinone (DBHQ)

Entry	Radical scavenger	Reaction time (days)	Ene conversion (%)
	PYR		
	GDMA:PYR		
C.1	1.000:0.0001	3	66
C.2	1.000:0.002	3	0
C.3	1.000:0.004	3	0
	DBHQ		
	GDMA:DBHQ		
D.1	1.000:0.0001	5	57
D.2	1.000:0.002	5	0
D.3	1.000:0.004	5	0

These results also highlight the fact that the spontaneous reaction is mainly if not only attributed to the radical mediated self-initiated process, excluding the contribution of the catalyzed mediated thiol-Michael addition. Contrary to the work reported by Esfiandari *et al.*,[5] no acidic compound was necessary to prevent the spontaneous reaction for the system based on GDMA/DATP.

Table 2.3. Ene conversion and final molar mass for GDMA-DATP polymers synthesized in presence of 0,003 equivalent of DBHQ with regards to GDMA.

Entry	GDMA:DATP	GDMA:DBHQ	Ene conversion (%)	Mw (kDa)
E	1.000:1.018	1.000:0.003	89	17
F	1.000:1.007	1.000:0.003	97	17

By controlling the onset of the polymerization, it seems that better reproducibility in terms of molar masses can be achieved, as seen in Table 2.3 with reaction of GDMA and DATP in presence of 0.5wt% of photoinitiator. Experimentally, GDMA was mixed with 0.003 equivalent of the radical scavenger DBHQ. The diene DATP and 0.5wt% of the photoinitiator TPO were then added to the reactional mixture. After 3 hours of UV exposure, poly(thioethers) with molar masses of 17kDa were obtained in reaction E and F, despite the stoichiometric ratio between thiol and ene monomer varying from one reaction to another and different conversion.

2.4. Conclusion

This study lays the foundation of thiol-ene challenges and limitations with the model thiol-ene pair based on GDMA and DATP. Results show that reproducibility and control of molar mass is challenging for this system, but as well by the nature of step growth polymerization and the purity of starting material. Indeed, in step growth linear polymerization, the final degree of polymerization is strongly impacted by stoichiometric balance between thiol and ene functionality and the overall extent of the reaction. Stoichiometric ratio between monomers can be biased because of the chemical instability of the neat GDMA, which pass spontaneous chemical reactions such as oxidized under molecular oxygen or thiol disulfide exchange, yielding to the formation of disulphide bonds with homodimers, trimers and even quadrimers. Besides inducing off-stoichiometric ratio between thiol and ene functionality, these disulphide bonds are capable to undergo rapid exchange with thiyl radicals. The latter can be responsible for premature polymerization, observed when the two neat monomers GDMA and DATP are mixed, by initiating the radical mediated step growth mechanism. The presence of

disulphide bonds within the GDMA-DATP polymer backbone could be appreciated by Raman analysis, and could explain the rapid decomposition of the polymer.

To improve reproducibility and control of molar masses, one strategy is to use radical inhibitor such as DBHQ and PYR. It is important to note that this strategy was efficient when working in bulk, but might be revisited when working in dispersed media. Indeed, when working in miniemulsion for exemple, the use of homogenization device such as sonicator may additionally form radicals capable to initiate the step-growth polymerization[36].

Therefore, in this work, another strategy in which chemical instability is turned into an advantage is proposed. Namely, the synthesis of thiol-ene oligomers by sonication was intentionally used to promote the obtainment of stable polymer particles in water. In that way, high molar masses polymer could be achieved with an additional step of photopolymerization, as described in Chapter 3.

2.5. References

(1) Lowe, A. B. Thiol-Ene "Click" Reactions and Recent Applications in Polymer and Materials Synthesis: A First Update. *Polym. Chem.* **2014**, *5* (17), 4820–4870. https://doi.org/10.1039/c4py00339j.

(2) Lowe, A. B. Thiol-Ene "Click" Reactions and Recent Applications in Polymer and Materials Synthesis. *Polym. Chem.* **2010**, *1* (1), 17–36. https://doi.org/10.1039/b9py00216b.

(3) Machado, T. O.; Sayer, C.; Araujo, P. H. H. Thiol-Ene Polymerisation: A Promising Technique to Obtain Novel Biomaterials. *Eur. Polym. J.* **2017**, *86*, 200–215. https://doi.org/10.1016/j.eurpolymj.2016.02.025.

(4) Resetco, C.; Hendriks, B.; Badi, N.; Du Prez, F. Thiol-Ene Chemistry for Polymer Coatings and Surface Modification-Building in Sustainability and Performance. *Mater. Horizons* **2017**, *4* (6), 1041–1053. https://doi.org/10.1039/c7mh00488e.

(5) Esfandiari, P.; Ligon, S. C.; Lagref, J. J.; Frantz, R.; Cherkaoui, Z.; Liska, R. Efficient Stabilization of Thiol-Ene Formulations in Radical Photopolymerization. *J. Polym. Sci. Part A Polym. Chem.* **2013**, *51* (20), 4261–4266. https://doi.org/10.1002/pola.26848.

(6) Sensfua, S.; Friedrich, M.; Kiemm, E. Untersuchungen Zur ThioVEn-Polymerisation: **1991**, *2900*, 2895–2900.

(7) Klemm, E.; Sensfuß, S.; Holfter, U.; Flammersheim, H. J. Free-Radical Stabilizers for the Thiol/Ene-systems. *Die Angew. Makromol. Chemie* **1993**, *212* (1), 121–127. https://doi.org/10.1002/apmc.1993.052120111.

(8) Klemm, E.; St. Sensfuß. Untersuchungen Zum Selbstinitiierungs-Mechanismus Der Thiol/En-Polymerisation. *Die Makromol. Chemie* **1991**, *192* (1), 159–164. https://doi.org/10.1002/macp.1991.021920114.

(9) Le, C. M. Q.; Morlet-Savary, F.; Chemtob, A. Role of Thiol Oxidation by Air in the Mechanism of the Self-Initiated Thermal Thiol-Ene Polymerization. *Polym. Chem.* **2021**, *12* (45), 6594–6605. https://doi.org/10.1039/d1py01301g.

(10) Jasinski, F.; Rannée, A.; Schweitzer, J.; Fischer, D.; Lobry, E.; Croutxé-Barghorn, C.; Schmutz, M.; Le Nouen, D.; Criqui, A.; Chemtob, A. Thiol-Ene Linear Step-Growth Photopolymerization in Miniemulsion: Fast Rates, Redox-Responsive Particles, and Semicrystalline Films. *Macromolecules* **2016**, *49* (4), 1143–1153. https://doi.org/10.1021/acs.macromol.5b02512.

(11) Infante Teixeira, L.; Landfester, K.; Thérien-Aubin, H. Nanoconfinement in Miniemulsion Increases Reaction Rates of Thiol-Ene Photopolymerization and Yields High Molecular Weight Polymers. *Polym. Chem.* **2022**, 2831–2841. https://doi.org/10.1039/d2py00350c.

(12) Hoyle, C. E.; Lee, T. Y.; Roper, T. Thiol-Enes: Chemistry of the Past with Promise for the Future. *J. Polym. Sci. Part A Polym. Chem.* **2004**, *42* (21), 5301–5338. https://doi.org/10.1002/pola.20366.

(13) Cramer, N. B.; Reddy, S. K.; O'Brien, A. K.; Bowman, C. N. Thiol - Ene Photopolymerization Mechanism and Rate Limiting Step Changes for Various Vinyl Functional Group Chemistries. *Macromolecules* **2003**, *36* (21), 7964–7969. https://doi.org/10.1021/ma034667s.

(14) Jasinski, F.; Lobry, E.; Tarablsi, B.; Chemtob, A.; Croutxé-Barghorn, C.; Nouen, D. Le; Criqui, A. Light-Mediated Thiol-Ene Polymerization in Miniemulsion: A Fast Route to Semicrystalline Polysul Fide Nanoparticles. *ACS Macro Lett.* **2014**, *3* (9), 958–962. https://doi.org/10.1021/mz500458s.

(15) Le, C. M. Q.; Vidal, L.; Schmutz, M.; Chemtob, A. Droplet Nucleation in Miniemulsion Thiol-Ene Step Photopolymerization. *Polym. Chem.* **2021**, *12* (14), 2084–2094. https://doi.org/10.1039/d1py00139f.

(16) Odian, G. *Principles of Polymerization*, 4th ed.; Sons., J. W. &, Ed.; 2004.

(17) Mutlu, H.; Ceper, E. B.; Li, X.; Yang, J.; Dong, W.; Ozmen, M. M.; Theato, P. Sulfur Chemistry in Polymer and Materials Science. *Macromol. Rapid Commun.* **2019**, *40* (1), 1–51. https://doi.org/10.1002/marc.201800650.

(18) D'Souza, V. .; Iyer, V. .; Szmant, H. H. Thiol-Olefin Cooxidation (TOCO) Reaction. 8. Solvent Effects in the Oxidation of Some Thiols with Molecular Oxygen. *J.Org.Chem.* **1987**, No. 52, 1725–1728.

(19) Fava, A.; Iliceto, A.; Camera, E. Kinetics of the Thiol-Disulfide Exchange. *J. Am. Chem. Soc* **1957**, *79*, 833–838.

(20) Lalevée, J.; Fouassier, J. P. Recent Advances in Sunlight Induced Polymerization: Role of New Photoinitiating Systems Based on the Silyl Radical Chemistry. *Polym. Chem.* **2011**, *2* (5), 1107–1113. https://doi.org/10.1039/c1py00073j.

(21) Fouassier, J. P.; Lalevée, J. *Photoinitiators for Polymer Synthesis: Scope, Reactivity, and Efficiency*; 2013.

(22) Hoyle, C. E.; Bowman, C. N. Thiol-Ene Click Chemistry. *Angew. Chemie - Int. Ed.* **2010**, *49* (9), 1540–1573. https://doi.org/10.1002/anie.200903924.

(23) Nair, D. P.; Podgórski, M.; Chatani, S.; Gong, T.; Xi, W.; Fenoli, C. R.; Bowman, C. N. The Thiol-Michael Addition Click Reaction: A Powerful and Widely Used Tool in Materials Chemistry. *Chem. Mater.* **2014**, *26* (1), 724–744. https://doi.org/10.1021/cm402180t.

(24) Kharasch, M. S.; Nudenberg, W.; Mantell, G. J. Reactions of Atoms and Free Radicals in Solution. XXV. the Reactions of Olefins with Mercaptans in the Presence of Oxygen. *J. Org. Chem.* **1951**, *16* (4), 524–532. https://doi.org/10.1021/jo01144a005.

(25) Bagiyan, G. A.; Koroleva, I. K.; Soroka, N. V.; Ufimtsev, A. V. Oxidation of Thiol Compounds by Molecular Oxygen in Aqueous Solutions. *Russ. Chem. Bull.* **2003**, *52* (5), 1135–1141. https://doi.org/10.1023/A:1024761324710.

(26) Goldstein, S.; Samuni, A.; Merenyi, G. Kinetics of the Reaction between Nitroxide and Thiyl Radicals: Nitroxides as Antioxidants in the Presence of Thiols. *J. Phys. Chem. A* **2008**, *112* (37), 8600–8605. https://doi.org/10.1021/jp804743g.

(27) D'souza, V. T.; Nanjundiah, R.; Jaime Baeza, J. B.; Szmant, H. H. Thiol-Olefin Cooxidation (TOCO) Reaction. 9. A Self-Consistent Mechanism under Nonradical-

Inducing Conditions. *J. Org. Chem.* **1987**, *52* (9), 1729–1740. https://doi.org/10.1021/jo00385a016.

(28) KOOYMAN, E. C.; Leiden. Thiyl Radicals. *Pure Appl. Chem.* **1967**, No. 15, 81. https://doi.org/10.1002/9780470034408.ch8.

(29) Nevejans, S.; Ballard, N.; Miranda, J. I.; Reck, B.; Asua, J. M. The Underlying Mechanisms for Self-Healing of Poly(Disulfide)S. *Phys. Chem. Chem. Phys.* **2016**, *18* (39), 27577–27583. https://doi.org/10.1039/c6cp04028d.

(30) Zhang, Q.; Qu, D. H.; Feringa, B. L.; Tian, H. Disulfide-Mediated Reversible Polymerization toward Intrinsically Dynamic Smart Materials. *J. Am. Chem. Soc.* **2022**, *144* (5), 2022–2033. https://doi.org/10.1021/jacs.1c10359.

(31) Somayajulu, G. R. Dissociation Energies of Diatomic Molecules. *J. Chem. Phys.* **1960**, *33* (5), 1541–1553. https://doi.org/10.1088/0256-307X/25/6/024.

(32) Nagy, P. Kinetics and Mechanisms of Thiol-Disulfide Exchange Covering Direct Substitution and Thiol Oxidation-Mediated Pathways. *Antioxidants Redox Signal.* **2013**, *18* (13), 1623–1641. https://doi.org/10.1089/ars.2012.4973.

(33) Kühne, G.; Diesen, J. S.; Klemm, E. New Results of the Self-Initiation Mechanism of SH/En Addition Polymerization. *Angew. Makromol. Chemie* **1996**, *242*, 139–145. https://doi.org/10.1002/apmc.1996.052420109.

(34) Moszner, N.; Schöb, W.; Rheingerger, V. Synthesis, Characterization and Thiol-Ene Polymerization of Hydrolyzed/Condensed Norbornenyl Silic Acid Ester. *Polym. Bull.* **1996**, No. 37, 289–295.

(35) Quoc Le, C. M.; Schmutz, M.; Chemtob, A. Ab Initio Batch Emulsion Thiol–Ene Photopolymerization. *Macromolecules* **2020**. https://doi.org/10.1021/acs.macromol.0c00265.

(36) Skinner, E. K.; Whiffin, F. M.; Price, G. J. Room Temperature Sonochemical Initiation of Thiol-Ene Reactions. *Chem. Commun.* **2012**, *48* (54), 6800–6802. https://doi.org/10.1039/c2cc32457a.

Chapter 3. Development of waterborne poly(thioether) coatings by polymerization in dispersed media

3.1. Introduction

As highlighted in the introduction of the thesis, the feasibility of thiol-ene photopolymerization in aqueous dispersed media is well documented in the literature, and has been performed in emulsion,[1,2] miniemulsion[3–9] and suspension,[10] giving rise to linear or crosslinked poly(thioethers) latexes. Among these processes, thiol-ene polymerization in miniemulsion turns out to be a privileged mean to obtain high sulfur content products with controlled colloidal properties and architecture.

As seen in Chapter 2, one of the main drawbacks in thiol-ene systems is the limited shelf-life resulting in premature polymerization, also referred to as thiol-ene dark reaction. The uncontrolled nature of thiol-ene spontaneous reaction may impact the experimental reproducibility, even more than in polymerization in homogeneous media.[4] The current strategies implemented to control thiol-ene reactivity consist of using radical scavengers to prevent the radical mediated initiation together with acidic compounds to prevent the nucleophilic pathway.[11]

In this chapter, two lines of investigation were simultaneously performed. In a first part, chemical stability of thiol-ene in miniemulsions based on the model monomer pair glycol dimercaptoacetate (GDMA) and diallyl terephtalathe (DATP) was targeted by using the radical scavanger 2,5-Di-tert-butylhydroquinone (DBHQ) to prevent premature polymerization occurring spontaneously and during sonication step. Thiol-ene miniemulsions were further converted to latexes by photopolymerization in presence of the photoinitiator lithium phenyl (2,4,6-trimethylbenzoyl)phosphinate (TPO-Li). This strategy allows a spatial and temporal control of the onset of the polymerization.

The second line of investigation implies a novel synthesis approach, in which thiol-ene chemical instability is turned into advantage. Namely, to prepare the miniemulsion, usually sonication is applied to break the monomer droplets dispersed in water, as already explained in Chapter 1. We took a benefit of the high thiol's reactivity during miniemulsification process by sonication that usually gives high monomer conversions and perform a sonopolymerization to synthesize "pre-polymers" without use of any initiator nor inhibitor. Ultrasound is a widely used tool in synthesis, and has already been applied to efficiently initiate radical chain-growth polymerization in dispersed media[12] of methacrylate monomers.[13,14] In the scope of thiol-ene chemistry, sonochemical initiation has been used to induce the coupling reaction of cysteamine chloride with various alkene in water in the presence and absence of thermal initiator 2,20-azobis(2-methylpropionitrile) (AIBN).[15] In our study, three sets of bifunctional monomer pairs were studied. In addition to the model pair GDMA-DATP, combination of DATP with the glycol dimercaptoproprionate (GDMP) and 2,2-(ethylenedioxy)diethanethiol (EDDT) were also tested.

In the current literature, poly(thioether) dispersions were synthesized with solids content in a range of 10% to 20%.[3–5,16] In order to fit more closely the industrial requirements, the synthetic approach has to be turned towards higher solids contents, which are indispensable for producing good quality films and generally desired to reduce the production and transport costs. Some attempts to meet this criterion were reported by Jasinsky *et al*., who reported the feasibility to work up to 50% solid content with a miniemulsion photopolymerization based on the monomers diallyl phthalate (DAP) and EDDT.[4] Le *et al*. emphasize the possibility to produce thiol-ene latexes based on the monomers DAP and EDDT by emulsion polymerization with solid content up to 40%.[2] However, their poly(thioether) dispersions synthesized at high solids content lacked a control of the process and product properties, as lower molar mass polymers (24 kDa with polydispersity index PDI of 3) were produced at higher solids content than these obtained at 10% solids content (39.2 kDa with PDI of 2.8). To fully unlock the potential of thiol-ene polymers obtained by polymerization in dispersed media, both the molar mass and the solids content need to be enhanced. As already mentioned, step-growth polymers are characterized with low molar masses, especially when produced in high-solids content dispersions.[17] In this work, to enhance the polymers' molar masses towards practical values for barrier coating required to reduce the migration of the polymer after film formation, a strategy of combining sonopolymerization and subsequent photopolymerization in presence of a water-soluble photoinitiator was implemented. In that way, "prepolymers" based on the monomer couples DATP/GDMA, DATP/GDMP and DATP/EDDT synthesized during the first step of sonopolymerization, were photopolymerized in the next step to produce up to 50% solids content film-forming poly(thioether) latexes with high molar masses. For the first time to the

best knowledge of the authors, film forming waterborne dispersions made of linear poly(thioether) polymers with huge molar masses, suitable for the intended application in food packaging were developed.

Related to the practical application of these dispersions in coatings, the main challenge that still persists is to obtain high-solids content dispersions of film-forming polymer formulation. Besides implementing new synthetic procedures and optimize them, an additional aim of the thesis is to obtain continuous film after water evaporation, suitable for waterborne coatings application that moreover display barrier properties. Hence, attention was turn toward the production of film forming poly(thioethers), which encompasses issues as glass transition temperature (T_g) of the polymers lower than film forming temperature and high solids content dispersions (40-50 wt. %). As emphasized in Chapter 1 Jasinski *et. al* reported the synthesis of linear poly(thioether ester) particles with film forming ability by photopolymerization in miniemulsion.[5] Linear chains based on the bifunctionnal monomers diallyl adipate (DAA) and ethylene glycol dithiol (EGDT) were synthesized with molar masses ranging between 35 and 57.5 kDa, with a PDI of 2.5. The polymer presents a low glass transition temperature (T_g) of -63ºC and yield an elastomeric film after water evaporation at room temperature. However, despite low solids content of the final dispersions that lack practical significance, the authors acknowledged the restraint utility of such film, due to a low melting point leading to poor mechanical properties. Introducing aromatic units in the polymer backbone is one of the strategies to stiffen significantly the final films obtained from thiol-ene aqueous dispersions. In another contribution, Jasinski *et. al* synthesized a film-forming poly(thioether) latex with a solid content of 20% based on the monomers DAP and EDDT with a molar mass of 54.3 kDa and

PDI of 2.7. [4] Introducing a rigid aromatic ring into the polymer building block resulted in increased T_g of -42ºC due to the less flexible chains. Although the authors emphasized the possibility to produce EDDT-DAP latexes by miniemulsion photopolymerization with solid content up to 50%, no data on the final molar mass reached in this case is reported.

Herein, a range of thiol and ene monomer combinations was studied, and strategies were explored to improve the quality and toughness of the final films, either by developing polymers with high molar masses, or crosslinked polymers by adding small amount of trifunctional monomers trimethylolpropan tri(3-mercaptopropionate) (TMPMP) and 1,2,4-Trivinylcyclohexane (TVCH). Addition of inorganic filler (graphene oxide and its reduced form) to the waterborne dispersions was studied, too.

3.2. Experimental

3.2.1. Material

Diallyl terephtalate (DATP, >98%), %), trimethylolpropan tri(3-mercaptopropionate) (TMPMP, >98%), 1.2,4-Trivinylcyclohexane (TVCH, >98%), lithium phenyl (2,4,6-trimethylbenzoyl)phosphinate (TPO-Li, >99%) were purchased from TCI chemicals. 2,2-(ethylenedioxy)diethanedithiol (EDDT, >95%) and hexadecane (HD, >98%), polyvinylpyrrolidone (PVP- M=10 000 g/mol) and hydrazine monohydrate and 2,2 -Azobis(2-methylpropionitrile) (AIBN, >98%) were purchased from Sigma Aldrich. Glycol dimercaptoacetate (GDMA, >95%) and glycol dimercaptopropionate (GDMP, >95%) were kindly supplied by Bruno Bock. Graphine oxide (10mg/mL) was obtained from Graphenea.

Dowfax 2A1 was kindly supplied by Dow chemicals. Tetrahydrofuran (THF 99.9% HPLC grade) was purchased from Scharlab and used as solvent for the GPC analysis. All chemicals were used as received without further purification, and de-ionised water was used as the dispersant media for the polymerization.

3.2.2. Synthesis

3.2.2.1. Poly(thioethers) synthesis by photopolymerization in miniemulsion

In a typical reaction, the organic phase was prepared by mixing the bifunctional monomers (1:1 equivalent thiol-ene) DATP and GDMA (Figure 3.1) and the radical inhibitor DBHQ at different concentration with respect to thiol monomers.

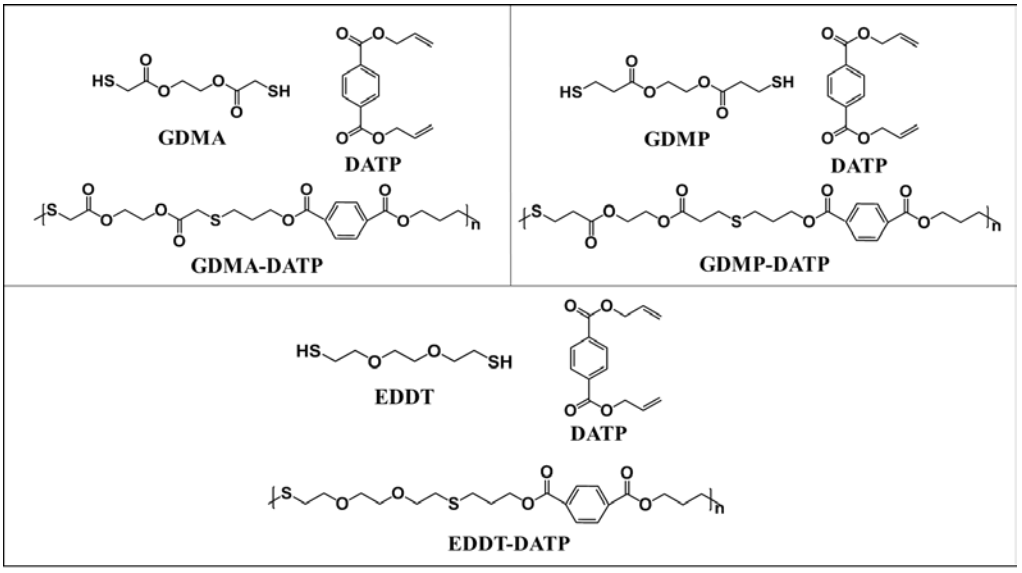

Figure 3.1. Chemical Structure of difunctionnal monomers DATP, GDMA, GDMP, EDDT and Poly(thioether) GDMA-DATP, GDMP-DATP and EDDT-DATP obtained from step-growth polymerization.

No costabilizer was used in the formulation, because of the poor solubility of GDMA with HD, typically used in the formulation of miniemulsions [18]. 20wt% solids content miniemulsions based on GDMA-DATP were prepared by dispersing monomer pairs in an aqueous solution of surfactant (Dowfax 2A1) for 5 min, followed by sonication step in an ice bath to pre-form small monomer droplets. Sonication was performed using a Branson Digital sonifier at 80% of amplitude, with a 0.5 sec on and 1 sec off pulsed program.

Table 3.1. Formulations and synthesis conditions of the 20% solid content moniemulsions of the bifunctional monomers DATP and GDMA.

Entry	Mass DATP (g)	Dowfax 2A1 (wt%)	DBHQ:GDMA	Stoechiometric ratio thiol:ene
M.1	6.1200	1.5	1.000:0.002	1.000:1.001
M.2	6.1225	4	1.000:0.002	1.000:0.999
M.3	6.1232	4	1.000:0.003	1.000:0.999
M.4	6.1261	4	1.000:0.004	1.000:1.001

0.5wt% (based on monomers mass) of the water soluble photoinitiator TPO-Li was added after the sonication step. The monomer pairs then were polymerized by step-growth radical photopolymerization performed in miniemulsion at ambient temperature under stirring (600 rpm). The photopolymerization was processed for 1 hour in a 630 mL quartz reactor placed in a UV chamber (model BS-03, Dr. Grobel UV-Elektronik GmbH) equipped with 20 mercury lamps with a maximum wavelength intensity at 368nm and an irradiance of 7 mW/cm^2. The formulations are depicted in Table 3.1.

3.2.2.2. Poly(thioethers) synthesis by sonopolymerization and photopolymerization

In a typical reaction, the organic phase was prepared by mixing the bifunctional monomers GDMA-DATP, GDMP-DATP or EDDT-DATP (Figure 3.1), with a targeted 1:1 mol ratio of thiol-ene functionality. In one formulation (Entry S.3., Table 3.2) 0.2 wt% (based on GDMA-DATP monomers' mass) of the thermal initiator AIBN was added to the organic phase.

In another formulation (Entry S.4, Table 3.2), 6wt% (based on EDDT-DATP monomers' mass) of HD was added to the organic phase as a costabilizer to prevent Ostwald ripening.

30 wt% solids content and 50% solid content dispersions were prepared by mixing the monomer pairs in an aqueous solution of surfactant (Dowfax 2A1. 1.5 wt%) for 5 min, followed by sonication in an ice bath to pre-form polymer particles. Sonication was performed using a Branson Digital sonifier at 70% of amplitude, with a 0.5 sec on and 1 sec off pulsed program. Synthesis conditions and formulations are depicted in Table 3.2.

For the additional photopolymerization step, 0.5 wt% (based on monomers mass) of the water soluble photoinitiator TPO-Li was added after sonication step. The reactional mixture was exposed for 1 hour to UV light under stirring in a 630mL quartz reactor, placed in a UV chamber (model BS-03, Dr. Grobel UV-Elektronik GmbH) equipped with 20 mercury lamps with a maximum wavelength intensity at 368 nm and an irradiance of 7 mW/cm^2.

Table 3.2. Formulations and synthesis conditions 30% and 50% solid content sonopolymers or pre-polymers obtained by sonopolymerization of the bifunctional monomers DATP, GDMA, EDDT and GDMP.

Entry	Monomers	Mass DATP (g)	AIBN (wt%) *	HD (wt%) *	Solid content (%)	Stoechiometric ratio thiol:ene	Sonication time (min)
S.1	GDMA-DATP	22.4483	-	-	30	1.000:0.999	10
S.2	GDMA-DATP	22.4463	-	-	30	1.000:0.999	10
S.3	GDMA-DATP	22.4488	0.2	-	30	1.000:1.000	10
S.4	EDDT-DATP	19.3880	-	6	30	1.000:1.000	7:30
S.5	EDDT-DATP	19.3893	-	-	30	1.000:1.000	7:30
S.6	GDMP-DATP	19.3995	-	-	30	1.000:1.000	7:30
S.7	GDMA-DATP	37.7575	-	-	50	1.000:1.000	20
S.8	EDDT-DATP	32.6515	-	-	50	1.000:1.000	10
S.9	GDMP-DATP	32.6453	-	-	50	1.000:1.007	10

*Based on monomers' mass

Another set of crosslinked poly(thioethers) based on the bifunctional monomers DATP, GDMA (Figure 3.1) and trifunctional monomers TVCH and TMPMP (Figure 3.2) was obtained by sonopolymerization only. For that aim, the organic phase was prepared by mixing the

bifunctional monomers DATP and GDMA, and small quantity (20mol% of the thiol mononmers) of one trifunctional monomer, either TMPMP or TVCH. The overall thiol-ene ratio functionality was 1:1. Formulations are as depicted in Table 3.3.

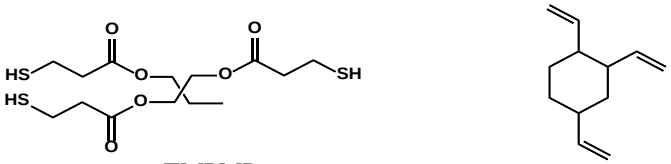

TMPMP

TVCH

Figure 3.2. Chemical Structure of trifunctional monomers TMPMP and TVCH

0.2 wt% (based on monomers' mass) of the thermal initiator AIBN was added to the organic phase and 6wt% (based on monomers' mass) of HD was added to the organic phase as a costabilizer to prevent Ostwald ripening. 30wt% solids content latexes were prepared in that way. Sonication was performed using a Branson Digital sonifier at 70% of amplitude, with a 0.5 sec on and 1 sec off pulsed program for 10 minutes.

Table 3.3. Formulations and synthesis conditions 30% solid content cross-linked sonopolymers obtained by sonopolymerization of the bifunctional monomers DATP, GDMA, and trifunctional monomers TVCH and TMPMP

Monomers	Mass DATP (g)
GDMA-DATP+TMPMP	6.2398
GDMA-DATP+TVCH	6.2462

3.2.2.3. Synthesis of nanocomposite based on thiol-ene polymer system and graphene oxide

- Preparation of reduced graphene oxide

Reduced graphene oxide (rGO) obtained by reduction of GO (10 mg/ml, Graphenea) using hydrazine monohydrate (Sigma Aldrich) in presence of polyvinylpyrrolidone (PVP-M=10 000 g/mol, Aldrich), as colloidal stabilizer. The preparation of rGO was carried out in few steps. First 100 ml of GO was stirred and sonicated in ice bath for 1 h with 0.5 s cycle and 70% amplitude. After that 2 g of PVP was added (2 %) which was previously dissolved in small amount of Milli-Q®. The third step was to introduce the dispersion in reactor that was heated to 60 oC, after which was added 0.2 ml of hydrazine monohydrate (GO: hydrazine monohydrate 5:1) as reducing agent, with continued stirring for 2 h. The last step was the dialysis of the dispersion for 2 weeks to eliminate side prodiucts of reduction reaction and excess PVP

- Blends thiol-ene system and graphene oxide

Dispersion of GO and rGO was added dropwise and under stirring with latexes based on thiol-ene polymers.

3.2.3. Film formation

Various films with a thickness in the following range 300-970 μm were prepared by casting of appropriate amount of the 30% and 50% solids content latexes into silicon moulds, and dried at standard atmospheric conditions (25ºC and 55% of relative humidity).). For sake of clarity, films based on the monomer couple GDMA-DATP are denoted F.AX, with F.A1 presenting lower molar mass than than F.A2. Films based on the monomer couple EDDT-DATP are denoted F.BX, and F.B1.HD displays lower molar masses than F.B2, and also contains 6wt% of HD. Finally, the film based on the monomer GDMP-DATP is referred to as film F.C. The main characteristics of the films are depicted in Table 3.4

Table 3.4 Films obtained after water evaporation of the latexes based on DATP, GDMA, EDDT and GDMP.

Film	Monomers	HD (wt%)	M_w (Da)
F.A1	GDMA-DATP	-	9135
F.A2	GDMA-DATP	-	22696
F.B1.HD	EDDT-DATP	6	52010
F.B2	EDDT-DATP	-	81152
F.C	GDMP-DATP	-	34618

3.2.4. Characterization

3.2.4.1. Miniemulsion and latex characterization

Average particle size of the miniemulsions and latexes was determined by dynamic light scattering (DLS) with a Zetasizer Nano ZS from Malvern Instrument. The samples for analysis were prepared by diluting a drop of the dispersion to approximately 1.5mL of MilliQ water, to avoid multiple light scattering.

The colloidal stability of the pre-polymer miniemulsion was assessed by measuring the backscattered signal over time with the equipment Turbiscan Lab.

Gel Permeation Chromatography (GPC) with THF as the carrier was utilized to determine molar mass (M_w) and polydispersity (PDI). Samples were prepared by dissolving dried polymers in THF at a concentration of 1mg/mL. The GPC instrument consists of an injector, a pump (Waters 510), three columns in series (Styragel HR2, HR4, and HR6), and a differential refractometer detector (Waters 2410). The equipment was calibrated using polystyrene standards. The molar masses reported were obtained by comparison with the polystyrene standards.

Proton nuclear magnetic resonance (^{1}H NMR) was used for the measurement of the final ene conversion, and the method is detailed in Appendix V. NMR spectra were recorded on a Bruker 400 MHz at 25 °C. Samples were prepared by dissolving dried 20mg aliquots in 0.5 mL of deuterated chloroform ($CDCl_3$-d^6) or deuterated Dimethylsulfoxide (DMSO-d^6).

3.2.4.2. Film characterization

The water uptake was measured by immersing films with similar rectangular shape (4.6 x 1.8 cm) and thickness (~0.6 mm) in distilled water in a close vial. The film were then withdrawn, gently dried with paper and weighted. The water uptake was determined as:

$$water\ uptake\ (\%) = \frac{m_t - m_0}{m_0} \times 100 \quad (3.1)$$

With m_0 weight of the film at t_0 ; m_t weight of the film at time t.

Chemical resistance was measured by immersing films with similar rectangular shape (4.6 x 1.8 cm) and thickness (~0.6 mm) in a 3% (w/v) acetic acid aqueous solution at a temperature of 25ºC. 3% (w/v) acetic acid solution is a frequently used as a test liquid for food packging application[19] to perform migration tests, and is reported as Food simulant B by Comission Regulation (EU) No 10/2011. The chemical resistance was evaluated by measuring the weight loss of the samples after 1 day, and 4 days of immersion. Samples were dried at 60ºC in order to be weighted.

Differential scanning calorimetry (DSC) was carried out on a differential scanning calorimeter Perkin Elmer DSC 8000 equipment from TA Instrument using an Intracooler II as a cooling system. Approximately 5 mg samples were encapsulated in aluminium pans. In the case of the films containing HD, a sealed aluminium pan was used. In this chapter, DSC was used to determine the glass transition temperature (T_g) of the films. For that aim, samples were heated at 20ºC/min up to 80ºC for the films F.A1 and F.A2, 90ºC for the films F.B1.HD and F.B2, 100ºC for the film F.C and 150ºC for the films FA, FB and their composites, and left 3

minutes in the melted state. They were then cooled at 10ºC/min until -30ºC for the films F.A1,F.A2 and F.C, -40ºC for the film F.C and -50ºC for the films FA, FB and their composites. Films were subsequently heated up at 20ºC/min to 80ºC (F.A1 and F.A2), 90ºC (F.B1.HD and F.B2) and 100ºC (F.C) and 150ºC (FA, FB, and their composites).

The morphology of the nanocomposite films was determined using scanning electron microscopy (SEM; Quanta 250 e-SEM, Philips Tecnai, Field emission, Schottky filaments). The samples were scanned without sputtering with metal. For cross-section imaging, the samples were fractured after being immersed in liquid nitrogen. Transmission electron microscopy (Philips TECNAI G2 20 TWIN) was used in order to examine the structure of the samples.

The mechanical properties of the films prepared for coatings application were evaluated by tensile test. The measurements were carried out using the TA.HD plus texture analyzer (Stable Micro Systems Ltd., Godalmming UK). Flat "dog-bone" shaped tensile test specimens with dimensions of 15 mm 3.5 mm 0.5 mm were cut from dry films for the tensile test measurements. With a constant strain velocity of 1.5 mm/s and a nominal strain rate of 0.1 Hz, stress-strain measurements were taken. Three specimens were prepared from each sample and the values presented are average of these measurements. The tensile properties for each material is represented in the stress-strain graphs.

Water vapour transmission rate experiments of the film F.A1 and F.C were performed at 25 °C with a gravimetric cell in which a small amount of liquid water was sealed by the film. The cell was put on a weighting scale with a readability of 10−5 g and the weight loss in time

(Permeate flow) of the cell, solely due to the permeation of the water vapor through the film,was registered by means of a computer connected to the scale. The water vapour transmission rate (WVTR) can be defined by:

$$WVTR = \frac{m \times f_{thickness}}{A \times (a_{int} - a_{ext})} \text{..... (3.2)}$$

Where m is the weight loss in time (Permeate flow) of the cell; $f_{thickness}$ is the film thickness (91.1μm for F.A1 and 30 μm for F.C); A is the exposed area of film (2.54 cm^2); a_{int} is the water activity which is equal to 1 inside de cell and a_{ext} is the penetrant activity outside the cell (assumed to be equal to the relative humidity in case of water). In all cases values of 0.3 of relative humidity (one percent) in the outside of the cell was considered.

3.3. Results and discussion

3.3.1. Photopolymerization in miniemulsion in presence of radical scavenger

In this part, the implemented strategy to obtain chemically and colloidally stable miniemulsions is explained with the model monomer pair GDMA-DATP.

As discussed in Chapter 2, premature polymerization is one of the main challenges of the thiol-ene chemistry. The spontaneous reaction between GDMA and DATP monomers could be efficiently prevented in bulk by using the DBHQ radical scavenger with 0.002 equivalent, calculated in bulk condition with regards to the amount of the thiol. When working in miniemulsion, chemical instability is worsen by the sonication step, which brings additional energy to the system and leads to significant monomers' conversion. It was reported more than

80 % conversion of DATP (measured by ^{1}H NMR) for a 20% solids content miniemulsion polymerization of GDMA-DATP, without the use of radical scavenger after 5 minutes of sonication.[3] Noteworthy, various miniemulsions based on GDMA-DATP monomers were prepared without the use of costabilizer, due to the limited solubility of HD in the thiol-ene monomers. To assure chemically stable miniemulsions, which is an indispensable condition for reproducible polymerization reactions, the addition of radical scavenger with at least 0.002 equivalent was necessary. Consequently, no polymer formation was observed by GPC after the sonication step, attesting for the preparation of chemically stable monomer droplets.

In Table 3.5, the formulations and average particle sizes of GDMA-DATP miniemulsions are shown, for various amounts of radical inhibitor DBHQ and surfactant Dowfax2A1. Four sets of experiments were performed, and are denoted as M.1, M.2, M.3 and M.4.

In the first set of experiments M.1, the miniemulsions obtained using 1.5 wt% surfactant Dowfax 2A1 and 0.002 equivalent of DBHQ displays very high average droplet size, higher than one micrometre (Entry M.1 Table 3.5). Although this miniemulsions is colloidally stable, as assessed by measurement of the intensity of the light backscattered from the miniemulsion in time (Figure I.1.a for miniemulsion M.1, Appendix I), high droplet sizes is precluded in our work because of the photopolymerization step, in which higher light scattering will limit the light penetration depth. It has been reported that for polymerization induced photochemically in miniemulsion, small droplet size impacts positively the reaction kinetics because of the decreased light scattering and improved light penetration depth.[20] In this case, probably there

was not enough amount of surfactant to stabilize the small droplets created during sonication, due to the important increase of the droplet surface area. Therefore, they aggregated forming larger droplets, as observed in Table 3.5. Hence, in the next batch of miniemulsions, the quantity of surfactant Dowfax 2A1was increased to 4 wt% (Entry M.2 Table 3.5), in which the droplet sizes decrease substantially, likely due to the surfactant stabilization effect over the small droplets created by sonication.

Table 3.5. Formulation and characterization 20% solid content miniemulsions prepared from the monomer pair GDMA-DATP. Sonication conditions were kept constant (5 minutes of sonication with 1sec on and 0.5sec off pulsed program, and 80% of amplitude).

Entry	GDMA:DBHQ	Dowfax 2A1 (wt%)*	Droplet size (nm)	Colloidal stability **
M.1	1.000:0.002	1.5	1600	Good
M.2	1.000:0.002	4	233	Good
M.3	1.000:0.003	4	1243	Bad
M.4	1.000:0.004	4	712	Good

*Weight based to monomer; ** determined from Figure I.1 in Appendix I

On the other hand, the increasing amount of radical scavenger affected negatively the droplet size DBHQ (Entries M.3 and M.4, Table 3.5) and the colloidal stability (M.3, Figure I.1.c, Appendix I). DBHQ is solubilized in organic phase of the miniemulsion, however it partitions between the both phases (partitioning coefficient octanol/water log P_{ow}=4.85[21]). In such conditions, the hydrophilicity of the monomer droplets is raised and their diffusional degradation (Ostwald ripening) is promoted.[22]

The colloidally and chemically stable 20 % solid content miniemulsions (M1, M.2 and M.4) were photopolymerized in the presence of water soluble initiator TPO-Li under UVA light with irradiance of 7 mW/cm^2. The molar mass and PDI, droplet size, particle size and double bond conversion (DBC) of the obtained latexes are shown in Table 3.6.

Table 3.6. Characterization of the 20% solid content latexes obtained from colloidally and chemically stable GDMA-DATP miniemulsions. For all formulations, the stoichiometric ratio GDMA:DATP is 1.000:1.000. Photopolymerization was performed in presence of 0.5wt% (based on monomers mass) of TPO-Li for 1 hour and irradiance of 7 mW/cm^2.

Latex	GDMA:DBHQ	Droplet size (nm)	Particle size (nm)	M_w (kDa)	PDI	DBC (%)
P.1	1.000:0.002	1600	210	26	2,01	98
P.2	1.000:0.002	233	153	34	1.87	98
P.4	1.000:0.004	712	151	22	4,12	97

Linear poly(thioether) latexes (P.X) were synthesized by photoinitiated miniemulsion polymerization with rather similar particle size, even though the miniemulsions presented large droplet sizes with important differences in diameter of the droplets, indicating rather emulsion polymerization like process. High conversion, above 97%, were reached through this process.

Molar masses are notably higher when miniemulsion's droplet size is smaller (Entry P.2 Table 3.6). This can be attributed to radical compartmentalization in dispersed system, leading to a decrease of termination reaction occurring by radical combination in thiol-ene polymerization.[7] Namely, for lower particle size, lower is the average number of radicals per

particle,[23] therefore the termination process is less important and the chains grow larger. In the thiol-ene miniemulsions, in the initial process there is large difference of droplet sizes. Under assumption that droplet nucleation (typical for miniemulsion polymerization) occurs, as initially mostly thiol-ene dimmers and smaller oligomers are formed, more pronounced termination in larger droplets/particles will likely lead to lower molar masses. Le *et al*.[6] reported that the use of the water-soluble photoinitiator lithium TPO-Li promoted –unfavourable- homogeneous nucleation in the preparation of linear poly(thioethers) based on DAP and EDDT.[24] Homogeneous nucleation occurred independently on monomer solubility, but was affected by droplet size. Indeed, when the droplet size was low enough (100 nm and below), droplet nucleation was prevalent. In our case, the lower droplet size in M.2 might promote droplet nucleation compared to other formulations in which homogeneous nucleation is happening, yielding to lower molar masses. Nevertheless, according to Table 3.6 (Entries P.2 and P.4) the important decrease of the particle size with respect to droplet size indicates that there is still homogenous nucleation occurring, promoted by the lack of costabilizer and probably important monomer diffusion throughout aqueous phase and high quantity of surfactant that stabilizes the new formed particles by homogeneous nucleation. This confirms the emulsion nature of the polymerization.

When 0.004 equivalent of DBHQ was used, slightly lower DBC (97%) and molar masses are obtained (Entry P.4, Table 3.6) than in case of P.3 reactions in which DBHQ of 0.002 equivalent was used (Entry P.3, Table 3.6). It might be a result on larger droplets initially and even more promoted monomer diffusion in presence of DBHQ which induced higher stoichiometric imbalance. This result show that a good balance between radical inhibitor and

radical initiator needs to be reached to optimize the step-growth mechanism and yield to poly(thioethers) with controlled molar masses (or radical inhibitor quantity can be another parameter to control the process and product).

It is worth mentioning that this line displays several limitations for the objective of this thesis. First, reproducibility was unsatisfactory, and colloidal stability issues occurred when reproducing miniemulsions M.1, M.2, M.3 and M.4. Possible reasons behind the irreproducibility can be the presence of DBHQ that destabilize the miniemulsions. Hence, the objective to increase the solid content of the dispersions is limited. Moreover, an additional aim of the thesis is to study in fine the crystalline behaviour of the film forming poly(thioethers). The crystalline behaviour can be highly influenced by the presence of additional species such as the radical inhibitor. Therefore, attention was drawn toward another strategy in which formulation had to be simplified.

3.3.2. Sonopolymerization combined with photopolymerization

3.3.2.1. Sonopolymerization step

Searching for a way to improve the control of the process and products, and simultaneously attempting to increase further the molar masses, advantage was taken from the high reactivity of the thiol-ene system. Namely, instead of addition of radical scavenger to prevent the premature reaction during sonication step employed to prepare the miniemulsion, this step was utilized to produce pre-polymers that can be photopolymerized afterwards to increase their molar masses.

For that aim, miniemulsions based on GDMA-DATP, GDMP-DATP and EDDT-DATP were prepared and rapidly converted into “pre-polymer” (S.X) during the homogenization step by sonication, without use of radical scavenger nor initiator. The reaction conditions and characteristics of the dispersions and polymers are depicted in Table 3.7. Due to the interest to increase the solids content for the film forming aims, 30% and up to 50% latexes were prepared. The effect of sonication time on the particle size, DBC and molar masses were studied for different thiol-ene pairs.

Table 3.7 Sonopolymers or pre-polymers obtained by sonopolymerization of the bifunctional monomers DATP, GDMA, EDDT and GDMP. Sonication was performed at 70% of amplitude, with a 0.5 sec on and 1 sec off pulsed program, in presence of 1.5wt% of Dowfax 2A1 (calculated based on monomers mass).

Entry	Monomers	AIBN (wt%)	HD (wt%)	Solids content (%)	Stoechiometric ratio thiol:ene	Sonication time (min)	Particle size (nm)	DBC (%)	Mw (kDa)	PDI
S.1	GDMA-DATP	-	-	30	1.000:0.999	10	237	96	9	2.53
S.2	GDMA-DATP	-	-	30	1.000:0.999	10	194	96	13	3.18
S.3	GDMA-DATP	0.2	-	30	1.000:1.000	10	202	97	11	2.83
S.4	EDDT-DATP	-	6	30	1.000:1.000	7:30	175	99	23	3.65
S.5	EDDT-DATP	-	-	30	1.000:1.000	7:30	191	95	5	2.62
S.6	GDMP-DATP	-	-	30	1.000:1.000	7:30	274	89	7	2.47
S.7	GDMA-DATP	-	-	50	1.000:1.000	20	195	95	8	2.80
S.8	EDDT-DATP	-	-	50	1.000:1.000	10	331	95	1	1.73
S.9	GDMP-DATP	-	-	50	1.000:1.007	10	213	96	9	2.85

Latexes from sonopolymers S.1, S.2, S.3, S.6, S.7 and S.9 (Table 3.7) were synthesized without costabilizer, due to a solubility issue of the conventional costabilizer HD with the thiol monomers GDMA and GDMP. As the dithiol EDDT is miscible with HD, miniemulsion based

on the monomer pair EDDT-DATP were prepared using HD as costabilizer (Entry S.4, Table 3.7). The same reactions were prepared without HD (Entries S.5 and S.8, Table 3.7) for comparison aim with the other reactions and allowing study on the effect of the costabilizer.

A portfolio of pre-polymer latexes based on a stoichiometric ratio of thiol and ene monomers were obtained from sonopolymerization, with solids content of 30% (latexes S.1, S.2, S.3, S.4, S.5 and S.6). The solids content was further increased to 50% (latexes S.7, S.8, S.9). These latexes were colloidally stable over time, as assessed by the repeatability of the light backscattered by the dispersions over time (Figures I.2 Appendix I) and by a particle size measured by DLS ranging from 175 to 331 nm (Table 3.7). Synthesizing pre-polymers during sonication i.e miniemulsification step, can be used as a strategy to obtain colloidally stable particles that can be further polymerized or functionalized in an additional step. Indeed, hydrophobic and high enough molar mass chains increased the hydrophobicity of the particles, preventing the monomer droplets diffusional degradation (Ostwald ripening), taking a role of costabilizers during the miniemuslification/sonopolymerization. In thiol-ene polymerization, following a step-growth mechanism, monomers are rapidly converted into dimers, trimers and oligomers in very restrained timescale. These oligomers delay Ostwald ripening effect because of slower rate of diffusion through the aqueous phase.[14] Combined with the surfactant preventing the droplet/particle degradation by coalescence, pre-polymer particles yet still reactive were prepared.

The pre-polymers or sonopolymers presented relatively high molar masses considering that they were polymerized by step growth mechanism and high conversion achieved through

sonication (above 89%, measured by ^{1}H NMR). At 30% solids content, sonopolymers with a molar mass of about 9 kDa (Entry S.1, Table 3.7) and 13 kDa (Entry S.2, Table 3.7) were obtained for the monomer pairs GDMA-DATP with PDI of 2,53 and 3.18 respectively. The different molar masses observed for the sonopolymers S.1 and S.2 can be induced either by smaller particle size, but most probably by a small stoichiometric imbalance between the thiol and ene monomer, smaller than the precision of the balance, as it is known that even such small imbalance results in differences in molar mass of resulting step-grown polymers.[17] As explained in Chapters 1 and 2, in the case of A-A and B-B monomers combination into linear addition polymers, the Carothers equation (Eq. 3.3) relates the degree of polymerization to the extent of reaction and the stoichiometric ratio between functionality, where $\bar{X}_n$ is the number-average degree of polymerization, p is the conversion and r is the monomers stoichiometric ratio (Eq. 3.4).

$$\bar{X}_n = \frac{1+r}{1+r-2pr} \quad \text{……. (3.3)}$$

$$r = \frac{[\mathrm{A-A}]}{[\mathrm{B-B}]} \quad \text{…….. (3.4)}$$

$$\text{with } [\mathrm{A-A}] \leq [\mathrm{B-B}]$$

The Carothers equation highlights the stringent requirements of the stoichiometric balance between thiol and ene monomers and conversion to enable molar mass control in step growth polymerization. Hence, it is unlikely to obtain the same molar mass for polymers synthesized from two different reaction, even though big efforts are implemented to reach the same reaction conditions. An attempt to increase the conversion and molar mass of

sonopolymers based on GDMA-DATP was carried out by adding 0.2 wt% (based on monomer mass) of the oil soluble thermal initiator AIBN (Entry S.3, Table 3.7), as the sonication step induces an increase of temperature within the reactional mixture. Even though an ice bath is used to limit this effect there is "hot spots" creation in the reaction mixture in which very high temperatures can be reached, which likely thermally initiate the step-growth polymerization and results in the synthesis of sonopolymers. In the presence of the thermal initiator AIBN, the DBC (97%) and final molar mass of sonopolymers S.3 (11 kDa) was not increased significantly in comparison to the same reaction without initiator S.1 (with a DBC of 96% and a molar mass of 9 kDa). Hence, the rest of the sonopolymers were synthesized without addition of initiator. Even though in presence of AIBN higher number of radicals were created, this likely increased the bimolecular termination process (or recombination of initiator radicals). Therefore, no positive effect on the molar mass was achieved.

For the monomer couple EDDT-DATP at 30% solids content with and without HD (entries S.4 and S.5, Table 3.7, respectively), polymers with a molar mass of about 23 kDa with a PDI of 3.65 and 5 kDa with PDI of 2.62 were obtained. The conversion reached in presence of HD is higher, with a DBC of 99% for S.4 and a DBC of 95% for S.5. The presence of HD provides improved colloidal stability and prevent monomer diffusion efficiently, which as mentioned is crucial to keep 1:1 molar ratio of the thiol to ene within each droplet/particle to ensure large chain lengths. Probably this is the main reason that the polymer synthesized in presence of HD presents the highest DBC and molar mass than all other sonopolymers, which have molar masses in the a range of 5 - 13 kDa. This fact highlights that, when the miniemulsion was prepared without HD, even though the oligomers are produced early in the reaction, still

there is a monomer diffusion that promotes the stoichiometric imbalance within individual particles (nanoreactors). Hence, the use of costabilizer seems to be an additional tool to increase the molar masses of the step-grow emulsion polymers.

When sonopolymerization is performed at increased solids contents of 50%, no significant change in molar mass is observed, except for the poly(thioethers) based on EDDT-DATP. The sonopolymer based on GDMA-DATP at 50% solids content presents a slightly lower conversion (DBC of 95%, Entry S.7 Table 3.7) and lower molar mass of about 8 kDa (Entry S.7, Table 3.7) than sonopolymers S.1 and S.2 synthesized at 30% solid content (DBC of 96 % and molar masses of 9-12 kDa). In the case of the sonopolymers based on the monomer pair GDMP-DATP, the BDC is increased from 89% to 96% and the molar mass is increased of about 7 to 9 kDa (Entry S.6 and S.9, Table 3.7) when sonication is performed at 50% solids content. A significant drop in molar mass from 5 kDa (Entry S.5, Table 3.7) to 1 kDa (Entry S.8, Table 3.7) is observed for the EDDT-DATP sonopoly(thioethers) synthesized at increased solids content. The higher viscosity of 50% dispersions than 30% implies the requirement of higher energy input to achieve the same particle sizes, polymerization extent and similar molar masses. To check this and to reach higher conversion and hence molar masses of the sonopolymers of 50% solids content dispersions, sonication time was increased further to 25 minutes for monomer pair GDMA-DATP (Latex S.10, Table 3.8) and up to 12 minutes for the monomer pair EDDT-DATP (Latex S11. Table 3.8).

Table 3.8. Synthesis conditions of 50% solid content polysulfide latexes produced by sonopolymerization in dispersed media of the monomer pairs GDMA-DATP and EDDT-DATP. S.10 and S.11 were synthesized with longer sonication time. Sonication was performed with the same pulsed program (0.5 sec on 1 sec off). No costabilizer was used.

Entry	Monomers	Stoechiometric ratio thiol:ene	Sonication time (min)	Particle size (nm)	DBC (%)	Mw (kDa)	PDI
S.7	GDMA-DATP	1.000:1.000	20	195	95	8	2,80
S.10	GDMA-DATP	1.000:1.000	25	280	94	8	3,46
S.8	EDDT-DATP	1.000:1.000	10	331	95	1	1.73
S.11	EDDT-DATP	1.000:0.999	12	198	89	6	2.93

This strategy did not extend the degree of polymerization as no important increase of the molar masses is observed after sonication for the polymer based on GDMA-DATP (Entries S.7 and S.10. Table 3.8). One on hand, this may be a result of high conversion of GDMA (and higher conversion 95%), thus, extended sonication did not introduce further important changes in the degree of polymerization and, molar mass.

Molar masses are substantially increased for longer sonication time of the EDDT-DATP dispersions (Entries S.8 and S.11, Table 3.8) although the DBC is lower after 12 min of sonication time. This result is not without ambiguity, as higher stoichiometric imbalance was also measured in that case, which should yield to lower molar masses. Perhaps for that system, the excess of thiol moieties from EDDT is beneficial to obtain higher molar masses, as thiol dimers might be present in the mixture. Similar observations have been made for the thiol-ene system based on EDDT-DAA in which the excess of ene moieties, certainly involved in other

side reactions (such as homopolymerization) than the thiol-ene step-growth mechanism, yielded to higher molar masses[7]. Thus, prolonged sonication together with stoichiometric imabalance promote further the molar masses in that case.

Noteworthy, expending sonication time even further led to coagulation. Indeed, higher sonication time can induce coagulation by increasing temperature and collision between droplets. Determining the optimal conditions for miniemulsification step can be challenging because the colloidal properties are changed, too, and they additionally affected the molar masses. On one hand, droplet size decreases with sonication time,[25] and the colloidal stability is ensured by the surfactant. On the other hand, too long sonication time provoke the collapse of monomer droplets, and the surfactant is no longer able to prevent coagulation. Herein, a good balance between these parameters was established in short sonication times that seems to be indispensable for attaining stable oligomers dispersions.

3.3.2.2. Photopolymerization step

The oligomers produced by sonopolymerization contain free thiol and ene functionalities, which is the pre-requisite to extend the molar mass in the second step of phopolymerization. For that aim, the pre-polymer latexes S.2 and S.4 to S.11 were photopolymerized in an additional step in the presence of the water-soluble photoinitiator TPO Li, yielding a range of photopolymers (SP.X, Table 3.9).

Table 3.9. Poly(thiolethers) obtained from sonopolymerization combined with photopolymerization step. Photopolymerization was performed for 1 hour at an irradiance of 7 mW/cm^2 in presence of 0.5 wt % of TPO-Li.

				After sonication step				After UV exposure			
Entry	Monomers	Costabilizer HD (wt%)	Solid content (%)	Particle size (nm)	DBC (%)	M_w (kDa)	PDI	Particle size (nm)	DBC (%)	M_w (Da)	PDI
SP.2	GDMA-DATP	-	30	194	96	13	3.18	185	99	23	4.02
SP.4	EDDT-DATP	6	30	175	99	23	3.65	173	99	52	4.07
SP.5	EDDT-DATP	-	30	191	95	5	2.62	222	99	81	2.53
SP.6	GDMP-DATP	-	30	274	89	7	2.47	299	99	35	4.22
SP.7	GDMA-DATP	-	50	195	95	8	2.80	257	99	20	3.91
SP.8	EDDT-DATP	-	50	331	95	1	1.73	308	99	20	3.48
SP.9	GDMP-DATP	-	50	213	96	9	2.85	293	99	28	4.32
SP.10	GDMA-DATP	-	50	280	94	8	3.46	271	98	18	5.62
SP.11	EDDT-DATP	-	50	198	89	6	2.93	208	99	120	15.72

The DBC are substantially increased (above 98%) and hence molar masses, and 30% solids content poly(thioethers) of 23kDa for SP.2, 52 kDa for SP.4, 81 kDa for SP.5 and 35 kDa for SP.6 were obtained (Table 3.9). The subsequent photopolymerization also increased slightly the polydispersity of the polymer chains, with PDI ranging from 2,63 to 4,22 (Table 3.9). During the process of photopolymerization, the initiator radicals, created from photoinitiator in combination with UVA light, react with the thiol-containing pre-polymers produced during sonopolymerization (Figure 3.3). The thiyl macroradical created reacts further with ene-containing pre-polymer chains, and so on, producing on one hand much larger molar masses chains and on the other hand wide distribution of chains with different molar masses.

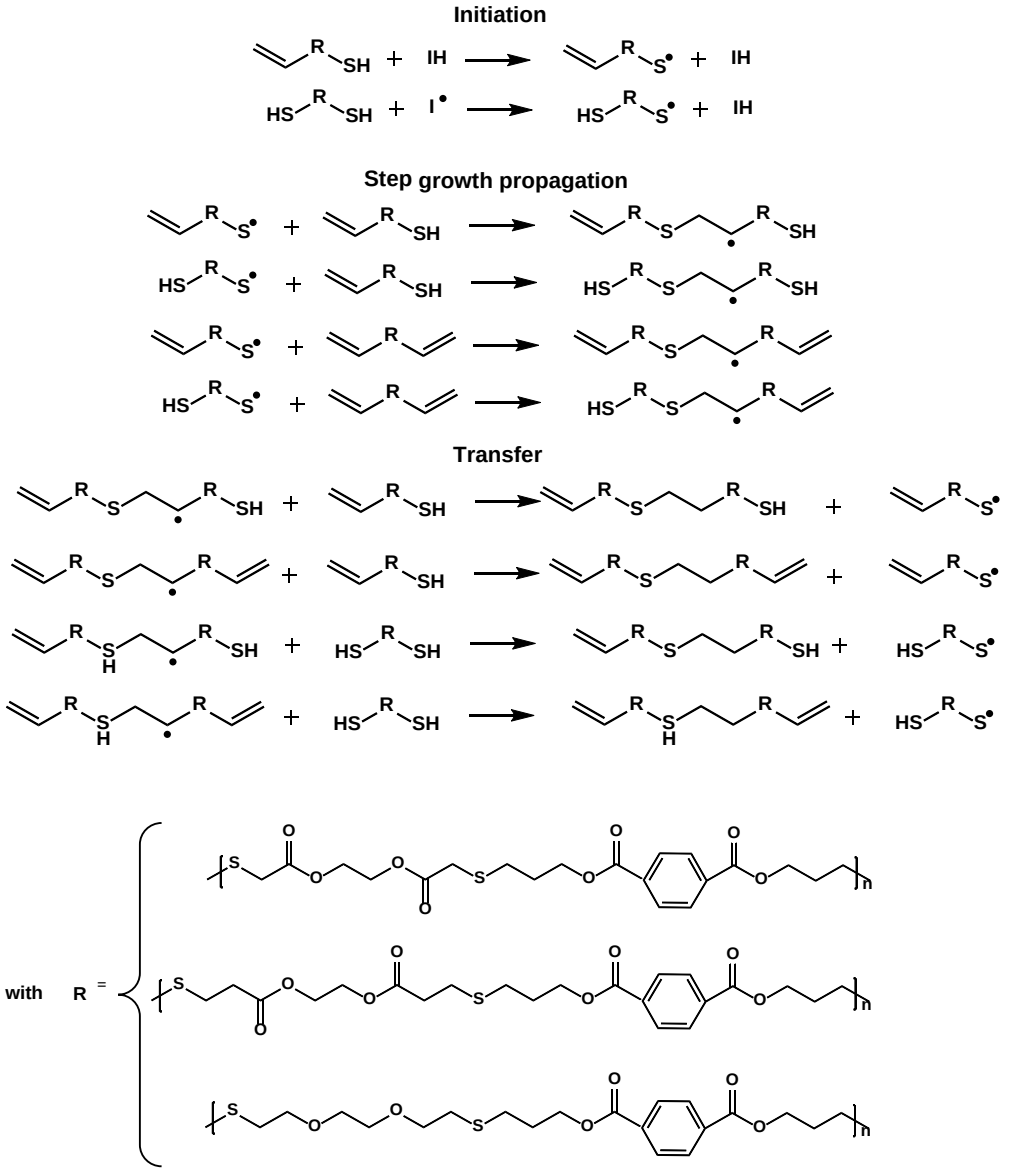

Figure 3.3. Photopolymerization mechanism of the thiol-containing pre-polymers.

The same trend is observed when miniemulsion of 50% solid content were prepared, giving rise to polymers with molar mass of 20 kD for SP.7, 196 kDa for SP.8 and 28 kDa for SP.9 and PDI ranging from 3,48 to 4,32 at high conversions (Table 3.9). Noteworthy, when sonopolymers based on EDDT-DATP were synthesized at extended sonication time, photopolymerization led to molar masses higher than 120 kDa (SP.11) up to 200 kDa (SP.8) with extended polidispersity up to 15.72 for SP.11 (Table 3.9). In thiol-ene photopolymerization, PDI between 2 and 3 are generally reported,[2,4,6] because of the step-growth mechanism. The increase of PDI after photopolymerization in all cases can be expected as pre-polymers with wide chain length distributions are combined, producing photopolymers with even further extended distribution of the chain lengths.

These results emphasize the fact that after sonopolymerization, the prepolymer chains are still reactive and very high molar masses can be achieved in an additional step of photopolymerization. Moreover, these results indicate that after sonopolymerization, the pre-polymers based on the pair EDDT-DATP are still bi-functional, because this can be explanation behind the huge molar masses obtained (up to 200 kDa). In the literature, the average molar mass (Mn) reported for poly(thioethers) containing EDDT monomers and synthesized in miniemulsion are in between 35 and 60 kDa with the dienes DAA[5,7], DAP[4,6], or divinyl adipate (DVA)[7]. For our system, hence, the combination of sonopolymerization and photopolymerization turns out to be an efficient tool to produce particularly high molar mass step-growth polymers.

It is worth mentioning that in the second step of photopolymerization, the presence of HD is not already crucial, as the SP.4 in presence of HD presented lower molar mass than SP.5 without the costabilizer. The reason behind this behaviour is already very low monomer concentration within the droplet and limited effect of the monomer diffusion.

In conclusion, the synthetic approach combining sonopolymerization and photopolymerization seems particularly suited for obtaining thiol-ene step growth polymers with high molar masses. This could be explained by the very good colloidal stability obtained after miniemulsification step for pre-polymer particles P2 to P8 allowing further efficient photopolymerization, even at high solids content such as 50%.

3.3.3. Film formation of linear poly(thioethers)

In the scope of the aimed application of the thiol-ene polymer dispersions in coatings displaying barrier properties, to combine excellent barrier properties and good film forming ability, the polymer microstructure is of the most importance, therefore, linear and crystallisable polymer chains are indispensable. Hence, attention is turned toward film forming ability of linear poly(thioethers), synthesized from bifunctional monomers.

The latex film formation can be divided into three steps.[26] After casting the latex on a substrate, the first step consists of water evaporation, leading to ordering of polymer particles and their close packaging. In the second step, the interstitial water remaining in-between the polymer particles disappears, allowing their deformation into a tetrahedral or honeycomb like shape. At this stage, the polymer particles integrity remains intact. The last step involves particle

coalescence and subsequent interdiffusion of polymer chains across particle interfaces to fuse the particles boundaries. This last step is of primary importance when it comes to mechanical properties, usually required for coating applications. Interdiffusion of polymer chains occurs at temperature above their T_g and is driven by Brownian motion. Indeed, obtaining of continuous coating films through film formation process from waterborne dispersions is very challenging, as each step affects drastically the final film morphology and therefore its properties. Good cohesion of a latex film is achieved when polymer particles deformed sufficiently and polymer chains from different particles have interdiffused between them and created entanglements. For this, it is important that the T_g of the polymer is lower than film forming temperature (lower than ambient temperature if the films should be formed at ambient conditions). On the other hand, too low T_g may result in very soft polymer film that does not respond to the minimum requirements of mechanical resistance. These two contradictory requirements are the main challenges of the film forming ability of polymer dispersions, especially when good mechanical properties are expected for targeted applications such as barrier coating.

Latexes based on the monomer pair GDMA-DATP, EDDT-DATP and GDMP-DATP at standard atmospheric conditions (temperature of 25ºC and relative humidity of 55%) gave rise to formation of homogeneous films. Herein, we focus only on the films obtained from the 30% solids content latexes, labelled F.A1 to F.C (Table 3.10 and photos in Figure I.3, Appendix I).

Table 3.10. Details on the films obtained after water evaporation from the latexes based on GDMA-DATP, GDMP-DATP and EDDT-DATP. For the synthetic processes, S stands for sonopolymerization and SP stands for sonopolymerization combined with photopolymerization.

Latex	Film	Monomers	Synthetic process	Solid content (%)	HD (wt%)	M_w (kDa)	T_g (ºC)*
S.1	F.A1	GDMA-DATP	S	30	-	9	-15.6
SP.2	F.A2	GDMA-DATP	SP	30	-	23	-7.8
SP.4	F.B1.HD	EDDT-DATP	SP	30	6	52	-22.3
SP.5	F.B2	EDDT-DATP	SP	30	-	81	-22.6
SP.6	F.C	GDMP-DATP	SP	30	-	35	-14.6

*T_g values were obtained from non-isothermal DSC analysis of the films, supplied in Figure I.4, Appendix I

The films are consistent and suitable for coatings application. Moreover, they are self-supported, which allows further characterizations. As the intended application is in food packing application, the barrier to humidity or oxygen are of upmost importance. In the thiol-ene polymers, this is expected to be provided by the crystalline structures created within these films, as reported previously.[4,5]The films based on EDDT-DATP (F.B1.HD, and F.B2 Table 3.10 and Figure I.3, Appendix I) and GDMP-DATP (F.C, Table 3.10 and Figure I.3, Appendix I) are opaque, white and ductile compared to the films based on GDMA-DATP (F.A1 and F.A2, Table 3.10 and Figure I.3, Appendix I) that are transparent and flexible. This could be first qualitative appreciation of the presence of crystalline domains. In Chapter 4, a deeper study of the crystallization behaviour of the thiol-ene polymer chains is presented, with attempts to control the crystallization kinetics.

Water sensitivity of polymer films aimed for coating application is an important characteristic, and is determined by water uptake measurements. For that aim, the water uptake of the films F.A1, F.A2, F.B1.HD, F.B2 and F.C was measured during 7 days and is shown in the Figure 3.4.

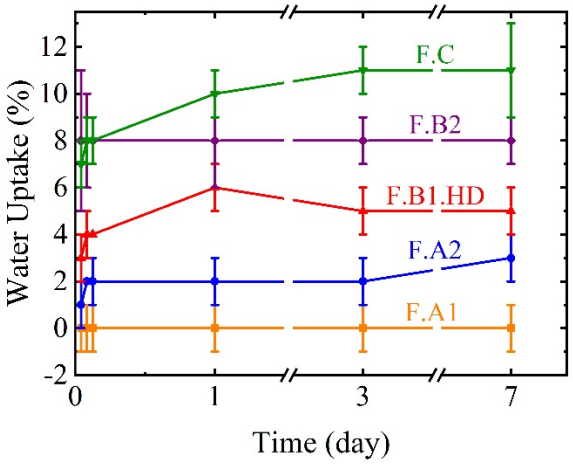

Figure 3.4 Water uptake F.A1, F.A2, F.B1.HD, F.B2 and F.C.

The water absorption of the waterborne films is often attributed to the migration of the hydrophilic surfactant during the film formation process, which creates aggregates within the film, able to absorb large water quantity from the surrounding. The presence of crystalline structures within the present films might limit water diffusion by forming physical obstacles to the water diffusion within the film. Indeed, in the case of PVDC, excellent barrier properties are provided by the presence of crystalline structures with a degree of crystallinity X_c ranging from 35% to 50%.[27,28]

The studied films present low water uptake after one day (below 12%), and noticeably the film F.A1 does not absorb any water with a water uptake close to 0%. This is a very unusual result for waterborne polymer films synthesized using conventional surfactants (Dowfax 2A1 in this case). The low T_g of the polymers in range -7.8ºC to -22.6ºC allows formation of very good quality films for all polymers studied. Probably the crystal structures developed during the film formation, along with the aromatic structure provided the necessary stiffness. Nevertheless, F.A1 presents the lowest molar mass from all of the studied films, which likely positively affected the film formation process. It is well known that the interdiffusion of the lower molar mass polymer chains between throughout the borders of polymer particles is easier[26]. Therefore, due to the such a low molar mass of about 9 kDa the interdiffusion of the polymer chains created strong entanglements, which along to the low Tg, resulted into very compact film. As only FA1 film was obtained without use of initiator, the lack of hydrophilic moities in the chains increased their hydrophobicity. Finally, the crystal structures likely formed inside probably improved further the water sensitivity.

Water vapour permeation tests were performed on the films F.A1 and F.C and results are presented in the Table 3.11. The films F.B1.HD and F.B2, too brittle, could not be tested, as sufficiently quality film for this test could not be prepared.

Table 3.11. Water vapour permeation through the films F.A1 and F.C

Film	**WVTR (g*mm/m^2*day)**
F.A1	2
F.C	11,9

In line with the data obtained by water uptake experiments, the film based on GDMA-DATP monomers (F.A1) presents the best results in terms of water vapour transfer. Moreover, the obtained value is within the range of water vapour permeations data reported for commonly used commercial barrier coating, which are between 0.1 and 30 g*mm/m^2*day.[29] This means that the crystalline structures are distributed within the amorphous matrix in a way to create a barrier to the paths that might be created by the hydrophilic species present in the film (initiator and surfactant). This result unlocks the potential of the waterborne poly(thioethers) in barrier coatings application as a possible and more environmental replacement of the current PVDC coatings.

The chemical resistance of poly(thioether) films based on the model monomer pair GDMA-DATP and synthesized with various processes was also investigated, to better understand which parameters affect this important property for coating application.

A first attempt to investigate the chemical resistance of linear GDMA-DATP films was performed by measuring the solvent uptake in ethanol, acetone, toluene, N,N-dimethylformamide (DMF) and diethyl ether. This study revealed the poor resistivity of linear GDMA-DATP films in contact with organic solvents, but differs from the requirements needed by the application we are targeting.

In order to get closer to the final application in food packaging, we decided to follow the standard testing methods that are usually used in packaging industry. For that aim, the films

were deepen in a 3% (w/v) acetic acid aqueous solution at a temperature of 25ºC and the resistance of films based on GDMA-DATP latexes was studied. 3%(w/v) acetic acid solution is a frequently used as a test liquid for food packaging application[19] to perform migration tests, and is reported as Food simulant B by Comission Regulation (EU) No 10/2011.

A range of linear GDMA-DATP latexes were synthesized via sonopolymerization (denoted S) or photopolymerization (denoted P) in dispersed media, with molar masses ranging from 7 kDa to 24 kDa as reported in Tables 3.12. Latex A was synthesized by sonopolymerization without addition of a radical initiator, whereas latex B was obtained from the same process with 0.2 wt% (based on monomers's mass) AIBN. Latexes C and D were obtained by photopolymerization in miniemulsion, initiated by 0.5 wt% of the water-soluble photoinitiator TPO-Li. Homogeneous films F1a, F1b, F2a, F2b, F3a, F3b and F4 (photos in Figure I.5, Appendix I) were obtained by water evaporation at different drying conditions (temperature and humidity), shown in Table 3.12. Namely by forming the film under higher temperature, the water evaporation rate increased, too, changing the properties of the obtained film. Humidity has opposite effect on the film forming process and usually increased humidity improved the quality of the film due to slower water evaporation. It is worth mentioning that the temperature was not changed importantly, to form the film at different ambient conditions (lower or higher humidity).

Table 3.12. Films obtained by water evaporation of GDMA-DATP latexes A, B, C and D for migration tests with food simulant B. The synthetic process employed to synthesize the latexes is labelles S for sonopolymerization and P for photopolymerization. The molar masses, PDI and drying conditions at wich the films were employed are also reported.

Latex	Synthesis process / Initiator (wt%)*	Solid content	Surfactant (wt%)*	Mw (Da)	PDI	Drying conditions		Film
						Temperature (°C)	Humidity (%)	
A	S	30 wt%	1.5wt%	7945	2.43	25	55	F1a
						23	80	F1b
B	S AIBN 0.2wt%	50 wt%	1.5wt%	7481	2.67	25	55	F2a
						23	80	F2b
C	P TPO-Li 0.5wt%	20 wt%	4wt%	23975	3.94	25	55	F3a
						23	80	F3b
D	P TPO-Li 0.5wt%	30 wt%	1.5wt%	14471	4.09	25	55	F4

***** present in the film after water evaporation based on GDMA-DATP monomers' mass

After 4 days of immersion in food simulant B under stirring, the tested films presented good chemical resistance, with low mass loss below 2wt%, except for the film F3a in which the mass loss is significantly higher (6 wt%).

Table 3.13. Films dissolution in contact with food simulant B. Mass loss (wt%) after 1 and 4 days in contact with food simulant B solution.

Film	Mass loss after 1 day in contact with food simulant B (wt%)	Mass loss after 4 days in contact with food simulant B (wt%)
F1a	1	1
F1b	1	2
F2a	2	2
F2b	1	1
F3a	4	6
F3b	2	2
F4	1	2

As explained previously, the water dissolution of waterborne polymer films is often attributed to the migration of the hydrophilic surfactant and small polymer chains to the aqueous phase. The polymers produced by photopolymerization contain fragments of water-soluble initiator in the chains, which increased their hydrophilicity. Moreover, they present larger PDI, indicating wider molar mass distribution than the polymers produced by sonopolymerization. Even though the molar masses of the last are much lower, the large PDI indicates that there are lower mass oligomers in the photopolymers, which additionally are more hydrophilic due the initiator fragments. The photopolymer film F3a was obtained by water evaporation of the latex C at 25ºC and 55% humidity, presenting a solid content of 20 wt%, 4wt% of surfactant and a molar mass of 23975 Da with a PDI of 3.94. Its poorer chemical resistance in water compared to other films could be explained by the presence of a higher amount of hydrophilic surfactant

and small molar mass polymer chains (oligomers) able to dissolve in the aqueous phase. The low solids content of the latex C likely worsens the film formation process. In relation to this discussion, the improved chemical resistance of films F3b, based on the same latex C, could be the result of the change of the drying conditions, 23ºC and 80% humidity. At increased humidity and decreased temperature, water evaporation is slower. At these conditions, a better interdiffusion of the polymer chains could eventually formed more entangled structures in which the smaller oligomeric chains would be strongly captured, preventing their dissolution. By comparison, the film F4 was obtained from the latex D (photopolymer) dried at 25ºC and 55% humidity, and also presents a high PDI in terms of molar mass. In this case, the better chemical resistance could be attributed to the higher solid content of latex D, promoting a better cohesion of the final film, but also to smaller amount of surfactant (1.5wt%). Noticeably, the films presenting the better chemical resistance combine the high solid content and low PDI (films F2b and F1a, sonopolymers). The use of oil-soluble initiator have important contribution, too, as even the oligomers of the same length as in photopolymer, in the sonopolymers will be more hydrophobic. As there are too many parameters included, it is better that the requirements to obtain chemical resistant films are evaluated on a case-by-case basis for each latex synthesized. The eventual crystallization within the film will be probably the most important parameter to control the chemical resistance and the other properties.

3.3.4. Film formation of cross-linked poly(thioethers) and reinforcement by inorganic filler

Another strategy to enhance mechanical resistance of the film is to add small amount of trifunctional monomers within the formulation based on GDMA-DATP, as it leads to creation of crosslinked chains[30]. Hence, the monomer pair GDMA-DATP and small amount (20 mol% of ene or thiol functionality) of trifunctional monomers either TMPMP or TVCH (Figure 3.2) were polymerized by sonication.

Soxhlet extraction under THF reflux was used to determine gravimetrically the gel content of the latexes. 30% solid content latexes DATP+TVCH/GDMA and DATP/GDMA+TMPMP with average particle size of 180nm were obtained and the polymers contain with 64% and 39% gel content, respectively (Table 3.14.).

Table 3.14. Characterization of the 30% solid content latexes based on DATP+TVCH/GDMA and DATP/GDMA+TMPMP, obtained by sonopolimerization in presence of 0.2 wt % of AIBN.

Latex	Particle size latex (nm)	M_w (kDa)	PDI	Gel content (wt%)	T_g by DSC (ºC)
DATP-BDMA+TVCH	180	11	2.14	65	-18ºC
DATP-GDMA+TMPMP	180	*	*	39	-16ºC

*Could not be measured

The latexes containing crosslinked polymer chains as well as linear chains were then casted into silicon moulds, and good quality films were obtained at 25°C and 55% of humidity, as shown in the Figure I.6 in Appendix I, with the film based on GDMA-DATP+TVCH denoted as F.D, and the film based on GDMA-DATP+TMPMP labelled F.E.

The T_g of the films F.D and F.E were determined by recording the second heating scan from non-isothermal DSC analysis, which are supplied in Figure I.7 in Appendix I. Likely due to the crosslinked structure, the T_g observed by DSC for the films containing trifunctional monomer are still low (-18 - -16)ºC as observed on the Table 3.14., but noticeably increased compared to the linear polysulfide film based on the DATP/GDMA latex which has a T_g below -25ºC. Beside low T_g, presence of small amount of trifunctional monomer in the formulation, and subsequently creation of cross-linked structure resulted in much better quality film as may be observed by comparison the films in the photos Figure I.6, Appendix I. Moreover, the molar mass of the soluble part of the film containing 65% crosslinks (GDMA-DATP+TVCH, F.D) presented in Table 3.14 was 11 kDa, indicating that the cross-linked structure will contained the higher molar mass chains incorporated within the gel part, which may be explanation for significant improvement of the quality of the film. According to the DSC traces in Figure I.7, Appendix I, no crystalline structures from the polymer are present in the sample (the observed melting in the second heating scan being attributed to the melting of HD). Therefore, good quality films are either obtained for increased T_g (but lower than the temperature at which the films are being forned) or the presence of crystalline structures.

Beside the various strategies planned to increase the T_g, attention was turned toward improving the film forming ability of already prepared latexes GDMA-DATP+TMPMP and GDMA-DATP+TVCH and potentially their barrier properties. Previous experience has shown that this may be achieved by addition of small amount of inorganic filler. Therefore, each of the latexes obtained was blended with graphene oxide (GO) or reduced graphene oxide (rGO) aqueous dispersions. Different amounts (between 0.2 wt% and 1 wt%) of GO and rGO related to polymer were added to reinforce the final films. In case of GO, only 0.2% was added because further increasing of this amount resulted in phase separation within the latex. The blending process diluted slightly our original latexes, which in principle influences negatively the film formation process. However, addition of graphene nanoplatelets, characterized with high surface area, creates large interface and many interactions within the aqueous dispersion (latex). As a result viscosity of the latex was improved and the film formation capability, too. Therefore, relatively nice composite films were obtained as shown in the Figure I.8 A and B, in Appendix I.

The T_g of the composite films are still low, as shown in the Table 3.15, determined from the second heating scan of DSC analysis, reported Figure I.7, Appendix I, and no crystalline structures are present. The slight T_g increase observed is probably result of the reduced mobility of polymer chains due to established interactions with GO and rGO, therefore more energy is necessary for movement of the chains.

Table 3.15. Glass transition temperature of the films based on DATP+TVCH/GDMA (FA) and DATP/GDMA+TMPMP (FB), and composite films by DSC

Latex	Inorganic filler	Film	T_g by DSC (ºC)
GDMA-DATP+TVCH	-	F.D	−17.6℃
	0.2 wt% GO	F.D-0.2GO	−14.1℃
	0.2 wt% rGO	F.D-0.2rGO	−14,1℃
	0.6 wt% rGO	F.D-0.6rGO	−16.3℃
	1 wt% rGO	F.D-1rGO	−15.9℃
GDMA-DATP+TMPMP	/	F.E	−15.9℃
	0.2 wt% GO	F.E-0.2GO	−16.2℃
	0.2 wt% rGO	F.E-0.2rGO	−17.0℃
	0.6 wt% rGO	F.E-0.6rGO	−16.9℃
	1 wt% rGO	F.E-1rGO	−15.8℃

It is well known that the graphene-based fillers improve the mechanical properties. Therefore, tensile tests were performed on the composite films to check their mechanical properties. The tensile measurements in Figure 3.5 show that the final composite films were importantly reinforced with respect to neat polymer film, with an important increase of the Young modulus of elasticity.

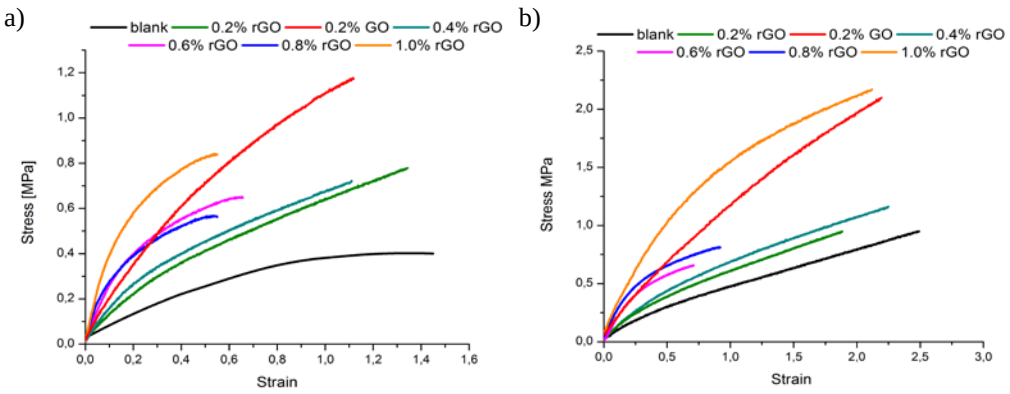

Figure 3.5. Tensile measurements of the prepared film a) F.E from the GDMA-DATP+TMPMP based latex and blends with GO and rGO and b) F.D from the GDMA-DATP+TVCH based latex and blends with GO and rGO

In general by increasing the loading of the filler, the reinforcement effect was higher, although there are some exceptions of this trend, probably due to defects of the formed films. Surprisingly for composite films, beside high augmentation of Young's moduli, no drop of the elongation at break was observed. This indicates that the GO and rGO are well distributed within the polymer matrix and that there are interactions established between the polymer and the filler.

To further investigate this, the morphology of the composite films was analysed by scanning electron microscopy (SEM) imaging. Figure 3.6 is representative image of the morphology of composite film containing 0.2% GO. In Figure 3.6, where the cross-section area of the composite is presented, the GO platelets (in white color) are very well distributed all over the polymer matrix (black areas), there is no aggregation and all the platelets are self-oriented perpendicularly to the cross-section view (Figure 3.6.A). Under higher magnification, as shown

in Figure 3.6.B, the individual polymer particles may be observed, due to the presence of the nanoplatelts that wrapped the nanoparticles and prevent complete interdiffusion and continuous film formation. The observed morphology is typical for waterborne systems.

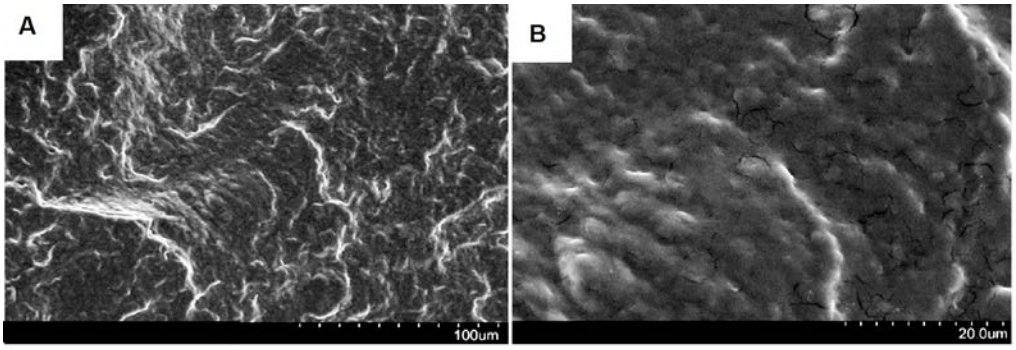

Figure 3.6. SEM images of the cross section of the composite film F.D prepared from the GDMA-DATP+TVCH based latex and blended with 0.2 wt% GO

The water uptake of the film GDMA-DATP+TVCH (F.D) and its rGO composites was measured for one month and is shown in the Figure 3.7.

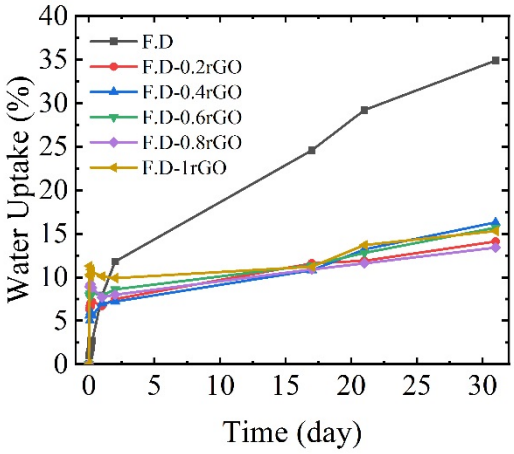

Figure 3.7. Water uptakes of the film GDMA-DATP+TVCH F.D and composite films F.D-0.2rGO; F.D-0.4rGO; F.D-0.6rGO; F.D-0.8rGO and F.D-1rGO

The composite films presented a relatively low water uptake after one month (~10%), and noticeably lower compared to the neat film F.D (~32%). This shows that the presence of rGO limits the water adsorption. This effect was attributed to the hydrophobicity of the graphene fillers, which may have an important role to humidity barrier properties of the films, due to the obstacles that rGO 2D platelet-like structures caused to water diffusion.

3.4. Conclusion

In this chapter, we report the synthesis of poly(thioether) latexes through two main processes, different in the strategy followed to overcome the challenge of the low chemical stability of thiol-ene system and premature polymerization that lead to irreproducibility.

In the first one chemical stability of thiol-ene miniemulsions based on the model monomer GDMA and DATP was achieved by using radical scavenger 2,5-Di-tert-butylhydroquinone (DBHQ) to prevent premature polymerization during miniemulsification by sonication. Stable thiol-ene miniemulsions were further converted to latexes by photopolymerization in present of a photoinitiator. This strategy allows a spatial and temporal control of the onset of the polymerization, but suffer from stability issue. Indeed, colloidally stable miniemulsions were challenging to obtain, as the presence of inhibitor DBHQ with high hydrophilicity increased the hydrophilicity of the particles and promoted monomer diffusion and stoichiometric imbalance. Consequently, lack of reproducibility especially in the molar masses was observed.

The other line of investigation in which sonopolymerisation is combined with photopolymerization, turned out to be very efficient for the synthesis of high solid content latexes based on diene monomer DATP and various dithiol monomers GDMA, GDMP and EDDT. In this line, the miniemulsification process of thiol-ene emulsion was used to perform sonopolymerization without use of any initiator or inhibitor, producing pre-polymer dispersions that were afterwards photopolymerized. The combination of two polymerisation processes allows to achieve colloidally stable latexes at solids content of 30% and up to 50% with high molar mass poly(thioether) as high as 200 kDa, the highest to the best knowledge of the author for this type of polymers. Colloidal instability is precluded, as stable pre-polymer particles are obtained after sonication likely due to the higher hydrophobicity of the oligomers that prevent monomer diffusion- Chemical instability was overcame, too because of the fast conversion of the monomers during the sonication, creating still reactive pre-polymers.

In addition, we report the synthesis of film forming linear poly(thioether), which will be of interest for the rest of the project. Indeed, latexes based on GDMA-DATP, GDMP-DATP and EDDT-DATP present good film forming abilities at room temperature. These films were characterized in terms of water and chemical resistance, which are important properties for the intended application in food packaging. The films based on GDMA-DATP turn out to be the more promising in terms of barrier properties, with low water uptake (below 2%) and water vapour diffusion rate (2 g*mm/m^2*day). Moreover, GDMA-DATP films presented good chemical resistance to food simulant B, with low mass loss values after 4 days immersed. In particular, the GDMA-DATP films obtained from high solid content latex and presenting low polydispersity in molar masses were the one presenting the chemical resistance, highlighting the fact that both film formation process and polymer's macrostructure are important for that matter.

Strategies were implemented to improve the final properties of the film by adding small amount of trifunctional monomer or inorganic filler (graphene oxide and reduced graphene oxide). The addition of a trifunctional monomer yields to the synthesis of cross-linked poly(thioethers), and further investigation in terms of crystalline behaviour are precluded as linear chains are preferred for this matter. However, the addition of inorganic filler could be a strategy to promote barrier properties, as water uptakes results were encouraging.

3.5. References

(1) Durham, O. Z.; Chapman, D. V.; Krishnan, S.; Shipp, D. A. Radical Mediated Thiol-Ene Emulsion Polymerizations. *Macromolecules* **2017**, *50* (3), 775–783. https://doi.org/10.1021/acs.macromol.6b02228.

(2) Quoc Le, C. M.; Schmutz, M.; Chemtob, A. Ab Initio Batch Emulsion Thiol–Ene Photopolymerization. *Macromolecules* **2020**. https://doi.org/10.1021/acs.macromol.0c00265.

(3) Amato, D. V.; Amato, D. N.; Flynt, A. S.; Patton, D. L. Functional, Sub-100 Nm Polymer Nanoparticles via Thiol-Ene Miniemulsion Photopolymerization. *Polym. Chem.* **2015**, *6* (31), 5625–5632. https://doi.org/10.1039/c4py01449a.

(4) Jasinski, F.; Rannée, A.; Schweitzer, J.; Fischer, D.; Lobry, E.; Croutxé-Barghorn, C.; Schmutz, M.; Le Nouen, D.; Criqui, A.; Chemtob, A. Thiol-Ene Linear Step-Growth Photopolymerization in Miniemulsion: Fast Rates, Redox-Responsive Particles, and Semicrystalline Films. *Macromolecules* **2016**, *49* (4), 1143–1153. https://doi.org/10.1021/acs.macromol.5b02512.

(5) Jasinski, F.; Lobry, E.; Tarablsi, B.; Chemtob, A.; Croutxé-Barghorn, C.; Nouen, D. Le; Criqui, A. Light-Mediated Thiol-Ene Polymerization in Miniemulsion: A Fast Route to Semicrystalline Polysul Fide Nanoparticles. *ACS Macro Lett.* **2014**, *3* (9), 958–962. https://doi.org/10.1021/mz500458s.

(6) Le, C. M. Q.; Vidal, L.; Schmutz, M.; Chemtob, A. Droplet Nucleation in Miniemulsion Thiol-Ene Step Photopolymerization. *Polym. Chem.* **2021**, *12* (14), 2084–2094. https://doi.org/10.1039/d1py00139f.

(7) Infante Teixeira, L.; Landfester, K.; Thérien-Aubin, H. Nanoconfinement in Miniemulsion Increases Reaction Rates of Thiol-Ene Photopolymerization and Yields High Molecular Weight Polymers. *Polym. Chem.* **2022**, 2831–2841. https://doi.org/10.1039/d2py00350c.

(8) Walley, S. E. Synthesis of Polythioether Nanoparticles via Thiol- Alkene / Alkyne Photopolymerization in Miniemulsion. **2017**, 34.

(9) Machado, T. O.; Cardoso, P. B.; Feuser, P. E.; Sayer, C.; Araújo, P. H. H. Thiol-Ene Miniemulsion Polymerization of a Biobased Monomer for Biomedical Applications. *Colloids Surfaces B Biointerfaces* **2017**, *159*, 509–517. https://doi.org/10.1016/j.colsurfb.2017.07.043.

(10) Durham, O. Z.; Shipp, D. A. Suspension Thiol-Ene Photopolymerization: Effect of Stabilizing Agents on Particle Size and Stability. *Polymer (Guildf).* **2014**, *55* (7), 1674–1680. https://doi.org/10.1016/j.polymer.2014.02.044.

(11) Esfandiari, P.; Ligon, S. C.; Lagref, J. J.; Frantz, R.; Cherkaoui, Z.; Liska, R. Efficient Stabilization of Thiol-Ene Formulations in Radical Photopolymerization. *J. Polym. Sci. Part A Polym. Chem.* **2013**, *51* (20), 4261–4266. https://doi.org/10.1002/pola.26848.

(12) McKenzie, T. G.; Karimi, F.; Ashokkumar, M.; Qiao, G. G. Ultrasound and Sonochemistry for Radical Polymerization: Sound Synthesis. *Chem. - A Eur. J.* **2019**, *25* (21), 5372–5388. https://doi.org/10.1002/chem.201803771.

(13) Teo, B. M.; Ashokkumar, M.; Grieser, F. Sonochemical Polymerization of Miniemulsions in Organic Liquids/Water Mixtures. *Phys. Chem. Chem. Phys.* **2011**, *13* (9), 4095–4102. https://doi.org/10.1039/c0cp01979h.

(14) Teo, B. M.; Prescott, S. W.; Ashokkumar, M.; Grieser, F. Ultrasound Initiated Miniemulsion Polymerization of Methacrylate Monomers. *Ultrason. Sonochem.* **2008**, *15* (1), 89–94. https://doi.org/10.1016/j.ultsonch.2007.01.009.

(15) Skinner, E. K.; Whiffin, F. M.; Price, G. J. Room Temperature Sonochemical Initiation of Thiol-Ene Reactions. *Chem. Commun.* **2012**, *48* (54), 6800–6802. https://doi.org/10.1039/c2cc32457a.

(16) Lobry, E.; Jasinski, F.; Penconi, M.; Chemtob, A.; Croutxé-Barghorn, C.; Oliveros, E.; Braun, A. M.; Criqui, A. Continuous-Flow Synthesis of Polymer Nanoparticles in a Microreactor via Miniemulsion Photopolymerization. *RSC Adv.* **2014**, *4* (82), 43756–43759. https://doi.org/10.1039/c4ra06814a.

(17) Odian, G. *Principles of Polymerization*, 4th ed.; Sons., J. W. &, Ed.; 2004.

(18) Asua, J. M. Miniemulsion Polymerization. *Prog. Polym. Sci.* **2002**, *27* (7), 1283–1346. https://doi.org/10.1016/S0079-6700(02)00010-2.

(19) Javed, A.; Ullsten, H.; Rättö, P.; Järnström, L. Lignin-Containing Coatings for Packaging Materials. *Nord. Pulp Pap. Res. J.* **2018**, *33* (3), 548–556. https://doi.org/10.1515/npprj-2018-3042.

(20) Jasinski, F.; Lobry, E.; Chemtob, A.; Croutxé-Barghorn, C.; Criqui, A. Photopolymerizable Monomer Miniemulsions: Why Does Droplet Size Matter? *Macromol. Chem. Phys.* **2013**, *214* (15), 1669–1676. https://doi.org/10.1002/macp.201300278.

(21) Danish Environmental Protection Agency. A LOUS Review Report Environmental Project No. 1477, 2013. **2013**, No. 1477, 1–28.

(22) Ugelstad, J.; Mork, P. C.; Mfutakamba, H. R.; E.Soleimany; I.Nordhuus; Schmid, R.; Berge, A.; Ellingsen, T.; Aune, 0.; Nustad, K. *Thermodynamics of Swelling of Polymer, Oligomer and Polymer- Oligomer Particles. Preparation and Application of Monodisperse Polymer Particles.*, Springer,.; 1983; Vol. 67.

(23) Costa, C.; Timmermann, S. A. S.; Pinto, J. C.; Araujo, P. H. H.; Sayer, C. Compartmentalization Effects on Miniemulsion Polymerization with Oil-Soluble Initiator. *Macromol. React. Eng.* **2013**, *7* (5), 221–231. https://doi.org/10.1002/mren.201200066.

(24) Priest, W. J. Particle Growth in the Aqueous Polymerization of Vinyl Acetate. *J. Phys. Chem* **1952**, *56* (3), 1077–1082.

(25) Do Amaral, M.; Arevalillo, A.; Santos, J. L.; Asua, J. M. Novel Insight into the Miniemulsification Process: CFD Applied to Ultrasonication. *Prog. Colloid Polym. Sci.* **2004**, *124*, 103–106. https://doi.org/10.1007/b12149.

(26) Keddie, J. L.; Routh, A. F. *Fundamentals of Latex Film Formation: Processes and Properties*; Springer US: Berlin, 2010.

(27) Patterson, M. C.; Dunkelberger, D. L. Additives for Processing Rigid PVDC Copolymers. *J. Vinyl Technol.* **1994**, *16* (1), 46–51. https://doi.org/10.1002/vnl.730160112.

(28) Chen, C. L.; Hsieh, T. H.; Ho, K. S. Studies on the Crystallization of Poly(Vinylidene Chloride-Co-Vinyl Chloride). *Polym. J.* **2001**, *33* (11), 835–841. https://doi.org/10.1295/polymj.33.835.

(29) Lange, B. J.; Wyser, Y. Recent Innovations in Barrier Technologies for Plastic Packaging – a Review. *Packag. Technol. Sci.* **2003**, *16*, 149–158.

(30) Li, Q.; Zhou, H.; Hoyle, C. E. The Effect of Thiol and Ene Structures on Thiol-Ene Networks: Photopolymerization, Physical, Mechanical and Optical Properties. *Polymer (Guildf).* **2009**, *50* (10), 2237–2245. https://doi.org/10.1016/j.polymer.2009.03.026.

Chapter 4. Study on the crystallization of film-forming poly(thioethers)

4.1. Introduction

As emphasized in Chapter 1, pertaining to waterborne barrier coatings, the polymer microstructure is of the utmost importance in combining excellent barrier properties and good film-forming ability. Therefore, linear and crystallisable polymer chains embedded within a soft amorphous polymer matrix are indispensable.

In Chapter 3, we reported a novel synthesis approach of high solids content film forming waterborne poly(thioethers) based on initiator-free step growth sonopolymerization. Copolymerization of bifunctional thiol and ene monomers dially terephthalate (DATP), glycol dimercaptoacetate (GDMA), glycol dimercaptopropionate (GDMP), and 2,2-(ethylenedioxy)diethanethiol (EDDT) gave rise to linear poly(thioethers) shown in Figure 4.1 with molar mass in a range between 23 and 7 k Da when synthesized at 30% solid content.

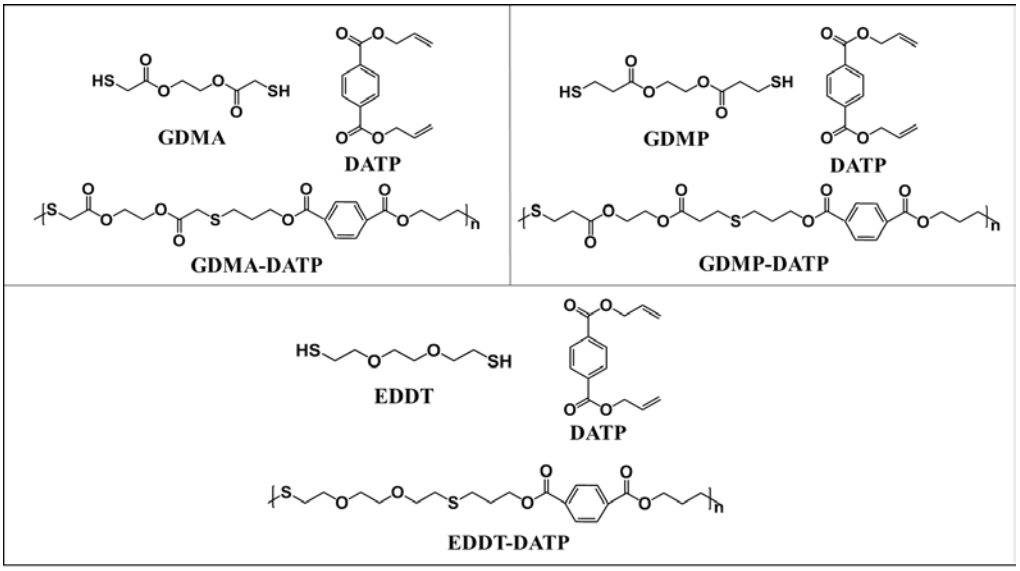

Figure 4.1 Chemical Structure of difunctional monomers DATP, GDMA, GDMP, EDDT, and Poly(thioether) GDMA-DATP, GDMP-DATP, and EDDT-DATP obtained from step-growth polymerization.

To further increase the polymers' molar mass, an additional photopolymerization step was performed in the presence of a water-soluble photoinitiator lithium phenyl-2,4,6-trimethylbenzoylephosphinate, yielding poly(thioethers) with a molar masses between 23 and 81 kDa. The polymer dispersions presented good film-forming ability at room temperature for the aimed application in coating. In that scope, the obtained films were first characterized in terms of thermal stability, using thermogravimetric measurements.

As already stated, polymer crystallization is another important property related to the waterborne barrier coating application. Crystallization has already been observed in linear

poly(thioether) films after water evaporation,[1,2] even though it has yet to be studied, up to the best knowledge of the authors. A controlled degree of crystallinity in the amorphous matrix films could yield smarter coatings presenting a passive barrier to oxygen and water. Flexible and linear chains are more prone to form crystalline domains within the film, but on the other hand, some rigidity in the polymer chain is required to form consistent films sufficiently good for coating application. Coping with this balance, we investigated for the first time the crystallization behaviour in linear and film-forming poly(thioether) films. For that aim, we have employed a self-nucleation strategy[3,4] to accelerate the crystallization kinetics of as-synthesized films and potentially improve the barrier properties and add value to the films produced from thiol-ene chemistry.

4.2. Experimental and method

4.2.1. Materials

Diallyl terephtalate (DATP, >98%), lithium phenyl (2,4,6-trimethylbenzoyl)phosphinate (TPO-Li, >99%) were purchased from TCI chemicals. 2,2-(ethylenedioxy)diethanedithiol (EDDT, >95%) and hexadecane (HD, >98%), and 2,2 -Azobis(2-methylpropionitrile) (AIBN, >98%) were purchased from Sigma Aldrich. Glycol dimercaptoacetate (GDMA, >95%) and glycol dimercaptopropionate (GDMP, >95%) were kindly supplied by Bruno Bock. Tetrahydrofuran (THF 99.9% HPLC grade) was purchased from Scharlab and used as solvent for the GPC analysis. All chemicals were used as received without further purification, and de-ionised water was used as the dispersant media for the polymerization.

4.2.2. Synthesis

The poly(thioether) latexes synthesis is described in Chapter 3. Molar masses and particle sizes of the latexes employed in this study are reported in Table 4.1.

Table 4.1. 30% solid content poly(thioethers) obtained from sonopolymerization alone (labelled S) or sonopolymerization combined with photopolymerization step (labelled SP).

			After sonication step			After UV exposure		
Process	**Monomers**	**Costabilizer HD (wt%)**	**Particle size (nm)**	**Mw (Da)**	**PDI**	**Particle size (nm)**	**Mw (Da)**	**PDI**
S	GDMA-DATP	-	237	9135	2.53	-	-	-
SP	GDMA-DATP	-	194	12848	3.18	185	22696	4.02
SP	EDDT-DATP	6	175	23008	3.65	173	52010	4.07
SP	EDDT-DATP	-	191	4966	2.62	222	81152	2.53
SP	GDMP-DATP	-	274	6828	2.47	299	34618	4.22

4.2.3. Film formation

Various films with a thickness in the following range 300-970 μm were prepared by casting of an appropriate amount of the 30% latexes into silicon moulds, and dried at standard atmospheric conditions (25ºC and 55% of relative humidity). For sake of clarity, films based on the monomer couple GDMA-DATP are denoted F.A, with F.A.1 presenting lower molar mass than F.A2. Films based on the monomer couple EDDT-DATP are denoted F.B, and F.B1.HD displays lower molar masses than F.B2 and also contains 6wt% of HD. Finally, the film based

on the monomer GDMP-DATP is referred to as film F.C. The main characteristics of the films are depicted in Table 4.2.

Table 4.2. Films obtained after water evaporation of the latexes based on DATP, GDMA, EDDT and GDMP.

Film	Monomers	HD (wt%)	M_w (Da)
F.A1	GDMA-DATP	-	9135
F.A2	GDMA-DATP	-	22696
F.B1.HD	EDDT-DATP	6	52010
F.B2	EDDT-DATP	-	81152
F.C	GDMP-DATP	-	34618

4.2.4. Characterizations

Thermogravimetric Analysis (TGA) of the films were carried out with a Perkin Elmer TGA 8000™ Thermogravimetric analyzer. Samples were heated from 40ºC to 800ºC at 10ºC/min (Purge gas: air at 40mL/min)

The crystallinity study was carried out on a differential scanning calorimeter Perkin Elmer DSC 8000 equipment using an Intracooler II as a cooling system. Approximately 5 mg samples were encapsulated in aluminium pans. In the case of the film based on the monomer pair EDDT-DATP containing HD, sealed aluminium pans were used.

- Non-isothermal crystallization

For the non-isothermal procedure, samples were heated 30ºC above their melting point at 20ºC/min, that is to say up to 80ºC for the films F.A1 and F.A2, 90ºC for the films F.B1.HD and F.B2 and 100ºC for the film F.C and left 3 minutes in the molten state. They were then cooled at either 1ºC/min or 10ºC/min until -30ºC for the films F.A1,F.A2 and F.C and -40ºC for the film F.C. Films were subsequently heated up at 20ºC/min to 80ºC (F.A1 and F.A2), 90ºC (F.B1.HD and F.B2) and 100ºC (F.C).

- Self-nucleation experiment

Self-nucleation (SN) is a thermal protocol in which self-seed or self-nuclei are being generated, so that nucleation density is greatly increased and the overall crystallization kinetics are sped up[5].

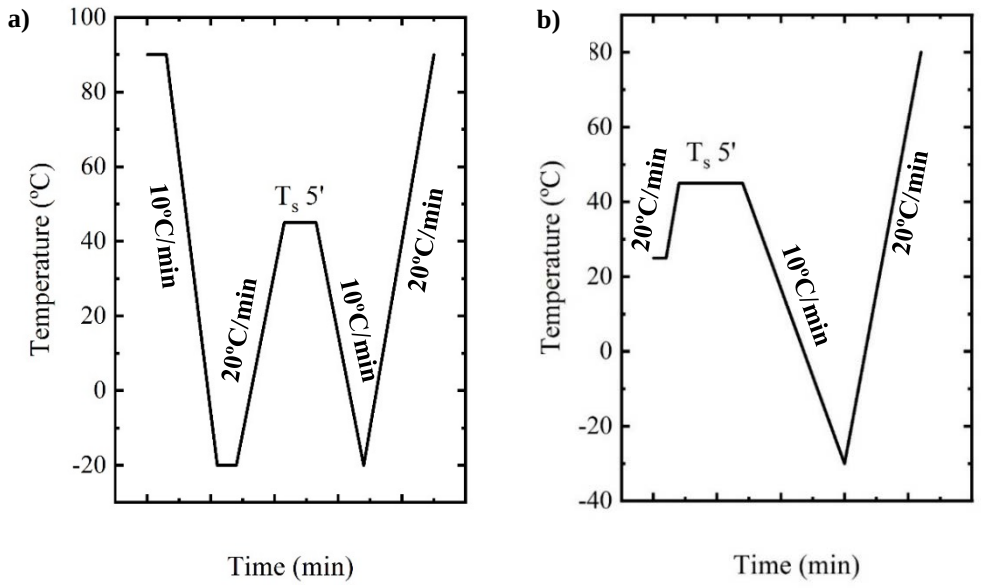

Figure 4.2. Schematic representation of SN thermal protocol performed on (a) poly(thioether) films based on EDDT-DATP and containing HD (F.B1.HD) and (b) poly(thioether) films based on GDMA-DATP (F.A1, F.A2), EDDT-DATP (F.B2) and GDMP-DATP (F.C). Cooling rates of 10ºC/min and heating rates of 20ºC/min were employed.

For the SN experiments on films F.A1, F.A2, F.B1.HD, F.B2 and F.C, two thermal protocols were employed, and are described below.

In the first procedure (see Figure 4.2.a), which is the typical SN protocol, the film F.B1.HD was heated to 90ºC and held 3 minutes at this temperature to erase thermal history. The film was then cooled from its isotropic melt at 10ºC/min to -20ºC. In this step, a standard thermal history is set up, and the polymer crystallizes until saturation. F.B1.HD is then heated up to a range of self-nucleation temperatures, denoted T_s, and kept for 5 minutes at this

temperature. During this thermal conditioning and depending on the T_s selected, the polymer can melt, self-nucleate, or self-nucleate and anneal. In the subsequent step, the film F.B1.HD is recrystallized by cooling from T_s to -20ºC at 10ºC/min. A final heating scan was performed up to 90ºC at 20ºC/min.

In the second SN thermal protocol Figure 4.2.b., which was applied to the films F.A1, F.A2, F.B2, and F.C, samples were directly heated up to a range of T_s at 20ºC/min and kept for 5 minutes at this temperature. T_s values were selected within the onset and the end of the melting peak obtained from the first heating scan of the non-isothermal procedure. Films were then cooled at 10ºC/min to -30ºC (F.A1, F.A2 and F.C) and -20ºC (F.B2), and subsequently heated at 20ºC/min to 80ºC (F.A1 and F.A2), 90ºC (F.B2) and 100ºC (F.C).

The degree of crystallinity was calculated as follows:

$$Xc = \frac{\Delta H_m}{\Delta H_{m,100\%\,crystalline}} \quad \text{.....(4.1)}$$

As $\Delta H_{m,100\%\,crystalline}$ of the polymers studied is not reported in the litterature, it was determined by using the group contribution theory. [6] The values are reported in the Table 4.3.

Table 4.3. Calculated $\Delta H_{m,100\%\ crystalline}$ with the group contribution theory for the films based on the polymers GDMA-DATP, GDMP-DATP and EDDT-DATP monomer pairs.

Film	Monomers	$\Delta H_{m,100\%\ crystalline}$ (J/g)
F.A1, F.A2	GDMA-DATP	108
F.B1.HD, F.B2	EDDT-DATP	151
F.C	GDMP-DATP	119

Wide-Angle X-ray scattering (WAXS) was carried out on the as casted films using a BRUKER D8 Advance X-Ray diffractometer with Cu Kα (λ=1.5418 Å) radiation.

4.3. Results and discussion

As emphasized in Chapter 3, latexes based on the monomer pair GDMA-DATP, EDDT-DATP and GDMP-DATP at standard atmospheric conditions (temperature of 25ºC and relative humidity of 55%) gave rise to the formation of homogeneous films F.A1 to F.C (Table 4.3 and photos in Appendix II, Figure II.1).

The films are consistent and suitable for coating applications. Moreover, they are self-supported which allows further characterizations. As the intended application is food packing, the barrier to humidity or oxygen are of upmost importance. In the thiol-ene polymers, this is expected to be provided by the crystalline structures created within these films, as reported previously[1,2]. In that scope, films based on EDDT-DATP F.B1.HD and F.B2 and GDMP-DATP F.C are opaque, white, and ductile compared to the films based on GDMA-DATP F.A1 F.A2 that are transparent and flexible (see Table 4.3 and photos in Appendix II, Figure II.1). This

could be the first qualitative appreciation of the presence of crystalline domains, which can scatter light as long as their superstructural aggregates (e.g., spherulites or axialites) have sizes larger than the wavelength of light. In the following, a deeper study of the crystallization behaviour of the thiol-ene polymer chains is presented, with attempts to control the crystallization kinetics.

4.3.1. Thermal stability

The thermal degradation curves of F.A1, F.A2, and F.B1.HD, F.B2, and F.C films are shown in Figure 4.3. Noticeably, all the studied thiol-ene films show degradation in the temperature range of 350-400 ºC which is at least 100 ºC higher than the common (meth)acrylic waterborne polymers that degrade at temperatures ranging from 150ºC to 300ºC.[7,8]

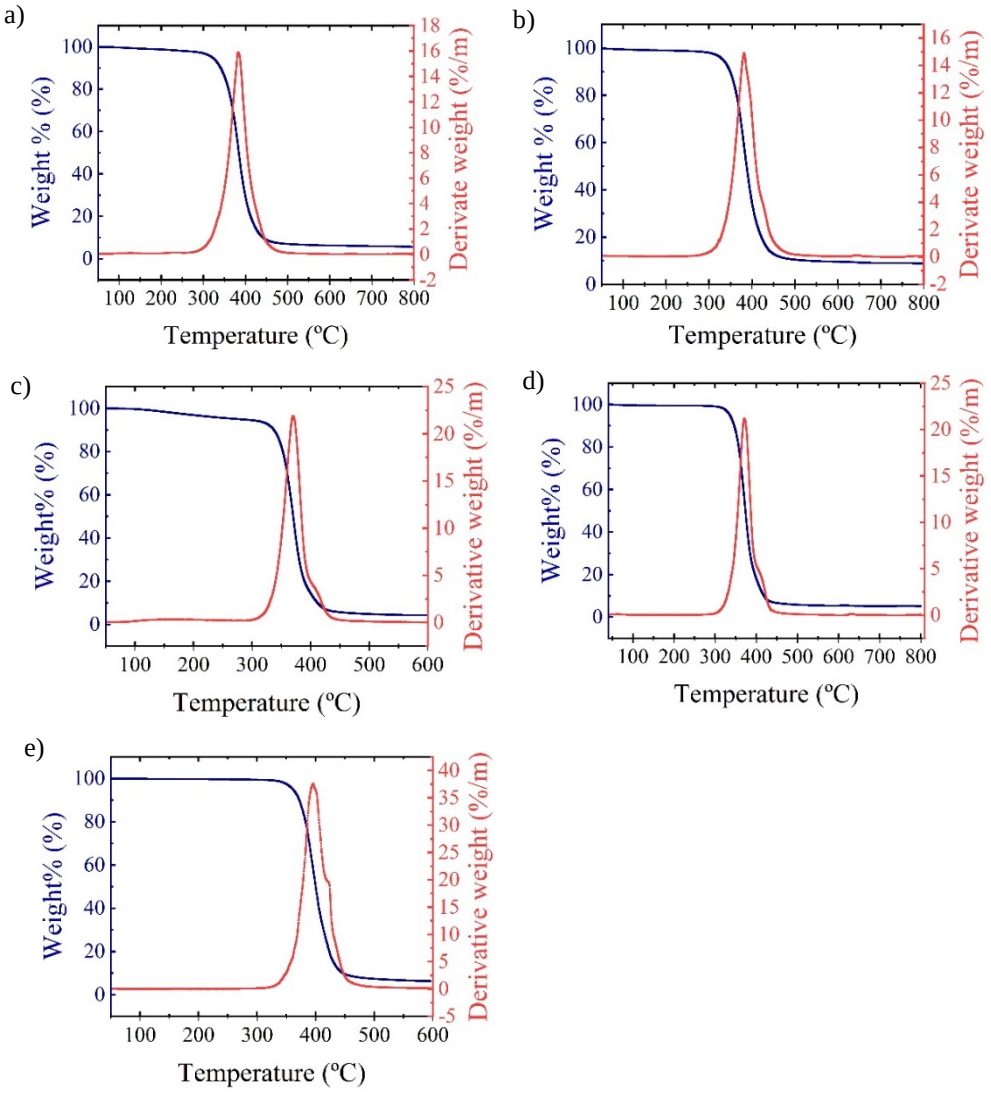

Figure 4.3. TGA of the films a) F.A1, b) F.A2, c) F.B1.HD, d) F.B2, and e) F.C

The presence of aromatic functionality within the backbone can be one of the possible causes for the improved thermal resistance. The thermal stability was not affected by the molar mass of the chains, but it was affected by the chemical compositions.

4.3.2. DSC results under non-isothermal conditions

The semi-crystalline behaviour of as-synthesized films is evidenced by a melting peak in the first heating scans of the non-isothermal DSC analysis (Figure 4.4), and the calorimetric values of interest obtained for the films are listed in Table 4.4.

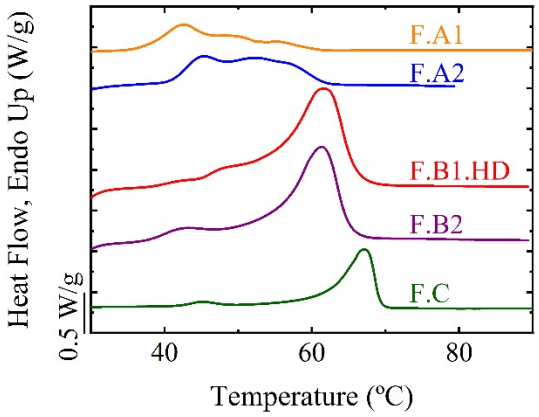

Figure 4.4. First, DSC heating scans at 20ºC/min of as-synthesized poly(thioether) films F.A1, F.A2, F.B1.HD, F.B2, and F.C.

The films F.A1 and F.A2, based on the same monomers combination GDMA-DATP, have a multimodal melting peak at 43°C and 45ºC, respectively, as shown on the first DSC heating scans (Figure 4.4 and Table 4.4). The melting point is slightly shifted to higher

temperature for photopolymers with respect to the sonopolymer (F.A2 versus F.A1) due to the larger molar masses.[9]

Table 4.4. Melting temperatures (T_m) and melting enthalpy (ΔH_m**)** values from the first heating scan. Cold crystallization enthalpy (ΔH_{cc}), T_m, ΔH_m and glass transition temperature (T_g) values from the second heating scan after cooling from the melt at 1ºC/min. Values are extracted from the non-isothermal experiments performed on F.A1, F.A2, F.B1.HD, F.B2 and F.C reported in Figures 4.4 and 4.6.

				First heating scan		Second heating scan			
Film	**Monomers**	**HD (wt%)**	**M_w (Da)**	**T_m (ºC)**	**ΔH_m (J/g)**	**ΔH_{cc} (J/g)**	**T_m (ºC)**	**ΔH_m (J/g)**	**T_g (ºC)**
F.A1	GDMA-DATP	-	9135	42.5 / 49.1 / 55.6	23	-	-	-	-15.6
F.A2	GDMA-DATP	-	22696	45.1 / 52.5 / 57.4	16	-	-	-	-7.8
F.B1.HD	EDDT-DATP	6	52010	48.2 / 61.7	37	5	25.3 / 60.9	27	-22.3
F.B2	EDDT-DATP	-	81152	42.5 / 61.6	33	-	61.3	15	-22.6
F.C	GDMP-DATP	-	34618	45.1 / 67.0	23	-	-	-	-14.6

The F.B1.HD and F.B2 films based on EDDT-DATP have a melting peak at 62ºC (Figure 4.4 and Table 4.4). In the sample F.B1.HD, a small endothermic peak is observed at 48ºC, which is attributed to the melting of HD (DSC scans Figure II.2, in Appendix II), which segregates from the polymer matrix in the film and forms crystalline structures. The F.C film based on monomer pair GDMP-DATP has a melting point of 67ºC, higher than the other films described previously.

The semi-crystalline behaviour of the films F.A1, F.A2, F.B1.HD, F.B2 and F.C could also be appreciated from WAXS diffractograms of the films (Figure 4.5).

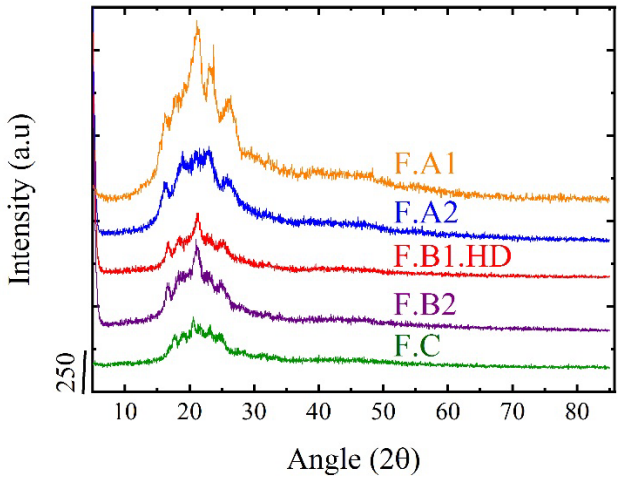

Figure 4.5. WAXS diffractograms of the films F.A1 F.A2 F.B1.HD F.B2 and F.C

The WAXS diffractograms of the films show several diffraction peaks with different intensities and sharpness. Namely, it may be observed in Figure 4.5 that the WAXS curves of all studied polymers contain one broad peak assigned to the amorphous structure and a few small sharp peaks that indicate the presence of crystalline domains within the films. The small contribution of the well-defined and sharp peaks with respect to the large wide peak highlights the low degree of crystallinity of the films.

The degree of crystallinity of each sample was determined from the first DSC heating scan, and the values reported in Table 4.5 using equation 4.1, see above[6].

Table 4.5. Calculated degree of crystallinity X_C for as-synthesized films F.A1, F.A2, F.B1.HD, F.B2 and F.C

Film	Monomers	ΔH_m (J/g)	X_c (%)
F.A1	GDMA-DATP	23	21
F.A2	GDMA-DATP	16	15
F.B1.HD	EDDT-DATP+HD	37	25
F.B2	EDDT-DATP	33	22
F.C	GDMP-DATP	23	20

All samples present similar degree of crystallinity of ~20%, which is within the range required for barrier coatings application [10,11]. F.A2 film, however, presents slightly lower degree of crystallinity compared to F.A1. As both contain the same chemical structure, the decreased degree of crystallinity is attributed to the higher molar mass of F.A2. Probably, the crystallization kinetics of this higher molar mass polymer is slower.[12–14]

Non-isothermal crystallization experiments were performed on the films, and DSC traces are reported in Figure 4.6.

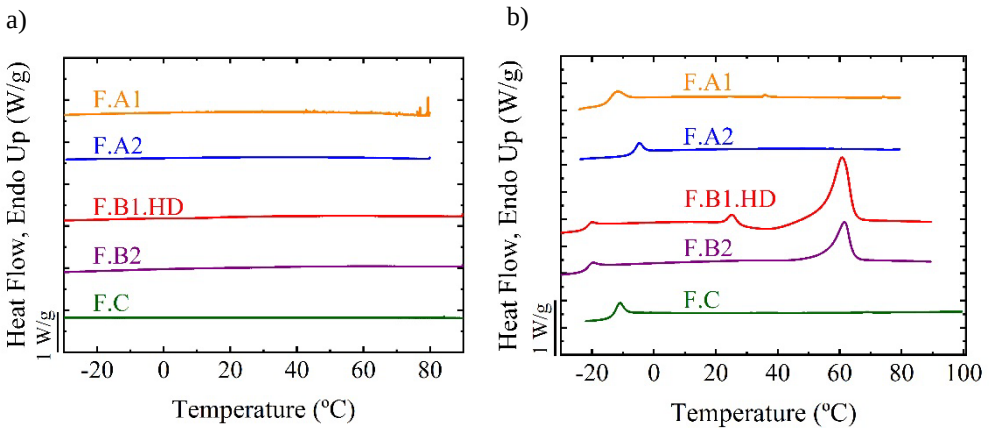

Figure 4.6. Non-isothermal crystallization of films F.A1, F.A2, F.B1.HD, F.B2 and F.C (a) DSC cooling scans from molten state at 1ºC/min and (b) subsequent heating scans at 20ºC/min

When the films are slowly cooled from the molten state at a cooling rate of 1ºC/min, no crystallization peak is observed in the DSC scans (Figure 4.6.a), demonstrating that these materials cannot crystallize from the melt, even when cooled at 1 ºC/min. They were able to crystallize during the film casting process, as illustrated in their first DSC heating runs (Figure 4.4). Once the polymer is molten and the crystalline history erased, they have difficulties in crystallizing from the melt. The presence of an aromatic ring in the polymers' backbone from the DATP monomer (Figure 4.1) conveys rigidity to the chains, and drastically slows down the ordering into crystalline domains. These poly(thioethers) probably need much smaller cooling rates (or longer times at specific temperatures) to allow the re-arrangement of the polymer chains in crystalline domains from the molten state. No melting peak is observed in the subsequent heating scan for the polymers F.A1, F.A2 and F.C based on GDMA-DATP and GDMP-DATP (Figure 4.6.b) as no crystalline structures were formed during the cooling step.

Interestingly, the films F.B1.HD and F.B2 based on EDDT-DATP present cold crystallization and subsequent melting peaks at 61ºC in the subsequent heating scan (Figure 4.6.b), showing that these polymers are able to organize into crystalline domains under the conditions studied. The lack of pending functional groups from the main backbone of EDDT based units, can be a cause behind this behaviour. For the film F.B1.HD, crystallization is occurring upon heating from the glassy state, as shown with the exothermic recrystallization peak at around 40ºC in Figure 4.6.b. This phenomenon, also referred to as cold crystallization, does not allow the full recovery of crystals, with ΔH_m in the second heating scan substantially lower that the ΔH_m of as-synthesized film (Table 4.4). F.B2 film behaves similarly, presenting lower ΔH_m in the second heating scan than in the as-synthesized film (Table 4.4). In the case of the film F.B2, the cold-crystallization peak could not be clearly observed by DSC, which can be attributed to slower crystallization during the scan (a fact that may difficult the observation of cold-crystallization, as it can be masked by the baseline), than its counterpart F.B1.HD. Likely F.B2 also crystallizes upon heating, and the exotherm is not detectable by the equipment. Film F.B1.HD contains 6 wt% of HD, which could act as a plasticizer or nucleating agent and slightly increase crystallization kinetics by comparison with F.B2. The non-isothermal DSC analysis of HD presented in Figure II.2 in Appendix II shows that HD crystallizes upon cooling at 20ºC, and melts at 30ºC. Hence, in the heating scan of film F.B1.HD in Figure 4.6.a, HD is in its semi-crystalline form at the onset of the cold crystallization exotherm, occurring around 24ºC, which means it can act as a heterogeneous nuclei and speed up EDDT-DATP crystallization kinetics. In a second phase occurring above 30ºC, HD is in its melted form and act as a plasticizer. Besides the presence of HD that induce slight difference in the crystallization behaviour of the

two films, F.B1.HD has substantially lower molar masses that F.B2 (Table 4.4) which could explain faster crystallization kinetics for the latter.

Additional analysis on films F.B1.HD and F.B2 was performed with a non-isothermal experiment in which the cooling rate was increased to 10ºC/min (Figure 4.7).

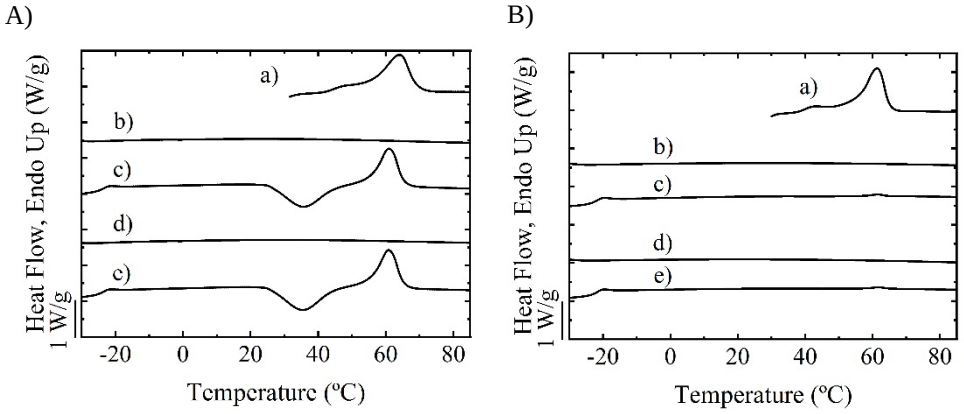

Figure 4.7. Non-isothermal crystallization of A) film F.B1.HD and B) film F.B2 with (a) first heating scan at 20ºC/min, (b) and (d) DSC cooling scans from molten state at 10ºC/min and (c) and (d) subsequent heating scan at 20ºC/min

As depicted in Figure 4.7, cold crystallization and subsequent melting are observed for the film F.B1.HD after a cooling scan at 10ºC/min, whereas no melting peak is observed for the film F.B2. The latter result shows that in the case of the F.B2, the occurrence of cold crystallization is dependent on the cooling rate. It is postulated that during the cooling rate at 1ºC/min, nuclei are formed and promote the organisation into crystalline region in the subsequent heating scan. When the cooling rate is increased to 10ºC/min, the nuclei are not

formed and cold crystallization is precluded. For the film F.B1.HD, which displays lower molar masses (Table 4.4) nuclei could be formed at cooling rates of 1ºC/min and 10ºC/min, supporting that lower molar masses promote crystallization.

All films present low T_g, below 0ºC (Figure 4.6.b and Table 4.4), indicating that soft rubbery films can be produced at room temperature in spite of the rigidity induced by the aromatic rings in the polymer chains, which is counterbalanced by the aliphatic parts. The polymer molar mass affects the T_g; thus, F.A1 with lower molar mass (Table 4.4) than its counterpart F.A2 is softer, which explains a T_g decrease from -7.8ºC to -15.6ºC. A T_g lower than film formation temperature ensures good cohesion of the obtained films. The soft chains interdiffuse and create entanglements efficiently in the last stage of the film formation process which together with the crystalline regions, yield tough rubbery materials at room temperature. The supplement of rigidity brought by the aromatic ring of DATP, along with the presence of crystalline structures increase the stiffness of the final material, and promote the formation of coherent coating films. As emphasized in the introduction, thiol-ene film forming polymers that have been studied in previous works suffered from very low melting point, which restrained their utility, because the crystalline domains are melted at room temperature[1]. Herein, the selected poly(thioethers) present significantly higher melting points than room temperature. The presence of crystalline domains within the films at room temperature could add value to the final properties of the materials, as crystallinity influences mechanical properties, thermal stability, and most importantly for the present work, the barrier properties.

4.3.3. Self-nucleation

As emphasized by the non-isothermal crystallization experiments on the films, the selected poly(thioethers) are slow-crystallizing materials when they are cooled from the melt. One way to accelerate crystallization kinetics is to implement a self-nucleation (SN) strategy, a thermal protocol in which self-nuclei are generated within the material at a selected T_s. [4] SN allows control of the nucleation step preceding the crystal growth. This step is substantially accelerated when polymer chains nucleate on pre-existing surfaces. In the case that polymer chains are allow to nucleate on preexisting crystals, the self-nucleation is very efficient, as the chains can epitaxially nucleate on the existing own crystals structures. SN exponentially increases the nucleation density and thus the overall crystallization kinetics are accelerated.[15]

In our case, the conventional SN thermal protocol (Figure 4.2.a) could be applied to the film F.B1.HD, as non-isothermal experiments have shown that this film could crystallize from the isotropic melt through cold crystallization, attesting for its slightly faster crystallization kinetics than films F.A1, F.A2, F.B2 and F.C.

For the film F.B1.HD, successful SN experiments were performed and the overall crystallization kinetics were accelerated, as exothermic recrystallization peaks could be observed by DSC during cooling at 10ºC/min from a range of T_s values (Figure 4.8.a).

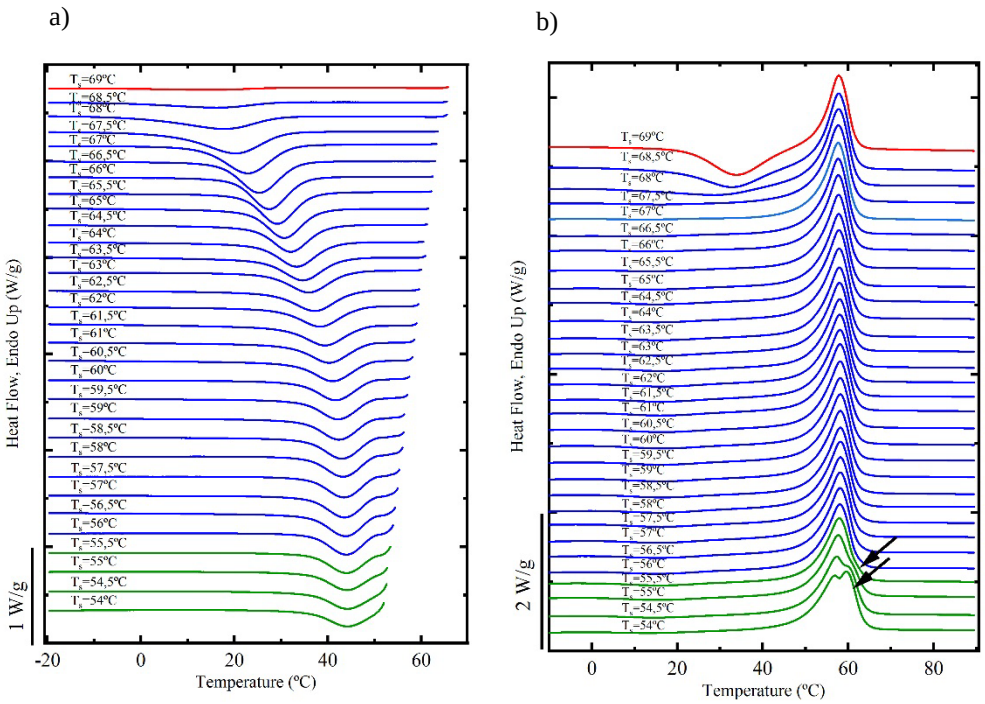

Figure 4.8. Self-nucleation experiments for poly(thioether) film F.B1.HD: (a) DSC cooling scan from the indicated T_s temperatures at 10ºC/min and (b) subsequent heating scans at 20ºC/min. Arrows show traces of annealing and sake of clarity, they are only presented in the first and last T_s of *Domain III.*

From the SN experiments, three domains can be defined as described by Fillon *et al.*[3]. In *Domain I*, which occurs for T_s values well above T_m, the polymer is completely melted. The thermal history and memory effect induced by previous crystallization are erased, and the crystallization temperatures (T_c) obtained upon cooling are constant. According to the DSC traces in Figure 4.8.a, F.B1.HD is in *Domain I* for T_s higher than 69ºC. The exothermic peak upon cooling is not visible by DSC, as the absence of self-nuclei could not speed up

crystallization kinetics. In this domain, the film displays the same behaviour as in the non-isothermal experiment shown in Figure 4.7.A.

In *Domain II*, T_s values are high enough to melt most of the crystals and low enough to create self-nuclei causing the so-called melt memory effect. In the present case, the self-nuclei are composed by crystal fragments that were not melted at T_s, as indicated by the fact that the T_s temperatures are always within the melting range of the polymer (see Figure 4.9). Self-seeds constitute ideal nucleation sites for epitaxially crystallizing the polymer, and they increase greatly the nucleation density, which is reflected by a crystallization peak from the melt shifted to higher temperatures.[3–5,16] According to the DSC traces in Figure 4.8.a, the F.B1.HD film is in *Domain II*, or self-nucleation domain, in the range of T_s from 56 ºC to 68.5 ºC: the overall crystallization kinetics is accelerated, with the crystallization peak visible on DSC traces upon cooling and clearly shifting towards higher temperature values while increasing its magnitude at the same time (see Figure 4.9 below).

In Figure 4.9, the T_c of F.B1.HD as a function of T_s temperature is presented superposed to the first heating scan of the film. The plot of T_c against T_s shows a clear increase of T_c as T_s decreases in the *Domain II* temperature range. Nevertheless, the range of T_s is still high enough to avoid annealing of the pre-existing crystals, which is the main difference with *Domain III*.

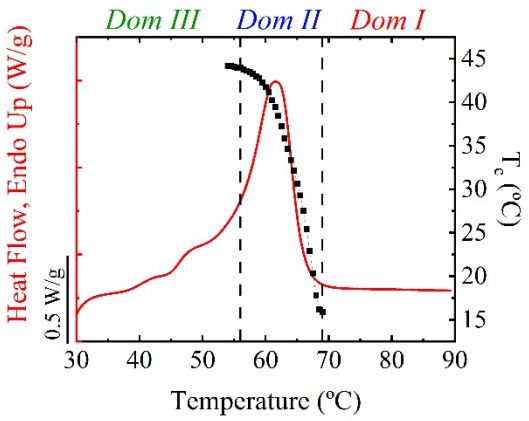

Figure 4.9. T_c as a function of T_s (right-hand temperature axis) for the F.B1.HD superimposed on its first melting endotherm. Values are taken from the self-nucleation experiments reported in Figure 4.8. and first heating scan of the film from Figure 4.4.

In *Domain III* or self-nucleation and annealing domain, T_s values are lower than in *Domain II*, so that the material is only partially melted. The unmolten crystals experience an annealing process during the 5 minutes holding time at T_s. Therefore, *Domain III* can be differentiated from *Domain II* by the presence of annealing traces in the final heating scan of the experiment. Annealing of the unmolten crystals is visible on the heating scans by DSC (Figure 4.8.b), as annealed crystals melt at higher temperatures. The film F.B1.HD is in *Domain III* at T_s lower than 55,5ºC. In Figure 4.9, the vertical lines divide the temperature range into the three different domains for the film F.B1.HD.

For the other samples, F.A1, F.A2, F.B2 and F.C, the thermal protocol had to be adapted, as these poly(thioethers) do not crystallize from molten state. The step in which films are cooled from isotropic melt to create a standard thermal history and polymers crystallize until saturation

is precluded. As presented in Figure 4.2.b, the films are directly heated up to a range of T_s values and conditioned 5 minutes at these temperatures. T_s values were selected within the onset and the end of the melting peak obtained from the first heating scan of the non-isothermal procedure (Figure 4.4). With this thermal protocol, it is expected that polymers from films F.A1, F.A2, F.B2, and F.C are in the SN *Domains II* and *III*.

The cooling rate in SN experiments was selected after a study of the films based on the model monomer pair GDMA-DATP, which were cooled at 1ºC/min, 10ºC/min, and 20ºC/min from a T_s of 45ºC. The results, reported in Figure 4.10, show that a crystallization peak can be observed when cooling at 10ºC/min and even at 20ºC/min after the self-nucleation step, which is not possible when the films are cooled from their molten state at these rates.

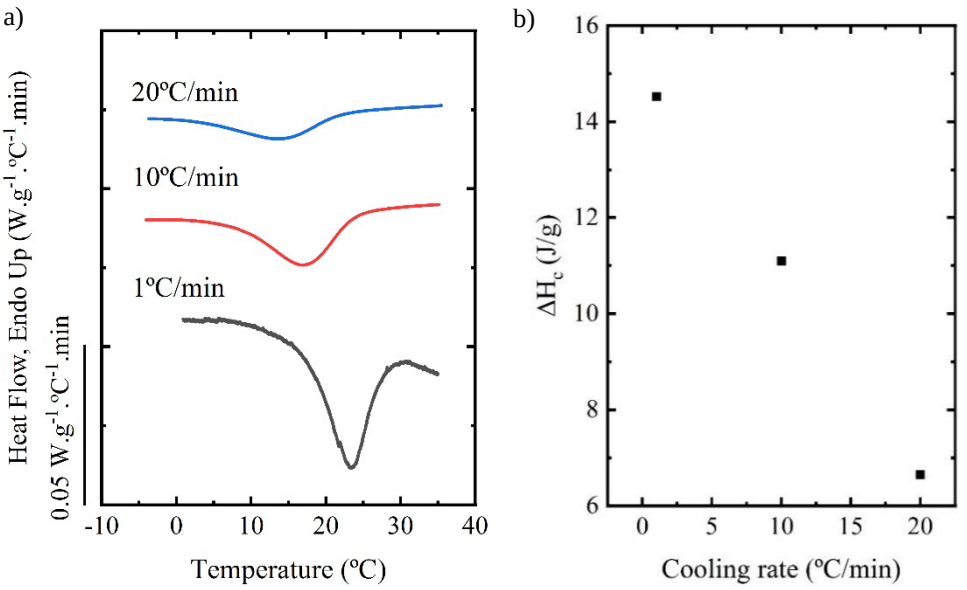

Figure 4.10. Preliminary tests to select the adequate cooling rate in SN experiments for the films based on GDMA-DATP. (a) DSC cooling scan from the T_s temperature of 45 ºC at the indicated cooling rate and (b) Crystallization enthalpy versus cooling rate.

A cooling rate of 10ºC/min was selected for the rest of SN experiments, as the results in Figures 4.10.a show that this cooling rate allows a better recovery of the crystallinity compared to a cooling rate of 20ºC/min. For the latter, as it can be observed in Figure 4.10.b, the crystallization enthalpy values are too low to permit work within a wide range of T_s.

Successful SN experiments were performed for F.A1, F.A2, F.B2 and F.C and the overall crystallization kinetics were accelerated, as exothermic recrystallization peaks can be observed by DSC upon cooling at 10ºC/min from a range of T_s (Figures 4.11.a, 4.12.a, 4.13.a, 4.14.a). Taking into consideration the thermal treatment, crystals that were present in the as-synthesized

film, and probably formed during film formation, are partially melted and act as self-nuclei in the subsequent cooling scans. A final heating scan at 20ºC/min is performed to observe the melting of the crystals formed (Figures 4.11.b, 4.12.b, 4.13.b, 4.14.b).

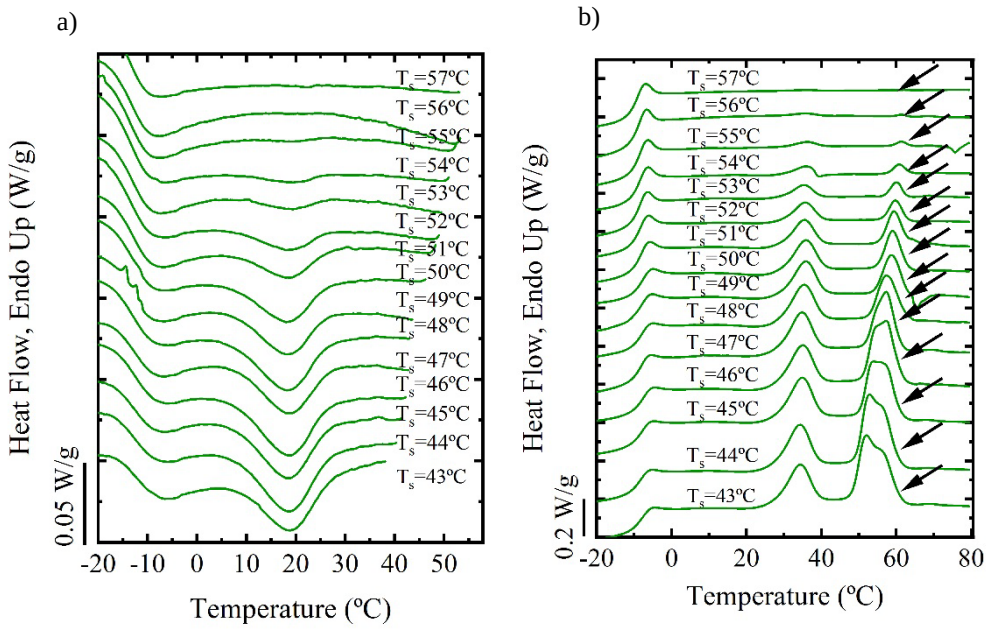

Figure 4.11. Self-nucleation experiments for poly(thioether) film F.A1: (a) DSC cooling scans from the indicated Ts temperatures at 10ºC/min and (b) subsequent heating scans at 20ºC/min. Arrows show traces of annealing.

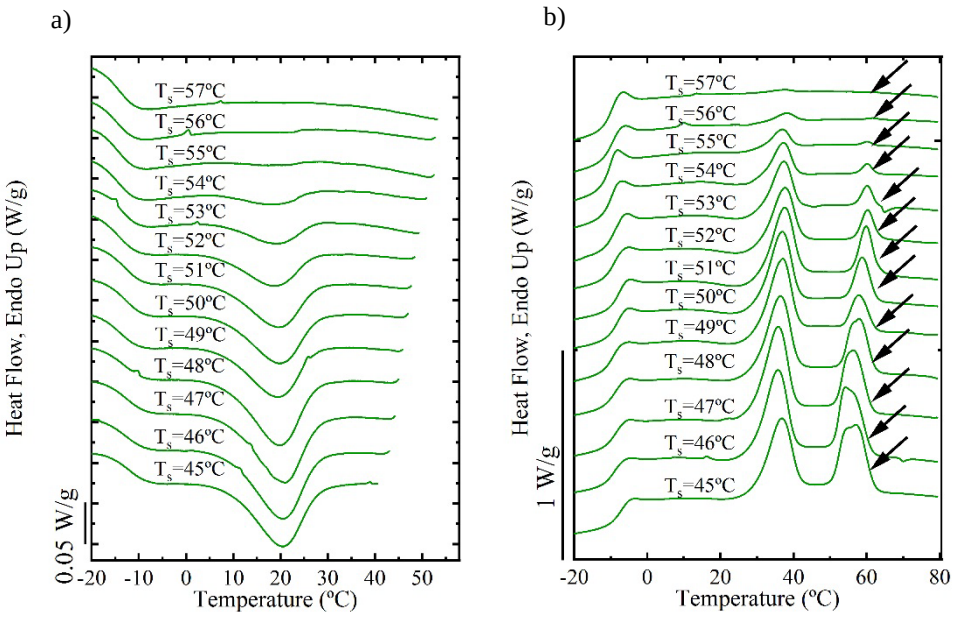

Figure 4.12.Self-nucleated poly(thioether) film F.A2: (a) DSC cooling scan from the indicated T_s temperatures at 10ºC/min and (b) subsequent heating scans at 20ºC/min. Arrows show traces of annealing.

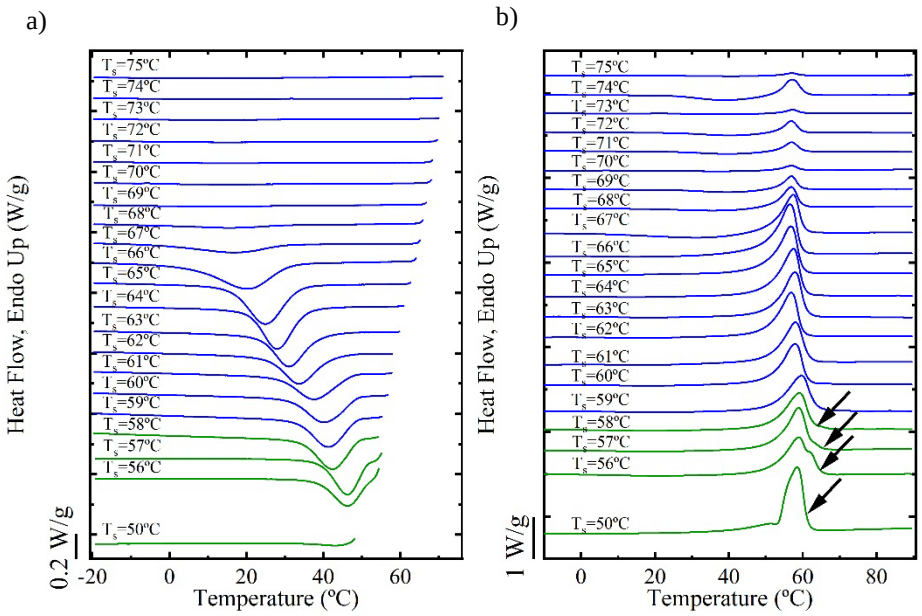

Figure 4.13 Self-nucleation experiments for poly(thioether) film F.B2: (a) DSC cooling scans from the indicated T_s temperatures at 10ºC/min and (b) subsequent heating scans at 20ºC/min. Arrows show traces of annealing.

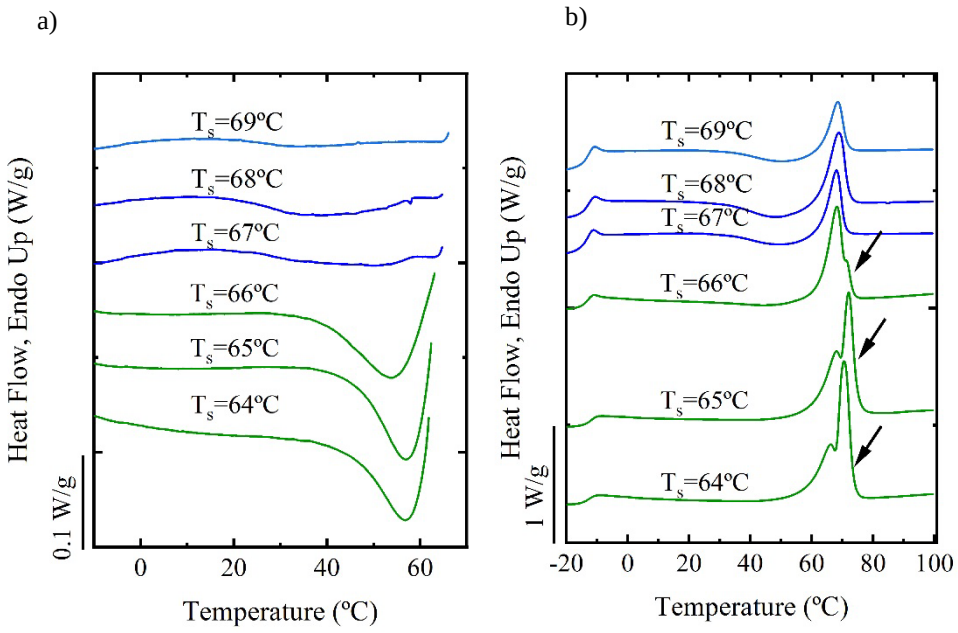

Figure 4.14. Self-nucleation experiments for poly(thioether) film F.C: (a) DSC cooling scan from the indicated T_s temperatures at 10ºC/min and (b) subsequent heating scans at 20ºC/min. Arrows show traces of annealing.

For the films F.A1 and F.A2 based on the monomer pair GDMA-DATP, similar behaviours can be appreciated. In the cooling scans from the range of T_s selected (Figures 4.11.a. and 4.12.a), T_c does not significantly change with T_s for F.A1 (Figure 4.15.a) and slightly increases at lower T_s for F.A2 (Figure 4.15.b.). In the following DSC heating scans, traces of annealing can be appreciated with clear multimodal peaks shown in Figures 4.11.b and 4.12.b.

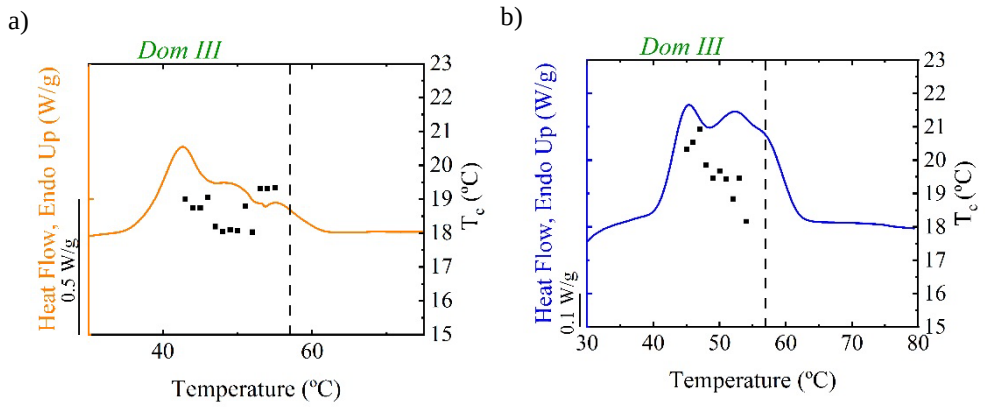

Figure 4.15. T_c as a function of T_s for a) F.A1 and b) F.A2 superimposed with the first melting endotherm of the films.Values are depicted from the self-nucleation experiments Figures 4.11 and 4.12 and first heating scan of the films Figure 4.4.

Hence, polymers based on GDMA-DATP are in the SN *Domain III* in the range of T_s selected. When T_s values were increased above 57ºC, no recrystallization peak could be observed by DSC, showing that GDMA-DATP polymer cannot recrystallize when in *Domain II* and above. The absence of *Domain II*, or self-nucleation domain, shows that GDMA-DATP polymer does not display a melt memory effect.

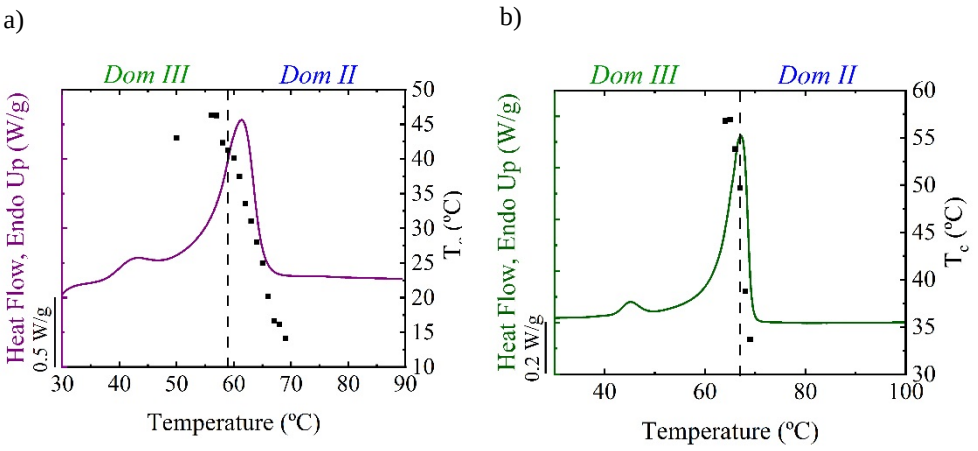

Figure 4.16. T_c as a function of T_s for a) F.B2 and b) F.C, superimposed with the first melting endotherm of the films.Values are depicted from the self-nucleation experiments Figures 4.13 and 4.14.

In the DSC heating scans Figures 4.13.b and 4.14.b, traces of annealing can be appreciated for the film F.B2 at T_s lower than 58ºC and for the film F.C at T_s lower than 66ºC showing that the films are in *Domain III* below these temperatures. At higher T_s, F.B2 and F.C are in *Domain II*, with a clear increase of T_c (and crystallization kinetics), as seen in Figure 4.16.

Table 4.6. Films characteristics and number of SN domains

Film	Monomers	HD (wt%)	M_w (KDa)	Domains	T_g (ºC)
F.A1	GDMA-DATP	-	9.135	Dom III	-15.6
F.A2	GDMA-DATP	-	22.696	Dom III	-7.8
F.B1.HD	EDDT-DATP	6	52.010	Dom III, II, I	-22.3
F.B2	EDDT-DATP	-	81.152	Dom III, II	-22.6
F.C	GDMP-DATP	-	34.618	Dom III, II	-14.6

Table 4.6. summarizes the characteristics of each film in terms of chemical structure, molar mass, T_g and number of domains. It was reported that while studying the melt-memory

effect by SN experiments, the effect of chemical structures could be investigated by comparing the width of self-nucleation domain (or domain II).[15] On behalf of the results obtained for the studied films, we propose here a comparison in terms of the number of SN domains. As highlighted in Table 4.6, the film F.B1.HD is the only one presenting the three SN domains. As supported by the previous non-isothermal study, F.B1.HD presents faster crystallization kinetics attributed to the linearity of the EDDT-DATP chains (promoting the organization into crystalline structures) and low T_g of -22.6ºC, but as well the presence of HD. When compared to its counterpart F.B2, which displays the same chemical structure and nearly same T_g but only two SN domains, F.B1.HD faster crystallization can be explained by the lower molar mass and presence of HD, as explained previously. The F.C film also exhibits two SN domains, highlighting slower kinetics than F.B1.HD. The presence of additional ester groups within the polymer backbone from GDMP monomer, and the higher T_g of -14.6ºC may enhance chain rigidity and slow down crystallization kinetics compared to F.B1.HD. Finally, SN experiments disclose that the films based on GDMA-DATP polymer (F.A1 and F.A2) present the slowest crystallization kinetics with crystallization occurring only in *Domain III*. The slowest crystallization kinetics of GDMA-DATP films is due to the chemical structure, which on one hand has the aromatic groups and on the other higher density of ester groups than in GDMA-based polymer.

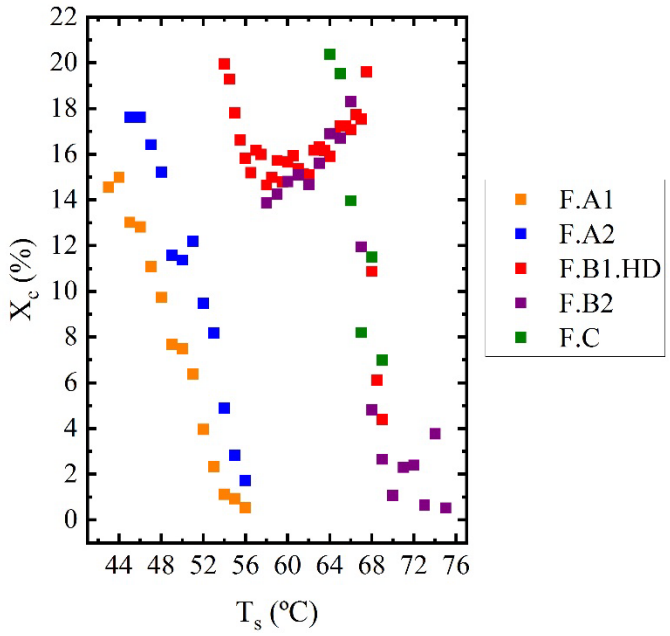

Figure 4.17. Degree of crystallinity (X_c) against T_s for the films F.A1, F.A2, F.B1.HD, F.B2 and F.C

To gain deeper insight on poly(thioethers) crystalline behaviour, the degree of crystallinity X_c at each T_s was calculated for the studied films using equation 4.1, and the results are shown in Figure 4.17. By comparison with X_c calculated for the as synthesized samples presented in Table 4.5, the degree of crystallinity after SN experiments is slightly decreased for the samples F.A1, F.B1.HD, F.B2, and F.C. Even though the crystals present in the as-synthesized samples were not fully recovered, fast crystallization from molten state was achieved for these polymers by the SN strategy. It is noteworthy that the degree of crystallinity after SN is increased in the case of the film F.A2 at T_s 45ºC, 46ºC and 47ºC with X_c above 16%.

4.4. Conclusion

In Chapter 3, we presented the synthesis of waterborne film-forming polysulfide latexes by sonopolymerisation combined with photopolymerisation, based on diene monomer DATP and various dithiol monomers GDMA, GDMP and EDDT. The combination of two polymerisation processes allows for first time to achieve ultra-high molar mass step-growth poly(thioethers) by photopolymerizing bifunctional thiol-ene sono-pre-polymers. A film forming, semicrystalline polymer latex with solids content of 30%, was synthesized for the first time.

As the selected monomers are bifunctionnal, the thiol-ene step-growth mechanism facilitates the synthesis of linear poly(thioether) with semicrystalline behaviour evidenced by DSC analysis. The as-synthesized films F.A1 to F.C present a degree of crystallinity of approximately 20% and slow crystallizing polymer chains. The SN thermal protocol turns out to be an efficient strategy to study the crystallization behaviour of such polymers, as the produced self-nuclei substantially sped up the overall crystallization kinetics. This study allowed to correlate the chemical structure of the poly(thioethers) with crystallization rate by comparing the number of SN domains that can be detected by the technique. Indeed, the film F.B1.HD, based on the monomer combination EDDT-DATP is the only one presenting the three SN domains described by Fillon et *al*. Its faster crystallization kinetics are attributed to the linearity of the EDDT-DATP chains (promoting the organization into crystalline structures) with low T_g of -22.6ºC. In addition, the presence of HD could act as a plasticizer and promote fast ordering of polymer chains.

4.5. References

(1) Jasinski, F.; Lobry, E.; Tarablsi, B.; Chemtob, A.; Croutxé-Barghorn, C.; Nouen, D. Le; Criqui, A. Light-Mediated Thiol-Ene Polymerization in Miniemulsion: A Fast Route to Semicrystalline Polysul Fide Nanoparticles. *ACS Macro Lett.* **2014**, *3* (9), 958–962. https://doi.org/10.1021/mz500458s.

(2) Jasinski, F.; Rannée, A.; Schweitzer, J.; Fischer, D.; Lobry, E.; Croutxé-Barghorn, C.; Schmutz, M.; Le Nouen, D.; Criqui, A.; Chemtob, A. Thiol-Ene Linear Step-Growth Photopolymerization in Miniemulsion: Fast Rates, Redox-Responsive Particles, and Semicrystalline Films. *Macromolecules* **2016**, *49* (4), 1143–1153. https://doi.org/10.1021/acs.macromol.5b02512.

(3) Fillon, B.; Wittmann, J. C.; Lotz, B.; Thierry, A. Self-nucleation and Recrystallization of Isotactic Polypropylene (α Phase) Investigated by Differential Scanning Calorimetry. *J. Polym. Sci. Part B Polym. Phys.* **1993**, *31* (10), 1383–1393. https://doi.org/10.1002/polb.1993.090311013.

(4) Michell, R. M.; Mugica, A.; Zubitur, M.; Muller, A. J. Self-Nucleation of Crystalline Phases within Homopolymers, Polymer Blends, Copolymers, and Nanocomposites. *Adv. Polym. Sci.* **2017**, *276* (August 2015), 215–256. https://doi.org/10.1007/12_2015_327.

(5) Sangroniz, L.; Cavallo, D.; Müller, A. J. Self-Nucleation Effects on Polymer Crystallization. *Macromolecules* **2020**, *53* (12), 4581–4604. https://doi.org/10.1021/acs.macromol.0c00223.

(6) Van Krevelen, D. W.; Te Nijenhuis, K. *Properties of Polymers*; 2009. https://doi.org/10.1016/B978-0-08-054819-7.X0001-5.

(7) Król-Morkisz, K.; Pielichowska, K. *Thermal Decomposition of Polymer Nanocomposites With Functionalized Nanoparticles*; Elsevier Inc., 2018. https://doi.org/10.1016/B978-0-12-814064-2.00013-5.

(8) Kholodovych, V.; Welsh, W. J. Thermal-Oxidative Stability and Degradation of Polymers. *Phys. Prop. Polym. Handb.* **2007**, No. 1, 927–938. https://doi.org/10.1007/978-0-387-69002-5_54.

(9) Witkowski, A.; Stec, A. A.; Hull, T. R. *Thermal Decomposition of Polymeric Materials*; 2016. https://doi.org/10.1007/978-1-4939-2565-0.

(10) Patterson, M. C.; Dunkelberger, D. L. Additives for Processing Rigid PVDC Copolymers. *J. Vinyl Technol.* **1994**, *16* (1), 46–51. https://doi.org/10.1002/vnl.730160112.

(11) Chen, C. L.; Hsieh, T. H.; Ho, K. S. Studies on the Crystallization of Poly(Vinylidene Chloride-Co-Vinyl Chloride). *Polym. J.* **2001**, *33* (11), 835–841. https://doi.org/10.1295/polymj.33.835.

(12) Godovsky, Y. K.; Slonimsky, G. L.; Garbar, N. M. Effect of Molecular Weight on the Crystallization and Morphology of Poly(Ethylene Oxide) Fractions. *J Polym Sci, Part C, Polym Symp* **1972**, *21* (38), 1–21. https://doi.org/10.1002/polc.5070380103.

(13) Chen, X.; Hou, G.; Chen, Y.; Yang, K.; Dong, Y.; Zhou, H. Effect of Molecular Weight on Crystallization, Melting Behavior and Morphology of Poly(Trimethylene Terephalate). *Polym. Test.* **2007**, *26* (2), 144–153. https://doi.org/10.1016/j.polymertesting.2006.08.011.

(14) Jenkins, M. J.; Harrison, K. L. The Effect of Molecular Weight on the Crystallization Kinetics of Polycaprolactone. *Polym. Adv. Technol.* **2008**, No. November 2007, 229–236. https://doi.org/10.1002/pat.

(15) Sangroniz, L.; Meabe, L.; Basterretxea, A.; Sardon, H.; Müller, A. J.; Cavallo, D. Chemical Structure Drives Memory Effects in the Crystallization of Homopolymers †. *Macromolecules* **2020**, *53* (12), 4874–4881. https://doi.org/10.1021/acs.macromol.0c00751.

(16) Quero, E.; Müller, A. J.; Signori, F.; Coltelli, M. B.; Bronco, S. Isothermal Cold-Crystallization of PLA/PBAT Blends with and without the Addition of Acetyl Tributyl Citrate. *Macromol. Chem. Phys.* **2012**, *213* (1), 36–48. https://doi.org/10.1002/macp.201100437.

(17) Kuru, A.; Aksoy, S. A. Cellulose–PEG Grafts from Cotton Waste in Thermo-Regulating Textiles. *Text. Res. J.* **2014**, *84* (4), 337–346. https://doi.org/10.1177/0040517513494251.

Chapter 5. Crystallization of aliphatic poly(thioethers)

The results presented in this Chapter were obtained in collaboration with Valentina Pirela and Prof. Alejandro J. Müller from the University of the Basque Country (Spain), with Brahim Bessif and Prof. Günter Reiter from Freiburg University (Germany) and with Dr. Cuong Minh Quoc Le and Dr. Abraham Chemtob from the University of Haute Alsace (France)

5.1. Introduction

It is well known that the crystallization behaviour is related to the final properties of the material. Hence, one way to evaluate a new type of material is by performing thermal, structural, and morphological characterization. It is a straightforward means to discard or motivate the use of new materials for an aimed application. In Chapter 4, we reported the crystalline behaviour of the film-forming and waterborne poly(thioethers) based on the monomers dially terephthalate (DATP), glycol dimercaptoacetate (GDMA), glycol dimercaptopropionate (GDMP), and 2,2-(ethylenedioxy)diethanethiol (EDDT). These polymers suffered from a low degree of crystallinity and slow crystallization kinetics, which limited the crystallinity study. However, a low degree of crystallinity is required to obtain continuous polymer films from the waterborne dispersions after drying at ambient conditions. It was shown that the presence of the aromatic ring within the polymer backbone was necessary for formation of films with sufficient

mechanical resistance to be applied as a protective coating. However, it drastically reduced the degree of crystallinity and slowed down the crystallization kinetics.

In this chapter, therefore, attention was turned toward three other poly(thioethers) composed of more linear backbones without aromatic or cyclic structures nor pending functionalities, based on monomers such as di(ethylene glycol) divinyl ether (DVE), 2,2'-dimercaptodiethyl sulfide (DMDS), triethylene glycol divinyl ether (TEGDVE) and 1,4-butanediol divinyl ether (BDDVE), which chemical structures are presented in Figure 5.1. Linear symmetric repeating units should increase the degree of crystallinity and provide sufficient mechanical resistance to the films for coating application.

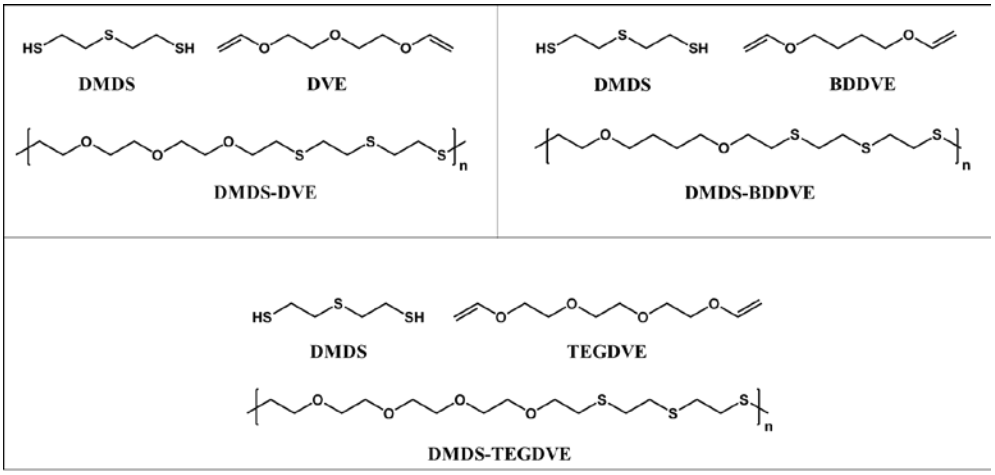

Figure 5.1. Chemical structures of the monomers DVE, DMDS, TEGDVE and BDDVE.

In this chapter, a preliminary study on the crystallization behaviour of polymers DVE-DMDS, TEGDVE-DMDS, and BDDVE-DMDS will be assessed by performing advanced

differential scanning calorimetry (DSC) analysis and morphologies will be observed by Polarized light optical microscope (PLOM).

5.2. Experimental and method

5.2.1. Materials

Poly(thioethers) based on the monomers 2,2'-dimercaptodiethyl sulfide (DMDS), di(ethylene glycol), divinyl ether (DVE), triethylene glycol divinyl ether (TEGDVE), and 1,4-butanediol divinyl ether (BDDVE) were kindly synthesized and provided by Institut de Sciences des Matériaux de Mulhouse (IS2M), from the Université de Haute-Alsace, France.

Herein, thiol-ene step-growth polymerization was performed between DMDS and three other diene monomers DVE, TEGDVE and BDDVE by Le *et al.*, following the synthetic process they developed for the monomers DMDS and diallyl phthalate (DAP)[1]. The synthesis is described in Appendix III, and the polymers' molar masses and glass transition temperatures (T_g) are reported in Table 5.1.

Table 5.1. Molar masses of the poly(thioethers) based on DVE-DMDS, TEGDVE-DMDS and BDDVE-DMDS

Polymer	M_n (kDa)	T_g(°C)
DVE-DMDS	9.8	-35
TEGDVE-DMDS	14.1	-27
BDDVE-DMDS	17.4	-40

5.2.2. Characterization

5.2.2.1. Differential scanning calorimetry (DSC)

The crystallization study was carried out on a differential scanning calorimeter Perkin Elmer DSC 8000 equipment using an Intracooler II cooling system. Approximately 5 mg samples were encapsulated in aluminium pans.

- **Non-isothermal protocol**

For the non-isothermal protocol, samples were heated up to 120ºC for DVE-DMDS, 100ºC for TEGDVE-DMDS, and 120ºC for BDDVE-DMDS at 20ºC/min and held 3 minutes in the molten state to erase thermal history. A subsequent cooling rate at 20ºC/min was performed until -40ºC for the samples DVE-DMDS and TEGDVE-DMDS and until 0ºC for the BDDVE-DMDS sample. A final heating scan was performed at 20ºC/min to the molten state.

- **Isothermal protocol**

First, the minimum isothermal crystallization temperature ($T_{c,min}$) in which the material can be cooled down at 60ºC/min without crystallizing has to be determined, following the protocol of Lorenzo *et al.* [7]. For that aim, samples were heated to 30ºC above their melting temperatures to erase thermal history, and cooled to the temperature T_c to be tested (generally the temperature at which the polymer starts to crystallize, and estimated from the non-isothermal DSC cooling scan) at 60ºC/min. When samples reach the selected T_c temperature, they are directly heated up. $T_{c,min}$ is the minimum temperature for which no melting peak is observed in

the latter heating scan, attesting that no crystals were formed during the cooling scan at 60ºC/min. With this method $T_{c,min}$ values of 60ºC, 46ºC and 79ºC were respectively obtained for the polymers DVE-DMDS, TEGDVE-DMDS and BDDVE-DMDS.

For the isothermal protocol, samples were heated to their molten state at 20ºC/min and kept 3 minutes at this temperature. They were then rapidly cooled down to a range of crystallization temperatures (T_c) with $T_c \geq T_{c,min}$ at 60ºC/min. In the last step, samples were heated up at 20ºC/min to record the melting of crystals formed isothermally. The schematic presentation of isothermal thermal procedure is depicted in Figure 5.2.

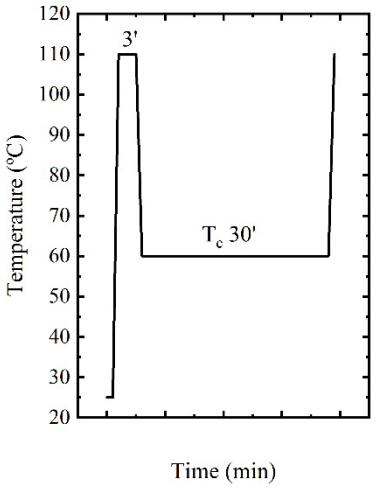

Figure 5.2. Schematic representation of an isothermal experiment, with heating rate of 20ºC/min and cooling rate of 60ºC/min

The isothermal polymer crystallization kinetics data were fitted to the Avrami equation. All the calculations needed to perform the Avrami fits were performed with an Origin

application software that was developed by Lorenzo et al. [7]. All fits were performed for a relative volumetric conversion range encompassing 0.03–0.2, i.e., from 3% to 20% relative conversion to the semi-crystalline state. From the origin plugin, the following values are measured: the experimental half-crystallization time ($\tau_{50\%,exp}$) (min), the Avrami index (n), the induction time (t_0) (min) and the correlation coefficient R^2 (that should be 0.9990 or larger[7]).

5.2.2.2. Polarized light optical microscope (PLOM)

For the non-isothermal, isothermal and self-nucleation protocols described below, a PLOM Olympus BX51 was employed incorporating a λ plate in between the polarizers at 45º to facilitate observation and determine the sign of the birefringence. The microscope was equipped with an Olympus SC50 digital camera. A Linkam LNP95 hot stage, which was connected to liquid nitrogen, was coupled to the equipment. Samples of DVE-DMDS, TEGDVE-DMDS and BDDVE-DMDS were dissolved in chloroform at a concentration of 5mg/mL and drop casted to glass slide at room temperature. Thin films were obtained after solvent evaporation, and were analysed uncovered.

- **Non-isothermal protocol**

For the non-isothermal protocol, samples DVE-DMDS, TEGDVE-DMDS and BDDVE-DMDS were respectively heated up to 120ºC, 93ºC and 126ºC at 20ºC/min and hold 3 minutes in their melted state in order to erase thermal history. Samples were subsequently slowly cooled down at 1ºC/min.

- **Isothermal protocol**

Following the isothermal thermal program performed with DSC, for the isothermal protocol under PLOM samples DVE-DMDS, TEGDVE-DMDS and BDDVE-DMDS were respectively heated up to 120ºC, 93ºC and 126ºC at 20ºC/min and kept 3 minutes at this temperature. They were then rapidly cooled down to a range of crystallization temperatures (T_c) at 50ºC/min, which is the fastest rate of cooling that can be achieved by the Linkam LNP95 hot stage, and kept at the selected T_c until the growth of single crystal could be isolated (*i.e.* does not get in contact with another growing crystal).

- **Successive isothermal protocol on sample DVE-DMDS**

For the thermal protocol described in this section, consisting of successive isothermal steps, thin polymer films based on DVE-DMDS polymer were prepared. As substrate, a commercially available silicon (Si) wafers (Silchem, Freiberg, Germany), which was cleaned via a UV (ultraviolet light)-ozone treatment was used. A sample of DVE-DMDS, was dissolved in chloroform at a concentration of 10 mg/mL at 50ºC until full dissolution. The solution was then spin-coated (WS-650MZ-23NPP, Laurell Technologies Corporation, North Wales, PA, USA) onto cleaned Si-substrate (2 x 2 cm2) at a rotation speed of 2000 rpm, for 1 min at room temperature. A dry and solid polymer film was obtained after total evaporation of the solvent. The dried thin polymer film was used for in-situ crystallization studies in an inert atmosphere (nitrogen) under an optical microscope (ZEISS A1, Oberkochen, Germany) equipped with a color camera (AXIOCAM, ICc 1, ZEISS). The temperature of the crystallization process was

controlled by a hot stage (Linkam TMS 94, Linkam Scientific Instruments Ltd, Redhill, UK) with a precision of 0.1°C. Morphological characterization of the polymers during and after crystallization in thin films was performed by PLOM, focusing on birefringence using crossed polarizers. The thermal procedure is explained in the *Results and discussion* section.

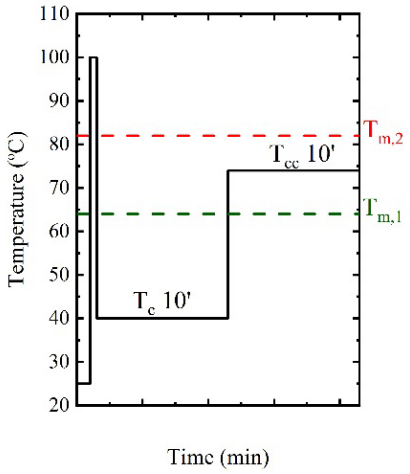

Figure 5.3 Thermal protocol applied to the sample DVE-DMDS to observe the morphology of polymorphs evidenced by DSC and in-situ WAXS.

Figure 5.3 shows the thermal protocol employed for investigating differences in morphology resulting from isothermal crystallization of DVE-DMDS thin film at temperatures T_c and T_{cc}, respectively. The experiment was performed in three steps. First the spin coated film was completely molten at a temperature of 100°C, which is well above the melting temperature of DVE-DMDS, to erase thermal history. Subsequently, the film was quenched to a chosen low crystallization temperature T_c of 40ºC, kept 10 min at this temperature, and the evolution of structural features was followed by PLOM. Finally, the resulting crystalline structures obtained

at T_c were molten by increasing the temperature to T_{cc} of 74ºC at a rate of 150 °C/min. The film was kept 10 min at this temperature, and the formation of crystals was followed by PLOM.

5.2.2.3. Wide angle X ray diffraction (WAXS)

Non-isothermal in-situ WAXS experiments were carried out at the ALBA Synchrotron Radiation Facility (Barcelona, Spain) at the beamline BL11 NCD-SWEET. DSC pans were employed to place samples in the beam path. A THMS 600 Linkam hot stage device was employed to first heat the samples from room temperature to the melt at 20 ºC/min and then from the melt to room temperature at the same rate, while WAXS data has been collected. The X-ray energy source amounted to 12.4 eV using a channel cut Si (1 1 1) monochromator (λ = 1.03 Å). The sample-detector distance was 132.6 mm with a 21.2° tilt angle, and chromium (III) oxide was employed for the calibration. A Rayonix LX255-HS detector, Evanston, IL, USA, with a resolution of 1920 × 5760 pixels and a pixel size of 44 μm^2 was employed.

5.3. Results and discussion

5.2.3. DSC results under non-isothermal conditions

Non-isothermal DSC analysis were performed on the samples based on DVE-DMDS, TEGDVE-DMDS and BDDVE-DMDS at 20ºC/min. The first heating scan of the samples and relevant values are reported in Figure III.1 and Table III.1, in Appendix III. The DSC cooling scans from the melt and subsequent heating scans are shown in Figure 5.4. and the relevant values obtained from it are listed in Table 5.2.

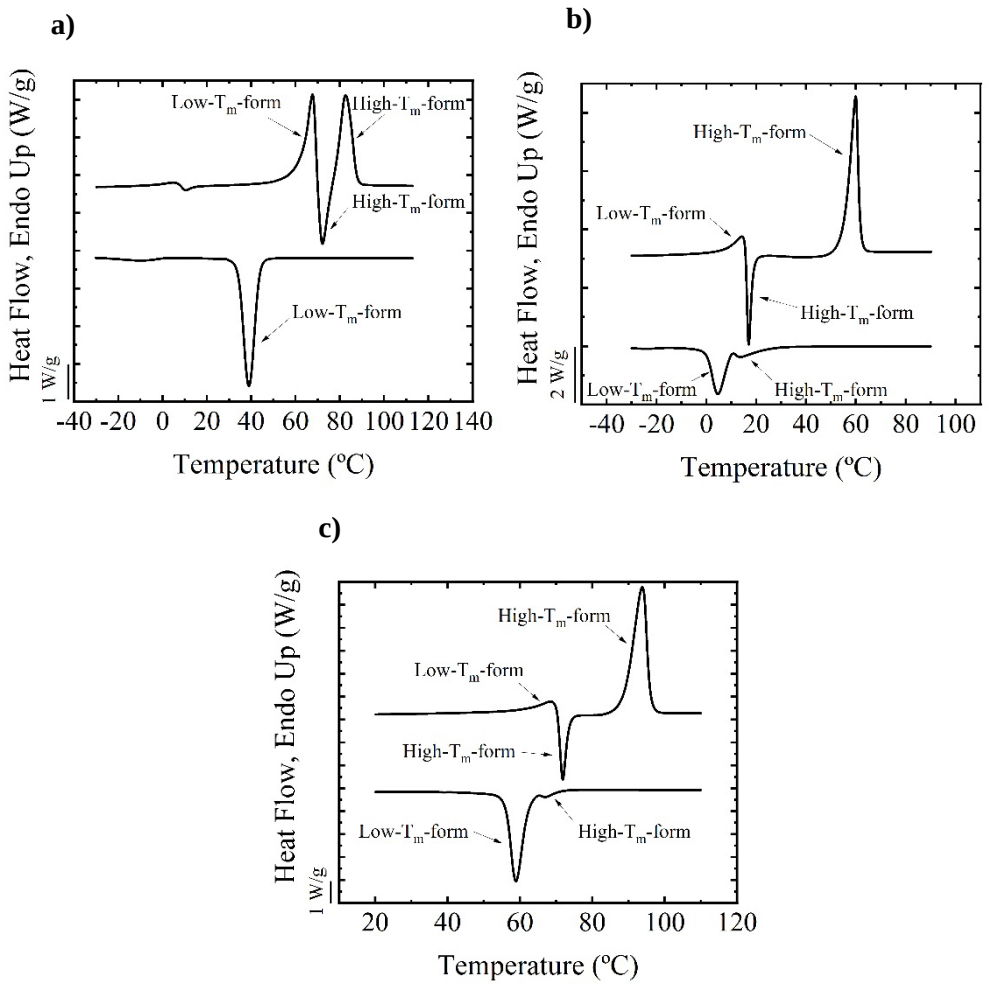

Figure 5.4. DSC cooling scans from molten state at 20ºC/min and subsequent heating scan at 20ºC/min for the polymers a) DVE-DMDS b) TEGDVE-DMDS and c) BDDVE-DMDS

The poly(thioethers) DVE-DMDS, TEGDVE-DMDS and BDDVE-DMDS crystallize upon cooling from the molten state, with an exothermic crystallization peak at T_c as seen in Figure 5.4. Noteworthy, for polymers TEGDVE-DMDS and BDDVE-DMDS, the

recrystallization peak displays a shoulder at higher temperatures. Upon heating, successive melting-crystallization-melting peaks are observed for the three polymers at respectively temperatures of $T_{m,1}$, T_{cc} and $T_{m,2}$ and reported in Table 5.2.

Table 5.2. Melting temperature (T_m), melting enthalpy (ΔH_m), crystallization temperature (T_c), crystallization enthalpy (ΔH_c), cold crystallization temperature (T_{cc}), cold crystallization enthalpy (ΔH_{cc}) of DVE-DMDS, TEGDVE-DMDS and BDDVE-DMDS. The values are obtained from non-isothermal DSC scans from Figure 5.4., with cooling scan from molten state at 20ºC/min and subsequent heating scan at 20ºC/min.

Polymer	Cooling		Second heating					
	T_c (ºC)	ΔH_c (J/g)	$T_{m,1}$ (ºC)	$\Delta H_{m,1}$ (J/g)	T_{cc} (ºC)	ΔH_{cc} (J/g)	$T_{m,2}$ (ºC)	$\Delta H_{m,2}$ (J/g)
DVE-DMDS	39.0	64	67.7	47	72.2	18	82.6	45
TEGDVE-DMDS	4.6 /14.7	45	14.1	23	17.0	14	59.9	81
BDDVE-DMDS	59.0 / 68.0	60	68.5	23	71.3	24	93.8	83

The first endotherm at $T_{m,1}$ (i.e., corresponding to the low melting temperature crystals) is attributed to the melting of the crystals formed upon cooling at T_c, with $T_{m,1} > T_c$. Subsequently, poly(thioethers) exhibit cold crystallization with an exotherm at $T_{cc} > T_{m,1}$, followed by the melting of the resulting crystals at $T_{m,2}$. The existence of two distinct melting peaks for the three polymers suggests that two different crystalline polymorphs exist. For sake of clarity, the crystals formed upon cooling and melting at $T_{m,1}$ are denoted as Low-T_m-form, and the crystals formed upon heating and melting at $T_{m,2}$ are referred to as High-T_m-form, as depicted in Figure 5.4 with arrows.

For the polymer DVE-DMDS, the high-T_m-form does not recrystallize from the melt, as emphasized by the single recrystallization peak at T_c upon cooling from the isotropic melt Figure 5.4.a. However, for the polymers TEGDVE-DMDS and BDDVE-DMDS, the behaviour is slightly different, as their crystallization peaks at T_c present shoulders at higher temperature (Figure 5.4 b and c). Hence, it is suggested that the Hight-T_m-form from polymers TEGDVE-DMDS and BDDVE-DMDS is capable to crystallize from the molten state.

Noticeably, the melting enthalpies of Low-T_m-form $\Delta H_{m,1}$ are substantially lower than the crystallization enthalpies ΔH_c (Table 5.2), indicating that their melting is masked by overlapping cold-crystallization. In addition, the melting temperatures of Low-T_m-form ($T_{m,1}$) and High-T_m-form ($T_{m,2}$) decrease when the T_g of the poly(thioethers) increases (TEGDVE-DMDS displays the highest T_g of -27ºC, and the lowest melting temperatures of 14.1ºC and 59.9ºC). Typically, a higher rigidity of the polymer chains in copolymers implies a higher T_g and melting temperature. Herein, such correlation is unmet, probably because the poly(thioethers) studied are alternating polymers.

Attention was turned towards the polymer DVE-DMDS, which displays a different behaviour than its counterparts. Non-isothermal DSC analysis were performed with various cooling rate (1ºC/min, 10ºC/min and 20ºC/min) and the DSC cooling scans from the melt and subsequent heating scans at 20ºC/min are shown in Figure 5.5. The relevant values are reported in Table 5.3, and show that crystallization upon cooling depends on the cooling rate.

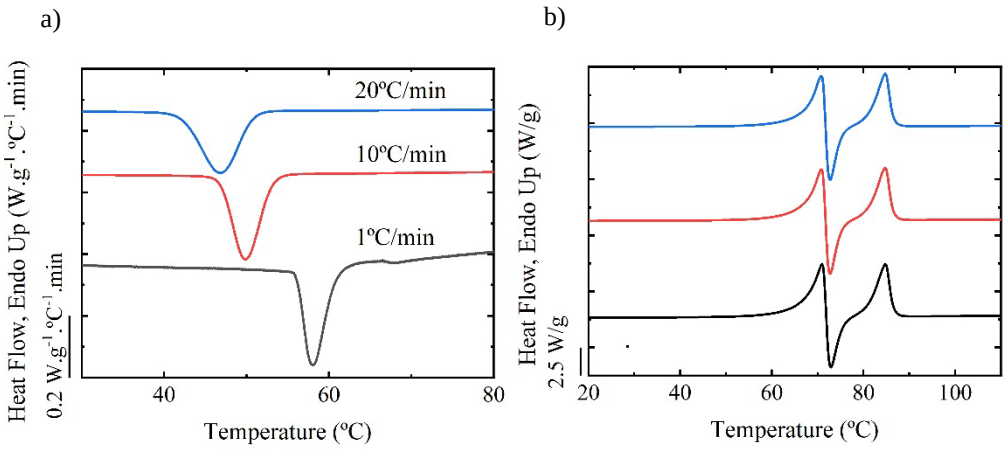

Figure 5.5. a) DSC cooling scans at 1ºC/min (black line), 10ºC/min (red line) and 20ºC/min (blue line) and b) subsequent heating scan at 20ºC/min for the polymer DVE-DMDS

Upon slow cooling rate ΔH_c increases, as an extended timeframe gives more time to the polymer chains to reorganize into crystalline domains, and a shift of T_c towards higher temperature is observed (Table 5.3). Hence, the formation of Low-T_m-form strongly depends on the cooling rate employed during the analysis.

Upon heating at 20ºC/min for the three samples, the same melting-crystallization-melting behaviour is observed, and the crystallization enthalpies ΔH_{cc} increases when a faster cooling rate is used in the previous step. From these results, it is shown that the appearance of High-T_m-form crystals upon heating also depend on the cooling rate used in the previous step and, somehow, on the Low-T_m-form formed in the previous step.

Table 5.3. T_m, ΔH_m, T_c, ΔH_c, T_{cc}, and ΔH_{cc} of the polymer DVE-DMDS. The values are obtained from non-isothermal DSC scan from Figure 5.5., with cooling scans at 1ºC/min, 10ºC/min and 20ºC/min and subsequent heating scan at 20ºC/min.

Cooling rate (ºC/min)	**Cooling**		**Second heating**					
	T_c (ºC)	**ΔH_c (J/g)**	**$T_{m,1}$ (ºC)**	**$\Delta H_{m,1}$ (J/g)**	**T_{cc} (ºC)**	**ΔH_{cc} (J/g)**	**$T_{m,2}$ (ºC)**	**$\Delta H_{m,2}$ (J/g)**
1	58.1	80	70.9	66	72.9	33	84.8	55
10	49.9	71	70.8	62	72.7	34	84.7	53
20	46.8	69	70.8	48	72.7	38	84.8	46

As emphasized previously, the successive melting-crystallization-melting behaviour suggests the existence of two different crystalline polymorphs High-T_m-form and Low-T_m-form. They could be due to differences in the way chains pack within the crystal unit cells. To support this assumption, further characterization techniques are required to reveal if structures obtained by crystallization below $T_{m,1}$ and at a temperature above $T_{m,1}$ are different. For that aim, non-isothermal Wide Angle X-ray scattering (WAXS) and PLOM were used to search for differences in morphological features in sample DVE-DMDS.

In analogy with the DSC experiments, non-isothermal in-situ WAXS scattering patterns were collected for the polymer DVE-DMDS, with a heating rate of 20ºC/min. The evolution of WAXS patterns with increasing temperature is shown in Figure 5.6.a, during the first heating scan of the as-synthesized sample (without any previous thermal treatment).

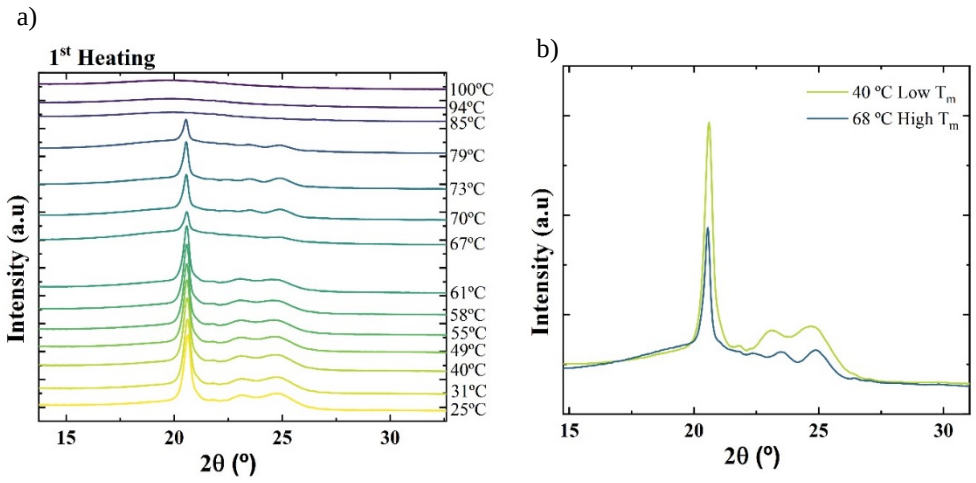

Figure 5.6. a) WAXS diffractograms of DVE-DMDS taken at the indicated temperature during the first heating ramp at 20ºC/min and b) WAXS diffractograns of DVE-DMDS at 40ºC and 60ºC.

Three distinct diffraction peaks can be observed at 20.6º, 23.2º and 24.9º. Upon heating, the Low-T_m-form starts to melt, and the intensity of the peaks decreases until it reaches 67ºC. Above this temperature, the intensity of the peaks increases again, suggesting that re-crystallization of the material i.e., the High-T_m-form is forming. Finally, the recrystallized material melts at 85ºC and above. Therefore, the results of WAXS and DSC show the same melting-crystallization-melting behaviour upon heating. Figure 5.6.b shows that a shift in the position of the peaks at 23.2 and 24.9ºC to higher angles is occurring above 67ºC. In addition, a fourth low-intensity peak appears at 22.5º on the WAXS diffractogram taken at 70ºC, which is not observed for the Low-T_m-form on the WAXS diffractogram taken at 46ºC (Figure 5.6.b). These differences in the scattering curves suggest that the crystal structures from Low-T_m- form and High-T_m-form are different, and attributed to two different polymorphs.

5.2.4. Non-isothermal analysis under PLOM

Non-isothermal crystallization was performed under a polarized light optical microscope (PLOM) for the polymers DVE-DMDS, TEGDVE-DMDS and BDDVE-DMDS. Samples were slowly cooled down at 1ºC/min from the molten state. Figure 5.7 displays the micrographs of the samples, which were taken at different temperature. Upon cooling, the growth of large birefringent spherulites is observed for the three samples.

As seen in Figure 5.7.a, for the polymer DVE-DMDS, the appearance of spherulites occurs at 54ºC upon cooling, which is attributed to the Low-T_m-form. Indeed, DSC results in Figure 5.4.a showed that High-T_m-form does not crystallize from the melt in the selected conditions, as only one single crystallization peak was detected upon cooling at T_c.

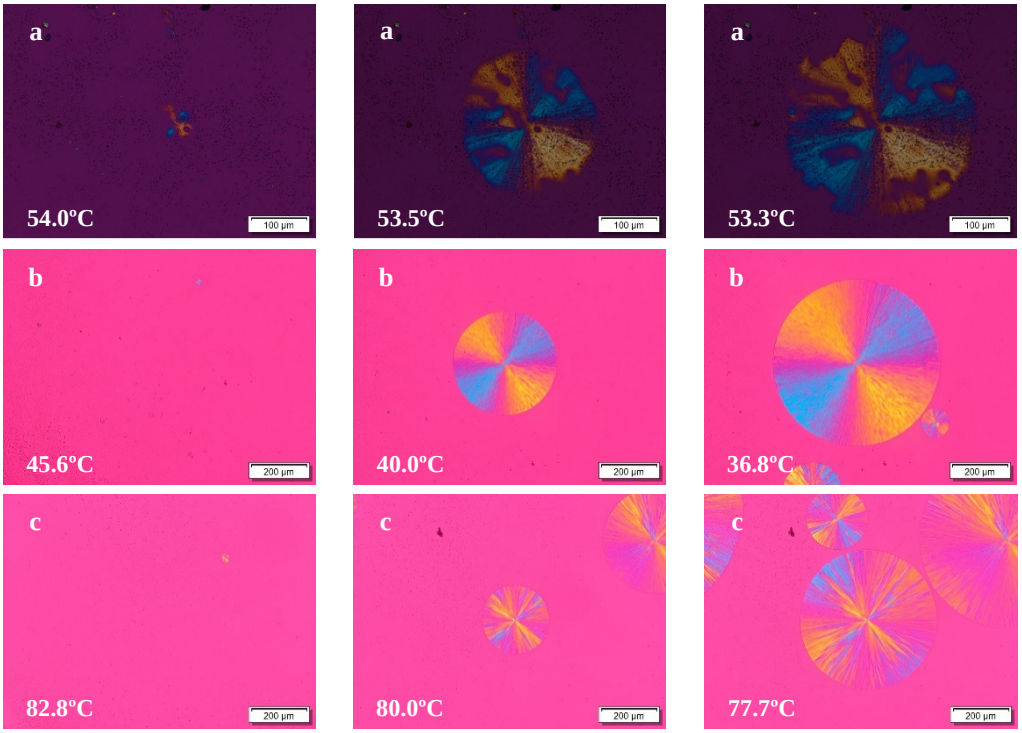

Figure 5.7. Non-isothermal crystallization under PLOM from a) DVE-DMDS, b) TEGDVE-DMDS and c) BDDVE-DMDS. Micrographs were taken at different temperatures, upon cooling at 1ºC/min. The scale bar represents a) 100 µm and b) and c) 200 µm.

For the polymers TEGDVE-DMDS and BDDVE-DMDS, the appearance of spherulites could be observed at temperatures of 45.6ºC and 82.6ºC respectively (Figure 5.7 b and c). Noteworthy, these temperatures are substantially higher than the melting of the Low-T_m-form which takes place at 14.1ºC for TEGDVE-DMDS ($T_{m,1}$ Table 5.2 and DSC heating scan Figure 5.4.b) and at 68.5ºC for BDDVE-DMDS ($T_{m,1}$ Table 5.2 and DSC heating scan Figure 5.4.c). Hence, the spherulites observed by PLOM are attributed to the High-T_m-form in these cases. The High-T_m-forms from TEGDVE-DMDS and BDDVE-DMDS display faster crystallization

kinetics that the High-T_m-form from DVE-DMDS, and can undergo crystallization upon cooling from the melt. This result is in line with the DSC scans in Figure 5.4 b and c, in which the crystallization from the melt of the High-T_m-form is also emphasized by the presence of a high-temperature shoulder in the main recrystallization exotherm at T_c.

5.2.5. DSC results under isothermal conditions

Isothermal crystallization measurements on polymers DVE-DMDS, TEGDVE-DMDS and BDDVE-DMDS were performed to give an insight into crystallization kinetics and give information about nucleation and crystal growth. Figures 5.8.a and 5.9. a and c show the isothermal DSC scans of the polymer DVE-DMDS, TEDGVE-DMDS and BDDVE-DMDS after erasing the thermal history of the samples and rapidly quench the samples to the isothermal crystallization temperatures (T_c) indicated. Figures 5.8 b and 5.9 b and d show the subsequent heating scans. Finally, Table 5.4. depicts the values of interest from isothermal and subsequent heating scans.

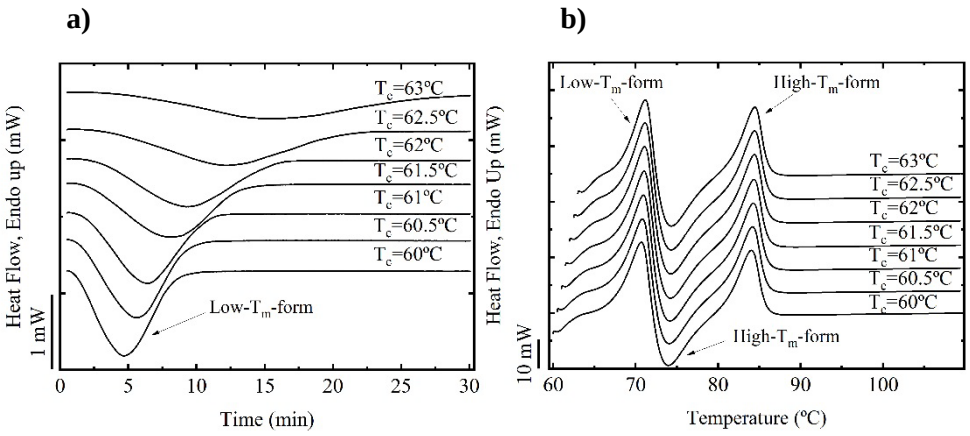

Figure 5.8. a) DSC isothermal scan from the indicated crystallization temperatures (T_c) and b) subsequent heating scan at 20°C/min of DVE-DMDS.

Figures 5.8.a shows that crystals from polymer DVE-DMDS were formed isothermally in a range of T_c temperatures between 60ºc and 63ºC. In the subsequent heating scans Figure 5.8.b, the melting of the crystals formed isothermally is observed at $T_{m,1}$ (Table 5.4) and is followed by the cold crystallization and subsequent melting of the High-Tm-form.

First, Table 5.4 shows that the values of melting enthalpy $\Delta H_{m,1}$ and crystallization enthalpy ΔH_c are very close, hence it confirms that the material did not crystallize during the cooling step at 60ºC/min and that the first melting at $T_{m,1}$ is attributed to the crystals formed isothermally at T_c. In the subsequent heating scan at 20ºC/min, the successive melting-crystallization-melting behaviour that was observed in the non-isothermal protocol is occurring. From this behaviour, it is clear that the crystals formed isothermally are from the Low-T_m-form.

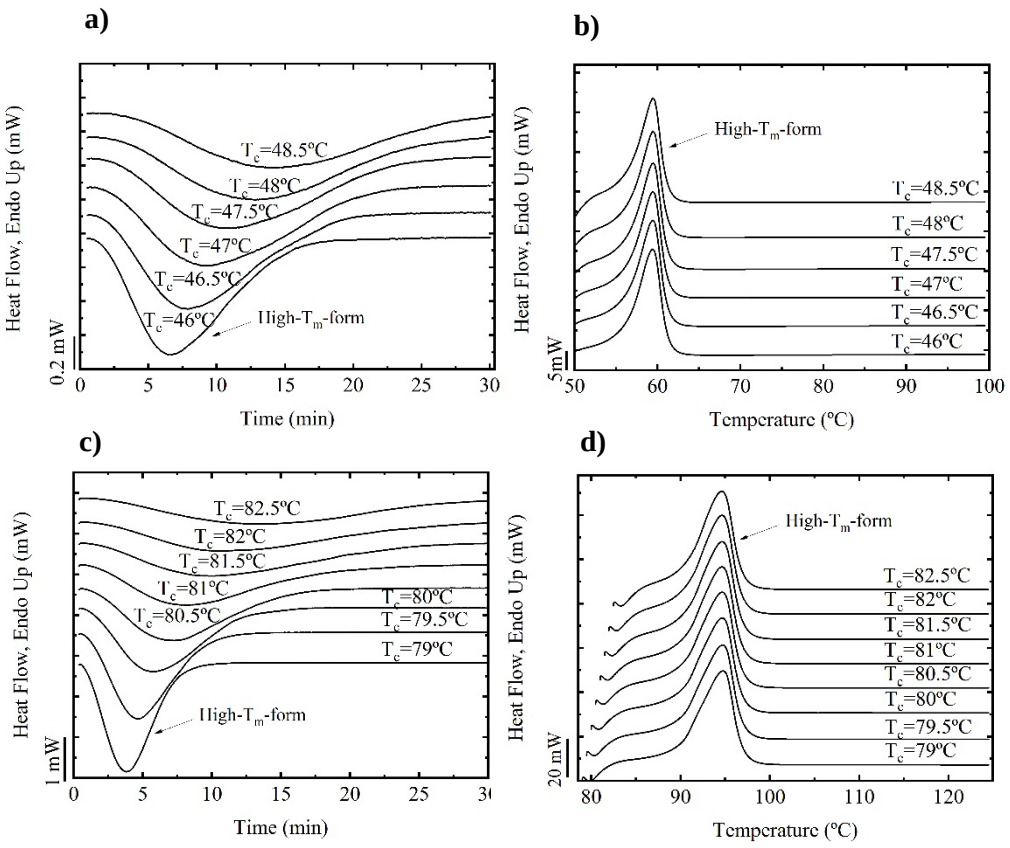

Figure 5.9. DSC isothermal scan from the indicated crystallization temperatures (T_c) of a) TEGDVE-DMDS and c) BDDVE-DMDS and subsequent heating scan at 20°C/min of b) TEGDVE-DNDS and d) BDDVE-DMDS.

For the polymers TEGDVE-DMDS and BDDVE-DMDS, the values ΔH_m and ΔH_c obtained from DSC isothermal scans are also very close (Table 5.4) confirming that no crystallization occurred during the quenching at 60ºC/min. For these polymers though, the successive melting-crystallization-melting behaviour is not observed is the heating ramp

following the isothermal crystallization (Figure 5.9.b and d). The range of T_c at which isothermal crystallization experiments were performed is higher than the melting of the melting of the Low-T_m-form in both cases (Table 5.2). Hence, the crystals formed isothermally are from the High-T_m-form for polymer TEGDVE-DMDS and BDDVE-DMDS.

Table 5.4 . T_m, ΔH_m, T_c, ΔH_c, T_{cc}, and ΔH_{cc} values from isothermal crystallisation experiments of DVE-DMDS, TEGDVE-DMDS and BDDVE-DMDS.

	Isothermal scan		**Heating scan**					
	T_c (°C)	**ΔH_c (J/g)**	**$T_{m,1}$ (°C)**	**$\Delta H_{m,1}$ (J/g)**	**T_{cc} (°C)**	**ΔH_{cc} (J/g)**	**$T_{m,2}$ (°C)**	**$\Delta H_{m,2}$ (J/g)**
DVE-DMDS	60	53	70.7	48	74.0	39	84.0	40
	60.5	52	70.8	47	74.0	38	84.2	41
	61	52	70.9	45	74.2	39	843	41
	61.5	51	71.0	43	74.2	41	84.3	39
	62	50	71.1	46	74.3	38	84.4	42
	62.5	51	71.1	44	74.3	38	84.5	42
	63	46	71.2	42	74.3	38	84.5	42
TEGDVE-DMDS	46	58	-	-	-	-	59.4	61
	46.5	57	-	-	-	-	59.4	62
	47	57	-	-	-	-	59.5	58
	47.5	53	-	-	-	-	59.5	59
	48	50	-	-	-	-	59.5	57
	48.5	47	-	-	-	-	59.5	53
BDDVE-DMDS	79	73	-	-	-	-	94.8	74
	79.5	74	-	-	-	-	94.7	79
	80	74	-	-	-	-	94.7	75
	80.5	73	-	-	-	-	94.7	76
	81	72	-	-	-	-	94.6	75
	81.5	74	-	-	-	-	94.7	77
	82	69	-	-	-	-	94.6	74
	82.5	62	-	-	-	-	94.6	72

The isothermal crystallization kinetics data were fitted to the Avrami equation with an Origins application software that was developed by Lorenzo et al.[7] The relevant values obtained

from the fitting are depicted in Table III.2 in Appendix III, and plotted in Figure 5.10 for the three poly(thioethers).

From the Avrami fitting, the first parameter to consider is the induction time (t_0), which is the time required to form stable nuclei. The inverse of the induction time gives us information about the nucleation rate. The values obtained for the Low-T_m-form crystals from the polymer DVE-DMDS, and the High-T_m-forms from TEGDVE-DMDS and BDDVE-DMDS are plotted against T_c in Figure 5.10.a. From the plot, the High-T_m-form from BDDVE-DMDS displays the higher nucleation rates, followed by the High-T_m-form from TEGDVE-DMDS and the Low-T_m-form DVE-DMDS. From these results, an effect of the molar mass on the nucleation rate can be emphasized, as nucleation rate increases with the molar mass of the poly(thioethers) (see Mn Table 5.1). Opposite results would be awaited, as polymers with lower molar mass are usually reported to crystallize faster[8–10]. In addition, faster nucleation rates are obtained for BDDVE-DMDS, which displays a lower glass transition temperature (T_g) (See Table 5.1). The latter results are expected, as polymers with lower T_g are more flexible, and hence more prone to aggregate and nucleate.

Another data that can be deduced from Avrami fitting is the measured half-crystallization time $\tau_{50\%,exp}$. The inverse of the half–crystallization time provides an experimental measure of the overall crystallization rate (which includes both nucleation and growth). From the plot Figure 5.10.b, the High-T_m-form from polymer BDDVE-DMDS reached the highest crystallization rates at low T_c, followed by Low-T_m-form from DVE-DMDS and High-T_m-form from TEGDVE-DMDS. Manifestly independent on the polymers' molar mass, the overall

crystallization rate could be influenced by the chemical structure of the poly(thioethers). As shown in Figure 5.1, DVE-DMDS, TEGDVE-DMDS and BDDVE-DMDS poly(thioethers) differs in terms of length of the repeating unit and the number of ether functionality in the polymer backbone, which are known to be very flexible liaisons. Faster crystallization rate were obtained for the polymer BDDVE-DMDS, which displays the shortest repeating unit followed by TEGDVE-DMDS. It is difficult to compare kinetics of different crystallographic forms. As DVE-DMDS does not form the High-Tm-form upon cooling from the melt, we assume that at least for this crystallographic form, it is the polymer that crystallizes slowest from the three examined. For these copolymer series, a high density of ether functionality within the polymer backbone (as observed in TEGDVE-DMDS) leads to slower crystallization kinetics of the High-T_m-form.

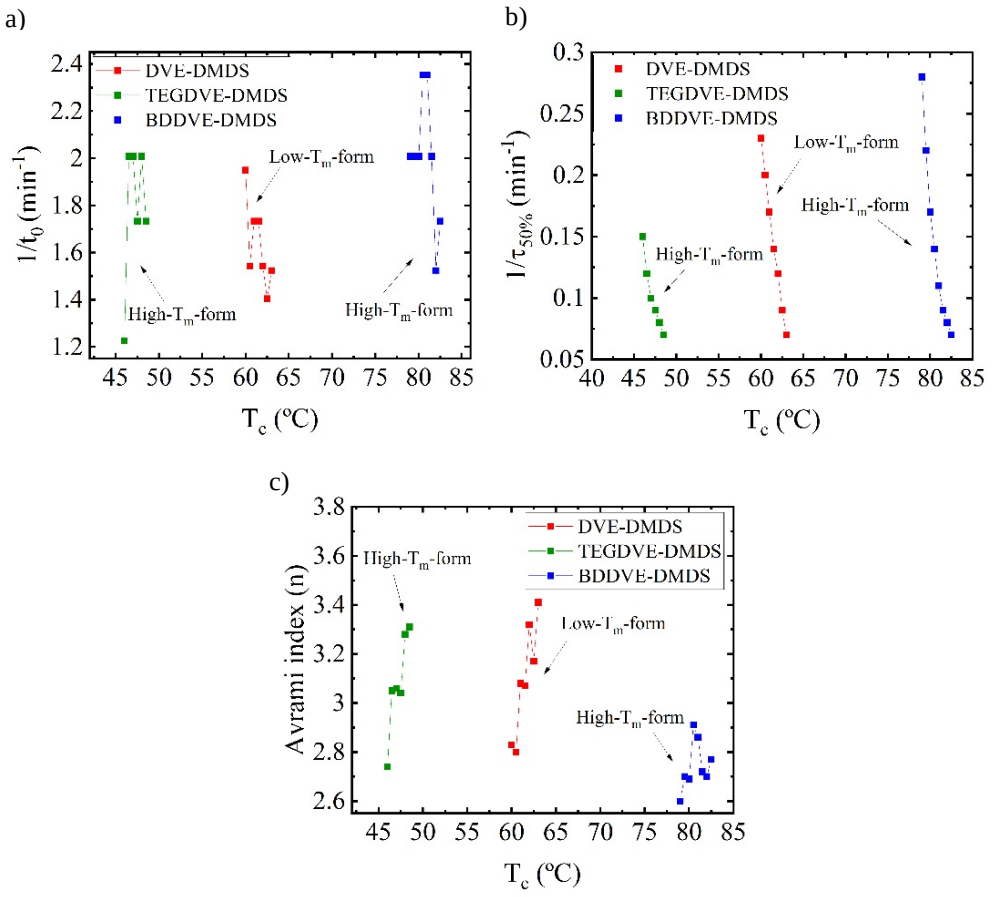

Figure 5.10. a) Nucleation rate $\frac{1}{t_0}$ as a function of T_c, b) $\frac{1}{\tau_{50\%,exp}}$ as a function of T_c and c) Avrami index n as a function of T_c for the polymers DVE-DMDS TEGDVE-DMDS and BDDVE-DMDS.

Finally, The Avrami index obtained from the fitting gives an additional indication of the morphology of the crystals that are formed isothermally. The Avrami index values are ranging between 2.80 - 3.41 for the Low-T_m-form of DVE-DMDS, 2.74 - 3.31 for the High-T_m-form from TEGDVE-DMDS and 2.60 - 2.91 for the High-T_m-form from BDDVE-DMDS (Figure 5.10c and Table III.2, in Appendix III). Values around 3 indicates that the spherulites

are nucleated instantaneously in the isothermal crystallization experiments of the three poly(thioethers).[11–13] In Figure 5.10.c, it is shown that the Avrami index tends to increase with T_c. This phenomenon is commonly observed as the nucleation changes from instantaneous (n=3) to sporadic nucleation (Avrami values around 4) when T_c increases.[12,13]

5.2.6. Isothermal crystallization under PLOM

- **Spherulite growth by isothermal crystallization under PLOM**

Under isothermal conditions, polymers DVE-DMDS, TEGDVE-DMDS and BDDVE-DMDS crystallize in spherulitic structures. Spherulite growth from the Low-T_m-form from DVE-DMDS and High-Tm-forms from TEGDVE-DMDS and BDDVE-DMDS can be monitored by performing isothermal crystallization under PLOM, and micrographs are reported in Figures 5.11, 5.12 and 5.13.

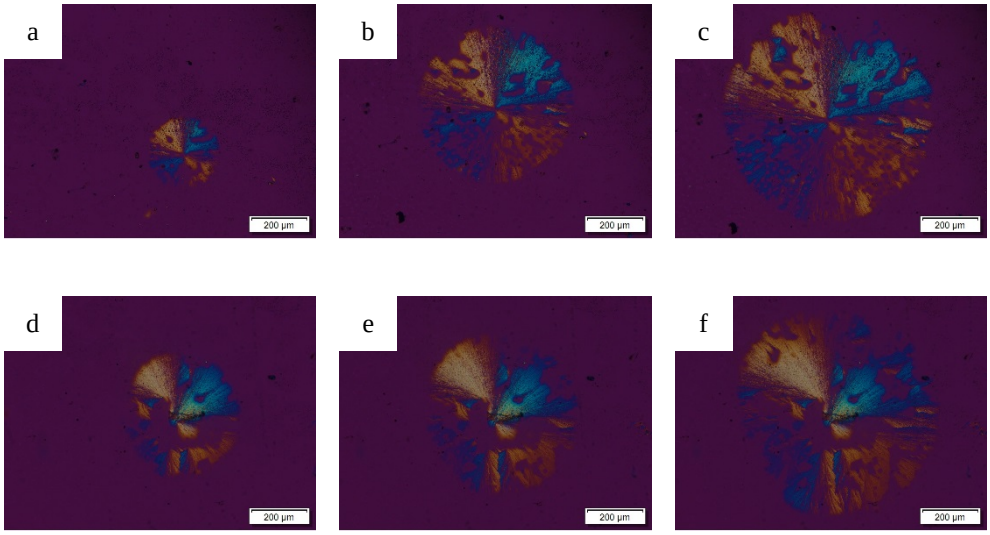

Figure 5.11. Isothermal crystallization under PLOM of the polymer DVE-DMD showing spherulite growth as a function of time at Tc 55ºC for a) 3 min b) 4min and c) 4 min 40sec and at Tc 57ºC for d) 2min 43 sec e) 3min 15sec and f) 4min. The scale bar represents 200 µm.

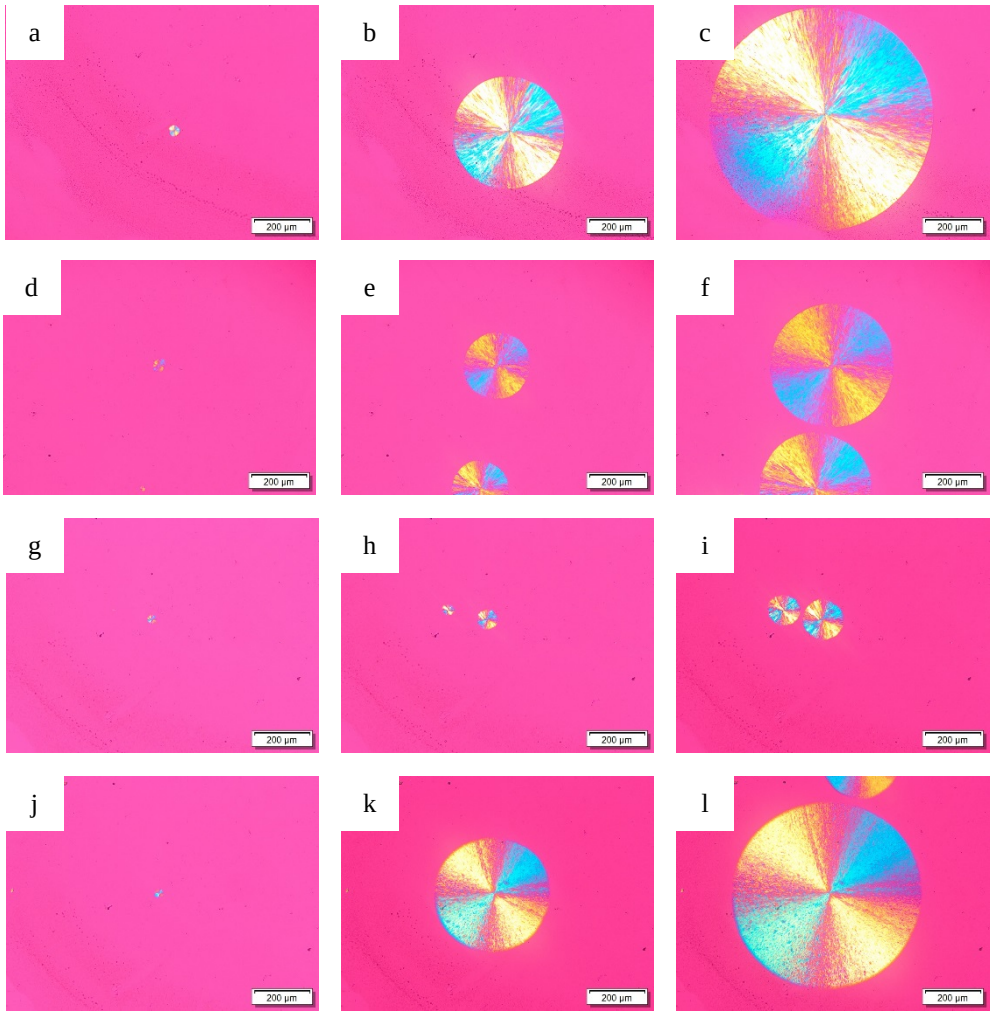

Figure 5.12. Isothermal crystallization under PLOM of the polymer TEGDVE- DMDS showing spherulite growth as a function of time at T_c 45ºC for a) 11min 39sec, b)18min and c) 25min; at at T_c 46ºC for d) 3min 13sec e)7min and f) 11min; at T_c 48ºC for g) 13min, h) 14min and i) 15min 40sec; and at T_c 50ºC for j) 27min 16sec, k) 37min, and l) 43min 20sec. The scale bar represents 200 µm.

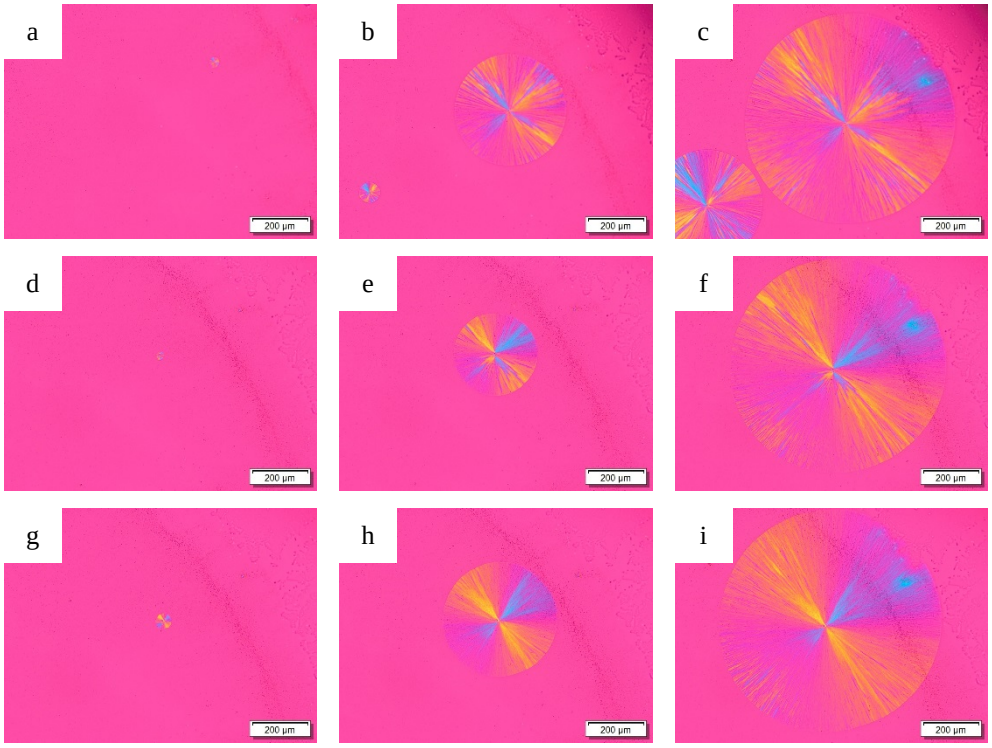

Figure 5.13. Isothermal crystallization under PLOM of the polymer BDDVE- DMDS showing spherulite growth as a function of time at T_c 79ºC for a) 29 sec, b) 3min 30sec and c) 6min 30sec; at T_c 81ºC for d) 45sec, e) 4min 30sec, f) 8min 54sec; and at T_c 83ºC for g) 1min, h) 6min 30sec, and i) 12min 30sec. The scale bar represents 200 µm

Unfortunately, due to reproducibility issues, the spherulitic growth rate could not be evaluated through this technique. Further work is required to avoid the effect of possible degradation during the measurements.

- **Evidence of the two polymorphs by successive isothermal crystallization on the polymer DVE-DMDS**

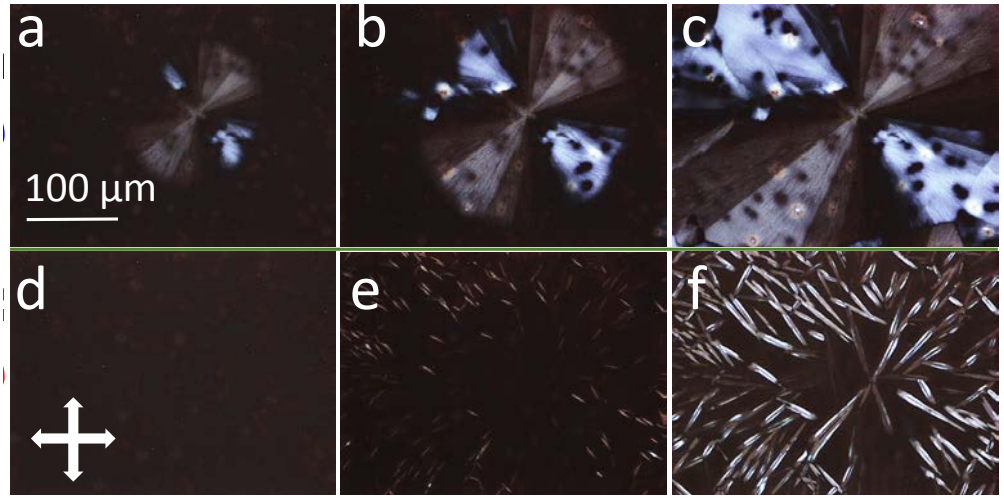

Figure 5.14. PLOM micrographs, taken between crossed polarizers (indicated by double-sided arrows), showing the growth as a function of crystallization time t of a spherulite at T_c 40ºC for a) 0 s, b) 10 s and c) 30 s. Subsequently, the sample was heated from T_c 40ºC to T_{cc} 74ºC at a rate of 150 °C/min. After melting of spherulite at $T_{m,1}$, the growth of anisotropic crystals at the higher temperature T_{cc} was followed in time d) 0 s , e) 130 s and f) 300 s. The scale bar represents 100 µm.

In Figure 5.14, it is shown that different types of crystalline objects grew in a 100 nm thick film of the polymer DVE-DMDS at T_c and at T_{cc}, respectively. After initial erasing thermal history at 100 °C for 30 seconds, the film was quenched to T_c=40 °C (T_c<$T_{m,1}$, see non-isothermal DSC scans in Figure 5.4.a and Table 5.2). At this temperature, the growth of large spherulites from Low-T_m-form could be observed by PLOM (Figure 5.14, a, b and c). After 10 min at T_c=40 °C, the whole sample was crystallized. Subsequently, the Low-T_m-form crystalline structures obtained at T_c were molten by increasing the temperature to T_{cc} =74ºC, which is above $T_{m,1,}$ but below $T_{m,2}$, i.e. the melting temperature of the High-T_m-form, (see non-isothermal DSC scans in Figure 5.4.a and Table 5.2). Because T_{cc}>$T_{m,1}$, the spherulites from

Low-T_m-form seen in Figure 5.14.c melts completely (Figure 5.14.d). During the isothermal step at T_{cc}=74 °C many birefringent, elongated crystals from High-T_m-form appear and become larger in time (Figure 5.14.e and f). The morphologies of the crystals observed at T_c (Low-T_m-form) differ significantly from the ones formed at T_{cc} (High-T_m-form). It is postulated that, within the molten spherulites, a large number of crystals formed at T_{cc} were nucleated. From the micrographs in Figure 5.14.e and f, it is observed that the orientation of these needle-like crystals at T_{cc} follows some pattern. Thus, these objects seem to have inherited some information (memory) from the initial spherulite. Probably, even when being molten above $T_{m,1}$, the polymer chains remembered their previous alignment within the crystalline Low-T_m-form for some time. Such preferential orientation of the poly(thioether) chains could nucleate the needle-like crystals formed at T_{cc}. This memory assists the nucleation and promotes the formation of the High-T_m-form.

5.4. Conclusion

This study on the crystallization of DVE-DMDS, TEGDVE-DMDS and BDDVE-DMDS shows the potential and peculiar behaviour of the poly(thioethers). Under non-isothermal conditions, DSC analysis show successive melting-crystallization-melting peaks upon heating for the three polymers. The two distinct melting peaks were attributed to two crystalline structures, denoted as Low-T_m-form and High-T_m-form. Upon cooling from the melt, the crystallization of the Low-T_m-forms could be observed for the three poly(thioethers). However, it was shown that the High-T_m-form could only form from the melt for the polymers TEGDVE-DMDS and BDDVE-DMDS.

For the polymer DVE-DMDS, it was shown by WAXS analysis that the two crystalline structures from Low-T_m-form and High-T_m-form are different, showing that two different polymorphs can be formed by the same polymer. The two polymorphs presented different morphologies, which could be observed under PLOM following a successive isothermal protocol. From the latter, it was found that upon heating the polymer chains from DVE-DMDS remembered their previous alignment within the crystalline Low-T_m-form, even above its melting temperature. This memory assisted the nucleation enabled the formation of the High-T_m-form.

Under isothermal conditions, crystallization kinetics of the Low-T_m-form from DVE-DMDS and High-T_m-form from TEGDVE-DMDS and BDDVE-DMDS could be implemented by DSC analysis. Experimental data were fitted to the Avrami equation, and give a first insight into crystallization kinetics. At this stage of the work, faster nucleation rate and crystallization rate are obtained for the high-T_m-form from polymer BDDVE-DMDS with the lowest T_g. The overall crystallization (which comprises nucleation and crystal growth) is mainly accelerated for shorter repeating unit in the polymer backbone and lower T_g. Overall, the polymer DVE-DMDS displays the slower kinetics, with only the Low-T_m-form capable to crystallize upon cooling from the melt. The High-T_m-form from this polymer presents very slow kinetics, that can be accelerated by self-nucleation from remaining self-nuclei or self-seeds of the Low-T_m-form slightly above its melting temperature.

5.5. References

(1) Le, C. M. Q.; Schrodj, G.; Ndao, I.; Bessif, B.; Heck, B.; Pfohl, T.; Reiter, G.; Elgoyhen, J.; Tomovska, R.; Chemtob, A. Semi-Crystalline Poly(Thioether) Prepared by Visible-Light-Induced Organocatalyzed Thiol-Ene Polymerization in Emulsion. *Macromol. Rapid Commun.* **2022**, *43* (5), 1–6. https://doi.org/10.1002/marc.202100740.

(2) Michell, R. M.; Mugica, A.; Zubitur, M.; Muller, A. J. Self-Nucleation of Crystalline Phases within Homopolymers, Polymer Blends, Copolymers, and Nanocomposites. *Adv. Polym. Sci.* **2017**, *276* (August 2015), 215–256. https://doi.org/10.1007/12_2015_327.

(3) Sangroniz, L.; Meabe, L.; Basterretxea, A.; Sardon, H.; Müller, A. J.; Cavallo, D. Chemical Structure Drives Memory Effects in the Crystallization of Homopolymers †. *Macromolecules* **2020**, *53* (12), 4874–4881. https://doi.org/10.1021/acs.macromol.0c00751.

(4) Fillon, B.; Wittmann, J. C.; Lotz, B.; Thierry, A. Self-nucleation and Recrystallization of Isotactic Polypropylene (α Phase) Investigated by Differential Scanning Calorimetry. *J. Polym. Sci. Part B Polym. Phys.* **1993**, *31* (10), 1383–1393. https://doi.org/10.1002/polb.1993.090311013.

(5) Sangroniz, L.; Cavallo, D.; Müller, A. J. Self-Nucleation Effects on Polymer Crystallization. *Macromolecules* **2020**, *53* (12), 4581–4604. https://doi.org/10.1021/acs.macromol.0c00223.

(6) Quero, E.; Müller, A. J.; Signori, F.; Coltelli, M. B.; Bronco, S. Isothermal Cold-Crystallization of PLA/PBAT Blends with and without the Addition of Acetyl Tributyl Citrate. *Macromol. Chem. Phys.* **2012**, *213* (1), 36–48. https://doi.org/10.1002/macp.201100437.

(7) Lorenzo, A. T.; Arnal, M. L.; Albuerne, J.; Müller, A. J. DSC Isothermal Polymer Crystallization Kinetics Measurements and the Use of the Avrami Equation to Fit the Data: Guidelines to Avoid Common Problems. *Polym. Test.* **2007**, *26* (2), 222–231. https://doi.org/10.1016/j.polymertesting.2006.10.005.

(8) Jenkins, M. J.; Harrison, K. L. The Effect of Molecular Weight on the Crystallization Kinetics of Polycaprolactone. *Polym. Adv. Technol.* **2008**, No. November 2007, 229–236. https://doi.org/10.1002/pat.

(9) Godovsky, Y. K.; Slonimsky, G. L.; Garbar, N. M. Effect of Molecular Weight on the Crystallization and Morphology of Poly(Ethylene Oxide) Fractions. *J Polym Sci, Part C, Polym Symp* **1972**, *21* (38), 1–21. https://doi.org/10.1002/polc.5070380103.

(10) Chen, X.; Hou, G.; Chen, Y.; Yang, K.; Dong, Y.; Zhou, H. Effect of Molecular Weight on Crystallization, Melting Behavior and Morphology of Poly(Trimethylene Terephalate). *Polym. Test.* **2007**, *26* (2), 144–153. https://doi.org/10.1016/j.polymertesting.2006.08.011.

(11) Coba-Daza, S.; Carmeli, E.; Otaegi, I.; Aranburu, N.; Guerrica-Echevarria, G.; Kahlen, S.; Cavallo, D.; Tranchida, D.; Müller, A. J. Effect of Compatibilizer Addition on the Surface Nucleation of Dispersed Polyethylene Droplets in a Self-Nucleated Polypropylene Matrix. *Polymer (Guildf).* **2022**, *263* (June), 125511. https://doi.org/10.1016/j.polymer.2022.125511.

(12) Müller, A. J.; Michell, R. M.; Lorenzo, A. T. Isothermal Crystallization Kinetics of Polymers. *Polym. Morphol. Princ. Charact. Process.* **2016**, 181–203. https://doi.org/10.1002/9781118892756.ch11.

(13) Gedde, U. W. *Polymer Physics*; Dordrecht, Ed.; Kluwer, 1995.

Chapter 6. Biobased polysulfide coatings

The results presented in this Chapter were obtained in collaboration with the research groups of Prof. R. Liska (Vienna University of Technology, Austria) and Dr. A. Chemtob (University of Haute Alsace, France)

6.1. Introduction

"Biobased polymers" are produced, wholly or partly, with monomers directly extracted or derived (after chemical modification) from biomass.[1] A large majority of these so-called "biobased monomers" are reacted by step-growth polymerizations in homogeneous conditions, either in bulk or in solution.[2] By contrast, biobased monomers are less susceptible to chain (radical) polymerization either because they lack the required carbon-carbon double bonds, or when these latter are present, they are generally sluggish towards this type of polymerization.[3] This is the case, for instance, of unsaturated vegetable oils containing internal unsaturations (1,2-disubstituted ethylenes), showing little or no tendency to undergo polymerization due to kinetic and thermodynamic limitations.[4] Another problem is that many biobased building blocks, such as fatty acids, terpene or phenol derivatives, are also prone to chain transfer reactions when they are chain polymerized, with the consequence of decreasing polymer molecular weights and monomer conversion.[5]

Although polymerizations in dispersed systems are already considered as eco-efficient due to the absence of volatile organic compounds and formation of waterborne products, the incorporation of biobased raw materials represents a further opportunity to make them even more sustainable and eco-friendly.[6] The biobased monomers able to react by chain polymerization in dispersed media have been recently reviewed by Molina-Gutierrez et al. in 2019.[7] More recently, a broader account of the subject was recently given by Aguirre et al. by including other biobased raw materials (surfactant, chain transfer agents, etc.) that make up waterborne polymer dispersions.[8] In very few cases, however, film formation and properties were investigated although coatings and adhesives are among the most important applications of polymer dispersions.[9] In most cases, fillers were added to the dispersions for mechanical reinforcement of the biobased polymer,[10–12] which has been an appropriate solution to the challenge of achieving biobased dispersed polymer products without scarifying performance and cost.

In this study, the possibility to carry out step-growth polymerizations in dispersed systems to yield biobased polymer dispersions for coatings has been revisited. Generally, the feasibility of step polymerizations in dispersed systems is severely decreased in presence of water, resulting in low molar mass products and low functional groups conversion.[13]

Interestingly, the radical-mediated polymerization of thiol with alkene monomers stands out as an exception since high molar mass poly(thioether) dispersions have been recently achieved by emulsion and miniemulsion thiol-ene polymerizations.[14–16] Thus, one important question remain, whether similar heterogeneous step polymerizations could be performed with

biobased thiol and ene monomers. There are precedents where bicomponent dithiol-diene monomer miniemulsions were polymerized. Between 2017 and 2019, the team of Araùjo used this process to polymerize petroleum-based dithiols with various biobased α,ω-diene monomers (these latter were obtained from castor oil-derived 10-undecanoic acid and 10-undecenoic acid[17,18]). In these previous studies, an application in the field of controlled drug delivery was targeted, and consequently, emphasis was made on particles' biocompatibility, cytotoxicity, degradability and cellular uptake. By contrast, monomer reactivity, polymer molar mass, film-forming properties after water evaporation, film mechanical and thermal properties have been poorly investigated.

In this Chapter, newly synthesized isosorbide-based dithiol (Iso-SH) and diallyl (Iso-A) biobased monomers were implemented in bulk or miniemulsion thiol-ene photopolymerization. The fully biobased bicomponent system Iso-SH/Iso-A was studied, but also three other formulations in which the biobased Iso-SH monomer was polymerized with three petroleum-based dienes: diallyl terephthalate (DATP), 3,9-divinyl-2,4,8,10-tetraoxaspiro [5.5]undecane (SPAC), and 1,4-bis(allyloxy)benzene (DAOB). The molecular structures of the monomers are shown in Figure 6.1.

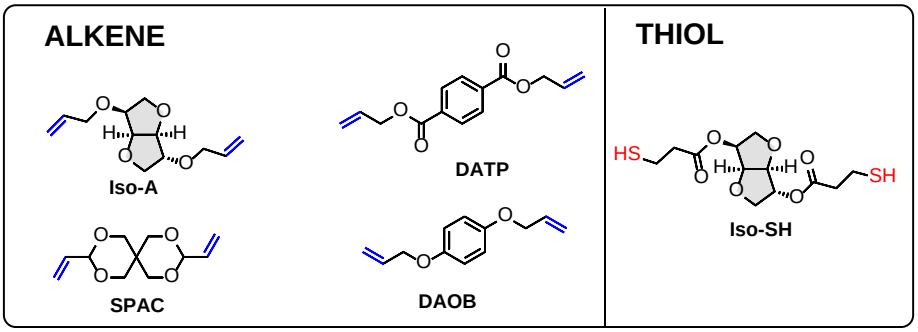

Figure 6.1. Chemical structure of dithiol and diene monomers

In order to assess the polymerization behaviour, photopolymerization of these four thiol-ene mixtures was firstly conducted in a solvent-free condition. Ene conversion, molar mass, and moduli were determined using two main techniques: photorheology combined with real-time Fourier-transform infrared spectroscopy (RT-FTIR) and size exclusion chromatography (SEC). The same systems were then subjected to a miniemulsion photopolymerization. In this process, particle nucleation proceeds by radical entry into monomer droplets, subsequently converted into polymer particles.[19,20] Such droplet nucleation mechanism is suitable to the relatively water-insoluble monomers used in our study, such as the isosorbide monomers Iso-A and Iso-SH. By contrast, emulsion polymerizations involves a monomer diffusion process through the aqueous continuous phase, from the monomer droplets to the nucleated polymer particles, which is likely to be slowed down or prevented with poorly water-soluble monomers.[7] Herein, we aim at achieving colloidally stable polymer dispersions with solids content of 30 w% and polymer chains with high molar masses (> 10 kDa) and film forming properties. The films exhibiting sufficient mechanical properties were subjected to a range of characterization by

thermogravimetric analysis (TGA), differential scanning calorimetry (DSC), tensile, water uptake and gloss tests.

6.2. Experimental

6.2.1. Material

The diene monomer diallyl terephtalate (DATP, 98%), the photoinitiator lithium phenyl(2,4,6-trimethylbenzoyl)phosphinate (TPO-Li, >99%), and the radical inhibitor 2,5-di-tert-butylhydroquinone (DBHQ, >98%) were purchased from TCI Chemicals. Hexadecane (HD, 98%), 3,9-divinyl-2,4,8,10-tetraoxaspiro[5.5]undecane (SPAC) and 1,4-bis(allyloxy)benzene (DAOB) wer purchased from Sigma. The surfactant Alkyldiphenyloxide disulfonate (Dowfax 2A1, 45%) was kindly provided by Dow chemicals. All chemicals were used as received without further purification, and de-ionised water was used as the dispersant media for the polymerization.

6.2.2. Synthesis of biobased monomers

The monomer isosorbide dithiol (Iso-SH) and isosorbide diallyl (Iso-A) were synthesized by the research group of Prof. R. Liska (Vienna University of Technology, Austria), and is reported in Appendix IV.

6.2.3. Synthesis of biobased polymers by bulk photopolymerization

Bulk photopolymerizations of the monomers Iso-SH with Iso-A, DATP, SPAC and DAOB were performed by the research group of Prof. R. Liska (Vienna University of Technology, Austria) and are reported in Appendix IV.

6.2.4. Synthesis of biobased polymers by miniemulsion photopolymerization

Miniemulsion photopolymerization of the monomers Iso-SH with Iso-A (Entries A1, A2 and A3 Table 6.1) DATP (Entry B1, Table 6.1), SPAC (Entry C1, Table 6.1) and DAOB (Entry D1, Table 6.1) were performed by the research group of Dr. A. Chemtob (University of Haute Alsace, France) and are reported in Appendix IV. The main characterization of the synthesized poly(thioethers) are reported Table 6.1, with the photoinitiator (PI) used, the Z-average diameter and particle size distribution (PSD) obtained from dynamic light scattering (DLS), and the molar mass and polydispersity index (PDI) obtained from gel permeation chromatography (GPC) (See Appendix IV).

Table 6.1. Poly(thioether) characterizations

Entry	Monomer	PI	Irradiance (mW cm^{-2})	% Coagulation	Z-average diameter (nm) / PSD	M_w (kDa)	PDI
A1	Iso-A/Iso-SH	TPO	3.7	43	305 / 0.24	8.20	2.32
A2	Iso-A/Iso-SH	TPO-Li	3.7	0	285 / 0.20	13.3	2.31
A3	Iso-A/Iso-SH*	TPO-Li	33	0	308 / 0.19	15.86	2.75
B1	DATP/Iso-SH	TPO-Li	3.7	0	168 / 0.06	-	-
C1	SPAC/Iso-SH	TPO-Li	3.7	0	191 / 0.15	69.5	5.5
D1	DAOB/Iso-SH	TPO-Li	3.7	0	141 / 0.16	136.4	7.8

6.2.5. Films and characterization

Self-supported films were prepared by casting the latex into silicon mold, and dried at controlled temperature (25ºC) and humidity (55%).

Water uptake was measured by immersing films with similar shape and thickness in milli-q water in a close vial. The film were then withdrawn, gently dried with paper and weighted. The water uptake was determined as:

$$water\ uptake\ (\%) = \frac{m_t - m_0}{m_0} \times 100 \ldots \text{(Eq 6.1)}$$

With m_0 weight of the film at t_0 ; m_t weight of the film at time t

Thermogravimetric Analysis (TGA) of the films were carried out with a Perkin Helmer TGA 8000™ Thermogravimetric analyzer. Samples of 5-10mg were heated from 40ºC to 800ºC at 10ºC/min

Differential scanning calorimetry (DSC) experiments were carried out on Perkin Elmer DSC 8000 equipment from TA instrument using an Intracooler II as a cooling system. Approximately 5 mg samples were encapsulated in sealed aluminium pans. For the non-isothermal procedure, the films based on Iso-SH/Iso-A and Iso-SH/DATP were heated up to 50ºC and the films based on Iso-SH/DAOB and Iso-SH/SPAC up to 100ºC at 20ºC/min, and kepts 3 minutes in the melted state to erase thermal history. The sample was then cooled at 20ºC/min until -30ºC for the films Iso-SH/Iso-A and Iso-SH/DATP and until -40ºC for the films

Iso-SH/DAOB and Iso-SH/SPAC. Films were subsequently heated at 20ºC/min, up to 50ºC (films Iso-SH/Iso-A and Iso-SH/DATP). For the non-isothermal analysis of hexadecane, the sample was heated until 60ºC at 20ºC/min, left 3 minutes in its melted state, and cooled at 20ºC/min until 0ºC. Then, a final heating ramp was performed at 20ºC/min until 60ºC. All DSC scans presented in this study show the cooling step after erasure of the thermal history and the second heating step.

The gloss of self-supported films was measured with a glossmeter from BYK Instrument at 20º, 60º and 85º.

The mechanical properties of the films prepared for coatings applications were evaluated by tensile test. The measurements were carried out using the TA.HD plus texture analyzer (Stable Micro Systems Ltd., Godalmming UK). Flat "dog-bone" shaped tensile test specimens with dimensions of 15 mm 3.5 mm 0.5 mm were cut from dry films for the tensile test measurements. With a constant strain velocity of 1.5 mm/s and a nominal strain rate of 0.1 Hz, stress-strain measurements were taken. Three specimens were prepared from each sample and the values presented are average of these measurements. The tensile properties for each material is represented in the stress-strain graphs.

Morphological characterization of thin films was carried out by atomic force microscope (AFM), with a scanning probe atomic force microscope with a Dimension ICON atomic force microscope with a Nanoscope V controller (Bruker) operating in tapping mode. An integrated silicon tip/cantilever with a resonance frequency of around 300 kHz and a spring constant of 40

N/m was used, performing measurements at a scan rate of 1 Hz s^{-1} with 512 scan lines. Different areas of each sample were analysed to ensure the final morphology of the investigated blends

6.3. Results and discussion

6.3.1 Synthesis of biobased polymers by bulk photopolymerization

The bio-based monomers Iso-A and Iso-SH were used in four different formulations for thiol-ene polymer synthesis: the biobased bicomponent formulation Iso-SH/Iso-A and formulations containing biobased Iso-SH with three other non-biobased dienes: DATP, SPAC, and DAOB.

In order to examine the reactivity of the above-mentioned newly developed thiol-ene formulations and their properties as stiffness, flexibility, and crystallinity, a photorheology study was carried out in solvent-free conditions (bulk photopolymerization) by mixing stoichiometric amount of thiol and ene monomers in presence of the photoinitiator TPO-Li. Through photorheology studies combined with real-time FTIR spectroscopy measurements, the materials' storage moduli (G'final) can be obtained with the corresponding double bond conversion (DBCfinal) and the time until 95% of the final double bond conversion is achieved (t95%). This method links mechanical data of the bulk polymers with molecular information, and is particularly beneficial before heading to more complicated systems in dispersed media. The polymer samples obtained by the photorheology measurements were subsequently analysed and characterized by GPC to polymer's molar mass M_w, and the molar mass polydispersity

index(PDI). The results of the RT-NIR-photorheology measurements combined with the subsequent GPC analysis of the thiol-ene polymers obtained are depicted in Table 6.2.

Table 6.2. Results of the RT-FTIR-photorheology measurements with the subsequent GPC analysis.

Formulation	G'final (kPa)	DBCfinal (%)	t95% (s)	M_w (kDa)	PDI
Iso-SH/Iso-A	13.8	92	43.7	6.0	3.8
Iso-SH/DATP	314.1	99	16.5	115.1	5.2
Iso-SH/SPAC	617.3	76	58.3	9.1	3.6
Iso-SH/DAOB	925.6	98	13.9	7.6	3.2

In the case of the formulation based on Iso-SH/Iso-A, a low final storage modulus of 13.8 kPa was measured. This result highlights the flexibility and softness of the poly(thioether) based on this monomer pair. A high double bond conversion of 92% was measured as it would be expected in a pure step-growth reaction, and the time until 95% of the final double bond conversion DBCfinal is reached is comparable long (43.7 s). This could be reasoned by either not very reactive thiol-ene monomers or a less efficient photoinitiator for this specific thiol-ene system. The weight average molar mass of the polymer is comparable low (6.0 kDa). From these results, it can be expected that the fully biobased latex would lead to soft and flexible latex film obtained from miniemulsion photopolymerization, which will lack necessary mechanical strength for coating formulation. To strengthen the final material, one could incorporate some aromatic ring[21] (with diallyl monomer such as DAOB) or spiro moieties[22] in the polymer building blocks. In addition, it is reported that thiol-ene polymer prepared with SPAC[22] can form semi-crystalline poly(thioether), and thus offering a way to improve mechanical property of its polymer film. As expected, a significantly higher final storage modulus was measured in the case of the formulations containing Iso-SH/DATP (314.1 kPa), Iso-SH/SPAC (617.3kPa)

and Iso-SH/DAOB (925.6kPa). In particular, the double bond conversion of the thiol-ene couple Iso-SH/DATP is over 99%, yielding to a very high molar mass of 115.1 kDa considering step-grow polymers. The reaction occurred rapidly, with 95% of the final double bond conversion reached at 16.5s, indicating very reactive monomers. Hence, it can be expected that a stiff waterborne film would be produced by miniemulsion photopolymerization with reasonably good material properties. The formulation containing Iso-SH and SPAC is less reactive than its counterparts with 95% of the double bond conversion reached after 58.3s. The double bond conversion is comparatively low (76%), which might indicate that the reaction is not only a pure step-growth reaction and to some extent a homopolymerization of the ene monomer SPAC is occurring. As a consequence, low molar mass of 9.1kDa is achieved for this poly(thioether). In case of Iso-SH/DAOB, presenting the highest final storage modulus and high conversion (98%), the molar mass is surprisingly low (7.6kDa). The GPC measurements might not have been successful and a higher number average molar mass and a higher weight average molar mass should be expected from these monomers. A reason why the numbers are comparably low could be the poor solubility of the polymer in the GPC solvent due to the aromatic π–π stacking of DAOB moieties. From these results obtained from photoreology measurements, the formulations containing biobased Iso-SH with the three other non-biobased dienes seem to be the most promising in terms of mechanical resistance for coating application. Despite this conclusion, the four monomers couples were further polymerized in miniemulsion to check if the reaction in dispersed media with its characteristic features might eventually affect the polymer properties and subsequently their performance, as it is the case for free radical emulsion polymerization of (meth)acrlyates.[23]

6.3.2. Synthesis of biobased polymers by miniemulsion photopolymerization

As emphasized in the introduction Chapter 1 and in Chapter 3, miniemulsion process has recently been shown to be particularly suited for the synthesis of polymers following a step growth mechanism, in which a stoichiometric ratio between monomers functionality is necessary to reach high conversion and molar masses.[16,21,24,25] Small stoichiometric imbalance induces a significant drop in molar masses, as explained by the Carothers equation (Eq. 6.2). In the case of linear addition polymers obtained by polymerization of bifunctionnal A-A and B-B monomers, the number-average degree of polymerization $\bar{X}_n$ is related to the conversion of the reaction p and the stoichiometric ratio r (Eq. 6.3) between monomers.[26]

$$\bar{X}_n = \frac{1+r}{1+r-2pr} \quad \text{..... (6.2)}$$

$$r = \frac{[\mathrm{A}-\mathrm{A}]}{[\mathrm{B}-\mathrm{B}]} \quad \text{..... (6.3)}$$

$$\text{with } [\mathrm{A}-\mathrm{A}] \leq [\mathrm{B}-\mathrm{B}]$$

Consequently, small irreproducibility in terms of molar masses from one reaction to another is quite likely to happen, as even very small experimental variations in the reactants mole quantity can induce the differences. In the scope of synthesis in dispersed media, miniemulsion process turns out to be a suitable option to cope with the matter. Indeed, contrary to the traditionally used emulsion polymerization, miniemulsion does not require monomer mass transfer through the aqueous phase to perform the reaction. The monomers droplets

obtained after miniemulsification process by sonication are stabilized against coalescence by surfactant and against diffusional degradation (Ostwald ripening) by costabilizer. By droplet nucleation process, these droplets are turned into particles, and become the main loci of the polymerization reaction, in which the monomers stoichiometric ratio theoretically is not affected. In this way, stoichiometric imbalance between monomers functionality that may be due to different rate of monomers mass transfer through the aqueous phase is prevented. Moreover, miniemulsion with such colloidal characteristic offers a suitable platform for synthesis of more colloidally challenging systems –such as bio-based formulations polymerized in dispersed media. Herein hexadecane is added to the formulation as a costabilizers and the surfactant Dowfax 2A1 is used to stabilize the miniemulsion against droplet coalescece. Dowfax 2A1, as well as hexadecane, are non-reactive compounds and hence are not incorporated into the polymer chains, but they are incorporated into the polymer films and may affect the performance.

In the first system studied Iso-SH/Iso-A, 30% solid content poly(thioether) latexes were obtained by photo-initiated miniemulsion polymerization (Entry A1-A3, Table 6.1 and Figure 6.2.a) and the synthetic process was optimized towards high monomer conversion and molar mass polymer chains. In a first attempt, the oil-soluble photoinitiator TPO was implemented to initiate the radical mediated step-growth polymerization, as it has been reported that it provides better particle size control than its water-soluble counterpart.[16] The oil-soluble photoinitiator by forming radicals in the monomer droplets could indeed facilitate droplet nucleation and mitigate the contribution of the secondary nucleation process that induce formation of novel particles in

aqueous phase. Secondary nucleation is usually undesired, because it widens the particle size distribution and affects the polymer properties.[23] However, up to 43% coagulation was obtained in the Iso-SH/Iso-A system after UV-exposure and the final particle size was of about 305 nm with relatively large PSD. Probably due to the light scattering by the large droplets/particles, the TPO did not get sufficient UV light (energy) to be activated. Therefore, low molar mass chains (8.2 kDa, entry A1, Table 6.1) were formed.

To avoid the mentioned challenges during synthesis, the oil-soluble PI was replaced by water soluble TPO-Li. Even though it gives rise to radicals in aqueous phase that start the polymerization with the few monomer units present in this phase, in the case of photopolymerization in dispersed media, likely there is an improved contact between the photoinitiator and the UV light. It seems that this contact is a key issue to unlock the possibility of implementation of this process for thiol-ene synthesis. Subsequently, this reaction (entry A2, Table 6.1) yielded a coagulation-free polymer dispersion with higher average polymer molar mass of 13.3 kDa, obtained for the same reaction conditions (irradiance 3.7 mW^{-2} and 1 hour of UV exposure). For the rest of the study, the water-soluble photoinitiator TPO-Li was hence preferred. No difference in molar mass was observed when the irradiance was increased to 33 mW cm^{-2} (entry A3, Table 6.1), meaning that he higher photon flukes did not affected the reaction and the polymer. Likely the main factor limiting the molar masses in such conditions is the step-growth nature of the polymerization.

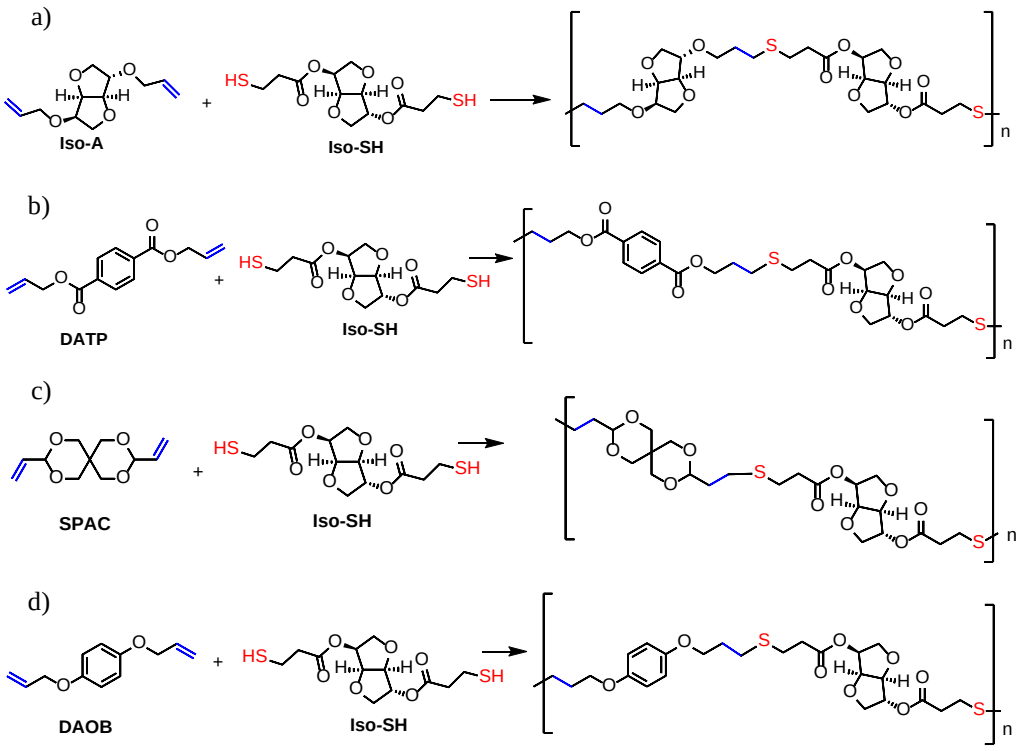

Figure 6.2 Poly(thioether) obatined by photopolymerization in miniemulsion of the monomer pairs a) Iso-SH/Iso-A and b) Iso-SH/DATP c) Iso-SH/SPAC and d) Iso-SH/DAOB

Even though decreasing the bio-based content, the previous bulk study demonstrated that the monomers containing aromatic ring or spiro moieties are promising in terms of material properties. This strategy was implemented by replacing the Iso-A monomer with DATP, SPAC or DAOB (Entries B1, C1 and D1, Table 6.1 and Figures 6.2.b, 6.2c and 6.2d) in the miniemulsion synthetic process. The idea here is to demonstrate that this strategy will work for the waterborne thiol-ene polymers produced from the bio-based thiol Iso-SH, which might be

followed by eventual replacement of the oil-based enes used in this study by bio-based similar molecules, when available.

30% solids content poly(thioether) aqueous dispersions were obtained by a photoinitiated polymerization in miniemulsion performed under the conditions optimized for the monomer couple Iso-SH/Iso-A. First, the polymer dispersion based on the monomer combination Iso-SH/DATP (Figure 6.2.b) was synthesized with an average particle diameter of 168 nm and with narrow particle size disptribution (PSD of 0.06, Entry B1, Table 6.1). The polymer molar mass could not be determined by conventional GPC using THF or DMF, because the polymer was not soluble in neither of the two solvents. This may be either due to high molar masses of the polymer chains or very high degree of crystallinity. As high degree of crystallinity is quite unlikely, because of the complexity of the chemical structure, that probably limits the rearrangement of polymer chains into crystal structure; we assume that the molecular mass could be at least above 10 kDa, which is also supported by the bulk experiment (Table 6.2). Concerning the formulation based on Iso-SH/SPAC, the least reactive thiol-ene combination according to the bulk polymerization results, a polymer dispersion with an average particle size of 191 nm and PSD of 0.15 (Entry C1, Table 6.2, Figure 6.2.c) was obtained. The molar mass achieved is 69.5kDa, much higher than the biobased Iso-SH/IsoA polymer. Finally, the polymer dispersion based on the very reactive combination Iso-SH/ DAOB presented an average particle diameter of 141 nm with a PSD of 0.16. The molar mass achieved is 136.4kDa, which is the highest obtained in this work and probably the highest reported for polymers obtained by step-growth polymerization. The high molar mass combined with stiff yet flexible polymer chains

could promote the formation of a coherent film. The four monomer couples, therefore might be polymerized in dispersed media, producing relatively concentrated polymer dispersions (30 %) with controlled particle size.

These results show that much higher molar masses were obtained when the reaction was performed in miniemulsion than the same in bulk. It is a consequence on the radical compartmentalization effect within the small monomer droplets/particles, typical for polymerization in dispersed media and observed previously in similarthiol-ene systems[27]. This phenomenon simultaneously provides fast polymerization rate and high molar masses, because of the decrease significance of the bimolecular termination reactions, which moreover are predominant way of termination in step-growth mechanism.

6.3.3. Film formation and properties

In the scope of the aimed application in decorative coating, a continuos film have to be formed by water evaporation from cast polymer dispersions. It is a complex process consisting of three main steps, as emphasized in Chapters 1 and 3. The first step involves evaporation of water and particle ordering. In the following step, particles are deformed into a tetrahedral shape and the water is fully evaporated. At this stage, polymer particles retain their integrity and the film becomes optically clear and as there is only one phase remained. The last step implies coalescence of the particles by polymer chains interdiffusion across particle-particle borders, which occurs at temperature above their glass transition temperature (T_g) and is driven by Brownian motion. Each step of the film formation process can result in differences in the final

film morphology and therefore will directly affect the final film properties. The last stage of the process is of primary importance when it comes to mechanical properties of the film. Indeed, good cohesion of a latex film is achieved when the polymer chains from different particles have interdiffused between them and created entanglements. For this, it is important that the T_g of the polymer is slightly lower than the film forming temperature (lower than ambient temperature if the films should be formed at ambient conditions). On the other hand, if too low the T_g, it may result in very soft polymer film that does not respond to the minimum requirements of mechanical resistance. These two contradictory requirements are the main challenge of the waterborne polymer dispersions, which limits the possibility of improvement of their mechanical properties.

After water evaporation at standard atmospheric conditions (temperature of 25ºC and relative humidity of 55%), the polymer dispersion based on the monomer couple Iso-SH/Iso-A gave rise to a soft and sticky film, as seen in Figure IV.3, Appendix IV. Consistent, tough and glossy coating films were obtained from the dispersions based on Iso-SH/DATP, Iso-SH/SPAC and Iso-SH/DAOB in the same conditions (Figures IV.3 b, c and d, Appendix IV), which is in accordance to the observation from bulk polymerizations. In addition, the films obtained are self-supported indicating a stiffness that can be attributed to the polymer structure (aromatic or cyclic structures) or/and to the presence of crystalline structures.

The production of continuous films at room temperature from the dispersions based on Iso-SH/Iso-A, Iso-SH/DATP and Iso-SH/DAOB suggests that the polymer chains efficiently interdiffused at this temperature and that the T_g of the polymers are lower than 25ºC. In the case

of the dispersion based on Iso-SH/SPAC, the appearance of cracks could indicate that the T_g is higher than the temperature at which the film was produced. The T_g of the films were measured by DSC analysis, reported in Figure IV.4 in Appendix IV, and the values are listed in Table 6. 3. In the DSC scans, the exothermic peak appearing upon cooling is attributed to the crystallization of hexadecane (occurring at around 10ºC), which subsequently melts in the heating scan around 20ºC as supported by the its DSC scans Figure IV.5 in Appendix IV. The multimodal crystallization peaks and melting peaks in the DSC scans of the films could indicate that different structures (either from HD or polymer chains, or other species present in the film such as the surfactant Dowfax 2A1) could crystallize, but were not further investigated. As emphasized previously, however, polymer chains with such complex chemical structure (presence of aromatic and cyclic structures) are unlikely to organize into crystalline domains.

Table 6.3 Tg values for the films based on Iso-SH/Iso-A, Iso-SH/DATP, Iso-SH/SPAC and Iso-SH/DAOB. The values are depicted from the DSC heating scans in Figure IV.4, Appendix IV.

Films	T_g (ºC)
Iso-SH/Iso-A	-2.3
Iso-SH/DATP	*
Iso-SH/SPAC	35.5
Iso-SH/DAOB	7.1

* The T_g could not be observed in the range of temperatures employed for the analysis (between -30ºC and 50ºC)

As expected, films based on Iso-SH/Iso-A, Iso-SH/DATP and Iso-SH/DAOB displays T_g below room temperature, whereas the film based on Iso-SH/DAOB has a higher T_g of 35.5ºC (Table 6.3), which is in line with the observations made previously.

Due to its flexibility and softness, the biobased film Iso-SH/Iso-A presents restrained utility as decorative coating film, but could find applications in other fields such as pressure sensitive adhesives (PSA), for example. The dispersions based on the monomer pairs Iso-SH/SPAC lead to brittle and rigid film (Figures IV.3.c, Appendix IV), which prevented further characterization as the typical flat "dog-bone" shaped tensile test specimens to measure mechanical properties by tensile test cannot be prepared. Noteworthy, the film based Iso-SH/DAOB (Figures IV.3.d, Appendix IV), would display the best characteristic for coating application, with a high T_g, but still low enough to efficiently obtain film at room temperature. For the latter, unfortunately, further characterization in terms of mechanical properties are prevented because the film, probably too rigid, was too fragile. Its film formation will be optimised in the future.

In the following, attention was turned toward the film based on Iso-SH/DATP monomer couple that presents high potential for the aimed application.

To elucidate the physical and mechanical properties of the film based on Iso-SH/DATP, further thermal analysis (TGA and DSC) and tensile tests were performed. The TGA thermogram of Iso-SH/DATP polymer is reported in Figure 6.3.a. In the investigated range of temperature, a first thermal decomposition occurred in a region of 100°C and 200°C and is attributed to the degradation of hexadecane. To confirm it, TGA was performed on hexadecane alone. The hexadecane thermogram is shown in Figure 6.3.b, confirming that it degrades between 100ºC and 200ºC.

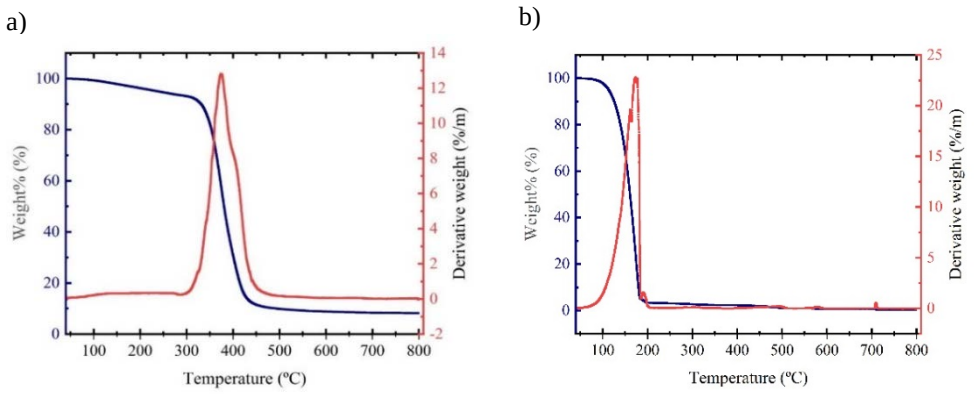

Figure 6.3. TGA of a) the film based on the monomer pair Iso-SH/DATP and b) Hexadecane

The Iso-SH/DATP polymer film was thermally stable until 300ºC, as highlighted by the second thermal decomposition on the thermogram in Figure 6.3.a, which is in a range of waterborne (meth)acrylic polymers currently used for coating applications .[28,29]

Mechanical resistance of the film Iso-SH/DATP was tested by tensile test measurements, as reported with the stress-strain plot in Figure 6.4.

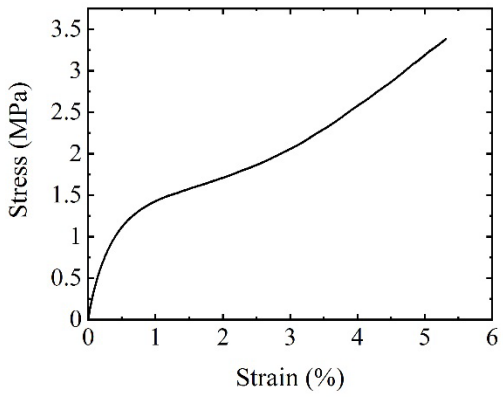

Figure 6.4. Stress-strain plot from tensile test from the tensile measurments of the film Iso-SH/DATP

Figure 6.4 shows that the Iso-SH/DATP film present a high Young's modulus of 3.72 MPa considering waterborne and step-grown polymers, and a high elongation at break of almost 55%, highlighting the flexibility of the material. The tensile tests were performed at 25°C, temperature at which the sample is completely amorphous as the melting peak of the crystalline structures observed by DSC is occurring at 21.5ºC. At lower temperatures, the presence of crystalline structures within the film could increase its stiffness and induce a drop in the elongation at break.

Water sensitivity of polymer films aimed for coating application is an important characteristic, and is determined by water uptake measurements. For that aim, the film based on Iso-SH/DATP was immersed in water and ecolution of the water absorption was followed. The water uptake results are shown in Figure 6.5. for the film based on Iso-SH/DATP, and compared

with two other coatings based on glycol dimercaptoacetate (GDMA) and DATP, labelled F.A1 and F.A2, reported in Chapter 3.

Table 6.4. Details on the films obtained after water evaporation from the latexes based on GDMA-DATP from Chaper 3. For the synthetic processes, S stands for sonopolymerization and SP stands for sonopolymerization combined with photopolymerization.

Latex	Film	Monomers	Synthetic process	Solid content (%)	HD (wt%)	M_w (KDa)
S.1	F.A1	GDMA-DATP	S	30	-	9.135
SP.2	F.A2	GDMA-DATP	SP	30	-	22.696

Films F.A1 and F.A2 were obtained by water evaporation of 30% solid content latexes S.1 and SP.2 synthesized by sonopolymerization and sonopolymerization combined with photopolymerization of the monomer pair GDMA-DATP, as reported in Table 6.4. Noteworthy, the latex SP.2 was synthesized in presence of 0.5wt% of the photoinitiator TPO-Li, whereas the latex S.1 was synthesized without radical initiator (See Latexes S.1 and SP.2 and films F.A1 and F.A2 in Chapter 3).

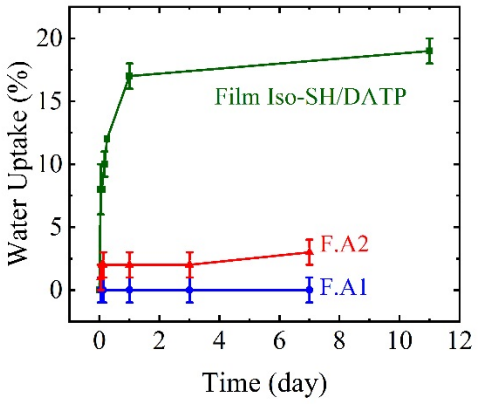

Figure 6.5. Water Uptake of the films F.A1, F.A2 and Iso-SH/DATP

The film Iso-SH/DATP presented relatively low water uptake after eleven days immersion in water of ~20%, which is on the lower line of the water uptake rang of common (meth)acrylic or other hydrophobic coatings produced by emulsion polymerization,[30] but significantly higher than the films F.A1 and F.A2 based on GDMA-DATP.

Various parameters affect the water sensitivity of film coatings. The presence of ionic species in the polymer matrix increases the osmotic pressure, which is the major driving force of water uptake.[31] In the synthesis of the present polymers, few hydrophilic species that can contribute to the increased water solubility were used, such as TPO-Li water soluble initiator and Dowfax 2A1 surfactant. Notably, films F.A2 and Iso-SH/DATP, which both contain TPO-Li, present higher water than the film F.A1, initiator-free. Indeed, hydrophilic moieties coming from the initiator are chemically incorporated within the polymer chains, increasing their hydrophilicity. Moreover, it has been shown in Chapter 4 that films F.A1 and F.A1 are semi-

crystalline at room temperature, with a calculated degree of crystallinity of 21% and 15% respectively. The presence of crystalline structures within the F.A1 and F.A2 films might limit water diffusion by forming physical obstacles and hence lower the water uptake by comparison to the film based on Iso-SH/DATP.

In addition, the water sensitivity of the coating Iso-SH/DATP can be explained by the presence of inhomogeneities in the coating. As shown by Atomic force microscope (AFM) images of the cross section of the films (Figure 6.6), the presence of pores in the biobased film Iso-SH/DATP could increase water penetration by comparison to the film F.A2, more homogeneous.

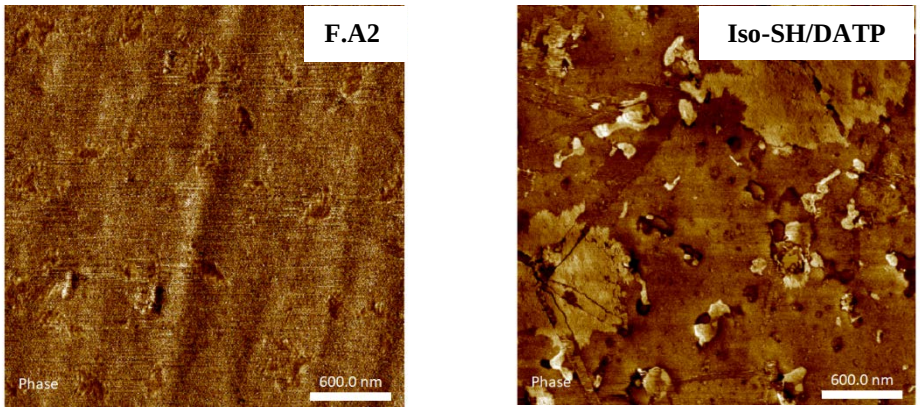

Figure 6.6. AFM images of the cross section of the films F.A2 based GDMA/DATP (image on the left) and IsoSH/DATP (image on the right)

In the case of waterborne coatings, the migration of the water soluble surfactant has been reported to be an important drawback in water sensitivity.[31] Indeed, surfactants molecules

provide hydrophilic channel that let the water soak in the coating. The surfactant Dowfax 2A1 is non-chemically bonded to the polymer, and its degree of compatibility with the polymer matrix affects its distribution within the film. However, the surfactant distribution is not static within the film. Free surfactant tends to migrate during and after the film formation process and affect the final properties of the film. If the chemical structures of the emulsifier and the polymer matrix are not compatible, emulsifier molecules aggregate within the polymer film matrix. These aggregates generate hydrophilic "pockets" able to absorb high water quantity from the surrounding. The reorganization of the surfactant depends on several factors, such as the hydrophobicity of the polymer matrix or its flexibility. Highly hydrophobic polymers tend to be less compatible with amphiphilic surfactant, and flexible chains allow the surfactant to migrate readily. Hence, the supposedly low T_g (that could not be measured by DSC in the range of temperature between -30ºC and 50ºC) and the hydrophobicity of the poly(thioether) based on Iso-SH/DATP tend to promote the reorganisation of Dowfax 2A1 within the films into hydrophilic pockets, and therefore the water uptake of the film. In that line, for the films based on GDMA/DATP, a T_g of -15.6ºC and -7.8ºC for F.A1 and F.A2 respectively could be measured by DSC (See Table 4.4, Chapter 4). Perhaps, these T_g are higher than the one of the film Iso-SH/DATP, which reduce the reorganization of the surfactant within the film and lower its water uptake.

In the decorative coating aimed application, the visual appearance of the final film is very important. The visual appearance with respect to its gloss level can be measured with a

gloss meter at different angles (20, 60 and 85°) and the results for the film Iso-SH/DATP are presented in Figure 6.7.

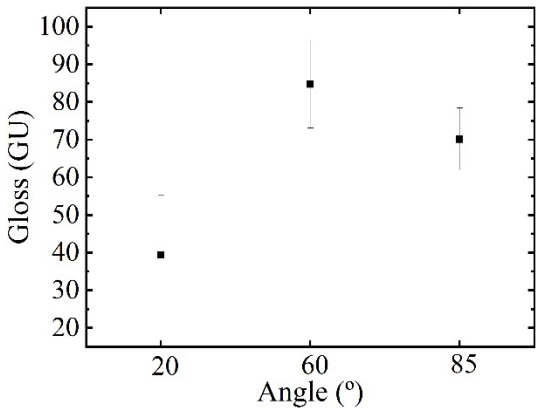

Figure 6.7 Gloss measurment at 20, 60 and 85º angle for the film based on Iso-SH/DATP

The coating Iso-SH/DATP presents high gloss, with a value higher than 80% at the angle 60°C (Figure 6.7). Besides the aesthetic purpose, the differences between a gloss and matte effect affects the practical aspects of the coating such as surface cleanability or texture. Glossy surfaces show every imperfection, whereas matte surfaces tend to hide scratches or imperfections. Moreover, the gloss can be an additional indication for migration of the surfactant to the film-air interface. For waterborne coatings, the higher the gloss, the less surfactant migrates to the film-air interface. Hence, in the case of the film Iso-SH/DATP, the surfactant may have mainly migrated within the coating forming the hydrophilic pockets, rather

than at the film-air interface. This resulted in hydrophilic aggregates increasing water uptakes and causing the milky or cloudy appearance of the film. Indeed, the presence of water pockets due to water that was trapped within the coating during film formation, displays a lower refractive index and lead to the scattering of light.

6.4. Conclusion

In this Chapter, we report the synthesis of 30% solid content poly(thioethers) latexes based on two newly synthesized biobased monomers Iso-SH and Iso-A. Namely, four thiol-ene monomer combination were implemented (Iso-SH/Iso-A, Iso-SH/DATP, Iso-SH/DAOB and Iso-SH/SPAC) and their applicability to step-growth polymerization in photoinduced miniemulsion polymerization process is reported.

Noteworthy, the four polymer dispersions based on the bio-monomers and their combination with oil-based monomers presented film forming abilities. Among them, the formulations containing bio-based Iso-SH with the non-biobased dienes DATP could be further characterized for the aimed application in coating. Indeed, the film based on Iso-SH-DATP presented good thermal stability until 300ºC, and good mechanical properties, investigated by tensile test measurement, with a measured Young's modulus of 3.72 MPa and a 55% elongation at break. In addition, the film Iso-SH/DATP presented relatively low water uptake after eleven days immersion in water of less than 20%, but significantly higher than the films F.A1 and F.A2 based on GDMA-DATP synthesized in Chapter 3. The latter present crystalline structures at room temperature, which could prevent the water diffusion through the coating and lower water

uptake, whereas the film Iso-SH/DATP is completely amorphous in these conditions. The higher water uptake could be explained by a lower T_g of the film Iso-SH/DATP, although not measured, which may promote the reorganization of the surfactant into hydrophilic "pockets" within the coating and increase its water sensitivity. In line with the aimed application in decorative coating, the film Iso-SH/DATP presents high gloss, with a value higher than 80% at the angle 60°C. Besides the aesthetic purpose, high gloss values provide another indication on the migration of the surfactant, which hence mainly migrates within the coating and not at the interface with air. Such behaviour is in line with the water uptake measurements.

Therefore, the synthesis in aqueous dispersed media, together with the incorporation of biobased building block within the polymer represents one step forward towards the production of fully biobased waterborne coating with added value.

6.5. References

1. Cywar, R. M., Rorrer, N. A., Hoyt, C. B., Beckham, G. T. & Chen, E. Y. X. Bio-based polymers with performance-advantaged properties. *Nat. Rev. Mater.* **7**, 83–103 (2022).

2. Kristufek, S. L., Wacker, K. T., Tsao, Y. Y. T., Su, L. & Wooley, K. L. Monomer design strategies to create natural product-based polymer materials. *Nat. Prod. Rep.* **34**, 433–459 (2017).

3. John, G., Nagarajan, S., Vemula, P. K., Silverman, J. R. & Pillai, C. K. S. Natural monomers: A mine for functional and sustainable materials – Occurrence, chemical modification and polymerization. *Prog. Polym. Sci.* **92**, 158–209 (2019).

4. Kohut, A. *et al.* Non-Conventional Features of Plant Oil-Based. *Molecules* **25**, 2990 (2020).

5. Li, W. S. J. *et al.* Cardanol-based polymer latex by radical aqueous miniemulsion polymerization. *Polym. Chem.* **9**, 2468–2477 (2018).

6. Jasinski, F., Zetterlund, P. B., Braun, A. M. & Chemtob, A. Photopolymerization in dispersed systems. *Prog. Polym. Sci.* **84**, 47–88 (2018).

7. Molina-Gutiérrez, S., Ladmiral, V., Bongiovanni, R., Caillol, S. & Lacroix-Desmazes, P. Radical polymerization of biobased monomers in aqueous dispersed media. *Green Chem.* **21**, 36–53 (2019).

8. Aguirre, M., Hamzehlou, S., González, E. & Leiza, J. R. *Renewable feedstocks in emulsion polymerization: Coating and adhesive applications*. *Advances in Chemical Engineering* vol. 56 (Elsevier Inc., 2020).

9. Molina-Gutiérrez, S. *et al.* Radical Aqueous Emulsion Copolymerization of Eugenol-Derived Monomers for Adhesive Applications. *Biomacromolecules* **21**, 4514–4521 (2020).

10. Sarkar, P. & Bhowmick, A. K. Terpene-Based Sustainable Elastomers: Vulcanization and Reinforcement Characteristics. *Ind. Eng. Chem. Res.* **57**, 5197–5206 (2018).

11. Lamparelli, D. H., Kleybolte, M. M., Winnacker, M. & Capacchione, C. Sustainable myrcene-based elastomers via a convenient anionic polymerization. *Polymers (Basel).* **13**, (2021).

12. Xu, Q., Ma, J., Zhou, J., Wang, Y. & Zhang, J. Bio-based core-shell casein-based silica nano-composite latex by double-in situ polymerization: Synthesis, characterization and mechanism. *Chem. Eng. J.* **228**, 281–289 (2013).

13. Choi, K. Y. & Mcauley, K. B. Step-Growth Polymerization. *Polym. React. Eng.* 273–314 (2008) doi:10.1002/9780470692134.ch7.

14. Durham, O. Z., Chapman, D. V., Krishnan, S. & Shipp, D. A. Radical Mediated Thiol-Ene Emulsion Polymerizations. *Macromolecules* **50**, 775–783 (2017).

15. Quoc Le, C. M., Schmutz, M. & Chemtob, A. Ab Initio Batch Emulsion Thiol–Ene Photopolymerization. *Macromolecules* (2020) doi:10.1021/acs.macromol.0c00265.

16. Le, C. M. Q., Vidal, L., Schmutz, M. & Chemtob, A. Droplet nucleation in miniemulsion thiol-ene step photopolymerization. *Polym. Chem.* **12**, 2084–2094 (2021).

17. Machado, T. O., Cardoso, P. B., Feuser, P. E., Sayer, C. & Araújo, P. H. H. Thiol-ene miniemulsion polymerization of a biobased monomer for biomedical applications. *Colloids Surfaces B Biointerfaces* **159**, 509–517 (2017).

18. Romera, C. D. O., De Oliveira, D., De Araújo, P. H. H. & Sayer, C. Biobased Ester 2-(10-Undecenoyloxy)ethyl Methacrylate as an Asymmetrical Diene Monomer in Thiol-Ene Polymerization. *Ind. Eng. Chem. Res.* **58**, 21044–21055 (2019).

19. Schork, F. J. *et al.* Miniemulsion polymerization. *Adv. Polym. Sci.* **175**, 129–255 (2005).

20. Asua, J. M. Miniemulsion polymerization. *Prog. Polym. Sci.* **27**, 1283–1346 (2002).

21. Jasinski, F. *et al*. Thiol-Ene Linear Step-Growth Photopolymerization in Miniemulsion: Fast Rates, Redox-Responsive Particles, and Semicrystalline Films. *Macromolecules* **49**, 1143–1153 (2016).

22. Sycks, D. G., Safranski, D. L., Reddy, N. B., Sun, E. & Gall, K. Tough Semicrystalline Thiol-Ene Photopolymers Incorporating Spiroacetal Alkenes. *Macromolecules* **50**, 4281–4291 (2017).

23. Asua, J. M. Emulsion Polymerization: From Fundamental Mechanisms to Process Developments. *J. Polym. Sci. Part A Polym. Chem.* **42**, 1025–1041 (2004).

24. Lobry, E. *et al.* Continuous-flow synthesis of polymer nanoparticles in a microreactor via miniemulsion photopolymerization. *RSC Adv.* **4**, 43756–43759 (2014).

25. Jasinski, F. *et al.* Light-mediated thiol-ene polymerization in miniemulsion: A fast route to semicrystalline polysul fide nanoparticles. *ACS Macro Lett.* **3**, 958–962 (2014).

26. Odian, G. *Principles of polymerization*. (2004).

27. Infante Teixeira, L., Landfester, K. & Thérien-Aubin, H. Nanoconfinement in miniemulsion increases reaction rates of thiol-ene photopolymerization and yields high molecular weight polymers. *Polym. Chem.* 2831–2841 (2022) doi:10.1039/d2py00350c.

28. Król-Morkisz, K. & Pielichowska, K. *Thermal Decomposition of Polymer Nanocomposites With Functionalized Nanoparticles. Polymer Composites with Functionalized Nanoparticles: Synthesis, Properties, and Applications* (Elsevier Inc., 2018). doi:10.1016/B978-0-12-814064-2.00013-5.

29. Kholodovych, V. & Welsh, W. J. Thermal-Oxidative Stability and Degradation of Polymers. *Phys. Prop. Polym. Handb.* 927–938 (2007) doi:10.1007/978-0-387-69002-5_54.

30. Boscán, F. *et al.* Incorporation of Very Insoluble Monomers in Waterborne Coatings. *Macromol. Mater. Eng.* **304**, 1–9 (2019).

31. Keddie, J. L. & Routh, A. F. *Fundamentals of Latex Film Formation: Processes and Properties*. (Springer US, 2010).

Chapter 7. Conclusions

The main aims of this thesis were the synthesis of novel film forming semi-crystalline poly(thioethers) by employing photopolymerization in dispersed media technique, and the study of their crystalline behaviour to develop application possibilities as waterborne barrier coatings for food packaging. In addition, the possibility to carry out polymerization in dispersed system to yield biobased polymer dispersions and coatings has been implemented, with an aimed application in decorative coating.

Chapter 1 lays the foundation of thiol-ene challenges and limitations with the model thiol-ene pair based on glycol dimercaptoactetate (GDMA) and diallyl terephtalate (DATP). Results show that reproducibility and control of molar mass is challenging for this system, but as well by the nature of step growth polymerization and the purity of starting material. Indeed, in step growth linear polymerization, the final degree of polymerization is strongly impacted by stoichiometric balance between thiol and ene functionality and the overall extent of the reaction. Stoichiometric ratio between monomers can be biased because of the chemical instability of the neat GDMA, which pass spontaneous chemical reactions such as oxidized under molecular oxygen or thiol-disulfide exchange, yielding to the formation of disulphide bonds with homodimers, trimers and even quadrimers. Besides inducing off-stoichiometric ratio between thiol and ene functionality, these disulfide bonds are capable to undergo rapid exchange with thiyl radicals. The latter can be responsible for premature polymerization, observed when the two neat monomers GDMA and DATP are mixed, by initiating the radical mediated step growth

mechanism. The presence of disulfide bonds within the GDMA-DATP polymer backbone could be appreciated by Raman analysis, and could explain the rapid decomposition of the polymer.

To improve reproducibility and control of molar masses, one strategy is to use radical inhibitor such as 2,5-Di-tert-butylhydroquinone (DBHQ) and Pyrogallol (PYR). It is important to note that this strategy was efficient when working in bulk, but might be revisited when working in dispersed media. Indeed, when working in miniemulsion for example, the use of homogenization device such as sonicator may additionally form radicals capable to initiate the step-growth polymerization[1].

Therefore, in this thesis, another strategy in which chemical instability is turned into an advantage is proposed. Namely, the synthesis of thiol-ene oligomers by sonication was intentionally used to promote the obtainment of stable polymer particles in water. In that way, high molar masses polymer could be achieved with an additional step of photopolymerization, as described in Chapter 3.

Indeed, in Chapter 3, we report the synthesis of poly(thioether) latexes through two main processes, different in the strategy followed to overcome the challenge of the low chemical stability of thiol-ene system and premature polymerization that lead to irreproducibility.

In the first one chemical stability of thiol-ene miniemulsions based on the model monomer GDMA and DATP was achieved by using radical scavenger DBHQ to prevent premature polymerization during miniemulsification by sonication. Stable thiol-ene miniemulsions were further converted to latexes by photopolymerization in presence of a

photoinitiator. This strategy allows a spatial and temporal control of the onset of the polymerization, but suffer from stability issue. Indeed, colloidally stable miniemulsions were challenging to obtain, as the presence of inhibitor DBHQ with high hydrophilicity increased the hydrophilicity of the particles and promoted monomer diffusion and stoichiometric imbalance. Consequently, lack of reproducibility especially in the molar masses was observed.

The other line of investigation in which sonopolymerisation is combined with photopolymerization, turned out to be very efficient for the synthesis of high solid content latexes based on diene monomer DATP and various dithiol monomers GDMA, glycol dimercaptopropionate (GDMP) and 2,2-(ethylenedioxy)diethanethiol (EDDT). In this line, the miniemulsification process of thiol-ene emulsion was used to perform sonopolymerization without use of any initiator or inhibitor, producing pre-polymer dispersions that were afterwards photopolymerized. The combination of two polymerisation processes allows to achieve colloidally stable latexes at solids content of 30% and up to 50% with high molar mass poly(thioether) as high as 200 kDa, the highest to the best knowledge of the author for this type of polymers. Colloidal instability is precluded, as stable pre-polymer particles are obtained after sonication likely due to the higher hydrophobicity of the oligomers that prevent monomer diffusion- Chemical instability was overcame, too because of the fast conversion of the monomers during the sonication, creating still reactive pre-polymers.

In addition, we report the synthesis of film forming linear poly(thioether), which will be of interest for the rest of the project. Indeed, latexes based on GDMA-DATP, GDMP-DATP and EDDT-DATP present good film forming abilities at room temperature. These films were

characterized in terms of water and chemical resistance, which are important properties for the intended application in food packaging. The films based on GDMA-DATP turn out to be the more promising in terms of barrier properties, with low water uptake (below 2%) and water vapour diffusion rate (2 g*mm/m^2*day). Moreover, GDMA-DATP films presented good chemical resistance to food simulant B (3% (w/v) acetic acid aqueous solution), with low mass loss values after 4 days immersed. In particular, the GDMA-DATP films obtained from high solid content latex and presenting low polydispersity in molar masses were the one presenting the chemical resistance, highlighting the fact that both film formation process and polymer's macrostructure are important for that matter.

Strategies were implemented to improve the final properties of the film by adding small amount of trifunctional monomer or inorganic filler (graphene oxide and reduced graphene oxide). The addition of a trifunctional monomer yields to the synthesis of cross-linked poly(thioethers), and further investigation in terms of crystalline behaviour are precluded as linear chains are preferred for this matter. However, the addition of inorganic filler could be a strategy to promote barrier properties, as water uptakes results were encouraging.

The films based on GDMA-DATP, GDMP-DATP and EDDT-DATP were further characterized in terms of crystalline behaviour in Chapter 4. As the selected monomers are bifunctionnal, the thiol-ene step-growth mechanism facilitates the synthesis of linear poly(thioether) with semicrystalline behaviour evidenced by differential scanning calorimetry (DSC) analysis. The as-synthesized films present a degree of crystallinity of approximately 20% and slow crystallizing polymer chains. The self-nucleation (SN) thermal protocol turns out to

be an efficient strategy to study the crystallization behaviour of such polymers, as the produced self-nuclei substantially sped up the overall crystallization kinetics. This study allowed to correlate the chemical structure of the poly(thioethers) with crystallization rate by comparing the number of SN domains that can be detected by the technique. Indeed, the film F.B1.HD, based on the monomer combination EDDT-DATP and containing hexadecane (HD) is the only one presenting the three SN domains described by Fillon et *al*.[2] Its faster crystallization kinetics are attributed to the linearity of the EDDT-DATP chains (promoting the organization into crystalline structures) with low glass transition temperature (T_g) of -22.6ºC. In addition, the presence of HD could act as a plasticizer and promote fast ordering of polymer chains.

In Chapter 5, attention was turned toward three other poly(thioethers) composed of more linear backbones without aromatic or cyclic structures nor pending functionalities, based on monomers such as di(ethylene glycol) divinyl ether (DVE), 2,2'-dimercaptodiethyl sulfide (DMDS), triethylene glycol divinyl ether (TEGDVE) and 1,4-butanediol divinyl ether (BDDVE). The study on the crystallization of DVE-DMDS, TEGDVE-DMDS and BDDVE-DMDS shows the potential and peculiar behaviour of the poly(thioethers). Under non-isothermal conditions, DSC analysis show successive melting-crystallization-melting peaks upon heating for the three polymers. The two distinct melting peaks were attributed to two crystalline structures, denoted as Low-T_m-form and High-T_m-form. Upon cooling from the melt, the crystallization of the Low-T_m-forms could be observed for the three poly(thioethers). However, it was shown that the High-T_m-form could only form from the melt for the polymers TEGDVE-DMDS and BDDVE-DMDS.

For the polymer DVE-DMDS, it was shown by wide angle X-ray scattering (WAXS) analysis that the two crystalline structures from Low-T_m-form and High-T_m-form are different, showing that two different polymorphs can be formed by the same polymer. The two polymorphs presented different morphologies, which could be observed under Polarized light optical microscope (PLOM) following a successive isothermal protocol. From the latter, it was found that upon heating the polymer chains from DVE-DMDS remembered their previous alignment within the crystalline Low-T_m-form, even above its melting temperature. This memory assisted the nucleation enabled the formation of the High-T_m-form.

Under isothermal conditions, crystallization kinetics of the Low-T_m-form from DVE-DMDS and High-T_m-form from TEGDVE-DMDS and BDDVE-DMDS could be implemented by DSC analysis. Experimental data were fitted to the Avrami equation, and give a first insight into crystallization kinetics. At this stage of the work, faster nucleation rate and crystallization rate are obtained for the high-T_m-form from polymer BDDVE-DMDS with the lowest T_g. The overall crystallization (which comprises nucleation and crystal growth) is mainly accelerated for shorter repeating unit in the polymer backbone and lower T_g. Overall, the polymer DVE-DMDS displays the slower kinetics, with only the Low-T_m-form capable to crystallize upon cooling from the melt. The High-T_m-form from this polymer presents very slow kinetics, that can be accelerated by self-nucleation from remaining self-nuclei or self-seeds of the Low-T_m-form slightly above its melting temperature.

Finally, in Chapter 6, we report the synthesis of 30% solid content poly(thioethers) latexes based on two newly synthesized biobased monomers isosorbide dithiol (Iso-SH) and

isosorbide diallyl (Iso-A). Namely, four thiol-ene monomer combination were implemented: the fully biobased bicomponent system Iso-SH/Iso-A was studied, but also three other formulations in which the biobased Iso-SH monomer was polymerized with three petroleum-based dienes: diallyl terephthalate (DATP), 3,9-divinyl-2,4,8,10-tetraoxaspiro [5.5]undecane (SPAC), and 1,4-bis(allyloxy)benzene (DAOB) (Iso-SH/Iso-A, Iso-SH/DATP, Iso-SH/DAOB and Iso-SH/SPAC). Their applicability to step-growth polymerization in photoinduced miniemulsion polymerization process is reported.

Noteworthy, the four polymer dispersions based on the bio-monomers and their combination with oil-based monomers presented film forming abilities. Among them, the formulations containing bio-based Iso-SH with the non-biobased dienes DATP could be further characterized for the aimed application in coating. Indeed, the film based on Iso-SH-DATP presented good thermal stability until 300ºC, and good mechanical properties, investigated by tensile test measurement, with a measured Young's modulus of 3.72 MPa and a 55% elongation at break. In addition, the film Iso-SH/DATP presented relatively low water uptake after eleven days immersion in water of less than 20%, but significantly higher than the films F.A1 and F.A2 based on GDMA-DATP synthesized in Chapter 3. The latter present crystalline structures at room temperature, which could prevent the water diffusion through the coating and lower water uptake, whereas the film Iso-SH/DATP is completely amorphous in these conditions. The higher water uptake could be explained by a lower T_g of the film Iso-SH/DATP, although not measured, which may promote the reorganization of the surfactant into hydrophilic "pockets" within the coating and increase its water sensitivity. In line with the aimed application in decorative coating, the film Iso-SH/DATP presents high gloss, with a value higher than 80% at

the angle 60°. Besides the aesthetic purpose, high gloss values provide another indication on the migration of the surfactant, which hence mainly migrates within the coating and not at the interface with air. Such behaviour is in line with the water uptake measurements.

Therefore, the synthesis in aqueous dispersed media, together with the incorporation of biobased building block within the polymer represents one step forward towards the production of fully biobased waterborne coating with added value.

References

(1) Skinner, E. K.; Whiffin, F. M.; Price, G. J. Room Temperature Sonochemical Initiation of Thiol-Ene Reactions. *Chem. Commun.* **2012**, *48* (54), 6800–6802. https://doi.org/10.1039/c2cc32457a.

(2) Fillon, B.; Wittmann, J. C.; Lotz, B.; Thierry, A. Self-nucleation and Recrystallization of Isotactic Polypropylene (α Phase) Investigated by Differential Scanning Calorimetry. *J. Polym. Sci. Part B Polym. Phys.* **1993**, *31* (10), 1383–1393. https://doi.org/10.1002/polb.1993.090311013.

Parts of this thesis have been presented in conferences, workshops, consortium meetings and Industrial Liaison Program (ILP) meetings, both as oral or poster presentation. In addition, parts of the work described in this thesis have been published or are planned to be published.

In the following, an overview of the oral and poster presentation is given, and a list of the publications (either planned or already published) is presented. The title and authors of planned publications may change.

Oral and poster presentations

Oral presentation “An introduction to thiol-ene waterborne coatings”, 1st Consortium Meeting project photo-emulsion, 2018, Mulhouse (France)

Oral presentation “High Barrier Waterborne Polysulfide Dispersions”, 19th ILP Meeting, 2019, San-Sebastián (Spain)

Oral presentation “High Barrier Waterborne Polysulfide Dispersions”, RISE seminar, 2019, Stockholm (Sweden)

Poster presentation “High Barrier Waterborne Polysulfide Dispersions”, 8th Working Party on Polymer Process Reaction Engineering (WPPRE), 2019, Hamburg (Germany)

Oral presentation “High Barrier Waterborne Polysulfide Dispersions”, 2nd Consortium Meeting project photo-emulsion, 2019, Mainz (Germany)

Oral presentation “Thiol-Ene Step-Growth Polymers: a New Matrix For Gas Sensor”, Training workshop Nato SfP PROJECT G5244, 2019, San-Sebastián (Spain)

Oral presentation “Waterborne Polysulfide Dispersions”, Prof. Günter Reiter research group seminar at Freiburg University, 2020, Freiburg (Germany)

Oral presentation “Resolving Challenges in Thiol-ene Polymerization System”, 20th ILP Meeting, 2020, Held Online

Oral presentation “Waterborne Polysulfide Dispersions”, 3rd Consortium Meeting project photo-emulsion, 2020, Held Online

Oral presentation “Thiol-ene waterborne coatings and their crystallization behaviour”, 4th Consortium Meeting project photo-emulsion, 2021, Maribor (Slovenia)

Oral presentation “Thiol-ene waterborne coatings and crystallization: towards innovative packaging”, GEP-SLAP conference, 2022, San-Sebastián (Spain)

Oral presentation “Thiol-ene waterborne coatings and crystallization: towards innovative packaging”, 22nd ILP Meeting, 2019, San-Sebastián (Spain)

Publications

Justine Elgoyhen and Radmila Tomovska. Self-initiation of thiol-ene polymerization by thiol oxidation. Under preparation

Justine Elgoyhen, Valentina Pirela, Alejandro J. Müller and Radmila Tomovska. Developing Synthesis Strategy for Ultra-high Molar Mass Step-grown Waterborne Poly(thioethers) and Unlock of their Semi-crystalline Nature. Under preparation

Justine Elgoyhen, Cuong Minh Quoc Le, Alexander Ricke, Stefan Baudis, Robert Liska, Abraham Chemtob and Radmila Tomovska. Biobased Polysulfide Coating for Decorative Application. Under preparation

Ana Trajcheva, Justine Elgoyhen, Maryam Ehsani, Yvonne Joseph, Jadranka B. Gilev, and Radmila Tomovska. Thiol-ene/rGO Nanocomposites - Novel Sensing Materials for Humidity Detection. Under preparation

Valentina Pirela, Justine Elgoyhen, Brahim Bessif, Cuong Minh Quoc Le, Barbara Heck, Thomas Pfohl, Abraham Chemtob, Günter Reiter, Radmila Tomovska and Alejandro J. Müller. Unraveling the Polymorphic Crystallization Behaviour and Kinetics of Aliphatic poly(thioethers). Unider preparation

Cuong Minh Quoc Le, Gautier Schrodj, Ibrahima Ndao, Brahim Bessif, Barbara Heck, Thomas Pfohl, Günter Reiter, Justine Elgoyhen, Radmila Tomovska, and Abraham Chemtob. Semi-

Crystalline Poly(thioether) Prepared by Visible-Light-Induced Organocatalyzed Thiol-ene Polymerization in Emulsion. *Macromol. Rapid Commun* 2022 doi: 10.1002/marc.202100740

Brahim Bessif, Barbara Heck, Thomas Pfohl, Cuong Minh Quoc Le, Abraham Chemtob, Valentina Pirela, Justine Elgoyhen, Radmila Tomovska, Alejandro J. Müller and Günter Reiter. Nucleation Assisted through the Memory of a Polymer Melt: A Novel Polymorph Emerging from the Melt of another One. Submitted to *Macromolecules*

Conclusiones

Los objetivos principales de esta tesis fueron la síntesis de nuevos poli(tioéteres) semicristalinos con capacidad de formar film mediante el empleo de la técnica de fotopolimerización en medio disperso, y el estudio de su comportamiento cristalino para desarrollar posibles aplicaciones como recubrimientos de barrera sintetizados en base agua para envases de alimentos. Además, se ha implementado la posibilidad de llevar a cabo la polimerización en un sistema disperso para producir recubrimientos y dispersiones de polímeros de biobasados, con una aplicación específica en recubrimientos decorativos.

El Capítulo 1 sienta las bases de los desafíos y limitaciones del tiol-eno usando el par tiol-eno modelo basado en dimercaptoactetato de glicol (GDMA) y tereftalato de dialilo (DATP). Los resultados muestran que la reproducibilidad y el control de la masa molar son un reto para este sistema, pero también por la naturaleza de la polimerización por crecimiento por etapas y la pureza los materiales de partida. De hecho, en la polimerización lineal de crecimiento por etapas, el grado final de polimerización se ve fuertemente afectado por el equilibrio estequiométrico entre la funcionalidad tiol y eno y la extensión general de la reacción. La relación estequiométrica entre los monómeros puede estar sesgada debido a la inestabilidad química del GDMA puro, que pasa por reacciones químicas espontáneas, como la oxidación bajo el oxígeno molecular o el intercambio tiol-disulfuro, dando lugar a la formación de enlaces disulfuro con homodímeros, trímeros e incluso tetrameros. Además de inducir una relación no estequiométrica entre la funcionalidad tiol y eno, estos enlaces disulfuro son capaces de

experimentar un intercambio rápido con los radicales tiilo. Este último puede ser responsable de la polimerización prematura, que se observa cuando se mezclan los dos monómeros puros GDMA y DATP, al iniciar el mecanismo de crecimiento escalonado mediado por radicales. La presencia de enlaces disulfuro dentro del esqueleto del polímero GDMA-DATP se podía apreciar mediante análisis Raman y podría explicar la rápida descomposición del polímero. Para mejorar la reproducibilidad y el control de las masas molares, una estrategia es utilizar inhibidores de radicales como 2,5-di-terc-butilhidroquinona (DBHQ) y pirogalol (PYR). Es importante tener en cuenta que esta estrategia fue eficiente cuando se trabajó en masa, pero podría revisarse cuando se trabaja en medios dispersos. De hecho, cuando se trabaja en miniemulsión por ejemplo, el uso de un dispositivo de homogeneización como un sonicador puede formar radicales adicionales capaces de iniciar la polimerización por etapas.

Por tanto, en esta tesis se propone otra estrategia en la que la inestabilidad química se convierte en una ventaja. Es decir, la síntesis de oligómeros de tiol-eno por sonicación se utilizó intencionalmente para promover la obtención de partículas poliméricas estables en agua. De esa manera, se podría lograr un polímero de masas molares altas con un paso adicional de fotopolimerización, como se describe en el Capítulo 3. De hecho, en el Capítulo 3, reportamos la síntesis de látex de poli(tioéter) a través de dos procesos principales, diferentes en la estrategia seguida para superar el desafío de la baja estabilidad química del sistema tiol-eno y la polimerización prematura que conduce a la irreproducibilidad.

En el primero, la estabilidad química de las miniemulsiones de tiol-eno basadas en el sistema modelo de los monómeros GDMA y DATP se logró mediante el uso del inhibidor de

radicales DBHQ para evitar la polimerización prematura durante la miniemulsificación por sonicación. Las miniemulsiones estables de tiol-eno se convirtieron además en látex mediante fotopolimerización en presencia de un fotoiniciador. Esta estrategia permite un control espacial y temporal del inicio de la polimerización, pero sufre un problema de estabilidad. De hecho, fue difícil obtener miniemulsiones coloidalmente estables, ya que la presencia del inhibidor DBHQ con alta hidrofilicidad aumentaba la hidrofilicidad de las partículas y promovía la difusión de monómeros y el desequilibrio estequiométrico. En consecuencia, se observó falta de reproducibilidad especialmente en las masas molares.

La otra línea de investigación en la que se combina la sonopolimerización con la fotopolimerización, resultó muy eficiente para la síntesis de látex de alto contenido en sólidos basados en el monómero dieno DATP y varios monómeros ditiol: GDMA, dimercaptopropionato de glicol (GDMP) y 2,2-(etilendioxi)dietanotiol (EDDT). En esta línea, se utilizó el proceso de miniemulsificación de la emulsión de tiol-eno para realizar la sonopolimerización sin el uso de ningún iniciador o inhibidor, produciendo dispersiones de prepolímeros que luego fueron fotopolimerizados. La combinación de los dos procesos de polimerización permite lograr látex coloidalmente estables con un contenido de sólidos del 30 % y hasta 50 % y con con poli(tioéteres) de alta masa molar de hasta 200 kDa. Estos valores son los más altos reportados para este tipo de polímeros, de acuerdo al mejor conocimiento de la autora. Se evita la inestabilidad coloidal, ya que se obtienen partículas de prepolímero estables después de la sonicación, probablemente debido a la mayor hidrofobicidad de los oligómeros que impiden la difusión del monómero. También se superó la inestabilidad química debido a la rápida conversión de los monómeros durante la sonicación, creando prepolímeros.

Además, reportamos la síntesis de poli(tioéter) lineal con capacidad de formar de filme, que será de interés para el resto del proyecto. De hecho, los látex basados en GDMA-DATP, GDMP-DATP y EDDT-DATP presentan buenas capacidades de formación de filme a temperatura ambiente. Estos filmes se caracterizaron en términos de resistencia al agua y a productos químicos, que son propiedades importantes para la aplicación prevista en el envasado de alimentos. Los filmes basados en GDMA-DATP resultaron ser los más prometedores en términos de propiedades de barrera, con baja absorción de agua (inferior al 2%) y velocidad de difusión del vapor de agua (2 g*mm/m^2*día). Además, los filmes de GDMA-DATP presentaron buena resistencia química al simulador alimentario B (solución acuosa de ácido acético al 3% (p/v)), con bajos valores de pérdida de masa después de 4 días de inmersión. En particular, los filmes GDMA-DATP obtenidos a partir de látex con alto contenido de sólidos y que presentan baja polidispersidad en masas molares fueron los que presentaron la mejor resistencia química, destacando el hecho de que tanto el proceso de formación de la filme como la macroestructura del polímero son importantes para este asunto.

Se implementaron estrategias para mejorar las propiedades finales de los filmes mediante la adición de una pequeña cantidad de monómero trifuncional o carga inorgánica (óxido de grafeno y óxido de grafeno reducido). La adición de un monómero trifuncional conduce a la síntesis de poli(tioéteres) reticulados, y se excluyen más investigaciones en términos del comportamiento cristalino, ya que se prefieren las cadenas lineales para este asunto. Sin embargo, la adición de cargas inorgánicas podría ser una estrategia para promover las propiedades de barrera, ya que los resultados de absorción de agua fueron alentadores. Los filmes basados en GDMA-DATP, GDMP-DATP y EDDT-DATP se caracterizaron más en

términos de comportamiento cristalino en el Capítulo 4. Como los monómeros seleccionados son bifuncionales, el mecanismo de crecimiento por etapas del tiol-eno facilita la síntesis de poli(tioéter) lineal con comportamiento semicristalino evidenciado por análisis de calorimetría diferencial de barrido (DSC). Los filmes sintetizados presentan un grado de cristalinidad de aproximadamente 20 % y cadenas poliméricas de cristalización lenta. El protocolo térmico de autonucleación (SN) resulta ser una estrategia eficiente para estudiar el comportamiento de cristalización de tales polímeros, ya que los autonúcleos producidos aceleraron sustancialmente la cinética de cristalización general. Este estudio permitió correlacionar la estructura química de los poli(tioéteres) con la tasa de cristalización comparando el número de dominios SN que pueden ser detectados por la técnica. De hecho, la filme F.B1.HD, basado en la combinación de monómeros EDDT-DATP y que contiene hexadecano (HD), es el único que presenta los tres dominios SN descritos por Fillon *et al*.[2] Su cinética de cristalización más rápida se atribuye a la linealidad de las cadenas EDDT-DATP (que favorecen la organización en estructuras cristalinas) con baja temperatura de transición vítrea (T_g) de -22,6 ºC. Además, la presencia de HD podría actuar como plastificante y promover el rápido ordenamiento de las cadenas poliméricas.

En el Capítulo 5, se centró la atención en otros tres poli(tioéteres) compuestos por esqueletos más lineales sin estructuras aromáticas o cíclicas ni funcionalidades pendientes, basados en monómeros como di(etilenglicol) divinil éter (DVE), 2,2'-dimercaptodietil sulfuro de hidrógeno (DMDS), trietilenglicol divinil éter (TEGDVE) y 1,4-butanodiol divinil éter (BDDVE). El estudio de la cristalización de DVE-DMDS, TEGDVE-DMDS y BDDVE-DMDS muestra el comportamiento potencial y peculiar de los poli(tioéteres). En condiciones no

isotérmicas, el análisis DSC muestra picos sucesivos de fusión-cristalización-fusión al calentar los tres polímeros. Los dos picos de fusión distintos se atribuyeron a dos estructuras cristalinas, denominadas forma de T_m baja y forma de T_m alta. Al enfriarse del fundido, se pudo observar la cristalización de las formas de T_m baja para los tres poli(tioéteres). Sin embargo, se demostró que la forma de T_m alta solo podía formarse a partir de la masa fundida para los polímeros TEGDVE-DMDS y BDDVE-DMDS.

Para el polímero DVE-DMDS, se demostró mediante análisis de dispersión de rayos X de gran angular (WAXS) que las dos estructuras cristalinas de forma de T_m baja y forma de T_m alta son diferentes, lo que demuestra que se pueden formar dos polimorfos diferentes por el mismo polímero. Los dos polimorfos presentaron morfologías diferentes, que pudieron observarse al microscopio óptico de luz polarizada (PLOM) siguiendo un protocolo isotérmico sucesivo. De este último, se encontró que al calentar las cadenas poliméricas de DVE-DMDS recordaban su alineación previa dentro de la forma cristalina de T_m baja, incluso por encima de su temperatura de fusión. Esta memoria ayudó a la nucleación y permitió la formación de la forma de T_m alta.

En condiciones isotérmicas, la cinética de cristalización de la forma de T_m baja de DVE-DMDS y la forma de T_m alta de TEGDVE-DMDS y BDDVE-DMDS podría implementarse mediante análisis DSC. Los datos experimentales se ajustaron a la ecuación de Avrami y dan una primera idea de la cinética de cristalización. En esta etapa del trabajo, se obtienen tasas de nucleación y cristalización más rápidas para la forma de T_m alta del polímero BDDVE-DMDS con la T_g más baja. La cristalización general (que comprende la nucleación y el crecimiento de

cristales) se acelera principalmente para unidades repetitivas más cortas en el esqueleto del polímero y una T_g más baja. En general, el polímero DVE-DMDS muestra una cinética más lenta, y solo la forma de T_m baja capaz de cristalizar al enfriarse del fundido. La forma de T_m alta de este polímero presenta una cinética muy lenta, que puede acelerarse mediante la autonucleación de los autonúcleos restantes o las autosemillas de la forma de T_m baja ligeramente por encima de su temperatura de fusión.

Finalmente, en el Capítulo 6, presentamos la síntesis de látex de poli(tioéteres) con un contenido de sólidos del 30 % basados en dos monómeros biobasados recientemente sintetizados, ditiol isosorbida (Iso-SH) y dialil isosorbida (Iso-A). A saber, se implementaron cuatro combinaciones de monómeros de tiol-eno: se estudió el sistema bicomponente biobasado Iso-SH/Iso-A, pero también otras tres formulaciones en las que el monómero Iso-SH de base biológica se polimerizó con tres dienos derivados del petróleo: tereftalato de dialilo (DATP), 3,9-divinil-2,4,8,10-tetraoxaspiro [5,5] undecano (SPAC) y 1,4-bis(aliloxi)benceno (DAOB) (Iso-SH/Iso-A, Iso -SH/DATP, Iso-SH/DAOB e Iso-SH/SPAC). Se presenta su aplicabilidad a la polimerización de crecimiento por etapas en el proceso de polimerización en miniemulsión fotoinducida.

Cabe destacar que las cuatro dispersiones de polímeros a base de biomonómeros y su combinación con monómeros a base de petróleo presentaron capacidades de formación de filme. Entre ellos, las formulaciones que contienen Iso-SH de biobasado con los dienos DATP de no base biológica podrían caracterizarse aún más para la aplicación prevista en el recubrimiento. De hecho, lel filme basado en Iso-SH-DATP presentó una buena estabilidad térmica hasta los

300 ºC y buenas propiedades mecánicas, concluidas por medición de prueba de tracción, con un módulo de Young medido de 3,72 MPa y un deformación a la rotura del 55 %. Además, el filme Iso-SH/DATP presentó una absorción de agua relativamente baja después de once días de inmersión en agua de menos del 20 %, pero significativamente mayor que las filmes F.A1 y F.A2 basados en GDMA-DATP sintetizados en el Capítulo 3. Estos últimos presentan estructuras cristalinas a temperatura ambiente, lo que podría impedir la difusión del agua a través del recubrimiento y una menor captación de agua, mientras que el filme Iso-SH/DATP es completamente amorfo en estas condiciones. La mayor absorción de agua podría explicarse por una menor T_g del filme Iso-SH/DATP, aunque no medida, lo que puede promover la reorganización del surfactante en "bolsillos" hidrofílicos dentro del recubrimiento y aumentar su sensibilidad al agua. En línea con la aplicación buscada en revestimiento decorativo, el filme Iso-SH/DATP presenta alto brillo, con un valor superior al 80 % en el ángulo de 60 °. Además del propósito estético, los valores altos de brillo brindan otra indicación sobre la migración del emulsificante, que por lo tanto migra principalmente dentro del recubrimiento y no en la interfaz con el aire. Tal comportamiento está en línea con las medidas de captación de agua.

Por lo tanto, la síntesis en medio disperso acuoso, junto con la incorporación de un componente de biobasado dentro del polímero, representa un paso adelante hacia la producción de recubrimientos a base de agua totalmente biobasados con valor añadido.

Appendix I: Supporting information Chapter 3

a)

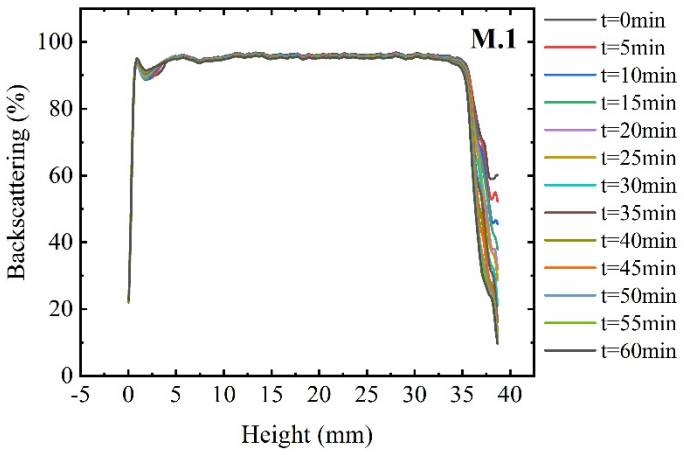

b)

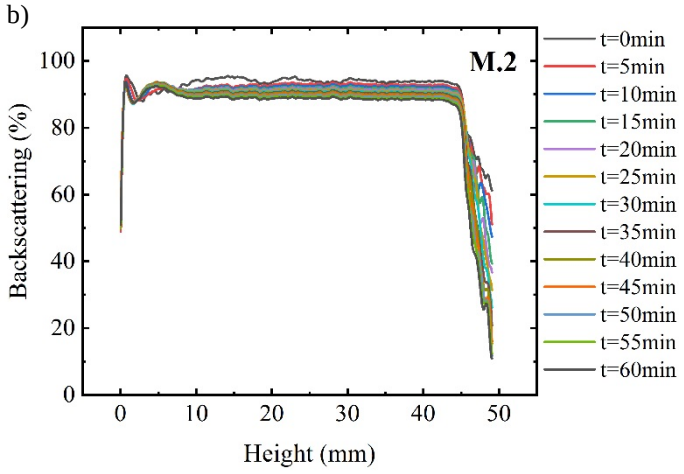

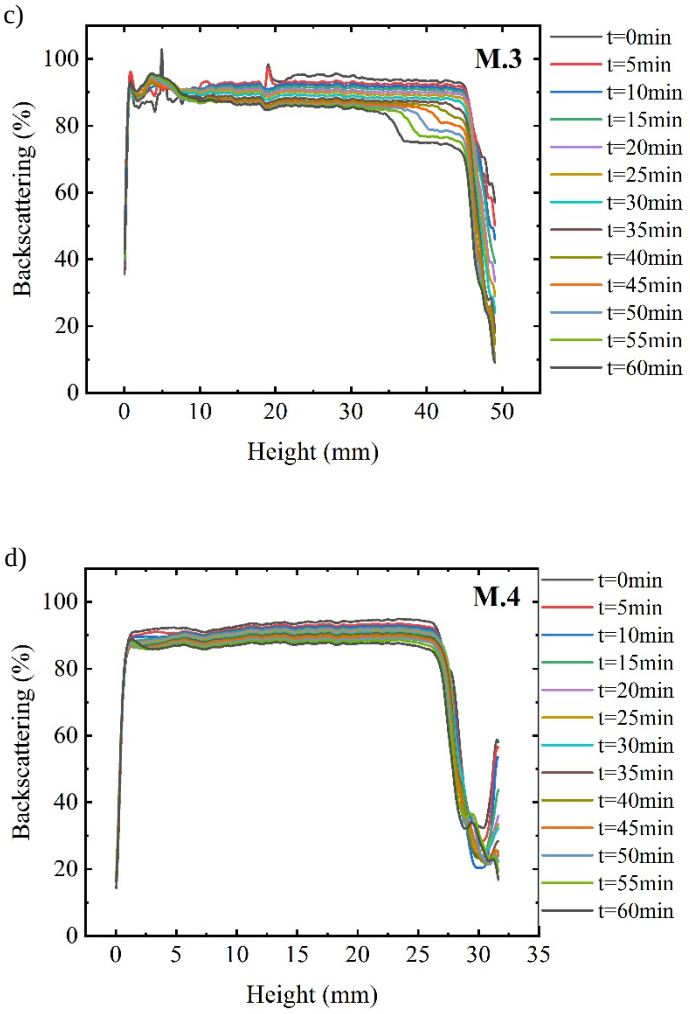

Figure I.1. Colloidal stability of 20% solid miniemulsions a)M.1 b) M.2 c) M.3 and d) M.4 based on GDMA-DATP monomer pair

a)

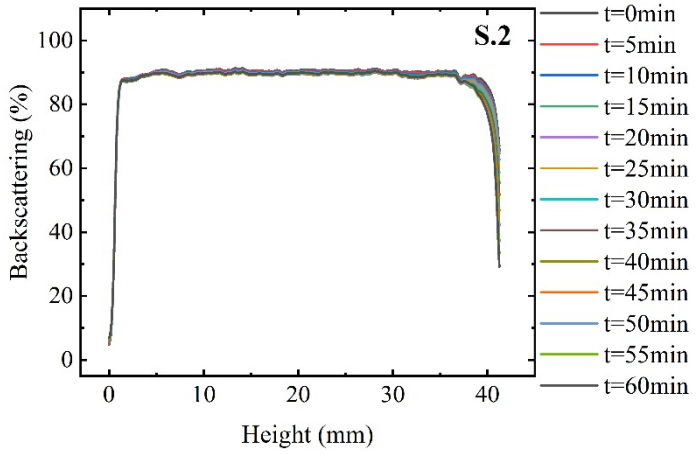
S.2
Backscattering (%)
Height (mm)
t=0min
t=5min
t=10min
t=15min
t=20min
t=25min
t=30min
t=35min
t=40min
t=45min
t=50min
t=55min
t=60min

b)

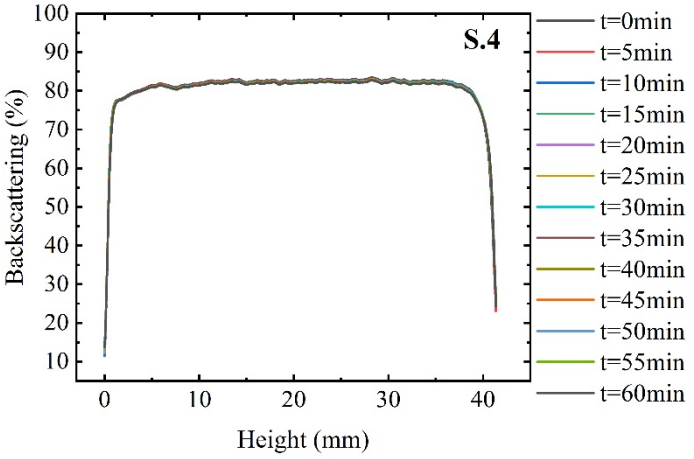
S.4
Backscattering (%)
Height (mm)
t=0min
t=5min
t=10min
t=15min
t=20min
t=25min
t=30min
t=35min
t=40min
t=45min
t=50min
t=55min
t=60min

c)

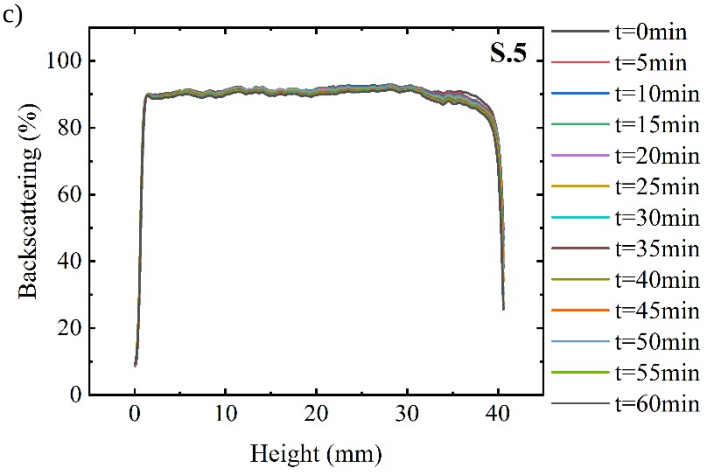
S.5
Backscattering (%)
Height (mm)
0
20
40
60
80
100
0
10
20
30
40
t=0min
t=5min
t=10min
t=15min
t=20min
t=25min
t=30min
t=35min
t=40min
t=45min
t=50min
t=55min
t=60min

d)

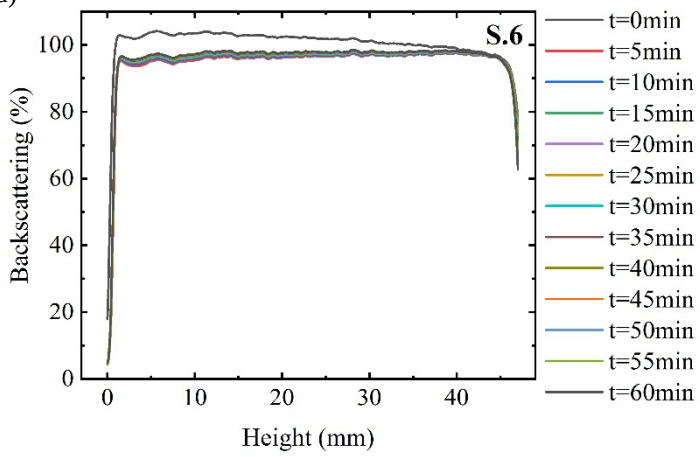
S.6
Backscattering (%)
Height (mm)
0
20
40
60
80
100
0
10
20
30
40
t=0min
t=5min
t=10min
t=15min
t=20min
t=25min
t=30min
t=35min
t=40min
t=45min
t=50min
t=55min
t=60min

e)

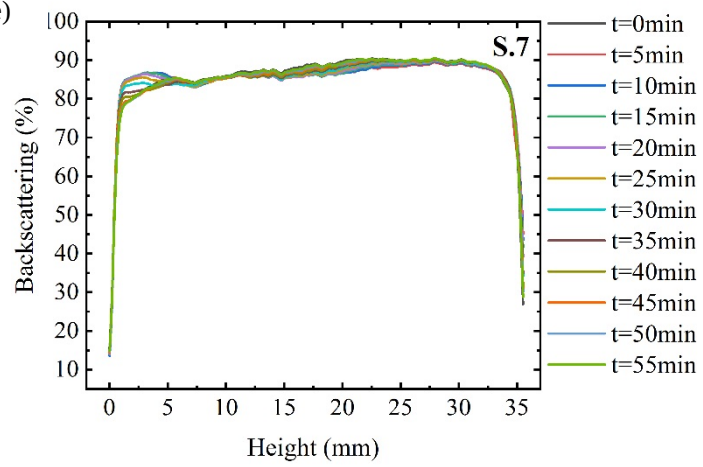
S.7
Backscattering (%)
Height (mm)
t=0min
t=5min
t=10min
t=15min
t=20min
t=25min
t=30min
t=35min
t=40min
t=45min
t=50min
t=55min

f)

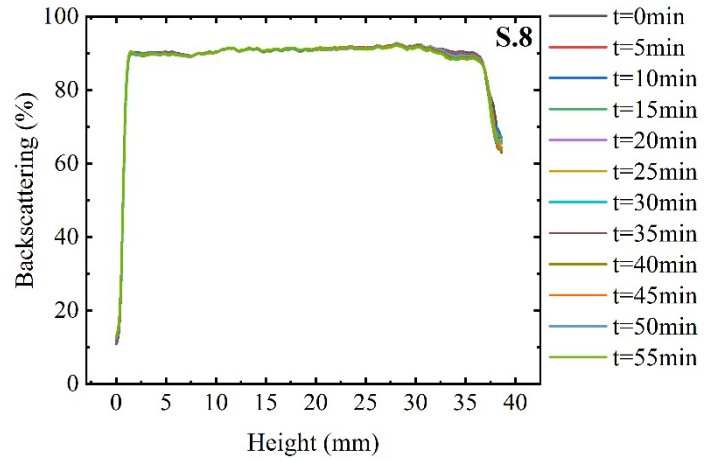
S.8
Backscattering (%)
Height (mm)
t=0min
t=5min
t=10min
t=15min
t=20min
t=25min
t=30min
t=35min
t=40min
t=45min
t=50min
t=55min

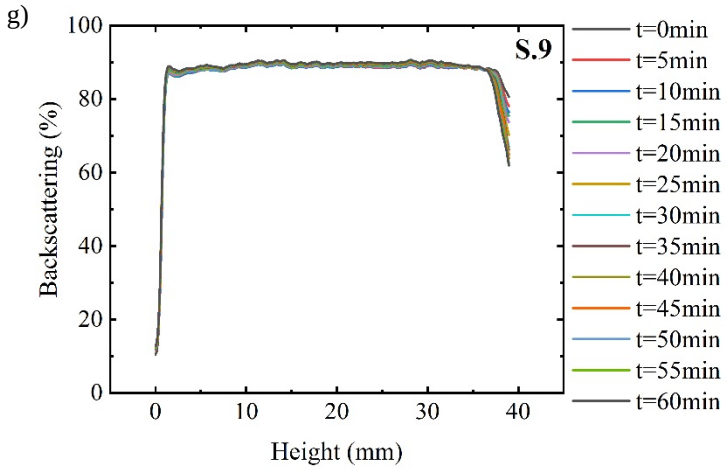

Figure I.2 Colloidal stability 30% solid content prepolymer latex a) S.2, b) S.4, c) S.5, d) S.6 e) S.7, f) S.8 and g) S.9

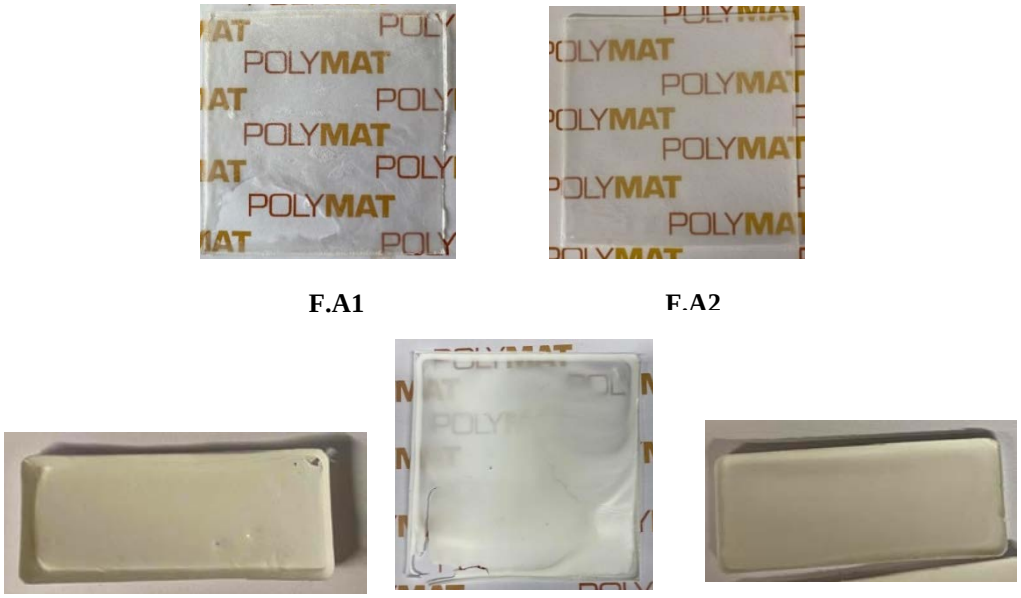

Figure I.3 Films FA.1 to FC obtained after water evaporation of the 30% solid content latexes based on GDMA-DATP, GDMP-DATP and EDDT-DATP at 25°C and 55% of humidity.

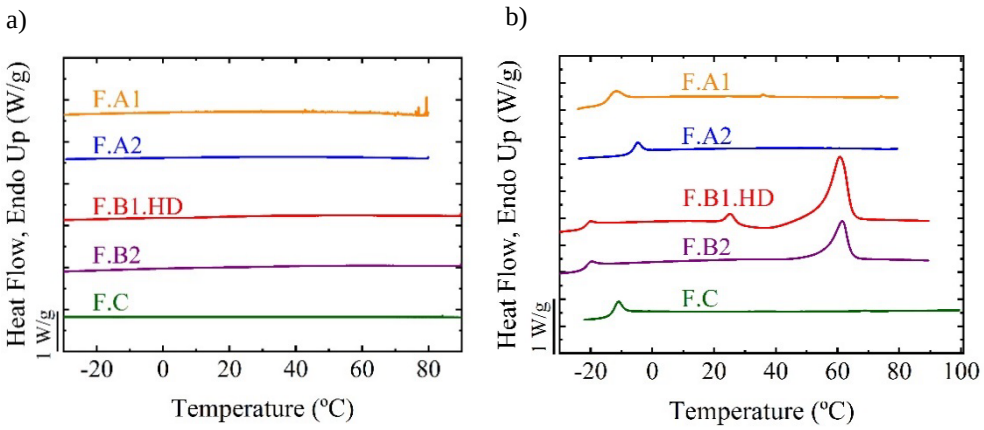

Figure I.4. Non-isothermal crystallization of films F.A1, F.A2, F.B1.HD, F.B2 and F.C (a) DSC cooling scans from molten state at 1ºC/min and (b) subsequent heating scans at 20ºC/min

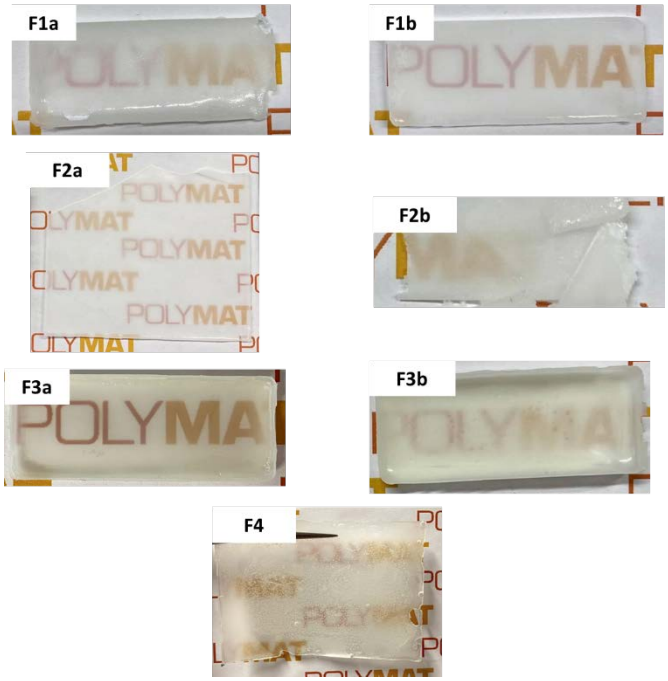

Figure I.5. Films obtained after water evaporation of the latexes A, B, C and D from Table 3.12.

A) **B)**

Figure I.6. Photos of the prepared film from **A**) the GDMA-DATP+TVCH based latex in silicone mold at 25°C and 55% of humidity **B**) the GDMA-DATP+TMPMP based latex in silicone mold at 25°C and 55% of humidity

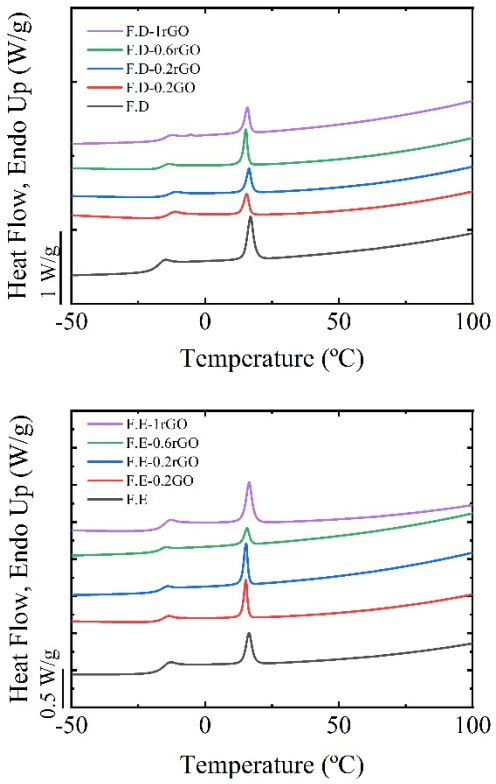

Figure I.7. DSC second heating scans from film F.D and composites and film F.E and composites. The melting point observed around 16ºC is attributed to the melting of HD

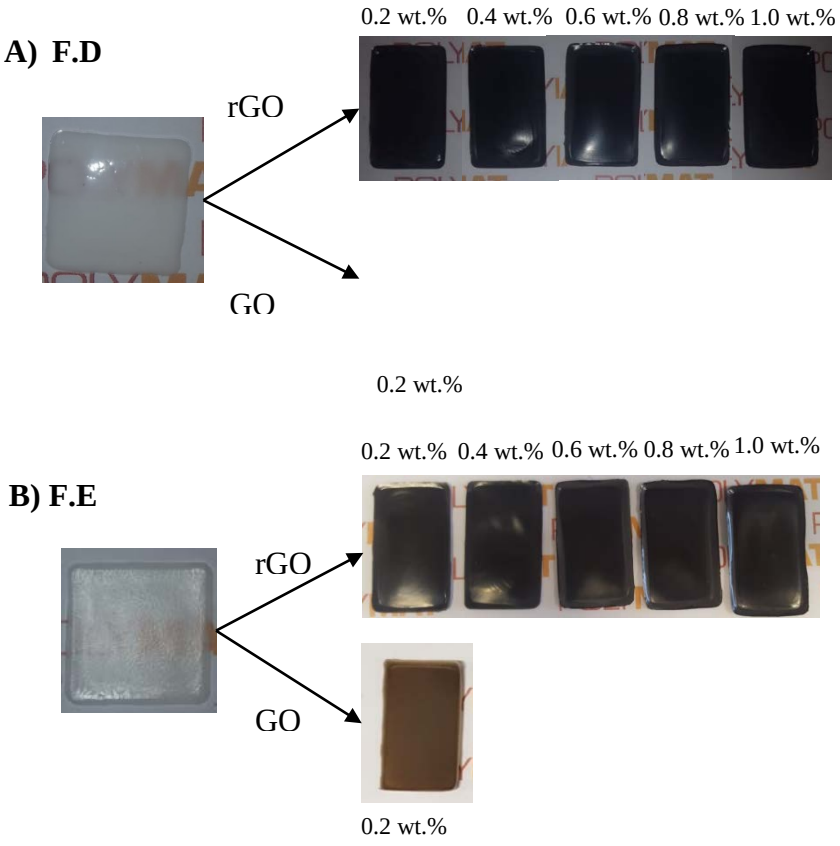

Figure I.8. Photos of the prepared film A) GDMA-DATP+TVCH based latex in silicone mold at 25°C and 55% of humidity and composite films B) GDMA-DATP +TMPMP based latex in silicone mold at 25°C and 55% of humidity and composite films

Appendix II: Supporting information Chapter 4

In this Appendix, another strategy that was implemented for the study of the crystalline behaviour of film based on GDMA-DATP monomers from Chapter 4 is reported.

Self-nucleation and isothermal crystallization

SN experiment can be used as a tool to speed up the nucleation step before isothermal crystallization when slow crystallizing materials are being used. In this way, the crystallization rate of self-nucleated polymers is accelerated, and crystal growth can be observed by isothermal DSC analysis[4].

SN and isothermal crystallization were performed for the film F.A1 based on the modelled monomer pair GDMA-DATP. For that aim, the first SN step is performed at T_s of 43ºC, temperature at which the SN step was successful (Figure 4.11, Chapter 4). The sample F.A1 is then rapidly cooled at 60ºC/min to the isothermal crystallization temperature T_c for 45 minutes and the results are depicted in Figure II.1.

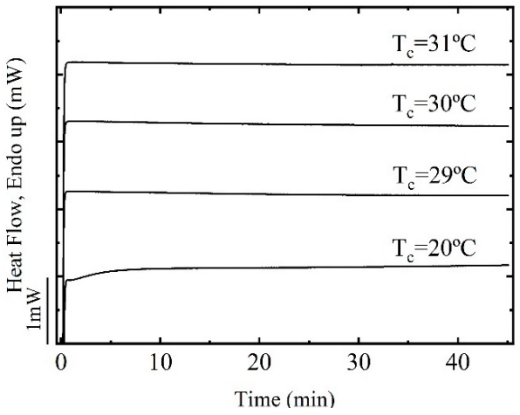

Figure II.1 Isothermal crystallization experiments of the film F.A1 at the indicated Tc after a self-nucleation step at 43 ºC.

No crystallization exotherm can be observed after 45 minutes at the selected T_c, despite the self- nucleation step. It means that, even with SN step and the presence of nuclei, crystallization kinetics are still too low to be studied by DSC isothermal crystallization.

Appendix III: Supporting information Chapter 5

III.1. Synthesis

Herein, thiol-ene step-growth polymerization was performed between DMDS and three others diene monomers DVE, TEGDVE and BDDVE by Quoc Le *et al*, following the synthetic process they developed for the monomers DMDS and diallyl phthalate (DAP)[1].

In a typical reaction, blends of monomers composed of 2,2'-dimercaptodiethyl sulfide (DMDS, 0.500 g, 3.2 mmol, 1 equiv.) and the chosen di-ene monomer di(ethylene glycol) divinyl ether (DVE, 0.516 g, 3.2 mmol) was added to 20 mL soda-lime glass vial (external diameter: 25 mm, height: 70 mm). To this monomer mixture, an aqueous phase containing a photo-catalyst (eosin disodium, 2 mg, 0.0026 mmol, 0.02 % w/w monomer), a surfactant (sodium dodecyl sulfate (SDS), 35 mg, 3.5 wt% with respect to monomers, 13.5 mM in water) and 9 mL of phosphate buffer 10 mM (pH = 8) were added. An emulsion with an organic phase content of 10 % w/w was prepared using a homogenizer (Ultra-Turrax, T25, IKA-Werke) at 15 000 rpm for 10 min. Photo-polymerization was performed immediately after emulsification at room temperature inside a circular photochemical reactor built with a green LED strip (530 nm, 3.0 mW·cm–2) around a quartz cylinder (internal diameter: 80 mm, length: 100 mm). Irradiation was continued for 60 min, while the vial was kept under continuous magnetic-stirring (1100 rpm).

Complementary polymers have been synthesized, where DVE has been replaced by triethylene glycol divinyl ether (TEGDVE), and 1,4-butanediol divinyl ether (BDDVE). Aqueous dispersions of the resulting polythioether were precipitated by adding ethanol, yielding a solid polymer powder, which was filtered, washed with ethanol and dried under vacuum. The molar masses of the obtained polythioethers was determined by gel permeation chromatography (GPC) of the polymers dissolved in dimethylformamide (DMF) (DVE-DMDS and TEGDVE-DMDS) and by proton nuclear magnetic resonance (1H- NMR) of the polymers dissolved in deuterated chloroform ($CDCl_3$) (BDDVE-DMDS), and are depicted in table 5.1. Typically, the obtained powders of these polythioether showed good solubility in chloroform and were used without further purification for the investigations described in this chapter. The glass transition temperatures of the three polymers were obtained by non-isothermal FLASH-DSC analysis, which are not reported in this manuscript.

III.2. Non-isothermal crystalline behaviour

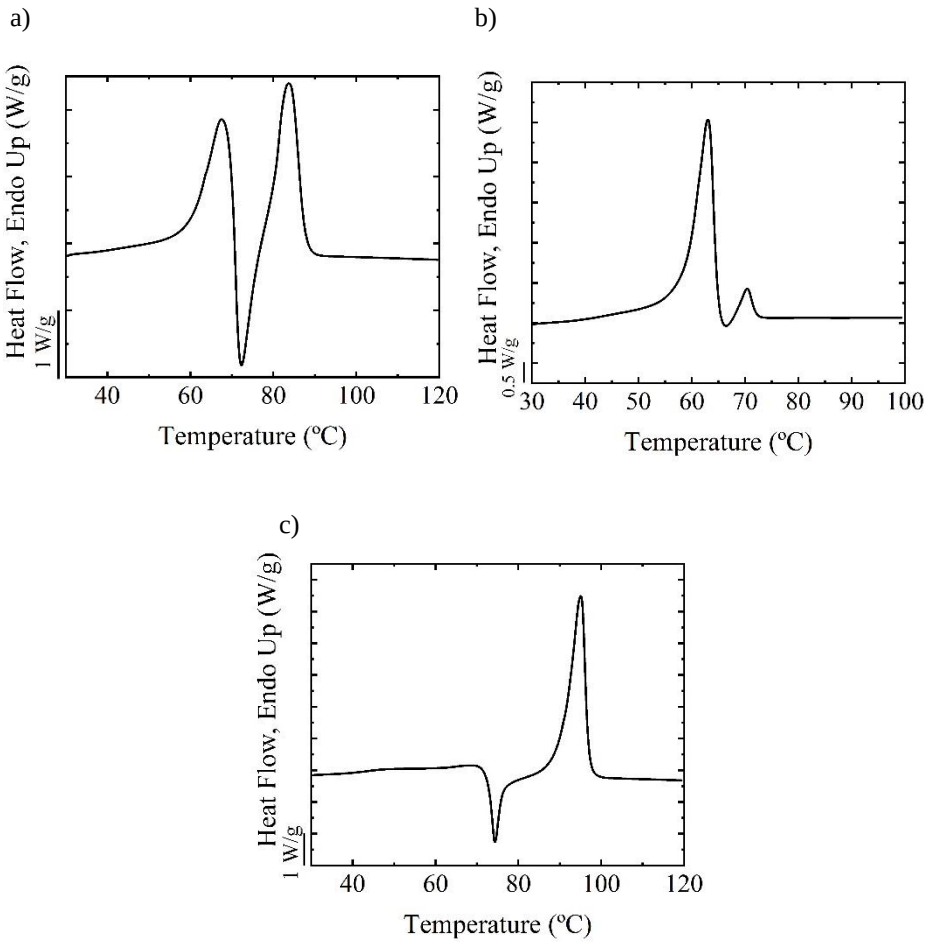

Figure III.1. First DSC heating scan at 20ºC/min for the polymers a) DVE-DMDS b) TEGDVE-DMDS and c) BDDVE-DMDS

Table III.1. Melting temperature (T_m), melting enthalpy (ΔH_m), cold crystallization temperature (T_{cc}), and cold crystallization enthalpy (ΔH_{cc}) of the polymer DVE-DMDS, TEGDVE-DMDS and BDDVE-DMDS. The values are obtained from the first DSC heating scan from Figure 5.2. at 20ºC/min.

Polymer	First Heating					
	$T_{m,1}$ (ºC)	$\Delta H_{m,1}$ (J/g)	T_{cc} (ºC)	ΔH_{cc} (J/g)	$T_{m,2}$ (ºC)	$\Delta H_{m,2}$ (J/g)
DVE-DMDS	67.5	55	72.3	16	83.7	46
TEGDVE-DMDS	60.6	72	-	-	67.5	4
BDDVE-DMDS	65.9	16	71.3	14	93.9	86

III.3. Avrami fit

Table III.2 . The overall crystallization rate $\frac{1}{\tau_{50\%,exp}}$, the nucleation rate $\frac{1}{t_0}$, the Avrami index n, the overall transformation constant K and the correlation coefficient R^2 values obtained after fitting isothermal crystallisation DSC scans of DVE-DMDS, TEGDVE-DMDS and BDDVE-DMDS to the avrami equation. t_{peak} was obtained directly from DSC cooling traces, and represents the time at which the crystallization exotherm reaches its maximum.

	T_c (ºC)	$1/t_{50\%\ exp}$ (min^{-1})	$1/t_{peak}$ (min^{-1})	$1/t_0$ (min^{-1})	Avrami index (n)	R^2
DVE-DMDS	60	0.23	0.21	1.95	2.83	1.0000
	60.5	0.20	0.18	1.54	2.8	1.0000
	61	0.17	0.16	1.73	3.08	1.0000
	61.5	0.14	0.12	1.73	3.07	0.9999
	62	0.12	0.11	1.54	3.32	1.0000
	62.5	0.09	0.08	1.40	3.17	0.9999
	63	0.07	0.07	1.52	3.41	0.9997

TEGDVE-DMDS	46	0.15	0.15	1.23	2.74	1.0000
	46.5	0.12	0.13	2.01	3.05	0.9997
	47	0.10	0.11	2.01	3.06	0.9997
	47.5	0.09	0.09	1.73	3.04	0.9998
	48	0.08	0.08	2.01	3.28	0.9995
	48.5	0.07	0.07	1.73	3.31	0.9997
BDDVE-DMDS	79	0.28	0.26	2.01	2.6	1.0000
	79.5	0.22	0.21	2.01	2.7	1.0000
	80	0.17	0.18	2.01	2.69	1.0000
	80.5	0.14	0.14	2.35	2.91	0.9999
	81	0.11	0.12	2.35	2.86	0.9996
	81.5	0.09	0.10	2.01	2.72	0.9998
	82	0.08	0.09	1.52	2.7	0.9999
	82.5	0.07	0.07	1.73	2.77	0.9998

Appendix IV: Supporting information Chapter 6

IV.1. Synthesis and purification of Iso-SH

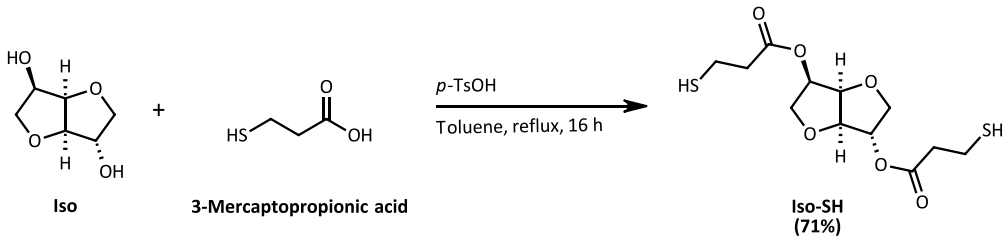

Figure IV.1 Synthesis of Iso-SH

In an oven-dried 1 L round-bottomed flask equipped with a Dean-Stark apparatus isosorbide (Iso) (1 eq., 342.1 mmol, 50.0 g), p-toluenesulfonic acid (0.1 eq., 34.2 mmol, 6.5 g) and 3-mercaptopropionic acid (2.5 eq., 855.3 mmol, 74.4 mL) were solved in dry toluene (500 mL). The reaction mixture was stirred vigorously and heated to 130 °C in an oil bath overnight for 16 h. The reaction progress was monitored via TLC (PE:EE = 6:4, Rf(product) = 0.38, stain = potassium permanganate solution). The reaction was transferred into a separation funnel and subsequently washed four times by the addition of an aqueous NaHCO3 solution (sat., 250 mL) and brine (2 x 150 mL). The organic phase was collected, dried over NaSO4, and the solvent was evaporated under reduced pressure. The crude product was purified three times by column chromatography (PE:EE = 1:0 → 1:1) to yield the final product Iso-SH (3R,3aR,6S,6aR)-hexahydrofuro[3,2-b]furan-3,6-diyl bis(3-mercaptopropanoate) 78.3 g (71%) as a colourless oil.

1H NMR (400 MHz, Chloroform-d) δ 5.25 – 5.22 (m, 1H), 5.22 – 5.15 (dt, J = 5.9, 5.2 Hz, 1H), 4.87 – 4.82 (m, 1H), 4.51 – 4.47 (m, 1H), 4.00 – 3.91 (m, 3H), 3.86 – 3.79 (m, 1H), 2.82 – 2.63 (m, 8H), 1.74 – 1.68 (t, J = 8.2 Hz, 1H), 1.65 – 1.59 (t, J = 8.3 Hz, 1H). 13C NMR (100 MHz, Chloroform-d) δ 171.1, 170.8, 86.0, 80.8, 78.3, 74.3, 73.4, 70.6, 38.4, 19.8. HPLC: 3.18 min (20% acetonitrile/(80% water + 0.1 vol% trifluoroacetic acid), v/v, detection at 210 nm).

IV.2. Synthesis and purification of Iso-A

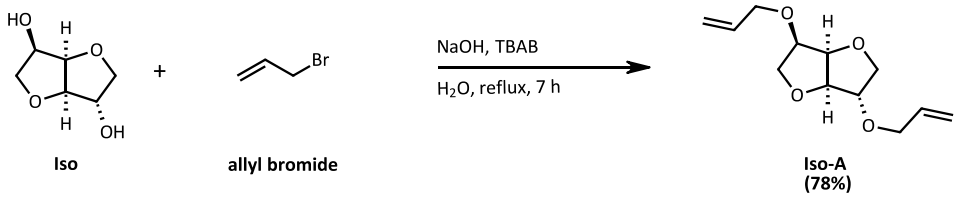

Figure IV.2 Synthesis od Iso-A

Isosorbide (Iso) (30.0 g, 1 equiv., 205.3 mmol) was mixed with NaOH (18.1 g) and 50 mL of water. After complete solubilization of isosorbide, TBAB (3.22 g) and allyl bromide (54.6 g, 451.6 mmol) were added. This mixture was refluxed for 7 h. After cooling to room temperature, the aqueous solution was extracted with CH2Cl2 (4 × 50 ml). The organic phase was collected and washed with 1 M HCl (200 mL) and with deionized water (4 × 50 mL) to remove salts. Finally, the organic phase was dried over anhydrous MgSO4, filtered, and CH2Cl2 was evaporated under vacuum. The crude product was purified two times via vacuum distillation (0.045 mbar, 95°C), yielding the final product Iso-A (3R,3aR,6S,6aR)-3,6-bis(allyloxy)hexahydrofuro[3,2-b]furan 36.3 g (78%) as a colourless oil. 1H NMR (400 MHz,

Chloroform-d) δ 6.00 – 5.81 (m, 2H), 5.33 – 5.23 (m, 2H), 5.22 – 5.15 (m, 2H), 4.64 – 4.59 (m, 1H), 4.52 – 4.44 (m, 1H), 4.23 – 4.15 (m, 1H), 4.07 – 3.89 (m, 8H), 3.63 – 3.55 (m, 1H). 13C NMR (101 MHz, Chloroform-d) δ 134.6, 134.3, 117.9, 117.6, 86.4, 83.9, 80.3, 79.6, 73.5, 71.7, 70.6, 69.9. HPLC: 2.54 min (20% acetonitrile/(80% water + 0.1 vol% trifluoroacetic acid), v/v, detection at 210 nm)

IV.3. Synthesis of biobased polymers by bulk photopolymerization

Bulk photopolymerization was performed by mixing thiol and ene in a stoichiometric ratio in presence of the photoinitiator TPO-Li and subjected to RT-NIR-photorheology measurments.

RT-NIR photorheology was performed on an Anton Paar MCR 302 WESP with a P-PTD 200/GL Peltier glass plate, a H-PTD 200 heating hood, and a disposable PP25 measuring system. The rheometer was coupled with a Bruker Vertex 80 FTIR spectrometer to be able to analyse the double bond conversion of the ene-monomer over time. For detection of the reflected beam, a MCT–detector was used. The measurements were performed in triplicates at room temperature (25°C). 180 µL sample volume was applied on a glass disk which was covered with PE tape. For detailed information about the the four formulations investigated, see Tables IV.1, IV.2, IV.3 and IV.4. The PE tape is necessary to remove the samples after irradiation. The gap size between the measuring system and the glass plate was set to 200 µm. UV curing was conducted with an Omnicure Series 200 EXFO as a light source equipped with a 200 W Hg lamp and an installed filter (wavelength of 400–500 nm). The light intensity at the surface of

the PE tape (attached to the glass plate) was measured via an Ocean Optics USB 2000 + spectrometer and set to 20 mW cm^{-2}. The samples were irradiated for 300 s. The photorheology measurements were analysed with the software Rheoplus V3.62 from Anton Paar, and the IR spectra were analysed with the software Opus 7.0 from Bruker.

Table IV.1. Formulation to prepare biobased bulk poly(thioether) with Iso-SH and Iso-A

Chemicals	**MW / g·mol^{-1}**	**n / mmol**	**wt%**	**m / mg**
Iso-SH	322.39	2.00	0.59	644.78
Iso-A	226.27	2.00	0.41	452.54
TPO-L	316.33	0.035	1.00	10.97

Table IV.2. Formulation to prepare biobased bulk poly(thioether) with Iso-SH and DATP

Chemical	**MW / g·mol^{-1}**	**n / mmol**	**wt%**	**m / mg**
Iso-SH	322.39	2.00	0.57	644.78
DATP	246.26	2.00	0.43	492.52
TPO-L	316.33	0.036	1.00	11.37

Table IV.3. Formulation to prepare biobased bulk poly(thioether) with Iso-SH and SPAC

Chemical	**MW / g·mol^{-1}**	**n / mmol**	**wt%**	**m / mg**
Iso-SH	322.39	2.00	0.60	644.78
SPAC	212.25	2.00	0.40	424.50
TPO-L	316.33	0.034	1.00	10.69

Table IV.4. Formulation to prepare biobased bulk poly(thioether) with Iso-SH and DAOB

Chemical	**MW / g·mol^{-1}**	**n / mmol**	**wt%**	**m / mg**
Iso-SH	322.39	2.00	0.63	644.78
DAOB	190.24	2.00	0.37	380.48
TPO-L	316.33	0.03	1.00	10.25

IV.4. Synthesis of biobased polymers by miniemulsion photopolymerization

In a typical reaction, an organic phase containing Iso-SH (3.4064 g, 10.57 mmol), Iso-A (2.3911 g, 10.57 mmol), the radical inhibitor DBHQ (0.0112 g, 10 mM with respect to monomer) and hexadecane (0.36 g, 6.2 wt.%/monomer) was mixed in a 25 mL vial. The organic phase was then mixed with a 14 mL aqueous phase containing Dowfax 2A1 surfactant (0.18 g, 3.1 wt.% respect to monomer), and the photoinitiatorTPO-Li (0.12 g, 0.40 mmol, 2.07 wt.%/monomer). In the reaction Entry A1 from Table 6.1 in Chapter 6 the oil soluble photoinitiator TPO was used instead of TPO-Li. A macroemulsion was then formed by high-speed mixing with Ultra-Turax setting at 15 000 rpm for 5 min. The resulting macroemulsion was further emulsified by using a Branson sonifier SFX250 for 5 min at 90 % amplitude and pulse mode 5 s ON / 1 s OFF cycles. The as-prepared monomer miniemulsion was irradiated for 60 min inside the custom-made photoreactor (3.7 mW cm^{-2}) with stirring speed at 1100 rpm. One miniemulsion was irradiated using a PESCHL photoreactor operating at an irradiance of 33 mW cm^{-2} (385 nm) (Table 6.1 in Chapter 6, entry A3). Table 6.1 in Chapter 6 summarizes the reaction parameters and the properties of the polymer dispersions prepared from the biobased monomers.

The formulation of the polymer dispersion based on DATP, SPAC, DAOB and Iso-SH are addressed Tables IV.5, IV.6 and IV.7. Their preparation followed the same protocol as it was explained for the dispersion based on the monomers Iso-A and Iso-SH, with reaction conditions and irradiation parameters described in Table 6.1 in Chapter 6.

Table IV.5. Formulation to prepare biobased latex with Iso-SH and DATP.

Chemicals	Quantity (g)	Mol number (mmol)
DBHQ	0.0112	0.049
Iso-SH	3.4013	10.55
DATP	2.6192	10.57
Hexadecane	0.3600	1.56
Dowfax 2A1	0.18	0.31
Water	14.0	
TPO-Li	0.120	0.40

Table IV.6. Formulation to prepare biobased latex with Iso-SH and SPAC

Chemicals	Quantity (g)	Mol number (mmol)
DBHQ	0.0112	0.049
Iso-SH	3.620	11.23
SPAC	2.383	11.23
Hexadecane	0.3600	1.56
Dowfax 2A1	0.18	0.31
Water	14.0	
TPO-Li	0.120	0.40
NaHCO3	0.0119	0.14

Table IV.7 Formulation to prepare biobased latex with Iso-SH and DAOB

Chemicals	Quantity (g)	Mol number (mmol)
DBHQ	0.0112	0.049
Iso-SH	3.75	11.63
DAOB	2.236	11.63
Hexadecane	0.3600	1.56
Dowfax 2A1	0.18	0.31
Water	14.0	
TPO-Li	0.120	0.40
$NaHCO_3$	0.0119	0.14

Gel permeation chromatography (GPC) measurements or size exclusion chromatography (SEC) experiments, were performed on a Malvern VISCOTEK TDA system equipped with a ViscotekTDA 305-021 RI+Viscdetector, a UV Detector Module 2550 for TDA 305, and a

VISCOTEK SEC-MALS 9 light scattering detector. Samples were prepared syringe-filtered (200 nm poly(tetrafluorethylene) syringe filters) 2-4 mg mL^{-1} THF-solutions spiked with 0.5 mg mL^{-1} butylated hydroxytoluene (BHT) as flow marker. Size exclusion chromatography was conducted through PSS SDC column using dry THF as mobile phase at a flow rate of 0.8 mL min^{-1} and a temperature of 35 °C. In the case of the triple detection, the dn/dc value was determined by injecting the sample at five different injection volumes between 80 and 120 µl and analyzing the slope of the signals. One narrow PS-standard ($\overline{M_w}$ = 105 kDa) and one broad PS standard ($\overline{M_w}$ = 245 kDa), both supplied by Malvern, were utilized for creating the triple detection calibration method. Analysis was conducted with the OmniSEC Software V5.12.461 (Malvern) to evaluate the elugrams and to calculate the number- and weight-average molecular weights and the dispersity $Đ$ of the polymers.

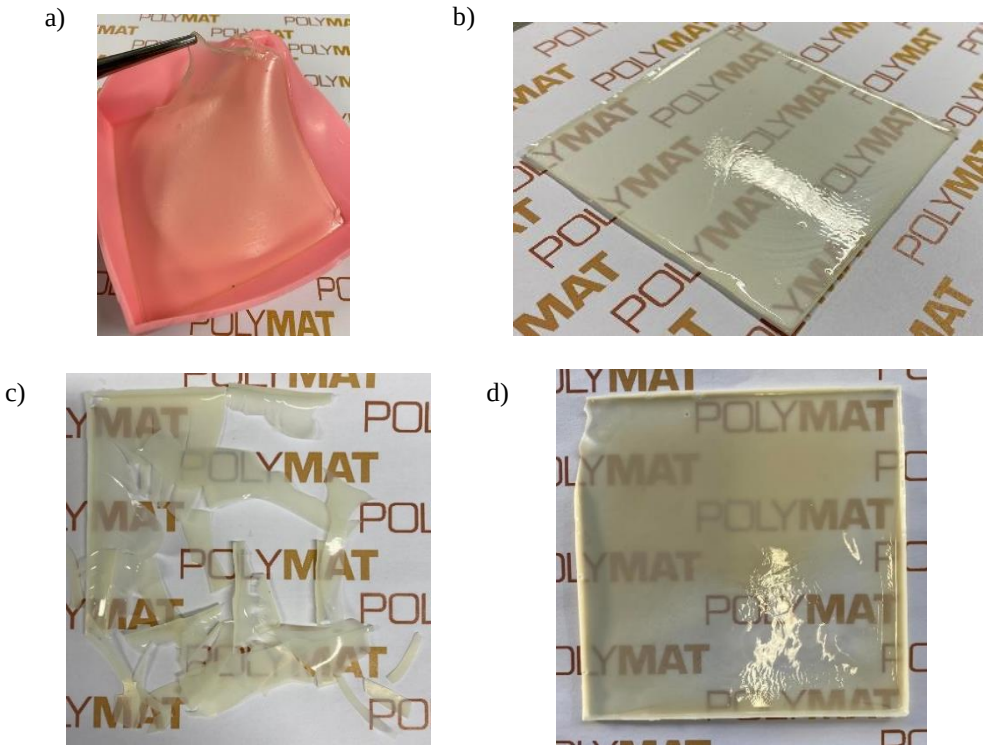

Figure IV.3. Film obtained by water evaporation of the latex based on the monomer pairs a)Iso-SH/Iso-A and b) Iso-SH/DATP c) Iso-SH/SPAC and d) Iso-SH/DAOB

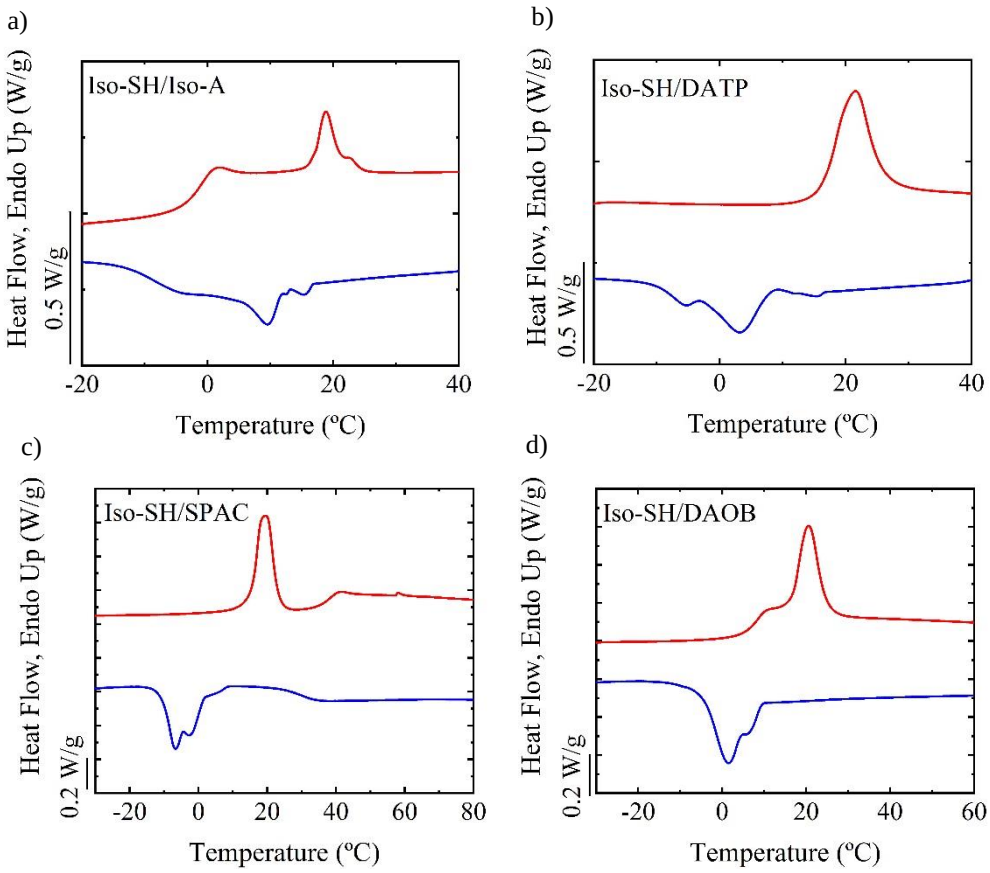

Figure IV.4. DSC cooling scans from molten state at 20ºC/min (blue) and subsequent heating scans at 20ºC/min (red) for the films based on a) Iso-SH/Iso-A, b) Iso-SH/DATP, c) Iso-SH/SPAC and c) Iso-SH-DAOB

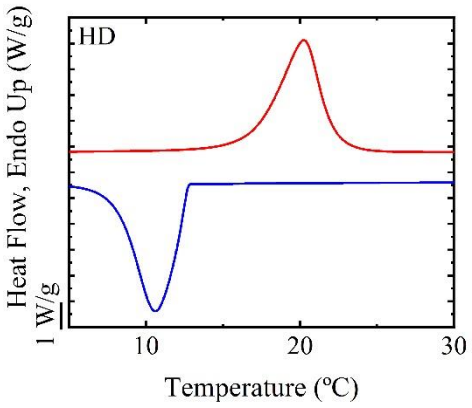

Figure IV.5. DSC cooling scans from molten state at 20ºC/min (blue) and subsequent heating scans at 20ºC/min (red) of HD

Appendix V: General characterization methods

Monomer conversion by proton nuclear magnetic resonance

Proton nuclear magnetic resonance (^{1}H NMR) was used for the measurement of the final ene conversion. NMR spectra were recorded on a Bruker 400 MHz at 25 °C. Samples were prepared by dissolving 20mg aliquots in 0.5 mL of deuterated chloroform ($CDCl_3$-d^6) or deuterated Dimethylsulfoxide (DMSO-d^6). The conversion was determined by following the disappearance of the peak at 4.81ppm and the appearance of the films at 4.32 ppm from diallyl terephtalate (DATP) monomer with the following equation:

$$Conv = \frac{I_{4,32ppm}}{I_{4,32\ ppm} + I_{4,81ppm}}$$

An example in the case of glycol dimercaptoacetate (GDMA) and DATP polymerization is presented in Figure V.1.

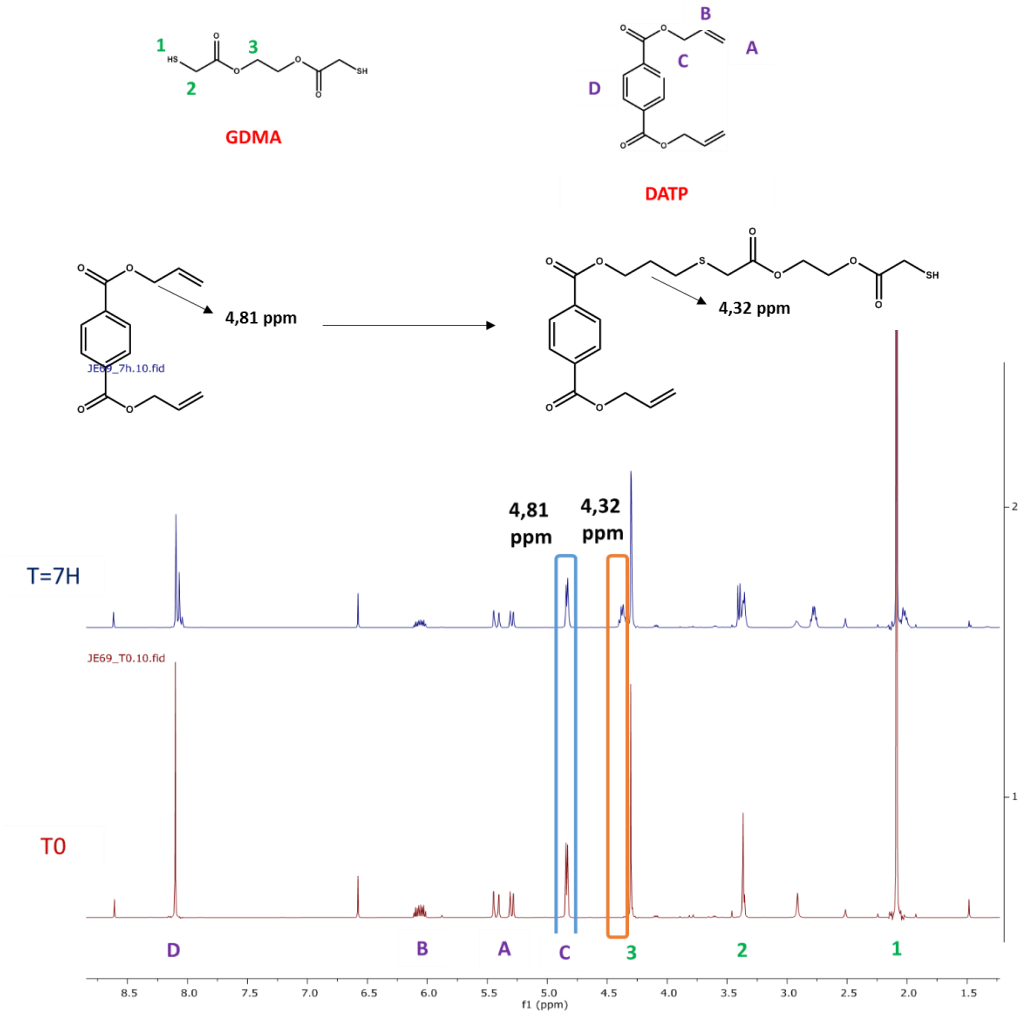

Figure V.1 NMR spectra of the monomers GDMA and DATP at T0 and the resulting poly(thioether) after 7 hours under UV exposure

Appendix VI. List of acronyms and abbreviations

AFM	Atomic force microscope
AIBN	2,2'-azobisisobutyronitrile
BDDVE	1,4-butanediol divinyl ether
DAOB	1,4-bis(allyloxy)benzene
DATP	Diallyl terephthalate
DBC	Double bond conversion
DBHQ	2,5-Di-tert-butylhydroquinone
DOSY	Diffusion ordered spectroscopy
DLS	Dynamic light scattering
DMDS	2,2'-dimercaptodiethyl sulfide
DOSY	Diffusion ordered spectroscopy
Dowfax 2A1	Alkyl diphenyl oxide disulfonate
DVE	Di(ethylene glycol) divinyl ether
EDDT	2,2-(ethylenedioxy)diethanethiol
EPR	Electron Paramagnetic Resonance
G	Graphene
G'	Storage moduli
GC	Gel content
GDMA	Glycol dimercaptoacetate
GDMP	Glycol dimercaptopropionate
GO	Graphene oxide
GPC	Gel permeation chromatography
$\Delta \boldsymbol{H_c}$	Crystallization enthalpy
$\Delta \boldsymbol{H_{cc}}$	Cold crystallization enthalpy
HD	Hexadecane

ΔH_m	Melting enthalpy
HPLC	High performance liquid chromatography
Iso-A	Isosorbide diallyl
Iso-SH	Isosorbide dithiol
MALDI-ToF	Matrix assisted laser desorption/ionization–time of flight mass
MS	spectrometry
MALS	Multi angle light scattering
Mw	Weight average molar mass
n	Avrami index
NMR	Nuclear magnetic resonance
PBN	N-tert-butyl-α-phenylnitrone
PDI	Polydispersity index-molar mass dispersity
PLOM	Polarized light optical microscope
PSD	Particle size distribution
PYR	Pyrogallol
r	Stoichiometric ratio
rGO	Reduced graphene oxide
R.H.	Relative humidity
RT-FTIR	Fourier-transform infrared spectroscopy
SEC	Size exclusion chromatography
S.C.	Solids content
SEM	Scanning electron microscopy
SN	Self-nucleation
SPAC	3,9-divinyl-2,4,8,10-tetraoxaspiro[5.5]undecane
$\mathbf{t_0}$	Induction time
$\tau_{50\%,exp}$	Experimental half crystallization time
$\mathbf{T_c}$	Crystallization temperature
$\mathbf{T_{cc}}$	Cold crystallization temperature
TEGDVE	Triethylene glycol divinyl ether

T_g	Glass transition temperature
TGA	Thermal gravimetric analysis
THF	Tetrahydrofuran
T_m	Melting temperature
TMPMP	Trimethylolpropan tri(3-mercaptopropionate)
TPO	Diphenyl(2,4,6-trimethylbenzoyl)phosphine oxide
TPO-Li	Lithium phenyl (2,4,6-trimethylbenzoyl)phosphinate
T_s	Self-nucleation temperature
TVCH	1,2,4-Trivinylcyclohexane
WAXS	Wide angle X-ray scattering
wt%	Weight percent
WVTR	Water vapour transmission rate
$\boldsymbol{Xc}$	Degree of crystallinity
$\boldsymbol{\bar{X}_n}$	Degree of polymerization